Interference and Transport of Bose-Einstein Condensates

by Bo Xiong, MSc

Thesis submitted to the University of Nottingham
for the degree of Doctor of Philosophy

November 2, 2009

PAGE

NUMBERING

AS ORIGINAL

Abstract

This dissertation studies the dynamics of atomic Bose-Einstein condensates (BECs) and Bose gases in a suddenly modified potential.

Firstly, we investigate the correlation between vortex formation and interference in merging Bose-Einstein condensates. This inherent correlation can explain some experiments in which vortices are formed in interfering condensates. Furthermore, we show the interference properties of merging condensates, particularly the relation of interference among colliding, expanding, and merging condensates, which can explain some complex interference phenomena in recent experiments.

Secondly, using the truncated Wigner approximation, we investigate the role of quantum fluctuations in different forms on the transport properties of bosonic atoms in a 1D optical lattice. The dynamics of transport with respect to quantum fluctuations in the plane-wave modes is distinct from that in the single-harmonic-oscillator modes. The discrepancies are demonstrated in detail. Quantum fluctuations in Bogoliubov modes lead to stronger damping behavior of the center-of-mass motion than quantum fluctuations in the plane-wave and single-harmonic-oscillator modes, which is in agreement with the experiment.

Thirdly, the role of the relative phase variation and velocity of two low-density condensates, and quantum noise on interference properties are discussed. In particular, the incoherent atoms have significant effect on the interference visability and microscopic dynamics. Although the interference pattern is not broken by quantum fluctuations, indicating the robust character of this interference, the process of inner correlations and dynamics is very complex and can not be understood purely with mean-field theory.

Finally, we investigate the elementary excitation spectrum and mode functions of a trapped Bose gas by numerically solving the Bogoliubov-De Gennes equation. The characteristic form of the Bogoliubov matrix, determined by the interatomic interactions, and the interaction between atoms and confining potential, specifies excitation spectra and mode functions. The role of these interactions on the properties of spectra and mode functions are shown.

Acknowledgements

I would like to express my thanks to my supervisor, Dr. Keith Benedict for his helpful suggestions and insights. I have been very fortunate to have a supervisor who permitted me to work across such broad areas. His precise deductions provided much theoretical support for my simulations. Our weekly discussions were invaluable.

For help during my research in Bose-Einstein condensations, I would like to thank Dr. Carlos Lobo for his suggestions about Bogoliubov theory and Truncated Wigner Method, Dr. Robin Scott for discussions about vortex, soliton and numerical methods, and Prof. Mark Fromhold for suggestions about my work and for allowing me to share his software.

I thank Mark Greenaway who taught me unselfishly in the use of mathematical software and gave me much knowledge about English culture and custom. I would like to thank Tom Judd who shared his ideas with me and helped me in parallel calculations, Dr. Su Chen for collaborating with me on quantum transport in optical lattice, Tim Preece for helping me tidy up my paper and oral English, especially for introducing me to his friends. I would also like to thank Tao Yang for discussion in the theory of Quantum field.

Finally, I will thank my family, Mum, Dad and brother for their continuous support for my work and study. Here, I would like to extend special thanks to my wife, Fen Xiao, for sending uncountable lunches and dinners to my office, for her understanding and support for my work and for all that I cannot express completely in this acknowledgment.

Definition of Symbols and Fundamental Constants

Fundamental Constants

h : Plank's constant, $\hbar = h/(2\pi)$.

e : The charge of an electron.

m_e : The mass of an electron.

μ_B : The Bohr magneton.

k_B : Boltzmann's constant.

Symbols

m : The mass of an atom.

T : The temperature of the system.

T_c : The critical temperature for Bose-Einstein condensation.

N : The number of atoms in the system.

N_0 : The number of condensed atoms in the system.

μ : The chemical potential of the system.

V : The volume of the system.

d : The period of an optical lattice.

a : The s-wave scttering length.

E_R : The recoil energy of a particle.

θ : The phase of condensed atomic wave function.

λ_B : de Broglie wavelength.

χ_W : The Wigner characteristic function.

Publications and Presentations

Papers

- *"Vortex Formation and Interference Properties of Merging Bose-Einstein Condensates"*. B. Xiong and Keith Benedict (in preparation for Phys. Rev. A).
- *"Interference Properties of Two Atomic Bose Gases: from Mean Field Theory to Truncated Wigner Method"*, B. Xiong, R. G. Scott, Y. H. Lee and Keith. Benedict (in preparation for Phys. Rev. A).
- *"Quantum Transport of a 1D Degenerate Bose Gase in a Lattice: The Role of Different Quantum Fluctuations"*. B. Xiong, S. Chen, T. Yang and Keith Benedict (in preparation for Phys. Rev. A).

Presentations

- *"Vortex Formation and Interference Properties of Merging Bose-Einstein Condensates."* (Oral presentation) Seminar, University of Durham, Durham, UK, August 27th 2008.
- *Quantum Transport of a 1D Degenerate Bose Gase in a Lattice: The Role of Different Quantum Fluctuations*, talk presentation.
- *"Interference and Transport of Bose-Einstein Condensates."* (Oral presentation) The University of Hannover, Hannover, Germany, November 19th 2008.

Contents

CHAPTER 1

Introduction

Bose-Einstein Condensation (BEC) of dilute atomic gases is a macroscopic quantum phenomenon with consequences for superfluidity, superconductivity and the laser. The realization of Bose-Einstein condensation in dilute atomic gases [1, 2] achieved several long-standing goals. First, since neutral atoms were cooled into the lowest energy state, the ultimate control over the motion and position of atoms can be limited only by Heisenberg's uncertainty relation, explicitly $\Delta x \Delta p \geq \frac{h}{2}$. Second, all atoms occupy the same quantum state and this macroscopic system leads to the realization of atom lasers, devices which generate coherent matter waves. An important application of this kind of matter waves is to process quantum information and sculpt wavefunctions by optical pulses or external fields [3]. Third, some possible measurement techniques provide some ways of exploring properties of many-body states in the dilute Bose gases which are difficult in the quantum liquids ^{3}He and ^{4}He. These have stimulated the rapid development in some experimental techniques, such as cooling atoms to extremely low-temperature, microscopic manipulation of atoms and precision measurements of the quantum properties of these atoms. Consequently, it is immediately necessary to understand the principles of these techniques.

In this chapter, we will descibe some experimental developements and principles used in the formation, control and measurement of BECs.

1.1 Production and Trapping of Cold Atoms

In order to create a Bose condensate in a dilute gas, atoms must be cooled and compressed in a trap until the thermal de Broglie wavelength, $\lambda_T = \sqrt{\frac{2\pi\hbar^2}{mk_BT}}$ [1], is on the order of the spacing between atoms. This can be achieved by trapping atoms with magnetic fields or with laser light inside ultra-high vacuum chambers. To understand the behaviour of atoms in a magnetic field and a laser field and how they are trapped, the Zeeman effect and atomic interactions with laser fields are explored in the following section. Subsequently the primary features of magnetic and optical traps are shown, particularly optical lattices produced by optical standing waves.

1.1.1 Magnetic-Optical Traps

The procedure for creating a BEC normally involves three steps. Firstly, non-charged atoms are cooled down to temperatures near absolute zero using circularly polarised laser light (Pre-cooling). Secondly, these atoms are trapped at a certain place using magnetic fields and laser light (Trapping). Thirdly, the final cooling of the atoms is done by evaporation.

With the addition of a magnetic field gradient, the velocity reduction of Doppler cooling (Pre-cooling) can be used to help confine and trap neutral atoms. In a weak inhomogeneous magnetic field the internal energy levels of the atoms are split into their Zeeman components. By using circularly polarized light to Doppler cool the atoms in the presence of this magnetic field, these atoms can also feel a spatially-dependent force that pushes them towards the zero of the magnetic field (Trapping). Using a quadrupole magnetic field and retroreflected, circularly polarized laser beams in a 3-D geometry enables cooling and trapping in all three dimensions. This type of magneto-optical trap, or MOT, was first demonstrated for the trapping and cooling of alkali metal atoms, but the method can be easily extended to atomic states that have broader cooling linewidths by increasing the applied magnetic field gradient.

[1] This formula refers to the thermal de Broglie wavelength for a free ideal gas of massive particles in equilibrium. k_B is Boltzmann's constant, m is the mass of one particle, and T is the temperature of the gas

Zeeman effect

To understand the mechanism of trapping it is crucial to briefly summarize the spin properties which determine the interaction of atomic systems with an external magnetic field, B. The atomic Hamiltonian in the presence of an external magnetic field has the following form

$$H = A\mathbf{I}\cdot\mathbf{J} + 2\mu_B J_z B, \tag{1.1}$$

where A is a coupling constant, and $\mathbf{I}$ and $\mathbf{J}$ are the nuclear and electronic angular momenta, respectively. $\mu_B = |e|\hbar/2m_e$ is the Bohr magneton and z indicates the direction of the magnetic field. Indeed, there exists also the interaction between external magnetic field and nuclear magnetic moment. However, the contribution from the nuclear magnetic moment is very small compared to the two terms in the Eq.(1.1) so we can neglect it from this point onwards.

The first part of Eq.(1.1) is usually called by hyperfine interaction. This interaction is related closely to the quantum numbers I, J and F [2]

$$\mathbf{I}\cdot\mathbf{J} = \frac{1}{2}[F(F+1) - I(I+1) - J(J+1)], \tag{1.2}$$

where $\mathbf{F} = \mathbf{I} + \mathbf{J}$ and $J = 1/2$ for the alkali atoms. The energy splitting produced by the interaction of the nuclear and electronic angular momenta between the two hyperfine states $F = I \pm 1/2$ is then easily calculated and is given by the formula $\Delta E = A(I + 1/2)$. Typical values range between 1 and 10 GHz.

We can consider two limits for Eq.(1.2). In weak magnetic fields, the second term can be considered as a perturbing part and the following result derived for the interaction energy between the atom and the external field :

$$< F, m_F|2\mu_B J_z B|F, m_F >= g_L \mu_B m_F B, \tag{1.3}$$

where m_F is the eigenvalue of F_z and

$$g_L = \frac{F(F+1) + J(J+1) - I(I+1)}{2F(F+1)} \tag{1.4}$$

[2]Eq.(1.2) is equivalent to mathematical transformation, $\mathbf{F}^2 = \mathbf{I}^2 + 2\mathbf{I}\cdot\mathbf{J} + \mathbf{J}^2$. Since the unperturbed eigenstates of $\mathbf{J}^2$, $\mathbf{I}^2$, and $\mathbf{F}^2$ are known and their corresponding eigenvalues are $\mathbf{J}^2 \to J(J+1)$, $\mathbf{I}^2 \to I(I+1)$, and $\mathbf{F}^2 \to F(F+1)$, Eq.(1.2) can be deduced.

is the Lande Factor. In strong magnetic fields, the nuclear and electronic angular momenta, $\mathbf{I}, \mathbf{J}$ are magnetized so that the direction of $\mathbf{I}$ and $\mathbf{J}$ is antiparallel or parallel to the direction of the magnetic field $\mathbf{B}$. Thus the eigenvalues of J_z are the same as the eigenvalues of $\mathbf{J}$, $\pm\frac{1}{2}$. Thus for $I = \frac{3}{2}$, the maximum total angular momentum $F = 2$ so that there exist $2F + 1 = 5$ states for m_F, namely $m_F = -2, -1, 0, 1, 2$. From Eq.(1.1) and Eq.(1.2), the eigenvalues for these relevant states of the alkali atoms in the strong magnetic field are,

$$\begin{aligned} E_{m_F=\pm 2} &= \frac{3}{4}A \pm \mu_B B \\ E_{m_F=\pm 1,0} &= -\frac{3}{4}A \pm \mu_B B. \end{aligned} \tag{1.5}$$

For arbitrary magnetic fields the eigenstates and eigenvalues of Eq.(1.1) should be determined by diagonalization. The structure of the group in the spin momentum has the following character $[\hat{I}_x, \hat{I}_y] = i\hbar\hat{I}_z$ and $[\hat{J}_x, \hat{J}_y] = i\hbar\hat{J}_z$. Thus we perform angular transformation $[\hat{I}_+, \hat{I}_-] = 2\hbar\hat{I}_z$ and $[\hat{J}_+, \hat{J}_-] = 2\hbar\hat{J}_z$ where the raising operator $\hat{I}_+ = \hat{I}_x + i\hat{I}_y$ and the lowering operator $\hat{I}_- = \hat{I}_x - i\hat{I}_y$[3]. By expressing $\mathbf{I} \cdot \mathbf{J}$ in terms of the raising and lowering operators according to $\mathbf{I} \cdot \mathbf{J} = I_z J_z + (I_+ J_- + I_- J_+)/2$, one can easily construct the matrix elements of Eq.(1.1) on the basis $|m_I, m_J>$ with $-I \leq m_I \leq +I$ and $m_J = \pm 1/2$. Thus Eq.(1.1) is rewriten as

$$H = A[I_z J_z + (I_+ J_- + I_- J_+)/2] + 2\mu_B J_z B. \tag{1.6}$$

For a nuclear spin $I = 3/2$, the maximum total angular momentum $F = 2$ so that there exist $2F + 1 = 5$ states for m_F, namely $m_F = -2, -1, 0, 1, 2$. The eigenvalues

[3]From the view of Lie group and Lie Algebra, this kind of transformation is similar to the transformation of operators $\{\hat{r}, \hat{p}\} \Rightarrow \{\hat{a}, \hat{a}^\dagger\}$.

for these relevant states of the alkali atoms are, thererfore[4],

$$E_{m_F=\pm 2} = \frac{3}{4}A \pm \frac{1}{2}C \tag{1.7}$$

$$E_{m_F=+1} = -\frac{1}{4}A \pm \sqrt{\frac{3}{4}A^2 + \frac{1}{4}(A+C)^2} \tag{1.8}$$

$$E_{m_F=-1} = -\frac{1}{4}A \pm \sqrt{\frac{3}{4}A^2 + \frac{1}{4}(A-C)^2} \tag{1.9}$$

$$E_{m_F=0} = -\frac{1}{4}A \pm \sqrt{A^2 + \frac{1}{4}C^2}, \tag{1.10}$$

where $C = 2\mu_B B$. From above analysis, one can see that for the maximum or minimum value of m_F, the magnetic fields play the role of shifting the initial energy level without the magnetic fields. For other m_F, the energy levels are split by the external magnetic fields. Meanwhile the width (gap) of split energy levels is increased with raising magnetic fields but approaches the constant levels $\pm\mu_B B$ for high magnetic fields. When considering the magnetic trapping of atoms, the variation of the direction of the field experienced by an atom is assumed to take place slowly compared to the inverse of the Larmor frequency [4]; consequently, atoms will remain in the same quantum state. Thus, an atom in a state whose energy increases with increasing field will move towards a minimum in the field, referred to as low-field seeking, and the reverse behavior referred to as high-field seeking.

From the above eigenvalues, we can see that E_{m_F} is determined by magnetic field B^2 under the condition of a fixed A. The existence of a maximum E_{m_F} requires $\partial B^2/\partial x_k = 0$ and $\partial^2 B^2/\partial x_k^2 < 0$ for each k. However, this is impossible for magnetic traps because

$$\nabla^2 B^2 = 2\frac{\partial}{\partial x_k}(B_i \frac{\partial B_i}{\partial x_k}) = 2B_i \nabla^2 B_i + 2(\frac{\partial B_i}{\partial x_k})^2 > 0, \tag{1.11}$$

where $\nabla^2 B_i = 0$. This means that the alkali metal atoms cannot be maintained in a stable stationary equilibrium configuration solely after a magnetic field is applied (Earnshow's theorem). The interaction between the magnetic field and the atoms forces the atoms to move to the point of minimum E_{m_F}.

[4]The Hamiltonian Eq.(1.6) conserves the z-component of total angular momentum F. $m_F = \pm 2$ have one state respectively and the other m_F have two different states

Atomic Interaction with Laser fields

The atomic interaction with laser fields is of importance to understand the confinement and manipulation of BECs by laser. Meanwhile it enriches the performances already available with magnetic trapping. In the dipole approximation[5], the interaction can be written as

$$V(\mathbf{r},t) = -\mathbf{d}\cdot\mathbf{E}(\mathbf{r},t), \tag{1.12}$$

where $\mathbf{d}$ is the electric dipole operator for a single atom and

$$\mathbf{E}(\mathbf{r},t) = \mathbf{E}(\mathbf{r})e^{-i\omega t} + c.c. \tag{1.13}$$

is a time-dependent electric field oscillating with frequency ω. In this field, the electric dipole moment is $< \mathbf{d} >= \alpha(\omega)\mathbf{E}(r,t)$, where

$$\alpha(\omega) = \hbar^{-1}\sum_{n} | < n|\mathbf{d}\cdot\hat{\epsilon}|0 > |^2 \frac{2\omega_{n0}}{\omega_{n0}^2 - (\omega+i\eta)^2}. \tag{1.14}$$

is the dipole dynamic polarizability and $\hat{\epsilon}$ is the unit vector in the direction of the electric field. In addition, the polarization produces a change in the energy of the system and this change is called the *AC Stark shift* which can be calculated by using second-order perturbation theory [4]. This energy change can be regarded as an effective potential

$$U(\mathbf{r}) = -\frac{1}{2}\alpha(\omega)\overline{\mathbf{E}^2(\mathbf{r},t)} \tag{1.15}$$

felt by each atom, where the bar indicates a time average. Usually the time variation of the laser field is much faster than the typical frequencies of the atomic motion so the time averaging of the potential is justified. Comparing Eq.(1.6) and Eq.(1.15), it is easy to see that the magnetic interaction energy is linear in B due to the intrinsic magnetic moment of atom while the electric interaction energy is quadratic in E as a result of the dipole atomic polarizability.

[5]In general, the wave-length of the type of electromagnetic radiation which induces, or is emitted during, transitions between different atomic energy levels is much larger than the typical size of a light atom. Thus, $exp[i(\omega/c)\mathbf{n}\cdot\mathbf{r}] = 1 + i\frac{\omega}{c}\mathbf{n}\cdot\mathbf{r} + \cdots$, can be approximated by its first term, unity. This approximation is known as the electric dipole approximation.

In classical mechanics, a potential generates a force $\mathbf{F} = -\nabla U(\mathbf{r})$ if the potential varies with position. So the effective potential (1.15) gives the force

$$\mathbf{f} = \alpha(\omega)\nabla\frac{\overline{\mathbf{E}^2(\mathbf{r},t)}}{2}, \tag{1.16}$$

which affects the motion of the atoms. The behaviour of the force is determined by the spatial variation of the radiation intensity $\overline{\mathbf{E}^2(\mathbf{r},t)}$ and on the exact value of the laser frequency. If the dipole polarizability (1.14) is dominated by a single resonant frequency ω_R, we define detuning $\delta = \omega - \omega_R$ ($|\delta| << \omega_R$), given by the difference between the laser and the resonant frequencies. Thus the polarizability behaves like $\alpha(\omega) = -| < R|\mathbf{d}\cdot\hat{\epsilon}|0 > |^2/\hbar\delta$, where $|R >$ is the resonant state. Obviously if $\delta > 0$ (blue detuning) the energy change (1.15) is positive and the laser field will force the atoms to move towards regions of low field (repulsive effect). In contrast, if the detuning is negative (red detuning) atoms will be attracted to the regions of higher electric field. In experiments, red detuning was employed to provide an optical confinement of BECs, namely *optical traps*. The blue detuning was applied to manipulate atoms away from the centre of quadrupole trap.

Optical Lattices

Optical traps, as discussed above, have many advantages. They can be employed to investigate the coexistence of multi-spin components with the possible occurrence of new magnetic phases. Also the value of the interaction between atoms can be tuned by adding a magnetic field. Most importantly, optical traps can be modulated into different traps like box traps, low-dimensional traps, optical lattices, rotating traps, etc to manipulate cold atoms. Among these optical lattices are applied frequently.

When considering the radiation field of an applied standing wave along the z-direction,

$$\mathbf{E}(\mathbf{r},t) = Ecos(qz)e^{-i\omega t} + c.c., \tag{1.17}$$

the time-averaged effective field (1.15) takes the form

$$U(\mathbf{r}) = -\alpha(\omega)E^2cos^2(qz). \tag{1.18}$$

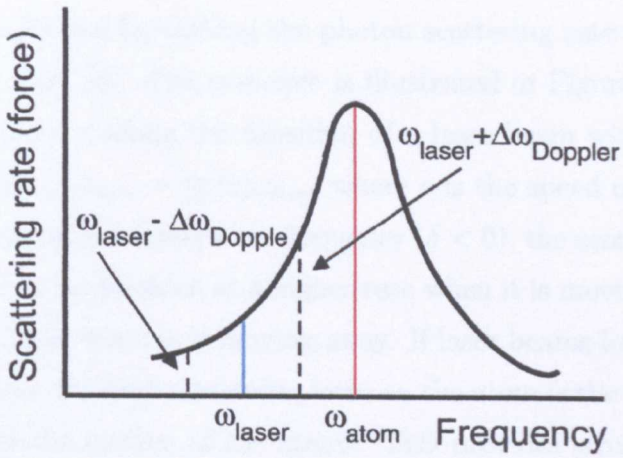

FIGURE 1.1: Atomic scattering rate versus laser frequency.

As a result, a periodic potential along the z-direction with wavelength π/q is formed and called an optical lattice. If the intensity of the laser is sufficiently high, this periodic potential with a magnetic trap can produce an array of condensates. Experiments can create a 3-dimensional optical lattice through three orthogonal lasers. Three optical standing waves are aligned orthogonal to each other, with their crossing point positioned at the centre of the atomic gas. Each standing wave laser field is created by focusing a laser beam to a waist of about one hundred μm at the position of the gas. A second lens and a mirror are then used to reflect the laser beam back onto itself, creating the standing wave interference pattern. Thus a 3-dimensional optical lattice can be formed [5].

1.1.2 Laser Cooling

The radiation-pressure force used in laser cooling and trapping is the recoil where momentum is transferred from photons scattering off an atom. Despite the infinitesimal momentum kick that the atom receives from each scattered photon, typically about 1cm/s, more than 10^7 photons per second are possibly scattered by exciting a strong atomic transition so that large accelerations are produced. Consequently the controlled radiation-pressure force can bring the atoms in a sample to a velocity near zero ("cooling") and hold them at particular point in space ("trapping").

The cooling is achieved by making the photon scattering rate velocity-dependent using the Doppler effect [6]. The principle is illustrated in Figure (1.1). If an atom is moving with velocity v along the direction of a laser beam with frequency ω_{laser}, the shifted frequency is $\omega_{laser} - (v/c)\omega_{laser}$ where c is the speed of light. If the laser frequency is below the atomic resonance frequency ($\delta < 0$), the atom, as a result of this Doppler shift, will scatter photons at a higher rate when it is moving toward the laser beam (v negative), than when it is moving away. If laser beams impinge on the atom from all six directions, the only remaining force on the atom is the velocity-dependent part, which opposes the motion of the atoms. This provides strong damping of any atomic motion and cools the atomic vapor.

1.1.3 Evaporative Cooling

Evaporative cooling is required because of the reality that to achieve BEC, the temperatures of atoms must be lower than those reached by laser or magnetic cooling. The essential ideas of evaporative cooling are to reach an extremely low temperature through reducing the mean kinetic energy of atoms in the system. Evaporative cooling is done by continuously removing the high-energy tail of the thermal distribution from trap. If there were a hole, produced by inducing a spin transition via the application of a radio frequency pulse, in the side of the trap, only atoms with kinetic energy no less than the potential energy of the trap at the point of the hole would escape [104]. These evaporated atoms carry away more than the average energy, which means the temperature of the remaining atoms decreases. The high energy tail must be constantly repopulated by collision, thus maintaining thermal equilibrium and sustaining the cooling process [7]. The only requirement for evaporative cooling to commence is a collisional re-thermalization time much shorter than the lifetime of an atom in the trap.

1.2 Experimental Probes

Much theoretical work tends to explain some experiments as well as guide experiments to realize some possible phenomena. It is fundamental and important to understand

experimental probes. The two most important techniques for observing Bose-Einstein condensates are in-situ and time-of-flight imaging. In both cases, one obtains an image which reflects the density distribution of the atoms either in a trapped state or in ballistic expansion.

1.2.1 Free Expansion and Direct Imaging

Free Expansion Imaging

Free expansion imaging in BEC is naturally the imaging of the momentum distribution of cold atoms. The process of imaging is shown below. After the formation of BEC, the trap spring constants were first adiabatically reduced and then suddenly reduced to nearly zero so that the atom cloud essentially expands ballistically [8]. A field gradient remains and supports the atoms against gravity to allow longer expansion times. After a few milliseconds expansion, the spatial distribution of the cloud was determined from the absorption of a few microseconds, polarized resonant laser pulse. The shadow of the cloud was imaged onto a charge-coupled device array, digitized, and stored for analysis.

This shadow image contains a large amount of easily interpreted information [8]. In general, a time-of-flight measurement of the velocity distribution is performed by experiments. At each point in the image, the optical density is *proportional* to the column density of atoms at the corresponding part of the expanded cloud. Thus, the recorded image is the initial velocity distribution projected onto the plane of the image. For all harmonic confining potentials, including the TOP trap, the spatial distribution is *identical* to the velocity distribution, if each axis is linearly scaled by the harmonic oscillator frequency for that dimension. Thus, from the single image one obtains both the velocity and coordinate-space distributions, and from these one also extracts the temperature and central density, in addition to characterizing any deviations from thermal equilibrium.

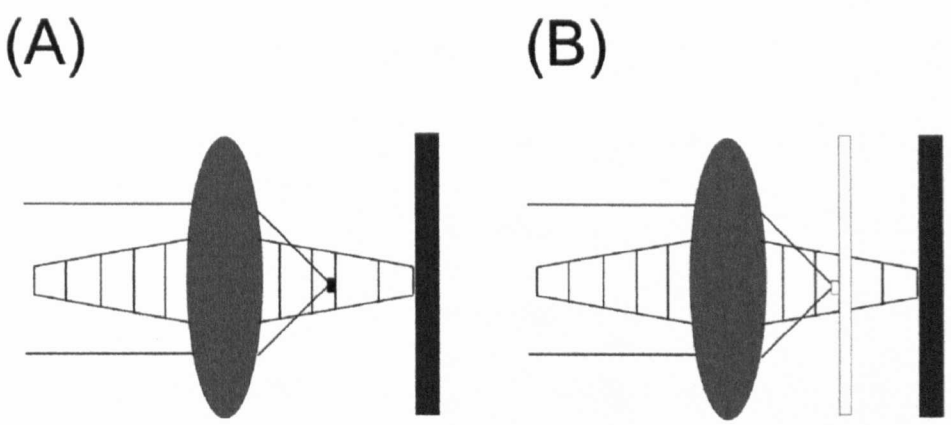

FIGURE 1.2: Dark-ground (A) and phase-contrast (B) imaging set-up. Probe light from the left is dispersively scattered by the atoms. In the Focal plane of the lens, the unscattered light is filtered. In dark-ground imaging (A), the unscattered light is blocked, forming a dark-ground image on the camera. In phase-contrast imaging (B), the unscattered light is shifted by a phase plate (consisting of an optical flat with a $\lambda/4$ bump or dimple at the center), causing it to interfere with the scattered light in the image plane.

Direct, Non-Destructive Imaging

After free expansion imaging was used in BEC, some groups commenced to explore the direct and non-destructive observation of the spatially localized condensate, in a gas of trapped atoms. The initial difficulty for this imaging was derived from the fact that because of the high optical density of the atom cloud near the critical temperature, direct observation by absorption imaging failed. For example, for typical experimental parameters the peak optical density (D_0) for resonant light is around 300, corresponding to a transmission coefficient of e^{-300} [9]. Thus the probe light is completely absorbed even in the wings of the spatial distribution, preventing direct imaging of the condensate. One applicable way to reduce the absorption is to detune the probe light. The light reveals major image distortions due to dispersive effects: the condensate acts as a lens and strongly deflects the light. However, by employing the "dark-ground" imaging technique the dispersively scattered light can be used to clearly image the condensate [7].

The central idea of dark-ground imaging is to obtain the imaging of scattered light and block the unscattered light by placing a small opaque object into the Fourier

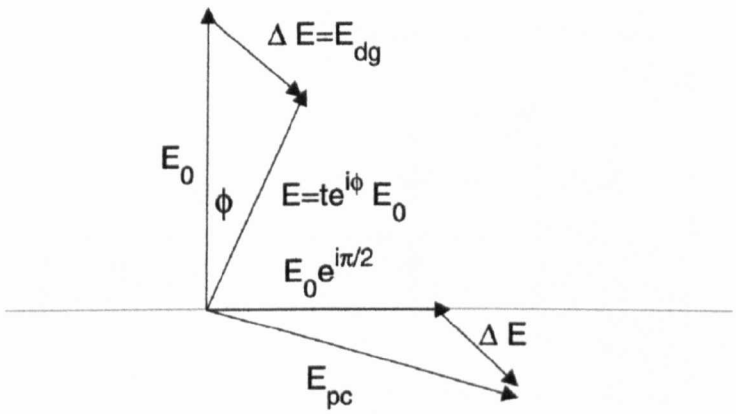

FIGURE 1.3: Phasor diagram of dark-ground and phase-contrast imaging. A ray of incident light with an electric field E_0 is scattered by the atoms, causing the light to be attenuated and shifted in phase, resulting in the electric field E. The dark-ground method images $\Delta E = E_{dg}$, the difference between incident and scattered electric fields. Phase-contrast methods cause ΔE and E_0 to interfere by rotating the phase of E_0 by 90°, resulting in the field E_{pc}

plane (Fig.1.2). In Fig.1.3, the probe light field after passing through the atoms can be separaated into the scattered (ΔE) and unscattered radiation (E_0),

$$E = tE_0e^{i\phi} = E_0 + \Delta E \tag{1.19}$$

Blocking the unscattered light gives the dark-ground signal:

$$< I_{dg} >= \frac{1}{2}|E - E_0|^2 = I_0[1 + t^2 - 2tcos\phi] \tag{1.20}$$

For small ϕ the dark-ground signal is quadratic in ϕ [7].

1.2.2 Phase-contrast Imaging

The purpose of phase-contrast imaging is to obtain the phase information by interfering the unscattered light (E_0) with the scattered radiation (ΔE). This is performed by shifting the phase of the unscattered light by $\pm\pi/2$ in the focal plane of the imaging lens (Fig.1.2). This is done with a "phase plate" which is an optical flat with a small bump or dimple in the center.

From Fig.1.3, the intensity of a point in the image plane is then

$$< I_{pc} >= \frac{1}{2}|E - E_0 + E_0e^{\pm i\frac{\pi}{2}}|^2 = I_0\left[t^2 + 2 - 2\sqrt{2}tcos\left(\phi \pm \frac{\pi}{4}\right)\right] \tag{1.21}$$

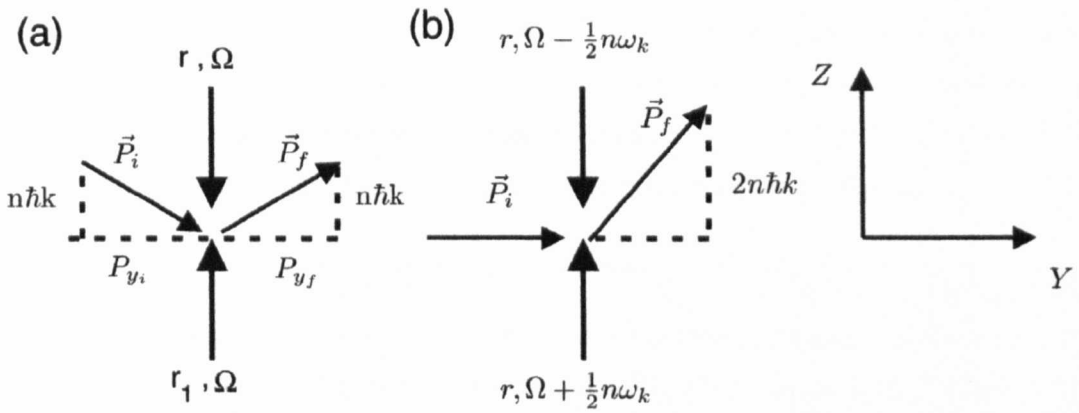

FIGURE 1.4: (a) Traditional geometry for Bragg scattering. The initial and final atomic momenta are $\mathbf{P}_i$ and $\mathbf{p}_f$, respectively. The fields' Rabi frequencies are denoted by r, r_1, and the fields' frequency by Ω. (b) In a reference frame moving with velocity $\mathbf{v} = -n(\hbar k/m)\hat{z}$, the atoms are incident orthogonal to the standing-wave field and the frequency of the traveling-wave components of the standing-wave field are Doppler shifted by $\pm n\omega_k/2 = \pm n\hbar k^2/m$.

For small ϕ one obtains

$$< I_{pc} > \approx I_0[t^2 + 2 - 2t \pm 2t\phi] \tag{1.22}$$

which is linear in ϕ. This makes phase-contrast imaging superior to dark-ground imaging for small signals [7].

1.2.3 2-photon Bragg Scattering

The standard Bragg scattering is performed by using two counterpropagating beams aligned perpendicularly to the weak axis of the trap (see Fig.1.4). A standing-wave field with spatial period $\pi/k = \lambda/2$ is directed along the z axis. The initial momentum components of scattered atomic beam are p_{i_y}, p_{i_z}, and final momentum components are p_{f_y}, p_{f_z}. For off-resonant scattering by the field, the atoms remain in their ground state. The momentum of the atoms can change by $p_{f_z} - p_{i_z} = 2n\hbar k$ ($n = \pm 1, \pm 2$, etc.), since the scattering process can result in an exchange of photons between the two traveling-wave components of the standing-wave field [11]. In general, the outgoing channel contains values of p_{f_z} corresponding to all values of n; however, in a sufficiently long time, $(p_{i_z} + 2n\hbar k)^2 = p_{i_z}^2$, or $p_{i_z} = -n\hbar k$ fulfills overall conservation

of energy. For a given value of n, resonant nth order Bragg scattering is achieved for an incident direction of the atomic beam given by $tan\theta = p_{i_z}/p_{i_y} = -nhk/p_{i_y}$; all other components of the scattering are suppressed.

Considering nth order Bragg scattering of atom beam with velocity

$$\mathbf{v} = (-nhk/m)\hat{\mathbf{z}},$$

where m is atomic mass, the field frequencies of the traveling-wave components of the field are Doppler shifted by $\pm(n\hbar k/m) = \pm n\omega_k/2$, where $\omega_k = \hbar(2k)^2/(2m)$ is the recoil frequency associated with a two-photon process. In this frame (see Fig.1.4), the atomic beam is incident in the y direction and the relative detuning of the two traveling-wave components of the field is $\delta = n\omega_k$. Thus resonant Bragg scattering can be viewed as arising from the interaction of an atomic beam with counter-propagating "pump" and "probe" fields that are detuned from one another [11].

This method of Bragg scattering can be used to probe density fluctuations of the system and thus to measure directly the dynamic structure factor $S(\mathbf{q}, v)$, which is the Fourier transform of the density-density correlation function and is central to the theoretical description of many-body systems [10].

1.3 Superfluidity

1.3.1 Overview of Physical Properties

Superfluidity is intimately connected with the phenomenon of Bose-Einstein condensation, a macroscopically occupied quantum state. In general, the property of superfluidity refers to the ability to flow through the narrowest capillaries without apparent friction [4]. The superfluidity of liquid ^{4}He, below the so-called λ-point, was discovered by Kapitza [12] and, independently, by Allen and Misener [13]. *The foundation for the description of superfluidity is a picture of the system as being comprised of a condensate and elementary excitations.* The earliest theory of superfluidity was developed by Landau, who showed that, if the spectrum of elementary excitations satisfies suitable criteria, the motion of the fluid below a critical flow velocity cannot give rise to dissipation. Landau's work marks the first explicit introduction

into condensed-matter physics of the seminal notion of a "quasiparticle", that is, an excitation of the system from the ground state, which is characterized by a definite energy and momentum, the total energy, momentum, etc., of the system can be regarded as the sum of that carried by the quasiparticles [48]. Next, Landau put forward two-fluid hydrodynamics to construct a quantitative theory of the flow properties of He-II: the "superfluid" component, which he identified, in an intuitive way, with the part of the liquid that remained in its ground state, and a "normal" component, which corresponded to the quasiparticles. Moreover, irrotationality of the superfluid plays a crucial role in this dissipationless motion. Irrotationality is directly related to Bose-Einstein condensation, being naturally associated with the phase of the order parameter which fixes the shape of the velocity potential.

1.3.2 Landau Criterion

Let us consider a liquid flowing along a capillary at a constant velocity $\mathbf{v}$. If one discusses the flow in a coordinate system moving with the liquid, the liquid helium is at rest, and the walls of the capillary move with velocity $-\mathbf{v}$. The entrainment of the liquid by the walls of the tube cannot initiate movement of the liquid as a whole. The motion must arise from a gradual excitation of internal motions, that is, from the appearance of elementrary excitations in the liquid. As elementary excitation appears in the liquid, the energy of the liquid E has the form

$$E = \epsilon + \mathbf{p} \cdot \mathbf{v} + \frac{1}{2} M v^2, \tag{1.23}$$

where M is the mass of the liquid and the expression $\epsilon + \mathbf{p} \cdot \mathbf{v}$ is the change in energy due to the appearance of the excitation. This change must be negative, since the energy of the moving liquid must decrease. In the conditon that $\mathbf{p}$ and $\mathbf{v}$ are antiparallel, one can get

$$v > \epsilon / p. \tag{1.24}$$

The minimum value of ϵ/p is clearly given by the point at which the line from the origin is a tangent to the curve. If this minimum is not zero, then, for velocities of flow below a certain value, excitations cannot appear in the liquid. This means that

the flow will not become slower, i.e. that the liquid exhibits the phenomenon of superfluidity [15]. One can see that any spectrum in which sufficiently small excitations are phonons will lead to superfluidity. One should notice that the arguments given above remain valid at any low temperature, since they made no direct use of the fact that the liquid was originally in the ground state.

Next, we consider the movement of quasi-particle gas as a whole with respect to the liquid, with a translational velocity $\mathbf{v}$. The distribution function for the gas moving as a whole is obtained from the distribution function $n(\epsilon)$ for the gas at rest by replacing the energy ϵ of a particle by $\epsilon - \mathbf{p} \cdot \mathbf{v}$. Thus the total momentum of the quasi-particle gas per unit volume is

$$\mathbf{P} = \int \mathbf{p} n(\epsilon - \mathbf{p} \cdot \mathbf{v}) d\tau. \tag{1.25}$$

Assuming that the velocity $\mathbf{v}$ is small, one expands the integrand in powers of $\mathbf{p} \cdot \mathbf{v}$. The zero-order term gives zero on integration over the directions of the vector $\mathbf{p}$, leaving

$$\mathbf{P} = -\int \mathbf{p}(\mathbf{p} \cdot \mathbf{v}) \frac{dn(\epsilon)}{d\epsilon} d\tau, \tag{1.26}$$

or, on averaging over the directions of $\mathbf{p}$,

$$\mathbf{P} = \frac{1}{3}\mathbf{v} \int \left(-\frac{dn}{d\epsilon}\right) p^2 d\tau. \tag{1.27}$$

From the fomula (1.27), one can see that the motion of the quasi-particle gas is accompanied by a transfer of mass: the effective mass per unit volume of the gas is determined by the proportionality coefficient between the momentum $\mathbf{P}$ and the velocity $\mathbf{v}$. On the othe hand, the fact that the quasi-particles collide with the walls of the tube and exchange momentum with them indicates that the excitation gas will be slowed down, like any ordinary gas flowing along a capillary.

Thus one fundamental result can be obtained. In a quantum Bose liquid there can exist simultaneously two motions, each of which has a corresponding "effective mass" such that the sum of these two masses is equal to the actual total mass of the liquid. One of these motions is "normal", i.e. has the same properties as that of an ordinary viscous liquid; the other is "superfluid". The two motions occur without

transfer of momentum from one to the other. In the hydrodynamic sense the density of a Bose liquid can be written as a sum $\rho = \rho_n + \rho_s$ of normal and superfluid parts, each corresponding to a hydrodynamic velocity $\mathbf{v}_n$ or $\mathbf{v}_s$. An important property of superfluid motion is that it is a potential flow:

$$\nabla \times \mathbf{v}_s = 0. \tag{1.28}$$

This property is the macroscopic expression of the fact that the elementary excitations with long wavelength (i.e. with small momentum) are sound quanta (phonons). When $T = 0$, the normal part of the density $\rho_n = 0$; the liquid can have only superfluid motion. For non-zero temperatures, ρ_n is given by (1.27):

$$\rho_n = \frac{1}{3}\int \left(-\frac{dn}{d\epsilon}\right) p^2 d\tau. \tag{1.29}$$

If we consider phonon excitation $\epsilon = up$ where u is the velocity of sound in the liquid,

$$\begin{aligned}(\rho_n)_{ph} &= -\frac{1}{3u}\int_0^\infty \frac{dn}{dp} p^2 \frac{4\pi p^2 dp}{(2\pi\hbar)^3} \\ &= \frac{4}{3\mu}\int_0^\infty np\frac{4\pi p^2 dp}{(2\pi\hbar)^3} \\ &= \frac{4}{3u^2}\int \epsilon n d\tau.\end{aligned} \tag{1.30}$$

The remaining integral here is just the energy of the phonon gas per unit volume; If one takes the form of the energy of the non-interacting liquid $E = V \cdot \pi^2 T^4/30(\hbar u)^3$, the density of normal fluid contributed by phonon excitation has the form,

$$(\rho_n)_{ph} = 2\pi^2 T^4/45\hbar^3 u^5. \tag{1.31}$$

In a similar way, one can deduce the roton contribution to ρ_n. Another important conclusion can be drawn. As the temperature increases, an increasing fraction of the mass of the liquid becomes normal. At the point where $\rho_n = \rho$, the properties of superfluidity disappear entirely. This is called the $\lambda - point$ of the liquid, and is a phase transition point of the second kind. One can notice that the quantitative formulae (1.31) is inapplicable near the $\lambda - point$, where the quasi-particle concentration becomes large, so that even the concept of quasi-particles is largely meaningless [15].

CHAPTER 2

Bose Gases

Since the experimental realization of Bose-Einstein condensation (BEC) in dilute atomic gases was achieved in 1995 [1, 2], the study of quantum gases in conditions of high degeneracy has become an emerging field of physics, attracting the interest of scientists from different areas. Experiments in cold atom systems allow access to regimes inaccessible in the Helium liquids, principally the weakly interacting limit. In addition, quite different properties became experimentally measureable. In particular, in these novel systems BEC shows up not only in momentum space but also in coordinate space, making the direct experimental investigation of the condensation feasible and providing new opportunities for interesting studies.

For temperature $T \to 0$, the fraction of non-condensed atoms is extremely small, for example, the number of particles in the condensate for a uniform ideal Bose gas varies as

$$N_0(T) = N\left[1 - \left(\frac{T}{T_c}\right)^{3/2}\right], \tag{2.1}$$

where N is total atom number and T_c is the critical temperature at which the dilute atomic gas undergoes the BEC phase transition. For $T \to 0$, the condensed atom number $N_0 \to 0$. Consequently, the thermal fluctuations will be neglected and mean field theory (Gross-Pitaeviskii equation (GPE)) can be applied to describe a large variety of physical phenomenon, including equilibrium configurations, collective oscillations, expansion, interference, quantized vortices, solitons, etc [4]. On the other hand, the number and distribution of noncondensed atoms can influence the properties of Bose

gas. In many cases, this number and distribution of noncondensed atoms are determined by the interatomic interaction and temperature in Bose gas. In general, the interatomic interaction can be modified to a large value by Feshbach resonances [16] or strong confinement [17], and the role played by finite temperature effects in the properties of Bose gases is also of importance. For example, due to thermal excitation, some quantities such as the spatial density of the condensate atoms [18] and the distribution of the number of particles in the condensate [19] are modified in thermal equilibrium. Some phenomena related to the role of finite temperature such as the damping and frequency shifts of collective modes [20,21], the evolution of the recently created vortices [22–24], must be explained by the noncondensed atoms and further by the interatomic interaction and temperature.

In this chapter, I will summarize existing theoretical approaches to Bose Gases upon which my work is based.

2.1 The Weakly-Interacting Bose Gases

As is well known, in the presence of Bose-Einstein condensation, an ideal Bose gas has infinite compressibility [1]. A weak interatomic interaction affects the properties of a Bose gas in a dramatic way, even for very dilute samples. On the other hand, the traditional perturbation techniques cannot be applied for uniform Bose gas because the ground state energy is zero in the absence of interactions. Therefore the Bogoliubov theory is an effective means to solve this kind of problem.

2.1.1 Uniform Interacting Bose gas

Uniform means translationally invariant. In the regime $T < T_c$, the typical atomic momentum always satisfies the inequality $pr_0/\hbar << 1$ where r_0 is the mean distance

[1] In the BEC phase, the pressure formula of the ideal Bose gas in a box is $P = \frac{k_B T}{\lambda_T^3} g_{5/2}(1)$. The Bose functions $g_P(z) = \frac{1}{\Gamma(p)} \int_0^\infty dx x^{p-1} \frac{1}{z^{-1}e^x - 1} = \sum_{l=1}^\infty \frac{z^l}{l^p}$, where $z = exp(\beta\mu)$ is the so-called fugacity and $\Gamma(p)$ is the factorial function $(p-1)!$. The thermal wavelength $\lambda_T = \sqrt{\frac{2\pi\hbar^2}{mk_B T}}$ [4]. Since the P does not depend on the volume, this implies that in the BEC phase the compressibility of the gas is infinite.

between atoms. At such momenta the scattering amplitude becomes independent of energy as well as of the scattering angle and can be safely replaced with its low-energy value which, according to standard scattering theory, is determined by a single parameter, the s-wave scattering length. First, we can consider a general Hamiltonian for a uniform Bose gas including two-body interaction,

$$\hat{H} = \frac{\hbar^2}{2m}\int \nabla\hat{\psi}^\dagger(r)\nabla\hat{\psi}(r)dr + \frac{1}{2}\int\int \hat{\psi}^\dagger(r)\hat{\psi}^\dagger(r')V(r-r')\hat{\psi}(r)\hat{\psi}(r')drdr'. \quad (2.2)$$

At low energy, the atomic interactions are essentially elastic, hard-sphere collisions between two atoms, and can be modeled in terms of the pseudo-potential, $V(r-r') = g\delta(r-r')$, where $g = 4\pi\hbar^2 Na/m$, with a the s-wave scattering length. Then, Eq.(2.2) can be rewritten as

$$\hat{H} = \frac{\hbar^2}{2m}\int \nabla\hat{\psi}^\dagger(r)\nabla\hat{\psi}(r)dr + \frac{g}{2}\int \hat{\psi}^\dagger(r)\hat{\psi}^\dagger(r)\hat{\psi}(r)\hat{\psi}(r)dr. \quad (2.3)$$

Eq.(2.3) can be rewritten in terms of the momentum basis by using

$$\hat{\psi}(r) = \frac{1}{\sqrt{V}}\sum_p \hat{a}_p e^{ip\cdot r/\hbar}, \quad (2.4)$$

where V is the volume of the system. So the Hamiltonian of the system in terms of the Bose field operators is simplified as

$$\hat{H} = \sum_p \frac{p^2}{2m}\hat{a}_p^\dagger\hat{a}_p + \frac{g}{2V}\sum_{p_1,p_2,q} \hat{a}_{p_1+q}^\dagger\hat{a}_{p_2-q}^\dagger\hat{a}_{p_1}\hat{a}_{p_2}. \quad (2.5)$$

The crucial point of the theory now is to replace the operator $\hat{a}_0$ with a C-number: $\hat{a}_0 \equiv \sqrt{N_0}$ in the Eq.(2.5). The advantages of this description is that it is simple and can explain some phenomenon in the Bose gas at extremely low temperature. But one can find that the substitution breaks Gauge symmetry and actually

$$\hat{a}_0 = \sqrt{\hat{N}}e^{i\hat{\theta}}.$$

Thus the problem with this approximation is that it breaks the conservation of particle number. In addition, the substitution, $V(r-r') \to g\delta(r-r')$, can not be made for a realistic potential since it would result in a poor approximation at short distances

of order r_0, where the potential is strong and quantum correlations are important. On the other hand, $\hat{a}_0|N_0>=\sqrt{N_0}|N_0-1>$ and $\hat{a}_0^\dagger|N_0>=\sqrt{N_0+1}|N_0+1>$. So Bogoliubov approximation becomes applicable when $N_0>>1$ and $N_0>>N-N_0$. For dilute Bose gas at the temperature $T\to 0$, the interatomic interaction is very weak and its perturbation is small at all distances so the replacement is accurate. In the case of $T\to 0$, all atoms drop almost into condensated atoms, $N_0\to N$. In the first approximation, the ground state energy takes the form

$$E_0=\frac{N^2g}{2V}. \tag{2.6}$$

where we notice some conclusions for homogeneous Bose gas: $E_0\propto\frac{1}{V}$; $E_0\propto N^2$. Contrary to the ideal case, the pressure of a weekly-interacting Bose gas does not vanish at zero temperature:

$$P=-\frac{\partial E_0}{\partial V}=\frac{N^2g}{2V^2}=\frac{gn^2}{2} \tag{2.7}$$

where n is the density. Accordingly, the *compressibility* is also finite:

$$\frac{\partial n}{\partial P}=\frac{1}{gn}, \tag{2.8}$$

which implies that it is more difficult to compress the gas for larger interatomic interaction gn. Using the hydrodynamic relation[2]

$$\frac{1}{mv^2}=\frac{\partial n}{\partial P}, \tag{2.9}$$

we can obtain $v=\sqrt{\frac{gn}{m}}$, where v is sound speed.

2.1.2 Bose gas in the isotropic harmonic traps

Now we consider a BEC confined within an isotropic trap, the Hamiltonian is

$$\hat{H}=\int(\frac{h^2}{2m}\nabla\hat{\Psi}^\dagger\nabla\hat{\Psi})d^3r+\int\frac{1}{2}m\omega^2r^2\hat{\Psi}^\dagger\hat{\Psi}d^3r+\frac{g}{2}\int\hat{\Psi}^\dagger\hat{\Psi}^{\dagger'}\hat{\Psi}\hat{\Psi}'d^3r \tag{2.10}$$

[2]In classical hydrodynamics, the mass density $\rho=\frac{mN}{V}$ and flux per unit time $V=v\times S$ where the velocity v is in the direction of a driving force F acting on the fluid, orthogonal to the transverse direction $\vec{S}$ of a rectangle shape of channel. Thus in an unit time, $F=\rho v\times Sv\Rightarrow mv^2=P/n$.

For a trapped gas, we expand the field operators $\hat{\Psi}$, $\hat{\Psi}^\dagger$ in the basis of simple harmonic oscillator,

$$\hat{\Psi}(r) = \sum_{n=(n_x,n_y,n_z)} \hat{a}_n \Phi_n(r) \quad \forall n_x, n_y, n_z \geq 0 \tag{2.11}$$

where $\Phi_n(r) = \phi_{n_x}(x)\phi_{n_y}(y)\phi_{n_z}(z)$ satisfies the Schrödinger equation

$$-\frac{\hbar^2}{2m}\nabla^2\Phi_n(r) + \frac{1}{2}m\omega^2 r^2 \Phi_n(r) = (n_x + n_y + n_z + \frac{3}{2})\hbar\omega\Phi_n(r).$$

Using Eq.(2.11), we expand the kinetic and potential parts as

$$\begin{aligned}
&\int (\frac{\hbar^2}{2m}\nabla\hat{\Psi}^\dagger\nabla\hat{\Psi})dr + \int \frac{1}{2}m\omega^2 r^2 \hat{\Psi}^\dagger\hat{\Psi}dr \\
&= \sum_{n,n'} \frac{\hbar^2}{2m}\hat{a}^\dagger_{n'}\hat{a}_n \int\int\int \nabla\Phi^*_{n'}\nabla\Phi_n dxdydz + \sum_{n,n'} \frac{1}{2}m\omega^2\hat{a}^\dagger_{n'}\hat{a}_n \int\int\int r^2\Phi^*_{n'}\Phi_n dxdydz \\
&= -\sum_{n,n'} \frac{\hbar^2}{2m}\hat{a}^\dagger_{n'}\hat{a}_n \int\int\int \Phi^*_{n'}\nabla\Phi_n dxdydz + \sum_{n,n'} \frac{1}{2}m\omega^2\hat{a}^\dagger_{n'}\hat{a}_n \int\int\int r^2\Phi^*_{n'}\Phi_n dxdydz \\
&= \sum_{n,n'} \hbar\omega(n_x + n_y + n_z + \frac{3}{2})\hat{a}^\dagger_{n'}\hat{a}_n \int\int\int \Phi^*_{n'}\Phi_n dxdydz \\
&= \sum_{n} l\omega(n_x + n_y + n_z + \frac{3}{2})\hat{a}^\dagger_n\hat{a}_n
\end{aligned} \tag{2.12}$$

For the interaction part,

$$\begin{aligned}
\frac{g}{2}\int \hat{\Psi}^\dagger\hat{\Psi}^\dagger\hat{\Psi}\hat{\Psi}dr &= \frac{g}{2}\sum_{n',m',n,m} \hat{a}^\dagger_{n'}\hat{a}^\dagger_{m'}\hat{a}_n\hat{a}_m \int\int\int \Phi^*_{n'}\Phi^*_{m'}\Phi_n\Phi_m dxdydz \\
&= \frac{g}{2}\sum_{n',m',n,m} \hat{a}^\dagger_{n'}\hat{a}^\dagger_{m'}\hat{a}_n\hat{a}_m A_{m',n',m,n}
\end{aligned} \tag{2.13}$$

where

$$A_{m',n',m,n} = \int\int\int \Phi^*_{n'}\Phi^*_{m'}\Phi_n\Phi_m dxdydz.$$

When $T \to 0$, the condensate fraction approaches 1, i.e., $N_0 \approx N$. From the Bogoliubov description, the ground state energy

$$\begin{aligned}
F_0 &\approx N\frac{3}{2}\hbar\omega + \frac{N^2 g A_{0,0,0,0}}{2} \\
&= N\frac{3}{2}\hbar\omega + \frac{N^2 g}{2V_{eff}},
\end{aligned} \tag{2.14}$$

where $V_{eff} = (2\pi)^{3/2} l^3$ is "effective volume" of the condensate. It is a little different from the homogeneous case; for every atom, its ground state energy is increased with zero-point energy. The *chemical potential*

$$\mu = \frac{\partial E_0}{\partial N} = \frac{3}{2}\hbar\omega + \frac{Ng}{V_{eff}}. \tag{2.15}$$

2.1.3 Penrose-Onsager Criterion for Bose-Einstein Condensation

Before demonstrating Penrose-Onsager Criterion for BEC, we first define the one-body density function by

$$\rho(r, r'; t) = < \hat{\Psi}^\dagger(r, t)\hat{\Psi}(r', t) >, \tag{2.16}$$

where the expection $< \cdots >$ is taken in the initial state. We suppose that $\phi_j(r', t)$ are a set of eigenvectors of $\rho(r, r'; t)$ with their eigenvalues $\xi_j(t)$ depending on the index j:

$$\int \rho(r, r'; t)\phi_j(r', t)dr' = \xi_j(t)\phi_j(r, t). \tag{2.17}$$

If the eigenvalue ξ_j is macroscopic, i.e., $O(N)$ where N is the total atom number, there exists BEC state. There is no BEC if all eigenvalues are very small, i.e., $O(1)$. This criterion is called Penrose-Onsager Criterion [26].

2.1.4 Off diagonal long-range order

We implement an example of a uniform and isotropic system of N particles occupying a volume V in the absence of external potentials to demonstrate the concept of off diagonal long-range order. In the thermodynamic limit, where $N, V \to \infty$ with the fixed density $n = N/V$, the one-body density depends only on the modulus of the relative variable $\mathbf{s} = \mathbf{r} - \mathbf{r}'$: $n^{(1)}(\mathbf{r}, \mathbf{r}') = < \hat{\Psi}^\dagger(\mathbf{r})\hat{\Psi}(\mathbf{r}') >= n^{(1)}(s)$, and one can write

$$n^{(1)}(s) = \frac{1}{V}\int d\mathbf{p} n(\mathbf{p}) e^{-i\mathbf{p}\cdot\mathbf{s}/\hbar}. \tag{2.18}$$

For a normal system the momentum distribution has a smooth behavior at small momenta and consequently the one-body density vanishes when $s \to \infty$. The situation is different if instead the momentum distribution exhibits the singular behavior

$$n(\mathbf{p}) = N_0\delta(\mathbf{p}) + \tilde{n}(\mathbf{p}) \tag{2.19}$$

characterized by a δ function term with a weight N_0 proportional to the total number of particles. This singular term arises from the macroscopic occupation of the single-particle state with momentum $\mathbf{p} = 0$. The macroscopic occupation of a single-particle state serves as a general definition of BEC and the quantity $N_0/N \leq 1$ is called the condensate fraction. From Eq.2.18, one finds that, in the presence of BEC, the one-body density matrix does not vanish at large distances but approaches a finite value:

$$n^{(1)}(s)_{s\to\infty} \to n_0, \tag{2.20}$$

fixed by the parameter $n_0 = N_0/V$. This behavior is often referred to as off-diagonal long-range order, since it involves the nondiagonal components ($\mathbf{r} \neq \mathbf{r}'$) of one-body density [4].

2.2 Approximation Schemes for Bose gas

2.2.1 Mean-field Approximation

We show the most simple way to derive the Gross-Pitaevskii equation (GPE) [27,28]. If readers hope to know about rigorous derivation of GPE, this paper [29] would be a nice work about it. The Hamiltonian of the weakly-interacting Bose gas has the following form,

$$\hat{H} = \int d^3\mathbf{r}\hat{\Psi}^\dagger(\mathbf{r})H_0\hat{\Psi}(\mathbf{r}) + \frac{g}{2}\int d^3\mathbf{r}\hat{\Psi}^\dagger(\mathbf{r})\hat{\Psi}^\dagger(\mathbf{r})\hat{\Psi}(\mathbf{r})\hat{\Psi}(\mathbf{r}), \tag{2.21}$$

where $H_0 = (\hbar^2/2m)\nabla^2 + V_{ext}$ is the single particle Hamiltonian and V_{ext} is the external potential acting on the system. Using the Bose commutation relations,

$$[\hat{\Psi}(\mathbf{r}'), \hat{\Psi}^\dagger(\mathbf{r})] = \delta(\mathbf{r}' - \mathbf{r}),\ [\hat{\Psi}(\mathbf{r}'), \hat{\Psi}(\mathbf{r})] = [\hat{\Psi}^\dagger(\mathbf{r}'), \hat{\Psi}^\dagger(\mathbf{r})] = 0, \tag{2.22}$$

then Heisenberg's time evolution equation becomes,

$$\begin{aligned} i\hbar\frac{\partial\hat{\Psi}(\mathbf{r}')}{\partial t} &= [\hat{\Psi}(\mathbf{r}'), \hat{H}] \\ &= [\hat{H}_0 + V_{ext} + g\hat{\Psi}^\dagger(\mathbf{r}')\hat{\Psi}(\mathbf{r}')]\hat{\Psi}(\mathbf{r}'). \end{aligned} \tag{2.23}$$

Since the condensate state involves the macroscopic occupation of a single state it is appropriate to decompose the Bose field operator in terms of a macroscopically-populated mean field term $\psi(\mathbf{r}') \equiv < \hat{\Psi}(\mathbf{r}') >$ and a fluctuation term $\hat{\Psi}'(\mathbf{r}')$,

$$\hat{\Psi}(\mathbf{r}') = \psi(\mathbf{r}') + \hat{\Psi}'(\mathbf{r}'). \tag{2.24}$$

Inserting Eq.2.24 into Eq.2.23 and taking only the leading order terms in ψ, Eq.2.23 leads to the time-dependent GPE,

$$i\hbar\frac{\partial\psi}{\partial t} = (-\frac{\hbar^2\nabla^2}{2m} + V_{ext} + g|\psi|^2)\psi. \tag{2.25}$$

Since the mean-field approximation neglects quantum fluctuation, i.e., neglects thermal and quantum depletion of the condensate, this is a valid approximation when (1) the temperature is much less than the transition temperature for the onset of condensation, and (2) when the condensate is sufficiently weakly-interacting so that s-wave scattering length a is much smaller than de Broglie wavelength of the particles λ_{dB}.

2.2.2 Normal Bogoliubov Approximation

We describe our system of N interacting bosons using the second quantized Hamiltonian in terms of the Bose field operator $\hat{\Psi}$. This operator is a function of space in the Schrödinger picture. The second quantized Hamiltonian is then given by,

$$\begin{aligned}\hat{H} = &\int d^3r\hat{\Psi}^\dagger(r)H_0\hat{\Psi}(r) \\ &+ \frac{1}{2}\int d^3r \int d^3r'\hat{\Psi}^\dagger(r)\hat{\Psi}^\dagger(r')V_{int}(r,r')\hat{\Psi}(r')\hat{\Psi}(r),\end{aligned} \tag{2.26}$$

Where $V_{int}(r,r')$ is the interaction potential acting between the bosons and $H_0 = -(h^2/2m)\nabla^2 + V_{ext}$ is the single particle hamiltonian, where m is the particle mass and V_{ext} is the external potential acting on the system. The bosonic creation and annihilation operators $\hat{\Psi}^\dagger(r)$, $\hat{\Psi}(r)$ fulfill the commutation relations

$$\begin{aligned}&[\hat{\psi}(r), \hat{\psi}^\dagger(r')] = \delta(r-r') \\ &[\hat{\psi}(r), \hat{\psi}(r')] = [\hat{\psi}^\dagger(r), \hat{\psi}^\dagger(r')] = 0.\end{aligned} \tag{2.27}$$

The gas is sufficiently dilute that the atomic interactions are dominated by low energy, two-body s-wave collisions. These are essentially elastic, hard-sphere collisions between two atoms, and can be modelled in terms of the pseudopotential

$$V_{int}(r, r') = g\delta(r' - r), \tag{2.28}$$

where $g = 4\pi\hbar^2 Na/m$, with a the s-wave scattering length. Through this potential, the Hamiltonian (2.26) is of the form

$$\hat{H} = \int d^3r \hat{\Psi}^\dagger(r) H_0 \hat{\Psi}(r) + \frac{g}{2} \int d^3r \hat{\Psi}^\dagger(r)\hat{\Psi}^\dagger(r)\hat{\Psi}(r)\hat{\Psi}(r). \tag{2.29}$$

We can expand the field operator $\hat{\Psi}(r, t = 0)$ in terms of the BEC ground-state amplitude $\hat{a}_0\psi_0$ with $< \hat{a}_0^\dagger \hat{a}_0 >= N_0$, and the excited states

$$\hat{\Psi}(r) = \psi_0(r)\hat{a}_0 + \delta\hat{\Psi}(r). \tag{2.30}$$

The c-number function $\psi_0(r)$ is the normalized one-body wave function for the condensate, and $\hat{a}_0$ is the corresponding destruction operator. In the Bogoliubov approximation, since the condensate contains most of the particles ($N - N_0 << N_0$) where N is total number of particles and N_0 the number in the condensate , the operator $\hat{a}_0$ is replaced by a c-number $N_0^{1/2}$ [30]. As a result, Eq.(2.30) can be written as

$$\hat{\Psi}(r) = \psi_0(r)N_0^{1/2} + \delta\hat{\Psi}(r), \tag{2.31}$$

It is convenient to work in the Grand Canonical ensenble so we introduce the chemical potential μ and a modified Hamiltonian

$$\hat{H}' \equiv \hat{H} - \mu\hat{N} = \hat{H} - \mu \int d^3r \hat{\Psi}^\dagger(r)\hat{\Psi}(r). \tag{2.32}$$

Substituting Eq.(2.31) into Eq.(2.29) and then putting them into Eq.(2.32), we obtain

$$\begin{aligned}\hat{H}' = \int d^3r \big[& N_0\psi_0^*(r)(H_0 - \mu + \frac{g}{2}|\psi_0(r)|^2)\psi_0(r) \\ & + N_0^{1/2}\psi_0^*(r)(H_0 - \mu + gN_0|\psi_0(r)|^2)\delta\hat{\Psi}(r) \\ & + N_0^{1/2}\delta\hat{\Psi}^\dagger(r)(H_0 - \mu + gN_0|\psi_0(r)|^2)\psi_0(r) \\ & + \delta\hat{\Psi}^\dagger(r)(H_0 - \mu + 2gN_0|\psi_0(r)|^2)\delta\hat{\Psi}(r)\big] \\ & + \frac{g}{2}\int d^3r \big[N_0\psi_0^{*2}(r)\delta\hat{\Psi}(r)\delta\hat{\Psi}(r) \\ & + 2N_0^{1/2}\psi_0^{*2}(r)\delta\hat{\Psi}^\dagger(r)\delta\hat{\Psi}(r)\delta\hat{\Psi}(r) \\ & + N_0\psi_0^2(r)\delta\hat{\Psi}^\dagger(r)\delta\hat{\Psi}^\dagger(r) \\ & + 2N_0^{1/2}\psi_0(r)\delta\hat{\Psi}^\dagger(r)\delta\hat{\Psi}^\dagger(r)\delta\hat{\Psi}(r) \\ & + \delta\hat{\Psi}^\dagger(r)\delta\hat{\Psi}^\dagger(r)\delta\hat{\Psi}(r)\delta\hat{\Psi}(r)\big]\end{aligned} \tag{2.33}$$

Since the scenario in which the number of noncondensate atoms, $N - N_0$, is far less than that of condensate, N_0, we consider terms up to second order in $\delta\hat{\Psi}$ and $\delta\hat{\Psi}^\dagger$ and ignore the interaction of noncondensate atoms. The linear terms vanish identically if ψ_0 obeys the following constraint

$$[H_0 - \mu + gN_0|\psi_0(r)|^2]\psi_0(r) = 0, \tag{2.34}$$

where Eq.(2.34) is the time-independent Gross-Pitaevskii equation. Consequently the Bogoliubov Hamiltonian can be written as

$$\begin{aligned}\hat{H}' = & \int d^3r N_0\psi_0^*(r)[H_0 - \mu + \frac{g}{2}N_0|\psi_0(r)|^2]\psi_0(r) \\ & + \int d^3r\delta\hat{\Psi}^\dagger(r)[H_0 - \mu + 2gN_0|\psi_0(r)|^2]\delta\hat{\Psi}(r) \\ & + \frac{1}{2}g\int d^3r\big[N_0\psi_0^{*2}(r)\delta\hat{\Psi}(r)\delta\hat{\Psi}(r) \\ & + N_0\delta\hat{\Psi}^\dagger(r)\delta\hat{\Psi}^\dagger(r)\psi_0^2(r)\big].\end{aligned} \tag{2.35}$$

Introducing the "quasiparticle" creation and annihilation operators $\hat{a}_j, \hat{a}_j^\dagger$ allows us to diagonalize the Hamiltonian (2.35) via

$$\delta\hat{\Psi}(r) = \sum_j [u_j(r)\hat{a}_j - v_j^*(r)\hat{a}_j^\dagger]. \tag{2.36}$$

Imposing bosonic commutation relations on $\hat{a}$ and $\hat{a}^\dagger$ leads to the constraints on $u_j(r)$ and $v_j(r)$

$$\begin{aligned}
&\sum_j [u_j(r)u_j^*(r') - v_j(r)v_j^*(r')] = \delta(r,r') \\
&\sum_j [u_j(r)v_j^*(r') - v_j^*(r)u_j(r')] = 0 \\
&\sum_j [u_j^*v_j(r') - v_j(r)u_j^*(r')] = 0.
\end{aligned} \tag{2.37}$$

Inserting Eq.(2.36) into Eq.(2.35), the Bogoliubov Hamiltonian becomes

$$\begin{aligned}
\hat{H}' = &\int d^3r N_0\psi_0^*[H_0 - \mu + \frac{g}{2}N_0|\psi_0|^2]\psi_0 \\
&+ \sum_{jk}\int d^3r\big[\hat{a}_j\hat{a}_k^\dagger(v_j\mathcal{L}v_k^* - \frac{1}{2}gN_0\psi_0^{*2}u_jv_k^* - \frac{1}{2}gN_0\psi_0^2u_k^*v_j) \\
&+ \hat{a}_j^\dagger\hat{a}_k\big(u_j^*\mathcal{L}u_k - \frac{1}{2}gN_0\psi_0^{*2}v_j^*u_k - \frac{1}{2}gN_0\psi_0^2v_ku_j^*\big) \\
&- \hat{a}_j\hat{a}_k\big(v_j\mathcal{L}u_k - \frac{1}{2}gN_0\psi_0^{*2}u_ju_k - \frac{1}{2}gN_0\psi_0^2v_jv_k\big) \\
&- \hat{a}_j^\dagger\hat{a}_k^\dagger\big(u_j^*\mathcal{L}v_k^* - \frac{1}{2}gN_0\psi_0^{*2}v_j^*v_k^* - \frac{1}{2}gN_0\psi_0^2u_j^*u_k^*\big)\big]
\end{aligned} \tag{2.38}$$

Here $\mathcal{L}$ is a Hermitian operator

$$\mathcal{L} = H_0 - \mu + 2gN_0|\psi_0(r)|^2, \tag{2.39}$$

which satisfies

$$\int d^3r u^*(r)\mathcal{L}v(r) = \int d^3r(\mathcal{L}^*u^*(r))v(r) \tag{2.40}$$

We require that u_j and v_j satisfy the Bogoliubov equations:

$$\mathcal{L}u_j(r) - gN_0\psi_0^2(r)v_j(r) = E_ju_j(r), \tag{2.41}$$

$$\mathcal{L}^*v_j(r) - gN_0\psi_0^{*2}(r)u_j(r) = -E_jv_j(r). \tag{2.42}$$

Using these results, the Hamiltonian (2.38) can be written as

$$\begin{aligned}\hat{H}' &= \int d^3r N_0\psi_0^*[H_0 - \mu + \frac{g}{2}N_0|\psi_0|^2]\psi_0 \\ &+ \frac{1}{2}\sum_{jk}\int d^3r\big[(E_j + E_k)(\hat{a}_j^\dagger\hat{a}_k u_j^* u_k - \hat{a}_j\hat{a}_k^\dagger v_j v_k^*) \\ &+ (E_j - E_k)(\hat{a}_j\hat{a}_k u_k v_j - \hat{a}_j^\dagger\hat{a}_k^\dagger u_j^* v_k^*)\big] \\ &= \int d^3r N_0\psi_0^*[H_0 - \mu + \frac{g}{2}N_0|\psi_0|^2]\psi_0 \\ &- \sum_j E_j\int d^3r|v_j|^2 + \sum_j E_j\hat{a}_j^\dagger\hat{a}_j.\end{aligned} \tag{2.43}$$

2.2.3 Elementary excitations of Bose gas in the isotropic harmonic traps

For elementary excitations of Bose gas in homogeneous system, readers can find it easily in some textbooks. Here we show elementary excitations of Bose gas in the isotropic traps. This work is the extended contents of section 2.1.2. The Bogoliubov scheme in homogeneous Bose gas can be extended to cover the harmonically trapped gases. Here we consider one-dimension situation. Eq.(2.13) is written as

$$\begin{aligned}\hat{V}_{int} &= \frac{g}{2}\sum_{m,n\neq 0}\Lambda_{m,n,0,0}(4\hat{a}_0^\dagger\hat{a}_m^\dagger\hat{a}_0\hat{a}_n + \hat{a}_m^\dagger\hat{a}_n^\dagger\hat{a}_0\hat{a}_0 + \hat{a}_0^\dagger\hat{a}_0^\dagger\hat{a}_m\hat{a}_n) \\ &+ \frac{g}{2}\sum_{n\neq 0}A_{n,0,0,0}(\hat{a}_n^\dagger\hat{a}_0^\dagger\hat{a}_0\hat{a}_0 + \hat{a}_0^\dagger\hat{a}_0^\dagger\hat{a}_0\hat{a}_n) + \frac{g}{2}A_{0,0,0,0}\hat{a}_0^\dagger\hat{a}_0^\dagger\hat{a}_0\hat{a}_0 + \cdots,\end{aligned} \tag{2.44}$$

where one must notice that due to the eigenfunctions $\phi_n^*(x) = \phi_n(x)$,

$$A_{m,n,0,0}^* = A_{m,n,0,0} = \left(\frac{m\omega}{2\pi^2 h}\right)^{1/2}(-1)^{(3m_j+n_j)/2}\frac{1}{\sqrt{m_j!n_j!}}\Gamma(\frac{m_j+n_j+1}{2}) \tag{2.45}$$

where m_j,n_j label excitation modes, m_j+n_j is even for all j and $\Lambda_{m,n,0,0} = 0$ otherwise. $\Gamma(n)$ is Gamma function. In Bogoliubov approximation, the normalization relation should be $\hat{a}_0^\dagger\hat{a}_0 + \sum_{n\neq 0}\hat{a}_n^\dagger\hat{a}_n = N$, and neglecting higher-order terms[3],

$$\hat{a}_0^\dagger\hat{a}_0^\dagger\hat{a}_0\hat{a}_0 = N^2 - 2N\sum_{n/0}\hat{a}_n^\dagger\hat{a}_n. \tag{2.46}$$

[3]The conditions for Eq.(2.46) are the condensate number $N_0 >> 1$ and the non-condensate number $N - N_0 << N_0$

Based on the new normalization relation, the sum of Eq.(2.2) and Eq.(2.44) yields the following expression for the Hamiltonian:

$$\begin{aligned}\hat{H} = &\frac{1}{2}\hbar\omega N + \frac{gN^2}{2}\left(\frac{m\omega}{2\pi\hbar}\right)^{1/2} + \sum_{n\neq 0}\hbar\omega(n+\frac{1}{2})\hat{a}_n^\dagger\hat{a}_n \\ &+ gN^{3/2}\sum_n A_{n,0,0,0}(\hat{a}_n^\dagger + \hat{a}_n) \\ &+ \frac{gN}{2}\sum_{m,n\neq 0} A_{m,n,0,0}(4\hat{a}_m^\dagger\hat{a}_n + \hat{a}_m^\dagger\hat{a}_n^\dagger + \hat{a}_m\hat{a}_n).\end{aligned} \tag{2.47}$$

The following ideas for dealing with Eq.(2.47) is based on Bogoliubov transformation, expressed in the language of matrix theory [31]. Let the indices m, n run over all the states denoted by vector indices m, n. To diagonalize Eq.(2.47) in order to obtain the energy spectrum, it is possible to write Eq.(2.47) in the following matrix form:

$$\begin{aligned}\hat{H} = &\hat{\mathbf{a}}^\dagger\boldsymbol{\epsilon}\hat{\mathbf{a}} + 2\lambda\sqrt{N}\left(\hat{\mathbf{a}}^\dagger\mathbf{A}_n + \hat{\mathbf{a}}^T\mathbf{A}_n\right) \\ &+ \lambda\left(4\hat{\mathbf{a}}^\dagger\mathbf{A}_{m,n}\hat{\mathbf{a}} + \hat{\mathbf{a}}^\dagger\mathbf{A}_{m,n}\hat{\mathbf{a}}^{\dagger T} + \hat{\mathbf{a}}^T\mathbf{A}_{m,n}\hat{\mathbf{a}}\right).\end{aligned} \tag{2.48}$$

In the above equation, $\hat{\mathbf{a}}$ and $\mathbf{A}_n$ are vectors of infinite dimension:

$$\hat{\mathbf{a}}^T = (\hat{a}_1, \hat{a}_2...), \hat{\mathbf{a}}^\dagger = (\hat{a}_1^\dagger, \hat{a}_2^\dagger, ...), \mathbf{A}_n = (A_{1,0,0,0}, A_{2,0,0,0}, ...),$$

the diagonal matrix $\boldsymbol{\epsilon} = \begin{pmatrix} \epsilon_1 & 0 & 0 & \dots \\ 0 & \epsilon_2 & 0 & \dots \\ \vdots & & \ddots & \end{pmatrix}$, and the matrix elements of $\mathbf{A}_{m,n}$ are the coefficients $A_{m,n,0,0}$. We have also written $\frac{gN}{2} = \lambda$.

In order to obtain the Hamiltonian in a diagonal form,

$$\hat{H} = \sum_n E_n\hat{\alpha}_n^\dagger\hat{\alpha}_n = \hat{\boldsymbol{\alpha}}^\dagger\boldsymbol{\mathcal{E}}\hat{\boldsymbol{\alpha}}, \tag{2.49}$$

which $\boldsymbol{\mathcal{E}}$ is the diagonal matrix with elements E_n, one can apply a generalization of the well-known Bogoliubov transformation demanding

$$\hat{\mathbf{a}} = \mathbf{X}\hat{\boldsymbol{\alpha}} + \mathbf{Y}\hat{\boldsymbol{\alpha}}^{\dagger T} + \mathbf{z}, \hat{\mathbf{a}}^\dagger = \hat{\boldsymbol{\alpha}}^\dagger\mathbf{X} + \hat{\boldsymbol{\alpha}}^T\mathbf{Y} + \mathbf{z}^T, \tag{2.50}$$

where $\mathbf{X}$ and $\mathbf{Y}$ are *Hermitian* square matrices of infinite dimension and $\mathbf{z}$ is a vector with *real* components. The Bosonic commutation relation of $\hat{\mathbf{a}}$ and $\hat{\mathbf{a}}^\dagger$, $\hat{\boldsymbol{\alpha}}$ and $\hat{\boldsymbol{\alpha}}^{\dagger T}$

require that matrices $\mathbf{X}$ and $\mathbf{Y}$ obey the following condition

$$\mathbf{X}^2 - \mathbf{Y}^2 = I, \tag{2.51}$$

where I is a unit matrix. Inserting Eq.(2.50) into Eq.(2.48) and simplifying the results, we can obtain separately the following parts if one hopes to eliminate the linear terms of $\hat{\alpha}, \hat{\alpha}^\dagger$ and $\hat{\boldsymbol{\alpha}}^\dagger\hat{\boldsymbol{\alpha}}^{\dagger T}$ and $\hat{\boldsymbol{\alpha}}^T\hat{\boldsymbol{\alpha}}$ terms,

$$\mathbf{z} = -2\lambda\sqrt{N}(\boldsymbol{\epsilon} + 6\lambda\mathbf{A}_{m,n})^{-1}\mathbf{A}_n, \tag{2.52}$$

and

$$\mathbf{X}\boldsymbol{\epsilon}\mathbf{Y} + 4\lambda\mathbf{X}\mathbf{A}_{m,n}\mathbf{Y} + \lambda\mathbf{X}\mathbf{A}_{m,n}\mathbf{X} + \lambda\mathbf{Y}\mathbf{A}_{m,n}\mathbf{Y} = 0 \tag{2.53}$$

$$\mathbf{Y}\boldsymbol{\epsilon}\mathbf{X} + 4\lambda\mathbf{Y}\mathbf{A}_{m,n}\mathbf{X} + \lambda\mathbf{Y}\mathbf{A}_{m,n}\mathbf{Y} + \lambda\mathbf{X}\mathbf{A}_{m,n}\mathbf{X} = 0. \tag{2.54}$$

Finally the energy matrix $\boldsymbol{\mathcal{E}}$ is

$$\boldsymbol{\mathcal{E}} = \mathbf{X}\boldsymbol{\epsilon}\mathbf{X} + \mathbf{Y}\boldsymbol{\epsilon}\mathbf{Y} + 4\lambda\mathbf{X}\mathbf{A}_{m,n}\mathbf{X} + 4\lambda\mathbf{Y}\mathbf{A}_{m,n}\mathbf{Y} + 2\lambda\mathbf{X}\mathbf{A}_{m,n}\mathbf{Y} + 2\lambda\mathbf{Y}\mathbf{A}_{m,n}\mathbf{X} \tag{2.55}$$

and its eigenvalues define the energy spectrum. If the interatomic interaction g is zero, the solutions for Eqs.(2.51, 2.53, 2.54) are $\mathbf{X} = I, \mathbf{Y} = 0$. In the condition that λ is very small, we apply matrix perturbation theory to expand the matrices $\mathbf{X}$ and $\mathbf{Y}$ into series over λ [31],

$$\mathbf{X} = I + 2\lambda^2\boldsymbol{\chi}^2 + \ldots, \quad \mathbf{Y} = \lambda\mathbf{v} + \lambda^2\mathbf{v}_1 + \ldots. \tag{2.56}$$

The matrices $\boldsymbol{\chi}, \mathbf{v}, \mathbf{v}_1$ can be found from Eqs.(2.51, 2.53, 2.54):

$$\mathbf{v} = 2\boldsymbol{\chi}, \quad \boldsymbol{\chi} = -\boldsymbol{\epsilon}^{-1}\mathbf{A}_{m,n}/2, \quad \mathbf{v}_1 = 4\boldsymbol{\epsilon}^{-1}\mathbf{A}_{m,n}\boldsymbol{\epsilon}^{-1}\mathbf{A}_{m,n}. \tag{2.57}$$

In the approximation up to λ^2 we obtain the matrix $\boldsymbol{\mathcal{E}}$:

$$\boldsymbol{\mathcal{E}} = \boldsymbol{\epsilon} + 4\lambda\mathbf{A}_{m,n} + \frac{\lambda^2}{2}\{(\boldsymbol{\epsilon}^{-1}\mathbf{A}_{m,n})^2\boldsymbol{\epsilon} - 3\mathbf{A}_{m,n}\boldsymbol{\epsilon}^{-1}\mathbf{A}_{m,n} - 2\boldsymbol{\epsilon}^{-1}\mathbf{A}_{m,n}^2\} \tag{2.58}$$

and the energy levels are given by $\mathcal{E}_n = \epsilon_n + 4\lambda A_{n,n,0,0} + \mathcal{O}(\lambda^2)$. For other situations, it is hard to solve analytically the Eqs.(2.51, 2.53, 2.54) and in general we must apply numerical methods to solve them. The details of numerical solutions and their applications will be demonstrated in Chapter 6.

2.2.4 Number-conserving Bogoliubov Approximation

In real experiments, only a few BECs can be regarded as a homogeneous gas: most are created in inhomogeneous potentials such as magnetic traps and optical lattice potentials. So it should be more realistic and meaningful to explore a series of theories for inhomogeneous Bose gases. Additionally, real condensates are generally influenced by the environments around them, resulting that few of them are completely "pure" condensates; that is to say, there exist quantum (thermal) fluctuations and condensates at the same time. In general, quantum (thermal) fluctuations play an important role in the properties of condensates. Especially in low-dimensional system. For example, the quantum damping of a Bose gas propagating in 1D optical lattices [17], the BKT transition and thermalization in 2D Bose gas [25]. Thus, these topics of interest require us to develop some theories to explore some properties of pure condensate, condensates with quantum/thermal fluctuation and more importantly, the dynamics of these Bose gases in realistic conditions.

In this section, I will derive the Bogoliubov theory conserving the total number of particles based on previous work [32]. This background knowledge is convenient for readers to understand the work of Chapters 5 and 6. Also, readers can identify the discrepancies between normal Bogoliubov theory and number-conserving Bogoliubov theory.

Hamiltonian constitution

A pure, homogeneous Bose gas appears rarely in real experiments. Bose-Einstein condensation in atomic gases was experimentally achieved in traps, where gases are naturally nonuniform. This nouniformity give rise to a new series of phenomena where the quantum nature of the system shows up in a peculiar way. The Hamiltonian of an inhomogeneous Bose gas is formed by adding an external potential term in the Hamiltonian of Eq.(2.3),

$$\hat{H} = \int \hat{\psi}^\dagger(r) H_0 \hat{\psi}(r) dr + \frac{g}{2} \int \hat{\psi}^\dagger(r)\hat{\psi}^\dagger(r)\hat{\psi}(r)\hat{\psi}(r) dr, \tag{2.59}$$

where $H_0 = -\frac{\hbar^2}{2m}\nabla^2 + U_{ext}(r)$ and U_{ext} is the potential function.

Constitution of condensate and non-condensate states

As is well known, a density matrix can be used to analyse some properties of a quantum system in thermal equilibrium or explore quantum decoherence of mixed states. To describe the properties of condensates and noncondensates, we first define the one-body density function by

$$\rho_1(r, r'; t) = < \hat{\psi}^\dagger(r, t)\hat{\psi}(r', t) > \tag{2.60}$$

where the expectation $< \cdots >$ is taken in the initial state. We assume in this section that the N-particle system is initially in thermal equilibrium at temperature T. I suppose that ϕ_0 be the eigenvector of ρ_1 with the largest eigenvalue N_0:

$$\int dr' \rho(r, r'; t)\phi_0(r', t) = N_0\phi_0(r, t) \tag{2.61}$$

The eigenvector fulfills the normalization condition, i.e., $< \phi_0|\phi_0 >= 1$. It is not difficult to understand that in the presence of a Bose-Einstein condensate, ϕ_0 is the condensate wave function and $N_0 \approx N$. As a description of the condensate and non-condensate in our system, the atomic field $\hat{\psi}$ is split into two parts:

$$\hat{\psi}(r) = \phi_0\hat{a}_0 + \delta\hat{\psi}(r), \tag{2.62}$$

where $\hat{a}_0$ annihilates a particle in the condensate ϕ_0. The remainder $\delta\hat{\psi}(r)$ is orthogonal to ϕ_0:

$$\int \phi_0^* \delta\hat{\psi} = 0 \tag{2.63}$$

For number conservation of particles, there is no single particle coherence between the condensate and the non condensed modes:

$$< \hat{a}_0^\dagger \delta\hat{\psi} >= 0. \tag{2.64}$$

Thus we define the operator $\hat{\Lambda}$ transferring one non condensed particle into the condensate:

$$\hat{\Lambda}(r) \equiv \hat{N}^{-1/2}\hat{a}_0^\dagger \delta\hat{\psi}(r). \tag{2.65}$$

Since the number of non-condensed particles $\delta N << N$ in the large N limit when the temperature is much lower than the critical temperature of BEC, and the trapping

potentials and mean interaction energy are fixed, one can make a systematic expansion of the exact condensate wavefunction ϕ_0 and of the fields $\hat{\Lambda}$ and $\hat{\Lambda}^\dagger$ in powers of the small parameter $\sqrt{\delta N/N} \sim 1/\sqrt{N}$. Formally,

$$\hat{\Lambda} = \hat{\Lambda}_{(0)} + \frac{1}{\sqrt{N}}\hat{\Lambda}_{(1)} + \frac{1}{N}\hat{\Lambda}_{(2)} + ... \tag{2.66}$$

$$\phi_0 = \phi_{(0)} + \frac{1}{\sqrt{N}}\phi_{(1)} + \frac{1}{N}\phi_{(2)} + ... \tag{2.67}$$

Order $\sqrt{\hat{N}}$: Gross-Pitaevskii equation

In order to simplify the understanding of the relation between condensate and non-condensate modes, we define the projector onto condensate wavefunction as

$$Q_c(r, r'; t) \equiv < r|\phi_0(t) >< \phi_0(t)|r' >$$

and thus the non-condensate space is orthogonal to condensate space [32], written as $Q_{non}(r, r'; t) \equiv \delta(r - r') - Q_c(r, r'; t)$. So

$$\begin{aligned}\delta\hat{\psi}(r, t) &= \hat{\psi}(r, t) - \phi_0(r, t)\int dr'\phi_0^*(r', t)\hat{\psi}(r', t) \\ &= \int dr'(\delta(r' - r) - \phi_0(r, t)\phi_0^*(r', t))\hat{\psi}(r', t) \\ &= \int dr' Q_{non}(r, r'; t)\hat{\psi}(r', t)\end{aligned} \tag{2.68}$$

From Eq.(2.65) and Eq.(2.68), we get

$$\begin{aligned}\frac{d}{dt}\hat{\Lambda} = &\frac{1}{\sqrt{\hat{N}}}\hat{a}_0^\dagger(\int dr'(\frac{d}{dt}Q_{non}(r, r'; t))\hat{\psi}(r', t)) \\ &+ \frac{1}{\sqrt{\hat{N}}}\hat{a}_0^\dagger\int dr' Q_{non}(r, r'; t)(\frac{d}{dt}\hat{\psi}(r', t)) \\ &+ \frac{1}{\sqrt{\hat{N}}}(\frac{d}{dt}\hat{a}_0^\dagger)\delta\hat{\psi}(r, t).\end{aligned} \tag{2.69}$$

Then we will simplify the three terms of Eq. (2.69). In the first term,

$$\begin{aligned}&\int dr'(\frac{d}{dt}Q_{non}(r, r'; t))\hat{\psi}(r', t) = -\int dr'(\frac{d}{dt}Q_c(r, r'; t))\hat{\psi}(r', t) \\ &= -\phi_0(r, t)\int dr'(\frac{d}{dt}\phi_0^*(r', t))(\phi_0(r', t)\hat{a}_0 + \delta\hat{\psi}(r', t)) - \frac{d}{dt}\phi_0(r, t)\hat{a}_0(t)\end{aligned} \tag{2.70}$$

If the lowest approximation is considered, $< \phi_0|\phi_0 >=< \phi_{(0)}|\phi_{(0)} >$ and

$$\frac{d}{dt}\int dr|\phi_{(0)}(r,t)|^2 = 0. \tag{2.71}$$

From Eq.(2.71), Eq.(2.70) can be rewritten

$$\begin{aligned}
\text{Eq.(2.70)} &= -(\frac{d}{dt}\phi_{(0)}(r,t))\hat{a}_0 \\
&+ \phi_{(0)}(r,t)\left[\int dr'(\frac{d}{dt}\phi_{(0)}(r',t))\phi^*_{(0)}(r',t)\hat{a}_0 - \int dr'(\frac{d}{dt}\phi^*_{(0)}(r',t))\delta\hat{\psi}(r',t)\right] \\
&= -\hat{a}_0\int dr'(\frac{d}{dl}\phi_{(0)}(r',t))(\delta(r'-r) - \phi_{(0)}(r,t)\phi^*_{(0)}(r',t)) \\
&- \phi_{(0)}(r,t)\int dr'(\frac{d}{dl}\phi^*_{(0)}(r',t))\delta\hat{\psi}(r',t)] \\
&= -\hat{a}_0\int dr' Q_{non}(r,r';t)(\frac{d}{dl}\phi_{(0)}(r',t)) \\
&- \phi_{(0)}(r,t)\int dr'(\frac{d}{dl}\phi^*_{(0)}(r',t))\delta\hat{\psi}(r',t)
\end{aligned} \tag{2.72}$$

In order to simplify the second term of Eq.(2.69), we first obtain a dynamic equation of $\hat{\psi}(r,t)$ through the Heisenberg equation of motion,

$$i\hbar\frac{d\hat{\psi}(r',t)}{dt} = [\hat{\psi}(r',t), \hat{H}], \tag{2.73}$$

and insert Eq.(2.59) into Eq.(2.73) so

$$\begin{aligned}
i\hbar\frac{d\hat{\psi}(r',t)}{dt} &= \int dr\hat{\psi}(r',t)\hat{\psi}^\dagger(r,t)[H_0 + \frac{1}{2}\hat{\psi}^\dagger(r,t)\hat{\psi}(r,t)]\hat{\psi}(r,t) \\
&- \int dr\hat{\psi}^\dagger(r,t)[H_0 + \frac{1}{2}\hat{\psi}^\dagger(r,t)\hat{\psi}(r,t)]\hat{\psi}(r,t)\hat{\psi}(r',t) \\
&= \int dr\delta(r-r')[H_0 + g\hat{\psi}^\dagger(r,t)\hat{\psi}(r,t)]\hat{\psi}(r,t) \\
&= H_0\hat{\psi}(r',t) + g\hat{\psi}^\dagger(r',t)\hat{\psi}(r',t)\hat{\psi}(r',t).
\end{aligned} \tag{2.74}$$

Then inserting Eq.(2.62) into Eq.(2.73) gives,

$$\begin{aligned} i\hbar\frac{d}{dt}\hat{\psi}(r',t) &= H_0\phi_0(r',t)\hat{a}_0 + g\hat{N}|\phi_0(r',t)|^2\phi_0(r',t)\hat{a}_0 \\ &+ H_0\delta\hat{\psi}(r',t) + 2g\hat{N}|\phi_0(r',t)|^2\delta\hat{\psi}(r',t) \\ &+ g\phi_0^2(r',t)\hat{a}_0\hat{a}_0\delta\hat{\psi}^\dagger(r',t) \\ &+ 2g\phi_0(r',t)\delta\hat{\psi}^\dagger(r',t)\delta\hat{\psi}(r',t)\hat{a}_0 + g\phi_0^*\delta\hat{\psi}(r',t)\delta\hat{\psi}(r',t)\hat{a}_0^\dagger \\ &+ g\delta\hat{\psi}^\dagger(r',t)\delta\hat{\psi}(r',t)\delta\hat{\psi}(r',t) \end{aligned} \tag{2.75}$$

In terms of the lowest approximation and ignoring all but terms of $\sqrt{\hat{N}}$, Eq.(2.75) is rewritten as

$$i\hbar\frac{d}{dt}\hat{\psi}(r',t) = H_0\phi_{(0)}(r',t)\hat{a}_0 + g\hat{N}|\phi_{(0)}(r',t)|^2\phi_{(0)}(r',t)\hat{a}_0 \tag{2.76}$$

Due to

$$\hat{a}_0 = \int dr\phi_0^*(r,t)\hat{\psi}(r,t), \tag{2.77}$$

$$\frac{d}{dt}\hat{a}_0 = \int dr[\frac{d}{dt}\phi_0^*(r,t)(\phi_0(r,t)\hat{a}_0 + \delta\hat{\psi}(r,t)) + \phi_0^*(r,t)\frac{d}{dt}\hat{\psi}(r,t)] \tag{2.78}$$

Combining Eq.(2.77) and the last term of Eq.(2.69), one can see that the last term of Eq.(2.69) is of the order $\hat{N}^0$ so it does not contribute to the present order $\sqrt{\hat{N}}$. From Eq.(2.69), Eq.(2.72), Eq.(2.76) and Eq.(2.77), one can get

$$\begin{aligned} \frac{d}{dt}\hat{\Lambda} &= -\frac{1}{\sqrt{\hat{N}}}\hat{a}_0^\dagger\hat{a}_0\int dr'Q_{non}(r,r';t)\frac{d}{dt}\phi_{(0)}(r',t) \\ &- \frac{1}{\sqrt{\hat{N}}}\hat{a}_0^\dagger\phi_{(0)}(r,t)\int dr'(\frac{d}{dt}\phi_{(0)}^*(r',t)\delta\hat{\psi}(r',t) \\ &+ \frac{1}{i\hbar\sqrt{\hat{N}}}\hat{a}_0^\dagger\int dr'Q_{non}(r,r';t)[H_0\phi_{(0)}(r',t) + g|\phi_{(0)}(r',t)|^2\phi_{(0)}(r',t)\hat{a}_0^\dagger\hat{a}_0]\hat{a}_0 \\ &+ \frac{1}{\sqrt{\hat{N}}}\int dr[\frac{d}{dt}\phi_0(r,t)(\phi_0^*(r,t)\hat{a}_0^\dagger + \delta\hat{\psi}^\dagger(r,t) + \phi_0(r,t)\frac{d}{dt}\hat{\psi}^\dagger(r,t))\delta\hat{\psi}(r,t) \end{aligned} \tag{2.79}$$

In the lowest approximation, we choose all terms of $\sqrt{\hat{N}}$, resulting in

$$i\hbar\frac{d}{dt}\hat{\Lambda} = \sqrt{\hat{N}}[\int dr'Q_{non}(r,r';t)[H_0 + g\hat{N}|\phi_{(0)}(r',t)|^2 - i\hbar\frac{d}{dt}]\phi_{(0)}(r',t) \tag{2.80}$$

From the requirement Eq.(2.64), $(d/dl) < \hat{\Lambda} >= 0$, and the expectation value of Eq.(2.80) determines the lowest-order approximation to $\phi_{(0)}$:

$$\sqrt{\hat{N}}[\int dr' Q_{non}(r,r';t)[H_0 + g\hat{N}|\phi_{(0)}(r',t)|^2 - i\hbar\frac{d}{dt}]\phi_{(0)}(r',t) = 0. \tag{2.81}$$

Since the orthogonality relation between Q_{non} and $\phi_{(0)}$, i.e.,

$$\int dr' Q_{non}(r,r';t)\xi(t)\phi_{(0)}(r',t) = 0, \tag{2.82}$$

where the $\xi(t)$ should be real constant because $|\phi_{(0)} >$ is the eigenstate of $H_0 + g\hat{N}|\phi_{(0)}(r',t)|^2$, we therefore have

$$[-i\hbar\frac{d}{dt} + H_0 + g\hat{N}|\phi_{(0)}(r',t)|^2]|\phi_{(0)} >= \xi(t)|\phi_{(0)} > \tag{2.83}$$

where the arbitrary real function $\xi(t)$ corresponds to an arbitrary global phase of the wave function $\phi_{(0)}$. The time-dependent Gross-Pitaevskii equation is recovered by choosing $\xi(t) = 0$.

Order $\hat{N}^0$: Time-dependent Bogoliubov-De Gennes equations

As one can see, the term of $\phi_{(1)}$ should contribute to the order of $\hat{N}^0$. In the next section, we will display the result of $\phi_{(1)} = 0$ and we will use directly this result to deduce the corresponding equation for $\hat{N}^0$. In the first term of Eq.(2.69), only the second term of Eq.(2.72) contributes to the order of $\hat{N}^0$. For the second term of Eq.(2.69), we can apply two means of deriving the same results contributing to the order $\hat{N}^0$ and here we will prove the equivalence of two means. In first case,

$$\begin{aligned}\frac{d}{dl}\delta\hat{\psi}(r,t) = &\int dr' Q_{non}(r,r';t)\frac{d}{dl}\hat{\psi}(r',t) - \int dr'(\frac{d}{dl}\phi_0^*(r',t))\phi_0(r,t)\hat{\psi}(r',t) \\ &- \int dr'\phi_0^*(r',t)(\frac{d}{dl}\phi_0(r,t))\hat{\psi}(r',t).\end{aligned} \tag{2.84}$$

Since $\frac{d}{dt}\hat{\psi}(r,t) = (\frac{d}{dt}\phi_0(r,t))\hat{a}_0 + \phi_0(r,t)\frac{d}{dt}\hat{a}_0 + \frac{d}{dt}\delta\hat{\psi}(r,t)$, the term of $\frac{d}{dt}\delta\hat{\psi}(r,t)$ can be simplified as

$$\begin{aligned}
\frac{d}{dt}\delta\hat{\psi}(r,t) &= \frac{d}{dt}\hat{\psi}(r,t) - (\frac{d}{dt}\phi_0(r,t))\int dr'\phi_0^*(r',t)\hat{\psi}(r',t) \\
&- \phi_0(r,t)\int dr'(\frac{d}{dt}\phi_0^*(r')\hat{\psi}(r',t) - \phi_0(r,t)\int dr'\phi_0^*(r',t)\frac{d}{dt}\hat{\psi}(r',t) \\
&= -(\frac{d}{dt}\phi_0(r,t))\int dr'\phi_0^*(r',t)\hat{\psi}(r',t) - \phi_0(r,t)\int dr'(\frac{d}{dt}\phi_0^*(r')\hat{\psi}(r',t) \\
&+ \int dr' Q_{non}(r,r';t)\frac{d}{dt}\hat{\psi}(r',t)
\end{aligned} \tag{2.85}$$

where we have use the condition of $\hat{a}_0 = \int dr'\phi_0^*(r',t)\hat{\psi}(r',t)$. Although we deduce the same term, $\frac{d}{dt}\delta\hat{\psi}(r,t)$ in two means shown separately in Eq.(2.84) and Eq.(2.85), it demonstrates the applicability of physical qualities, such as Q, Q_{non}, and $\hat{\psi}$. Since we only collect those terms with the order $\hat{N}^0$, Eq.(2.84) is simplified as

$$\begin{aligned}
\text{Eq.(2.84)} = &\int dr'\frac{1}{i\hbar}Q_{non}(r,r';t)\Big\{\Big[II_0 + 2g\hat{a}_0^\dagger\hat{a}_0|\phi_{(0)}(r',t)|^2\Big]\delta\hat{\psi}(r',t) \\
&+ g\phi_{(0)}^2(r',t)\hat{a}_0^2\delta\hat{\psi}^\dagger(r',t)\Big\} \\
&- \int dr'(\frac{d}{dt}\phi_{(0)}^*(r',t))\phi_{(0)}(r,t)\delta\hat{\psi}(r',t)
\end{aligned} \tag{2.86}$$

Through the previous results, $\frac{d}{dt}\psi_{(0)}^*(r',t) \to \psi_{(0)}^*(r',t)$ so the last term of Eq.(2.86) is equal to zero.

In the same order approximation,

$$\begin{aligned}
i\hbar\frac{1}{\sqrt{\hat{N}}}\frac{d}{dt}\hat{a}_0 &= \frac{i\hbar}{\sqrt{\hat{N}}}[\int dr\frac{d\phi_{(0)}^*(r,t)}{dt}\hat{\psi}(r,t) + \int dr\phi_{(0)}^*(r,t)\frac{d\hat{\psi}(r,t)}{dt}] \\
&= -\frac{i\hbar}{\sqrt{\hat{N}}}\int dr\frac{d\phi_{(0)}(r,t)}{dt}\phi_{(0)}^*(r,t)\hat{a}_0 \\
&+ \int dr\phi_{(0)}^*(r,t)[H_0 + g\hat{N}|\phi_{(0)}(r,t)|^2]\phi_{(0)}(r,t)\hat{a}_0 \\
&= \frac{1}{\sqrt{\hat{N}}}\int dr\phi_{(0)}^*(r,t)[H_0 + g\hat{N}|\phi_{(0)}(r,t)|^2 - i\hbar\frac{d}{dt}]\phi_{(0)}(r,t)\hat{a}_0 \\
&= \xi(t)\frac{1}{\sqrt{\hat{N}}}\hat{a}_0
\end{aligned} \tag{2.87}$$

Inserting Eq.(2.86) and Eq.(2.87) into Eq.(2.69) and we collect the previous results and identify ϕ_0 and $g\hat{a}_0^\dagger\hat{a}_0$ with $\phi_{(0)}$ and $g\hat{N}$, respectively, in a manner consistent with the order $\hat{N}^0$ of the calculation.

$$\begin{aligned} i\hbar\frac{d}{dt}\hat{\Lambda} = \frac{1}{\sqrt{\hat{N}}}\hat{a}_0^\dagger \int dr' Q_{non}(r,r';t)\Big\{ \left[H_0 + 2g\hat{a}_0^\dagger\hat{a}_0|\phi_{(0)}(r',t)|^2\right]\delta\hat{\psi}(r',t) \\ + g\phi_{(0)}(r',t)\hat{a}_0^2\delta\hat{\psi}^\dagger(r',t)\Big\} - \frac{1}{\sqrt{\hat{N}}}\xi(t)\hat{a}_0^\dagger\hat{\psi}(r',t) \end{aligned} \tag{2.88}$$

Here, we utilize $\delta\hat{\psi}(r',t) = \int dr Q_{non}(r',r;t)\delta\hat{\psi}(r,t)$ and Eq.(2.88) can be rewritten as

$$\begin{aligned} i\hbar\frac{d}{dt}\hat{\Lambda} = \frac{1}{\sqrt{\hat{N}}}\hat{a}_0^\dagger[H_0 + g\hat{N}|\phi_{(0)}(r',t)|^2 - \xi(t)]\delta\hat{\psi}(r,t) \\ + \frac{1}{\sqrt{\hat{N}}}\hat{a}_0^\dagger \int dr' Q_{non}(r,r';t) g\hat{N}|\phi_{(0)}(r',t)|^2 \int dr Q_{non}(r',r;t)\delta\hat{\psi}(r,t) \\ + \frac{1}{\sqrt{\hat{N}}}g\hat{N}\int dr' Q_{non}(r,r';t)\phi_{(0)}^2(r',t)\hat{a}_0 \int dr Q_{non}^*(r',r;t)\delta\hat{\psi}^\dagger(r,t) \end{aligned} \tag{2.89}$$

Thus, we can obtain the time evolution of the operators $\hat{\Lambda}, \hat{\Lambda}^\dagger$ through Eq.(2.89),

$$i\hbar\frac{d}{dt}\begin{pmatrix} \hat{\Lambda}(t) \\ \hat{\Lambda}^\dagger(t) \end{pmatrix} = \mathcal{L}(t) \circ \begin{pmatrix} \hat{\Lambda}(t) \\ \hat{\Lambda}^\dagger(t) \end{pmatrix} \tag{2.90}$$

with

$$\mathcal{L}(t) = \begin{pmatrix} A & B \\ -B^* & -A^* \end{pmatrix} \tag{2.91}$$

where $A = H_{GP}(t) + gNQ_{non}|\phi_{(0)}(r,t)|^2 Q_{non} - \xi(t)$ and $H_{GP} = H_0 + g\hat{N}|\phi_{(0)}(r',t)|^2$ and $B = gNQ_{non}\phi_{(0)}^2(r,t)Q_{non}^*(t)$. The $\circ$ describes the integral relation shown in Eq.(2.89). Although the means of writing in Eq.(2.90) is much simper than Eq.(2.89), we should keep clear in mind the integral relation shown in Eq.(2.90).

Order $\hat{N}^{-1/2}$: Corrections to the Gross-Pitaevskii equation

As one can see, the fact of $\phi_0 = \phi_{(0)}$ in the lowest approximation permits to derive the next order $\hat{N}^{-1/2}$ by inserting $\phi_0 = \phi_{(0)} + \frac{1}{\sqrt{\hat{N}}}\phi_{(1)}$ into Eq.(2.81) and ignoring

other terms,

$$\frac{1}{\sqrt{\hat{N}}}[\int dr' Q_{non}(r,r';t)[H_0\phi_{(1)}(r',t) + 2g\hat{N}|\phi_{(0)}(r',t)|^2\phi_{(1)}(r',t) \\ + g\hat{N}\phi^2_{(0)}(r',t)\phi^*_{(1)}(r',t) - i\hbar\frac{d}{dt}\phi_{(1)}(r',t) - \xi\phi_{(1)}(r',t)] = 0. \tag{2.92}$$

One needs to notice that the last term corresponds to the global phase of the condensate wavefunction ϕ_0 because of the orthogonality relation, $\int dr' Q_{non}(r,r';t)\phi_0(r',t) = 0$. Through minimal manipulation, one can obtain

$$\begin{pmatrix} Q_{non}(t) & 0 \\ 0 & Q^*_{non}(t) \end{pmatrix} \left(i\hbar\frac{d}{dt} - \mathcal{L}_{GP}(t)\right) \begin{pmatrix} \phi_{(1)}(t) \\ \phi^*_{(1)}(t) \end{pmatrix} = 0 \tag{2.93}$$

where

$$\mathcal{L}_{GP} = \begin{pmatrix} H_0 + 2gN|\phi_0|^2 - \xi & gN\phi_0^2 \\ -gN\phi_0^{*2} & -H_0 - 2gN|\phi_0|^2 + \xi \end{pmatrix}. \tag{2.94}$$

From the Eq.(2.93), one can see that $\phi_{(1)}(t) = 0$ if $\phi_{(1)}(t=0) = 0$ in that $\phi_{(1)}$ is linear and homogeneous. This assumption is easily satisfied in real systems. The system is initially in thermal equilibrium; in this case, from a time-reversal symmetry argument, the N-particle wave function is real, consequently $\phi_{(0)}, \phi_{(1)}$ can be real. However, the $\phi_{(1)}$ must be orthogonal to $\phi_{(0)}$ because of the normalization condition. The wave function $\phi_{(1)}$ should be zero through the above equation.

2.3 Classical Field Method

2.3.1 Introduction

A key focus of the explosion of interest in the dilute atomic gas Bose-Einstein condensates has been the study of the time evolution of condensates from some initial state. Among many works, the description of condensate using the time-dependent Gross-Pitaevskii equation (GPE) or coupled Gross-Pitaevskii equation (or their equivalent hydrodynamic versions) has succeeded in explaining some phenomena, such as shaking the trap to excite sound waves [33, 34], removing a potential barrier to allow two condensates to interfere [35, 36], applying electromagnetic fields to transfer condensate population into other, possibly untrapped states [37, 42], or stirring a condensate

to excite vortices [43, 44]. However, there is an increasing number of works which focus on coherence [45] and the diffusion of relative phase between two condensates held separately [46], probing for many-body states in two- or one-dimensional quasicondensates [25] and the pairwise scattering of condensate atoms into unoccupied modes [47]. Since the GPE can be derived as an equation for the condensate amplitude assuming that the condensate state is multimode coherent state,it is impossible to describe these phenomena. So we must seek an applicable theory to explore these interests.

In research on quantum optics, early work suggested that the coherence properties in atom lasers may be strongly influenced by the nonlinear interactions and the processing of quantum noise by nonlinearities leads to interesting statistical properties. In addition, it is well known that in quantum optics a classical electromagnetic field obeying Maxwell's equations arises as an assembly of photons all in the same quantum state. The motivation of the classical field method (Truncated Wigner method) is that in the same way a Bose-Einstein condensate, composed of Bosonic atoms all in the same quantum state, might behave very much like a classical field, whose equation of motion is the Gross-Pitaevskii equation.

In this section, we will focus on a very useful method, the truncated Wigner method (TWA), from quantum optics used in Bose-Einstein condensates. The truncated Wigner method is one of the classical field methods. The basic idea of this method is to expand a quantum field operator equation in the Wigner representation and derive a generalized Fokker-Planck equation. The diffusion matrix of the Fokker-Planck equation for the Wigner distribution vanishes identically and dynamical quantum noise acts via third-order derivatives. These result in a deterministic equation for the classical field, which coincides with the Gross-Pitaevskii equation. We will give the derivation of the truncated Wigner method. Prior to this, the essential idea of the classical field method is shown in the flow diagrams and some recent developments about this method will be shown in the middle part of this chapter.

2.3.2 Truncated Wigner method

Hamiltonian constitution

In weakly-interacting Bose gas systems, the range r_0 of the interatomic forces is much smaller than the average distance $d = n^{-1/3}$ between particles, fixed by the density $n = N/V$ of the gas. This allows one to consider only configurations involving pairs of interacting particles, while configurations with three or more particles interacting simultaneously can be safely neglected [4]. Thus the Hamiltonian of the system in terms of quantum fields $\hat{\psi}^\dagger(\mathbf{r}, t), \hat{\psi}(\mathbf{r}, t)$ can be written:

$$\begin{aligned}\hat{H}(t) = &\int d\mathbf{r}\hat{\psi}^\dagger(\mathbf{r}, t)\big[-\frac{\hbar^2\nabla^2}{2m} + U_{ext}(\mathbf{r}) + \delta U_{ext}(\mathbf{r}, t)\big]\hat{\psi}(\mathbf{r}, t) \\ &+ \frac{1}{2}\int d\mathbf{r}\int d\mathbf{r}'\hat{\psi}^\dagger(\mathbf{r}, t)\hat{\psi}^\dagger(\mathbf{r}', t)U_{2b}(\mathbf{r}-\mathbf{r}')\hat{\psi}(\mathbf{r}', t)\hat{\psi}(\mathbf{r}, t),\end{aligned} \tag{2.95}$$

where $U_{ext}(\mathbf{r})$ and $\delta U_{ext}(\mathbf{r}, t)$ are respectively a time-invariant external potential and a time-dependent potential, while $U_{2b}(\mathbf{r}-\mathbf{r}')$ is the two-body scattering potential. Under appropriate conditions, and with appropriate qualifications, the true interaction potention $U_{2b}(\mathbf{r}-\mathbf{r}')$ may be replaced by a delta function $\delta(\mathbf{r}-\mathbf{r}')$ of strength U_0, where $U_0 = 4\pi\hbar^2 a/m$, where a is the s-wave scattering length [48]. The second-quantized field operator $\hat{\psi}(\mathbf{r})$ annihilates a particle from position $\mathbf{r}$ and obeys the equal-time commutation relations for identical bosons,

$$\begin{aligned}[\hat{\psi}(\mathbf{r}), \hat{\psi}(\mathbf{r}')] = [\hat{\psi}^\dagger(\mathbf{r}), \hat{\psi}^\dagger(\mathbf{r}')] = 0 \\ [\hat{\psi}(\mathbf{r}), \hat{\psi}^\dagger(\mathbf{r}')] = \delta(\mathbf{r}-\mathbf{r}'),\end{aligned} \tag{2.96}$$

where $\delta(\mathbf{r})$ is the three-dimensional Dirac delta function.

Second quantization for bosonic field operator

By decomposing the field operator onto a single-particle basis

$$\hat{\psi}(\mathbf{r}, t) = \sum_j \psi_j(\mathbf{r})\hat{a}_j(t),$$

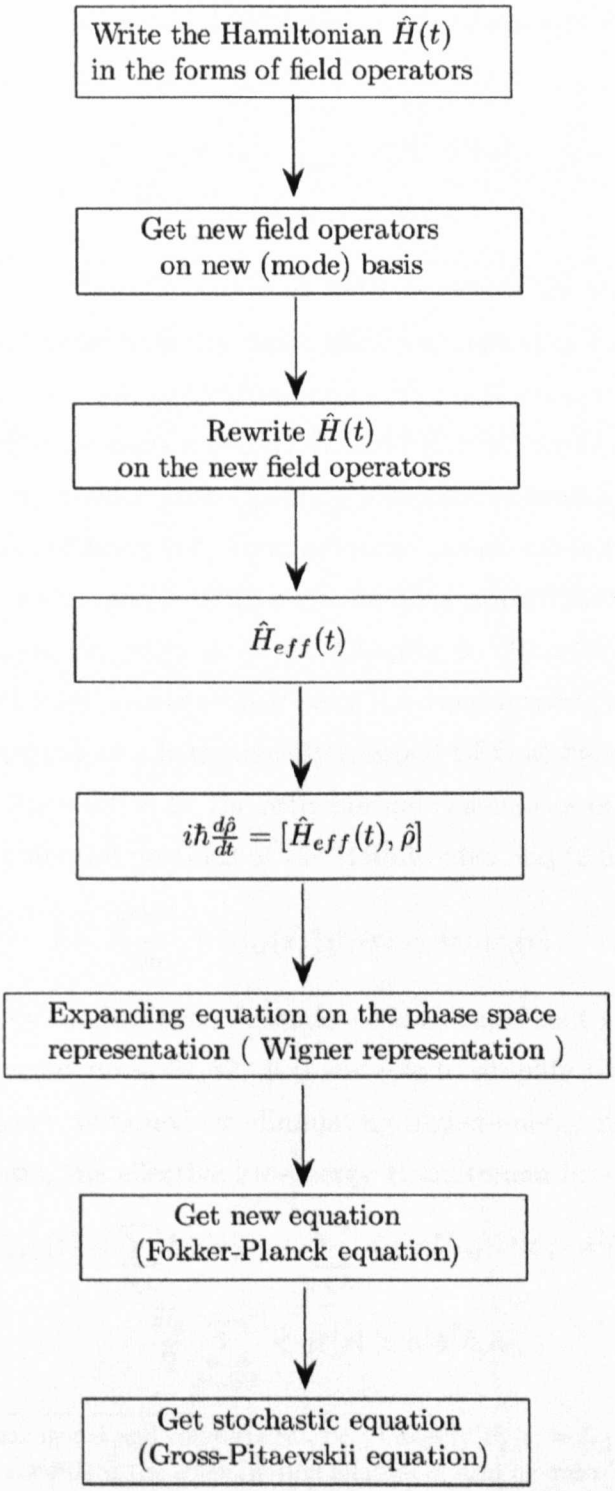

FIGURE 2.1: The flow diagrams about the procedure of the classical field method.

where the mode operators $\hat{a}_j(l)$ and $\hat{a}_j^\dagger(l)$ also obey bosonic commutation relations[4], we can obtain the full Hamiltonian on this basis, written as [5]

$$\begin{aligned}\hat{H}(l) = &\sum \hbar\omega_j \hat{a}_j^\dagger \hat{a}_j + \sum < j|\delta U_{ext}(l)|l > \hat{a}_j^\dagger \hat{a}_l \\ &+ \frac{U_0}{2} \sum < jr|st > \hat{a}_j^\dagger \hat{a}_r^\dagger \hat{a}_s \hat{a}_l.\end{aligned} \tag{2.97}$$

One can notice that the application of TWA is similar for the plane-wave basis (PW) and single-harmonic-oscillator basis (SHO) except that the quantum fluctuations in the inital state are introduced by adding half an average quanta into a limited number of different basis modes (PW and SHO) with a Gaussian distribution in amplitude (here, we assume that $U_{ext}(\mathbf{r})$ is harmonic potential). Physics must be independent of choice of basis but, once approximations are made, some bases are more natural than others and lead to more obvious approximation schemes. The above point of view is one motivation for Chapter 5. Recently, the effect of the plane wave basis and harmonic oscillator basis has been investigated with respect to the equilibrium properties of a harmonically trapped BEC at finite temperature [50]. Here we choose the basis set to be the orthonormal eigenstates of the noninteracting and time-invariant potential portions of the Hamiltonian, Eq.(2.95), i.e.,

$$\{ -\frac{\hbar^2\nabla^2}{2m} + U_{ext}(\mathbf{r})\}\psi_j(\mathbf{r}) = \hbar\omega_j\psi_j(\mathbf{r}). \tag{2.98}$$

Since in higher-energy modes, time dependence is so rapid as to be unobservable in experiments on ultracold gases [51,52], it is suitable to simplify Hamiltonian by using an effective field theory, obtained by eliminating higher-energy modes. Thus within the Heisenberg picture, the effective low-energy Hamiltonian becomes

$$\begin{aligned}\hat{H}_{eff}(t) = &\sum_{j\in L} \hbar\omega_j \hat{a}_j^\dagger \hat{a}_j + \sum_{jt\in L} < j|\delta U_{ext}(t)|t > \hat{a}_j^\dagger \hat{a}_t \\ &+ \frac{U_0}{2} \sum_{jrst\in L} < jr|st > \hat{a}_j^\dagger \hat{a}_r^\dagger \hat{a}_s \hat{a}_t,\end{aligned} \tag{2.99}$$

[4]Here, $\{\psi_j\}$ is an orthogonal and complete set, i.e., $\int dr\psi_i^*(r)\psi_j(r) = \delta_{i,j}$ and $\sum_i \psi_i^*(r)\psi_i(r') = \delta(r-r')$. Under these conditions,the commutation relation of field operator $\hat{\psi}(r), \hat{\psi}^\dagger(r)$ lead to the bosonic commutation relations of mode operator $\hat{a}, \hat{a}^\dagger$.

[5]Indeed, Eq.(2.97) is obtained in the condition that the single-particle functions $\psi_j(\mathbf{r})$ is the eigenfunctions of $-\frac{\hbar^2\nabla^2}{2m} + U_{ext}(\mathbf{r})$.

where L describes the low-energy modes. It should be noticed that in numerical calculations, the low-energy modes include both condensed modes and low-energy excitation modes. Since the BEC is initially weakly interacting and confined in a harmonic trap with no optical lattice, the main contribution to the matter wave coherence comes from the thermal and quantum fluctuations of low-energy phonons [55]. Here, the treatment of TWA gives a uniform average distribution of quantum noise in every low-energy mode. This might be inappropriate for dealing with the distribution of quantum fluctuation in a strongly confined harmonic trap. However, the Bogoliubov theory can correct the distribution of quantum fluctuation in low-energy excitation modes. Thus it provides further motivation for the work in Chapter 5. Let us define the density operator of the restricted basis field to be $\hat{\rho}(t)$, whose time evolution is straightforwardly obtained using the Von Neumann equation

$$i\hbar\frac{d\hat{\rho}(t)}{dt} = [\hat{H}_{eff}(t), \hat{\rho}(t)]. \tag{2.100}$$

The construction of dynamic equation in Wigner representation

In quantum mechanics, the role of harmonic oscillator arises from the fact that in practice very many forces are nearly harmonic as well as from the all pervading nature of electromagnetic fields, which, like all Bose fields, are exactly equivalent to assemblies of harmonic oscillators. The harmonic oscillator has an infinite number of equally spaced energy levels. In general, systems with a finite number of energy levels do not exist. However, in many situations it is possible to consider that interesting processes involve only a few energy levels of some system, and in these situations it is advantageous to consider an idealized Hamiltonian whose full range of energy levels comprises only those of interest. As discussed in the above section, Bose-Einstein condensates satisfy this situation: a large number of atoms occupy limited low-energy states, and the properties of high-energy states occupied by a few atoms are hard to explore and measure by experiments and thus can be neglected.

From the regime of quantum optics there have been developed a very rich profusion of techniques for dealing with these kinds of system. Much of the thrust of these techniques lies in their ability to exploit classical analogues-most particularly analogues

with classical noise theory. Using these techniques, namely phase space techniques, such as the P-representation of Glauber and Sudarshan and the Wigner representation, purely harmonic systems can be reduced to *non-operator* systems. However the essentially quantum mechanical nature of the problem is present in terms of the interpretation of the apparently classical variables. These phase space techniques are not actually applicable to their fullest advantage until quantum noise systems are dealt with but even in the case of non-noisy systems they bring a clarity to the problem of the transition from the quantum world to the classical world. The central idea which unifies all the harmonic oscillator techniques is the *coherent state*, first introduced by Glauber, which is the quantum state which most closely approaches the classical description of harmonic physics.

Since the earliest period when the phase space techniques, i.e., the positive-P function and the Wigner distribution have been applied to trapped Bose-Einstein condensates [53], the methods have played an important role in the regime of Bose gases, such as the prediction of quantum turbulence [47] and quantum correlations [54] in colliding condensates, and damping quantum transport of 1D Bose gas in the lattice [55]. To obtain the time evolution of $\hat{\rho}(t)$ we may represent $\hat{\rho}(t)$ in a suitable phase-space. Here we make use of the Wigner representation and the multimode Wigner function is defined:

$$W(\alpha_j, \alpha_j^*, t) = \frac{1}{\pi^{2M}} \int d^2\lambda_1 \cdots \int d^2\lambda_M \prod_{j=1}^{M} exp[-\lambda_j \alpha_j^* + \lambda_j^* \alpha_j] \chi_W(\lambda_j, \lambda_j^*, t), \tag{2.101}$$

where the multimode Wigner characteristic function is

$$\chi_W(\lambda_j, \lambda_j^*, t) = Tr\left\{\hat{\rho}(t) \prod_{j=1}^{M} exp[\lambda_j \hat{a}_j^\dagger - \lambda_j^* \hat{a}_j]\right\}. \tag{2.102}$$

Here $\hat{a}_j^\dagger(\hat{a}_j)$ creates (annihilates) atoms in the jth single particle mode. For converting between expectation values of the multimode density operator and averages over the corresponding multimode Wigner function, we use the multimode operator

correspondences [56]

$$\begin{aligned}
\hat{a}_j\hat{\rho}(t) &\leftrightarrow (\alpha_j + \frac{1}{2}\frac{\partial}{\partial\alpha_j^*})W(\alpha_j,\alpha_j^*,t)\\
\hat{a}_j^\dagger\hat{\rho}(t) &\leftrightarrow (\alpha_j^* - \frac{1}{2}\frac{\partial}{\partial\alpha_j})W(\alpha_j,\alpha_j^*,t)\\
\hat{\rho}(t)\hat{a}_j &\leftrightarrow (\alpha_j - \frac{1}{2}\frac{\partial}{\partial\alpha_j^*})W(\alpha_j,\alpha_j^*,t)\\
\hat{\rho}(t)\hat{a}_j^\dagger &\leftrightarrow (\alpha_j^* + \frac{1}{2}\frac{\partial}{\partial\alpha_j})W(\alpha_j,\alpha_j^*,t).
\end{aligned} \tag{2.103}$$

Here, we give a proof for one of them and others can be verified in a similar way. This process of deducing correspondences can help us understand the nature of TWA and know how to use them. For simplification, we consider the case of a single mode and the Wigner characteristic function is expanded on coherent state,

$$\chi_W(\lambda,\lambda^*,t) = \int \frac{d\alpha^* d\alpha}{2\pi i} e^{-\alpha^*\alpha} < \alpha|\hat{\rho}\hat{D}|\alpha > \tag{2.104}$$

where $\hat{D} = exp[\lambda\hat{a}^\dagger - \lambda^*\hat{a}]$. Thus

$$\frac{d\chi_W(\lambda,\lambda^*,t)}{d\lambda^*} = Tr\{\hat{\rho}(-\hat{a} + \frac{\lambda}{2})\hat{D}\} \tag{2.105}$$

Using partial integration, we can obtain

$$\begin{aligned}
\frac{1}{2\pi i}\int d\lambda d\lambda^* exp[-\lambda_j\alpha_j^* + \lambda_j^*\alpha_j]Tr\{\hat{\rho}\hat{a}\hat{D}\} &= \frac{1}{2\pi i}\int d\lambda d\lambda^* \frac{\lambda}{2} exp[-\lambda_j\alpha_j^*\\
&\quad + \lambda_j^*\alpha_j]Tr\{\hat{\rho}\hat{D}\} + \alpha W(\alpha,\alpha^*,t)\\
&= -\frac{\partial}{2\partial\alpha^*}W(\alpha,\alpha^*,t) + \alpha W(\alpha,\alpha^*,t).
\end{aligned} \tag{2.106}$$

so

$$\hat{\rho}a \leftrightarrow (\alpha - \frac{\partial}{2\partial\alpha^*})W(\alpha,\alpha^*,t),$$

and other results can be obtained in a similar way.

On the other hand, one can see easily the correspondences of time differentiation of density operator,

$$\frac{d\hat{\rho}(t)}{dt} \leftrightarrow \frac{\partial W(\alpha,\alpha^*,t)}{\partial t}. \tag{2.107}$$

Defining the multimode Wigner function $W(\alpha_j, \alpha_j^*, t)$ to be the quasiprobability analogue of the density operator $\hat{\rho}(t)$, the quantum-mechanical Eq.(2.100), inserted with Eq.(2.99) can immediately be written in Wigner representation as

$$\frac{\partial W}{\partial t} = \frac{\partial W^{diag}}{\partial t} + \frac{\partial W^{pert}}{\partial t} + \frac{\partial W^{nonlin}}{\partial t}, \tag{2.108}$$

where the diagonal, perturbing and nonlinear portions of the partial differential equation correspond respectively to the first, second and third terms of dynamic equation Eq.(2.99). The diagonal portion of the evolution, corresponding to the free rotation of the modes, is obtained as

$$i\hbar \frac{\partial W^{diag}}{\partial t} = -\sum_{j \in L} \hbar\omega_j \Big(\frac{\partial}{\partial \alpha_j}\alpha_j - \frac{\partial}{\partial \alpha_j^*}\alpha_j^* \Big) W. \tag{2.109}$$

Similarly, the Wigner function evolution due to the perturbing potential can be shown to become

$$i\hbar \frac{\partial W^{pert}}{\partial t} = -\sum_{jt \in L} < j|\delta U_{ext}|t > \Big(\frac{\partial}{\partial \alpha_j}\alpha_t - \frac{\partial}{\partial \alpha_t^*}\alpha_j^* \Big) W. \tag{2.110}$$

The more complicated term is expanded and simplified as

$$\begin{aligned} i\hbar \frac{\partial W^{nonlin}}{\partial t} = & -\frac{U_0}{2} \sum_{jrst \in L} < jr|st > \Big[\frac{\partial}{\partial \alpha_j}\alpha_r^*\alpha_s\alpha_t \\ & + \frac{\partial}{\partial \alpha_r}\alpha_j^*\alpha_s\alpha_t - \frac{\partial}{\partial \alpha_s^*}\alpha_j^*\alpha_r^*\alpha_t - \frac{\partial}{\partial \alpha_l^*}\alpha_j^*\alpha_r^*\alpha_s \\ & - \frac{1}{2}\frac{\partial}{\partial \alpha_j}\alpha_s\delta_{r,l} - \frac{1}{2}\frac{\partial}{\partial \alpha_j}\alpha_l\delta_{r,s} - \frac{1}{2}\frac{\partial}{\partial \alpha_r}\alpha_s\delta_{j,l} \\ & - \frac{1}{2}\frac{\partial}{\partial \alpha_r}\alpha_l\delta_{j,s} + \frac{1}{2}\frac{\partial}{\partial \alpha_s^*}\alpha_j^*\delta_{r,l} + \frac{1}{2}\frac{\partial}{\partial \alpha_s^*}\alpha_r^*\delta_{j,l} \\ & + \frac{1}{2}\frac{\partial}{\partial \alpha_t^*}\alpha_j^*\delta_{r,s} + \frac{1}{2}\frac{\partial}{\partial \alpha_t^*}\alpha_r^*\delta_{j,s} \\ & - \frac{1}{4}\frac{\partial^3}{\partial \alpha_j \partial \alpha_r \partial \alpha_s^*}\alpha_t - \frac{1}{4}\frac{\partial^3}{\partial \alpha_j \partial \alpha_r \partial \alpha_t^*}\alpha_s \\ & + \frac{1}{4}\frac{\partial^3}{\partial \alpha_j \partial \alpha_s^* \partial \alpha_t^*}\alpha_r^* + \frac{1}{4}\frac{\partial^3}{\partial \alpha_r \partial \alpha_s^* \partial \alpha_t^*}\alpha_j^* \Big], \end{aligned} \tag{2.111}$$

where some commutation relations have been applied to deduce the above result, as

shown below

$$[\alpha_i, \frac{\partial}{\partial \alpha_j}] = -\delta_{i,j} \qquad [\alpha_i, \frac{\partial}{\partial \alpha_j^*}] = 0$$
$$[\alpha_i, \alpha_j] = 0 \qquad [\alpha_i, \alpha_j^*] = 0. \tag{2.112}$$

Due to the presence of the summations, the specific indices involved in each term are mutable. We can therefore write the nonlinear Wigner function evolution component as

$$i\hbar \frac{\partial W^{nonlin}}{\partial t} = -U_0 \sum_{jrst \in L} < jr|st > \Big[\Big(\frac{\partial}{\partial \alpha_j}\alpha_t - \frac{\partial}{\partial \alpha_t^*}\alpha_j^*\Big)(\alpha_r^*\alpha_s - \delta_{r,s})$$
$$- \frac{1}{4}\Big(\frac{\partial^3}{\partial \alpha_j \partial \alpha_r \partial \alpha_s^*}\alpha_t - \frac{\partial^3}{\partial \alpha_r \partial \alpha_s^* \partial \alpha_t^*}\alpha_j^*\Big)\Big]W. \tag{2.113}$$

In order to proceed analytically, we shall restrict ourselves to a multi-mode Wigner function which at some time τ is factorisable into single-mode functions, thus

$$W(\alpha_j, \alpha_j^*, \tau) = \prod_{j \in L} \frac{\Gamma_j}{\pi} exp\big[-\Gamma_j|\alpha_j - \alpha_{j0}|^2\big]. \tag{2.114}$$

Substituting the given Wigner function Eq.(2.114) into the nonlinear portion of the equation of motion Eq.(2.113) gives the evolution at time τ as

$$i\hbar \frac{\partial W^{nonlin}}{\partial t} = U_0 \sum_{jrst \in L} < jr|st > \big[\Gamma_j(\alpha_j^* - \alpha_{j0}^*)\alpha_t$$
$$- \Gamma_t \alpha_j^*(\alpha_t - \alpha_{t0})\big] \times \Big\{\big[\alpha_r^*\alpha_s - \delta_{r,s}\big]$$
$$- \frac{\Gamma_r}{2}\Big[\frac{\Gamma_s}{2}(\alpha_r^* - \alpha_{r0}^*)(\alpha_s - \alpha_{s0}) - \delta_{r,s}\Big]\Big\}W \tag{2.115}$$

Given that the process giving rise to the cubic noise is local in coordinate space, we now introduce

$$\Psi_{\mathcal{P}}(\mathbf{r}) = \sum_{j \in L} \psi_j(\mathbf{r})\alpha_j, \tag{2.116}$$

which represents a possible state of the total restricted basis field in coordinate space. For the purposes of the present analysis we also find it useful to define the wavefunction

$$\xi_{\mathcal{P}}(\mathbf{r}) = \sum_{j \in L} \psi_j(\mathbf{r})\frac{\Gamma_j}{2}\alpha_j, \tag{2.117}$$

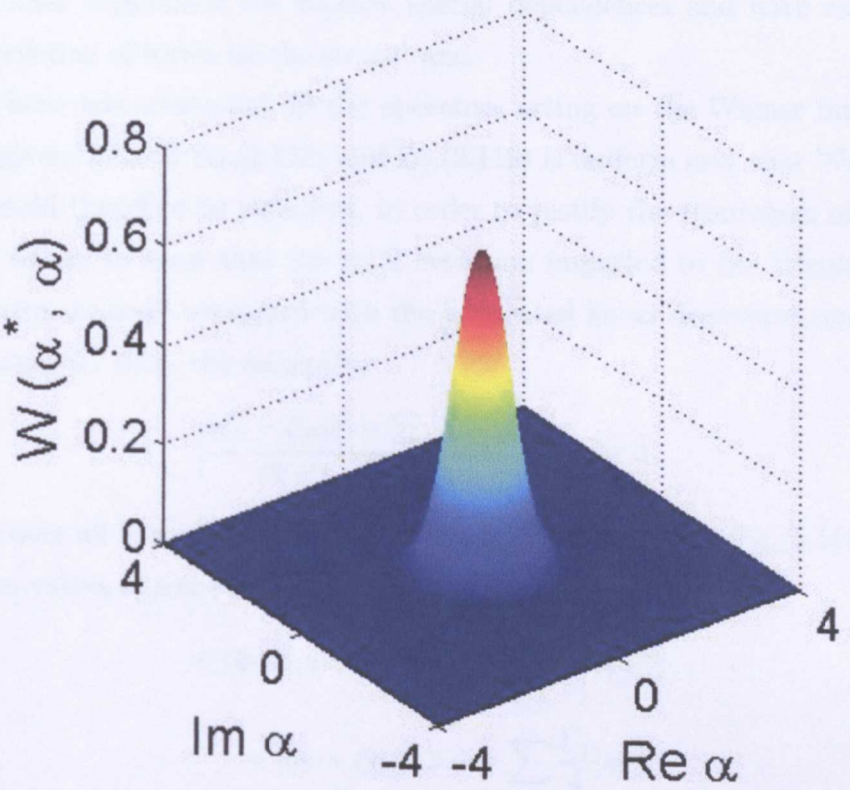

FIGURE 2.2: The plots of Wiger distribution function $W(\alpha^*, \alpha) = \frac{2}{\pi} exp(-2|\alpha|^2)$.

and the related

$$\xi_{\mathcal{P}0}(\mathbf{r}) \equiv < \xi_{\mathcal{P}}(\mathbf{r}) >_W = \sum_{j \in L} \psi_j(\mathbf{r}) \frac{\Gamma_j}{2} \alpha_{j0}, \tag{2.118}$$

where we have calculated the (classical) expectation values using the particular form of the multimode Wigner function given by Eq. (2.114). These definitions (Eq.(2.116), Eq.(2.117), Eq.(2.118)) allow us to rewrite the evolution of the multimode Wigner function due to the pairwise collisions at time τ as

$$\begin{aligned} i\hbar \frac{\partial W^{nonlin}}{\partial t} &= 2U_0 \int dx \left[(\xi^*_{\mathcal{P}} - \xi^*_{\mathcal{P}0}) \Psi_{\mathcal{P}} - \Psi^*_{\mathcal{P}} (\xi_{\mathcal{P}} - \xi_{\mathcal{P}0}) \right] \\ &\times \Big\{ \left(|\Psi_{\mathcal{P}}|^2 - \sum_{j \in L} |\psi_j|^2 \right) - \left(|\xi_{\mathcal{P}} - \xi_{\mathcal{P}0}|^2 \right. \\ &\left. - \sum_{j \in L} \frac{\Gamma_j}{2} |\psi_j|^2 \right) \Big\}, \end{aligned} \tag{2.119}$$

where we have suppressed the explicit spatial dependences and have retained the previous ordering of terms on the second line.

As we have now evaluated all the operators acting on the Wigner function, the evolution given by both Eq.(2.115) and Eq.(2.119) is uniform over that Wigner function. It would therefore be sufficient, in order to justify the truncation of the cubic derivative terms, to show that the total evolution imparted to the Wigner function by these terms is small compared with the integrated linear derivative terms. Under this local analysis then, the inequality

$$\left|\frac{|\xi_{\mathcal{P}} - \xi_{\mathcal{P}0}|^2 - \sum_{j\in L}\frac{\Gamma_j}{2}|\psi_j|^2}{|\Psi_{\mathcal{P}}|^2 - \sum_{j\in L}|\psi_j|^2}\right| << 1, \tag{2.120}$$

must hold over all space. Using the multimode Wigner function Eq.(2.114), we find expectation values of some terms in Eq.(2.120),

$$\begin{aligned} < |\Psi_{\mathcal{P}}|^2, \tau >&= |\Psi_{\mathcal{P}0}|^2 + \sum_{j\in L}\frac{1}{\Gamma_j}|\psi_j|^2, \\ < |\xi_{\mathcal{P}} - \xi_{\mathcal{P}0}|^2 >_W&= \sum_{j\in L}\frac{\Gamma_j}{4}|\psi_j|^2, \end{aligned} \tag{2.121}$$

where

$$\Psi_{\mathcal{P}0}(\mathbf{r}) = \sum_{j\in L}\psi_j(\mathbf{r})\alpha_{j0},$$

is the expectation value of the coordinate space field, and can be identified as the condensate wavefunction. Applying the multimode correspondence between Wigner function averages and mode operator expectation values [56],

$$< \{a^r(a^\dagger)^s\}_{sym} >= \int d^2\alpha \alpha^r(\alpha^*)^s W(\alpha, \alpha^*), \tag{2.122}$$

we also find that in the general case

$$< |\Psi_{\mathcal{P}}(\mathbf{r})|^2 >_W =< \hat{\Psi}^\dagger_{\mathcal{P}}(\mathbf{r})\hat{\Psi}_{\mathcal{P}}(\mathbf{r}) > + \frac{1}{2}\delta_{\mathcal{P}}(\mathbf{r}, \mathbf{r}), \tag{2.123}$$

where $\delta_{\mathcal{P}}(\mathbf{r}, \mathbf{r}') = \sum_{j\in L}\psi_j^*(\mathbf{r}')\psi_j(\mathbf{r})$ is defined as the restricted delta function [52]. Using these results Eq.(2.120) and Eq.(2.123) we are led to the condition

$$\left| < \hat{\Psi}^\dagger_{\mathcal{P}}(\mathbf{r})\hat{\Psi}_{\mathcal{P}}(\mathbf{r}) > - \frac{1}{2}\delta_{\mathcal{P}}(\mathbf{r}, \mathbf{r})\right| >> \sum_{j\in L}\frac{\Gamma_j}{4}|\psi_j(\mathbf{r})|^2. \tag{2.124}$$

Thus in order to justify the truncation it is required that the real particle density be large compared with some function of the density of modes $\sum_{j\in L}|\psi_j|^2$. Based on the above condition, the total Wigner function evolution given above (Eq.(2.109), (2.110), (2.113)) can be written as the Fokker-Planck equation

$$\begin{aligned} i\hbar\frac{\partial W}{\partial t} \approx & -\sum_{j\in L}\frac{\partial}{\partial\alpha_j}\Big[\hbar\omega_j\alpha_j+\sum_{\iota\in L}<j|\delta U_{ext}|t>\alpha_t \\ & +U_0\sum_{rst\epsilon L}<jr|st>(\alpha_r^*\alpha_s-\delta_{r,s})\alpha_t\Big]W \\ & +\sum_{j\in L}\frac{\partial}{\partial\alpha_j^*}\Big[\hbar\omega_j\alpha_j^*+\sum_{\iota\in L}<j|\delta U_{ext}|\iota>^*\alpha_t^* \\ & +U_0\sum_{rst\epsilon L}<jr|s\iota>^*(\alpha_r\alpha_s^*-\delta_{r,s})\alpha_t^*\Big]W. \end{aligned} \tag{2.125}$$

Within the Ito calculus, the Fokker-Planck equation governing the evolution of a multi-mode distribution function $P(\mathbf{z},t)$ over the vector of variables $\mathbf{z}=\{z_j\}$ can be written as [57]

$$\begin{aligned} \frac{\partial P(\mathbf{z},\iota)}{\partial t} = & -\sum_j\frac{\partial}{\partial z_j}[A_j(\mathbf{z},t)P(\mathbf{z},t)] \\ & +\frac{1}{2}\sum_{i,j}\frac{\partial^2}{\partial z_i\partial z_j}\{[\mathbf{B}(\mathbf{z},t)\mathbf{B}^T(\mathbf{z},t)]_{ij}P(\mathbf{z},t)\}, \end{aligned} \tag{2.126}$$

where $\mathbf{A}(\mathbf{z},t)$ and $\mathbf{B}(\mathbf{z},t)$ are respectively the drift vector and diffusion matrix. The corresponding stochastic differential equation to Eq.(2.126) is [6]

$$d\mathbf{z}(t)=\mathbf{A}(\mathbf{z},t)dt+\mathbf{B}(\mathbf{z},t)d\mathbf{W}(t), \tag{2.127}$$

where $d\mathbf{W}(t)$ is a vector of independent Wiener processes, and describes gaussian random fluctuations about the drift evolution. Our truncated Wigner Fokker-Planck equation Eq.(2.125) contains only drift terms, enabling us to write the stochastic differential equation for low-energy mode amplitude α_j using Eq.(2.127) straightfor-

[6] Actually, it is not difficult to understand Eq.(2.127) providing one applies the skills of partial differential equation. $dz=\frac{\partial A(\mathbf{z},t)P(\mathbf{z},t)}{\partial P(\mathbf{z},t)}dt+\frac{1}{2}\sum_i\frac{\partial^2}{\partial z_i\partial P(\mathbf{z},t)}\{[\mathbf{B}(\mathbf{z},t)\mathbf{B}^T(\mathbf{z},t)]_iP(\mathbf{z},t)\}$.

wardly as

$$i\hbar\frac{d\alpha_j(t)}{dt} = \hbar\omega_j\alpha_j + \sum_{t\in L} < j|\delta U_{ext}(t)|t > \alpha_t(t) + U_0 \sum_{rst\in L} < jr|st > (\alpha_r^*(t)\alpha_s(t) - \delta_{r,s})\alpha_t(t). \tag{2.128}$$

Introducing the time-dependent restricted basis wavefunction,

$$\Psi_{\mathcal{P}}(\mathbf{r}, t) = \sum_{j\in L} \psi_j(\mathbf{r})\alpha_j(t), \tag{2.129}$$

we find that the mode amplitude evolutions can be rewritten as

$$i\hbar\frac{d\alpha_j}{dt} = \hbar\omega_j\alpha_j + \int dr\psi_j^*\{\delta U_{ext} + U_0[|\Psi_{\mathcal{P}}|^2 - \delta_{\mathcal{P}}(\mathbf{r},\mathbf{r})]\}\Psi_{\mathcal{P}} \qquad (j \in L), \tag{2.130}$$

where $\delta_{\mathcal{P}}(r,r) = \sum_{j\in L}\psi_j^*(r)\psi_j(r)$. $\delta_{\mathcal{P}}(r,r)$ depends on the low energy modes, L, and are spatially invariant so one can remove the anomalous term from the evolution by a simple energy rescaling. Thus, the form of the stochastic differential equation becomes

$$i\hbar\frac{d\alpha_j}{dt} = \hbar\omega_j\alpha_j + \int dx\psi_j^*[\delta U_{ext} + U_0|\Psi_{\mathcal{P}}|^2]\Psi_{\mathcal{P}} \qquad (j \in L). \tag{2.131}$$

Eq.(2.131) implies the evolution of every mode satisfies the same equation of classical trajectory and the modes display essentially Gaussian statistics at all times, with minimal correlations between the modes. Consequently, the truncated Wigner stochastic differential Eq.(2.131) expressed in a fully coordinate space form becomes

$$i\hbar\frac{\partial\Psi_{\mathcal{P}}}{\partial t} = \left[-\frac{\hbar^2\nabla^2}{2m} + U_{ext}\right]\Psi_{\mathcal{P}} + \mathcal{P}\left[\delta U_{ext} + U_0|\Psi_{\mathcal{P}}|^2\right]\Psi_{\mathcal{P}}. \tag{2.132}$$

Finally, some concepts and central ideas about Truncated Wigner method will be described below as well as some misunderstandings about the method and the motivation of work in presence of Chapter 6 will be discussed. Firstly, we must identify the difference between many-body state $\Psi_{1,2,...,n} = |\psi_1, \psi_2, ..., \psi_n >$ and the mode state $\sum_j \alpha_j\phi_j$ here. α_j in classical field refers to the amplitude function in the j-th low-energy mode while one particle state ψ_j in many body state is constituted

possibly by the states of several modes. Due to the noise part of α_j with random Gaussian distribution, it causes some states in a single trajectory behavior like many body states but the average effect of so many trajectories is equivalent to single particle behavior. For understanding conveniently the central ideas and applicability of Truncated Wigner method, we give a simple example in quantum physics. As is well known, $\int a_i^* \psi_i^*(r) a_j \psi_j(r) dr = \delta_{i,j}$ in normal case where a_i, a_j are constant. However, in the classical field, a_i, a_j are variables and the integral above might not be true and is confirmed if the average of many trajectories is performed for these variables $< a_i^* a_j >_W = \delta_{i,j}$. Secondly, in the condition of single trajectory, $\alpha_j = \alpha_{j0} + \chi_j$, where α_{j0} is condensate part and χ_j is noise part, and

$$\alpha_i^* \alpha_j = \alpha_{i0}^* \alpha_{j0} + \alpha_{i0}^* \chi_j + \chi_i^* \alpha_{j0} + \chi_i^* \chi_j. \tag{2.133}$$

In many trajectories,

$$< \alpha_i^* \alpha_j >_W = < \alpha_{i0}^* \alpha_{j0} >_W + < \chi_i^* \chi_j >_W . \tag{2.134}$$

From Eq.(2.131) and Eq.(2.134), one infers that if the number of non-condensed atoms is small compared with the condensed number, it will not affect the nature of dynamics from classical field theory in every mode and the dynamics is independent of the mode functions. However, we can see in Eq.(2.133) and Eq.(2.131) that if the noise number is large and its contribution to the nonlinear term cannot be ignored, a small change might cause dynamic instability so that the dynamics might depend on the choice of basis.

CHAPTER 3

Vortex Formation and Interference Properties of Merging Bose-Einstein Condensates

Interference is the superposition of two or more waves that result in a new wave pattern. In general, the term interference refers to the interaction of waves which are *correlated* or *coherent* with each other. In BECs, matter wave interference implies the long-distance coherence of cold atoms in analogy to the coherence phenomena exhibited by light. Distinguishing from light interference, this interference from many massive atoms can be controlled and modulated freely, particularly in local regime of position and in some parameters. Meanwhile this interference might be sensitive to some factors, such temperature, interatomic interaction, the geometric shape of atom clouds, etc. Thus it is used to sense accelerations [93, 112], monitor quantum decoherence [41] and measure fundamental constants [112, 113].

A quantum vortex is a topological defect exhibited in superfluids, superconductors and BECs. In BECs, there is the relation between the velocity of the condensate flow $\mathbf{v}$ and the phase of condensate θ, $\mathbf{v} = \frac{\hbar}{m}\nabla\theta$, so that $\nabla \times \mathbf{v} = 0$. This implies that the velocity field is irrotational, unless the phase of the order parameter has a singularity [104]. Possible motions of the condensate are therefore very restricted. In terms of a single-particle wave function of the condensate, around a closed contour the change $\Delta\theta$ in the phase of the wave function must be a multiple of 2π, or $\Delta\theta = \oint \nabla\theta \cdot d\mathbf{l} = 2\pi l$,

where l is an integer. The corresponding *circulation* Γ around a closed contour is given by $\Gamma = \oint \mathbf{v} \cdot d\mathbf{l} = \frac{\hbar}{m} 2\pi l = l\frac{h}{m}$, which shows that it is quantized in units of h/m. This quantized circulation indicates the possibility of forming quantum vortices.

Considering purely azimuthal flow in a trap invariant under rotation about the z axis, to satisfy the requirement of single-valuedness, the condensate wave function must vary as $e^{il\theta}$, where θ is the azimuthal angle. It is easy to obtain $v_\theta = l\frac{h}{2\pi mr}$, which indicates that if $l \neq 0$, the condensate wave function must vanish on the axis of the trap $r = 0$ and the structure of the flow pattern is that of a vortex line. In the case of a uniform medium, the analytic form $\psi(\vec{r}) = \frac{nx}{\sqrt{2\,|\,x^2}} e^{il\theta}$, where n^2 is the BEC density far from the vortex, $x = \frac{r}{l\xi}$ with ξ is healing length of the condensate. Correspondingly, a singly-charged vortex ($l = 1$) energy ϵ_v is given by $\epsilon_v = \pi n \frac{\hbar^2}{m} ln(1.464\frac{b}{\xi})$ where b is the farthest distance from the vortex considered. For multiply-charged vortices ($l > 1$), the energy is equal approximately to $\epsilon_v \approx l^2 \pi n \frac{\hbar^2}{m} ln\left(\frac{b}{\xi}\right)$, which is greater than that of l singly-charged vortices. This implies that these multiply-charged vortices are unstable to decay [4].

3.1 Introduction

Experiments in which a Bose condensed cloud of ultra-cold atoms is divided into two spatially separated components and then allowed to overlap spatially have been widely reported [68, 94, 103]. These experiments have a fundamental interest, for example, in demonstrating the quantum nature of the condensate, and in investigating decoherence. In addition, such processes are central to matter wave interferometry using ultra-cold atom condensates, which may have many technological applications. In general, there are two ways in which initially separated clouds can be made to evolve so that they subsequently overlap. Firstly, they can be allowed to expand by relaxing the confining potential that holds them apart [35, 94, 105]. Secondly, they can be subjected to external potential gradients that cause the clouds to move together and collide whilst maintaining their form [106]. In realistic scenarios, a merging process will, to some extent, involve both of these mechanisms. The resulting interference pattern will be more complex than in either of the idealized cases. To date, there

has been little study of this general case or how it compares with either the purely expanding or purely colliding scenarios.

It is now known that while the behaviour of very low density condensates in such situations can be well described using elementary single-particle quantum mechanics, systems in which the interactions are stronger show behaviour which is quantitatively, and frequently qualitatively, different. In particular it was shown by [86] that the interference pattern formed when two counterpropagating interacting clouds overlap can give rise to the formation of persistent dark solitary waves and, subsequently, the nucleation of linear arrays of vortex rings. As well as having implications for real matter wave interferometers, these processes are of intrinsic interest as an experimentally controllable route to homogeneous quantum turbulence [69]. Recently, experiments have observed the formation of spontaneous vortcies in the merging and interfering of three part BECs [38]. Correspondingly, some theoretical works focus on the role of ramping down and phase imprinting in the formation of these spontaneous vortices [39, 40]. Although the role of interference in the formation of vortices has been pointed out [39, 40], the detailed description of how the interference affects the formation of nonlinear excitations has not been shown.

In this part, we investigate the interference instability and vortex formation of two merging BECs in a simple heuristic model, which is *equivalent* to curve a single trap into a double minimum trap using an atom chip [94], optical barriers [103] or an acousto-optic modulator [105]. Our results show that the formation of vortex rings arises in the regions which evolved from interference minimu. Through the analysis of our simulations and known experiments, we argue that the role of the interference in merging BECs is of critical importance for the spontaneous vortex formation: interference of atom clouds generates high-density peaks and extremely low-density valleys. These additional degrees of freedom might be produced by thermal/quantum fluctuations [25], dynamic instability [103], external potential or perturbation [86, 92, 94]. Therefore the additional degrees of freedom excitate high-density region from original peaks or condensate patches reeling around low-density regions evolved from initial valleys, resulting in the formation of vortices. Moreover, an intrinsic relation among colliding, expanding, and merging BECs is deduced based on simulations using

a large range parameters. Our interference formula derived from the analysis of these simulations can explain well the spatial nonuniformity and dynamic properties of the fringe patterns in some experiments [35] and our simulation. Finally, we propose that the interference dynamics of merging BECs can be observed experimentally under presently available conditions [94, 105, 106].

Our general protocol involves preparing each of a pair of clouds such that it is in the lowest (mean field) energy state of a harmonic trap. The prepared clouds are then displaced in opposite directions and allowed to evolve when subject to a harmonic trap potential which need not be the same as that used to prepare the initial clouds. In general two dynamical processes will occur before the two clouds overlap. Firstly the clouds can undergo (ballistic) centre-of-mass motion in response to the trap potential. Secondly the clouds can change shape as they evolve (most notably expanding or contracting). In general, of course, both processes will occur but we can identify two extreme limits. If two copies of a non-interacting Bose gas are prepared in the lowest energy state of a given harmonic trap and are then placed at symmetric points away from the centre of that trap, the clouds will move ballistically without changing volume until they overlap spatially. We refer to this as a "colliding process". Alternatively two (interacting) clouds prepared as above can be placed a fixed distance apart and then allowed to evolve in the absence of any trap potential. In this case the clouds will expand until they overlap. We refer to such a process as an "expanding" process. Intermediate cases where neither ballistic centre-of-mass motion nor expansion dominate will be referred to as "merging" processes. .

3.2 Simulations

In the most general case our simulations have the following general features. We begin with a trap potential of the form

$$V_0(r,z) = \frac{1}{2}m\omega_{\perp,0}r^2 + \frac{1}{2}m\omega_{\parallel,0}z^2 \quad , \tag{3.1}$$

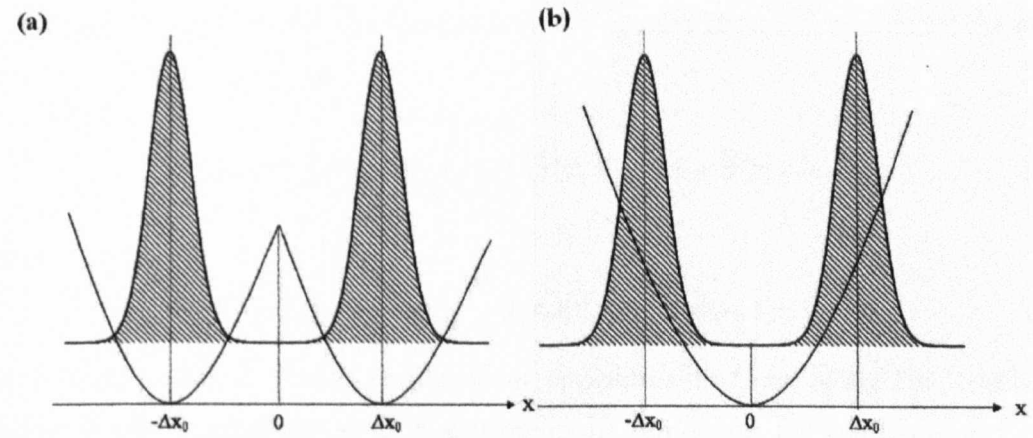

FIGURE 3.1: Solid curves show the effective potential and Shaded areas in the two pictures represent the initial atom density profile $|\Psi(x,0,0)|^2$.

where (r,θ,z) are polar coordinates of positions within the trap. We choose the form for the function $\overline{\phi}(r,z)$ which minimizes the GP energy functional

$$E[\overline{\phi}] = 2\pi \int_{-\infty}^{\infty} dz \int_{0}^{\infty} dr\, r\Big\{ \frac{\hbar^2}{2m} \left|\nabla\overline{\phi}\right|^2 + V_0(r,z) \left|\overline{\phi}\right|^2 + \frac{1}{2} g \left|\overline{\phi}\right|^4 \Big\}, \tag{3.2}$$

subject to the constraint

$$N = 2\pi \int_{-\infty}^{\infty} dz \int_{0}^{\infty} dr\, r \left|\overline{\phi}\right|^2 r dr dz \tag{3.3}$$

where $g = 4\pi\hbar^2 a_s/m$ is the usual GP coupling constant and a_s is the s-wave scattering length for inter-atomic collisions. In all of these simulations we use the value a_s = 2.9nm and $m = 3.82 \times 10^{-26}$kg, appropriate for a Sodium-23 condensate. In practice the minimization is effected by evolving an initially Gaussian form according to the imaginary time Gross-Pitaevskii equation

$$\frac{\partial\overline{\phi}(r,z,\tau)}{\partial\tau} = -\Gamma \frac{\delta E[\overline{\phi}(r,z,\tau)]}{\delta\overline{\phi}(r,z,\tau)} \tag{3.4}$$

where Γ is a suitablly chosen friction co-efficient. To conserve the total particle number, we normalize $\overline{\phi}(r,z,\tau)$ in every time step using Eq.(3.3).

The initial condition for the main simulation is then obtained by setting the order parameter to have the form

$$\phi(r,z,t=0)=\sqrt{\frac{1}{2\left(1+Q\right)}}\left(\overline{\phi}(r,z-\Delta)+\overline{\phi}(r,z+\Delta)\right), \tag{3.5}$$

where

$$Q=\frac{1}{N}2\pi\int_{-\infty}^{\infty}dz\int_{0}^{\infty}drr\overline{\phi}(r,z-\Delta)\overline{\phi}(r,z+\Delta), \tag{3.6}$$

representing a pair of clouds displaced in opposite directions along the z-axis. Q ensures correct normalization of ϕ and might be important for tunneling and incoherence. It is worth pointing out that the representation in terms of a single order parameter, ϕ implies that the two clouds are fully coherent and it is not the case that there are $N/2$ atoms in each cloud. In all of the simulations described below, the two clouds are spatially non-overlapping so that $Q=0$.

The subsequent evolution of the system is determined by numerically solving the Gross-Pitaevskii equation

$$i\hbar\frac{\partial\phi}{\partial t}=-\frac{\hbar^2}{2m}\nabla^2\phi+V(r,z)\phi+g\left|\phi\right|^2\phi \tag{3.7}$$

assuming that the initial rotational symmetry in the xy-plane is preserved using a 2d Crank-Nicholson algorithm adapted to correctly treat the polar variable r. The potential is now

$$V(r,z)=\frac{1}{2}m\omega_{\perp}r^2+\frac{1}{2}m\omega_{\parallel}z^2 \quad , \tag{3.8}$$

where, in general $\omega_{\parallel}\leq\omega_{\parallel,0}$ etc..

3.3 General description of two condensates coming together

By analyzing the interference pattern generated by the merger of two condensates we indetify three types of behaviour and their corresponding parameter regimes. We refer to the two extreme cases as *colliding* and *expanding*, and to the generlized intermediate case as *merging*. To explore the role of the repulsive interatomic interaction in the interference fringes, we calculate the half center of mass (c.m.), $<x>_{+}(t)=\int_{0}^{\infty}x|\psi(x,t)|^2dx$ in a 1D freely expanding single condensate through

various atom number. From Fig.3.2, we observe that the strong interaction tends to speed up linearly the expansion of condensate. Genuinely, our simulations are well in agreement with *ab initio* calculation [110]. $< x >_+ (t) \approx \sqrt{1 + (\omega t)^2} R(0)$ where $R(0)$ is initial radius of condensate and ω is trap frequency for generation of condensates and is larger than $2\pi \times 800$ rads s^{-1} here. Thus at $t > 3\mu s$ the second part in the square is much larger than 1 and $< x >_+ (t)$ is increased approximately linearly. Therefore we take heuristically into account the atomic cloud internal expansion due to the nonlinear term, approximate as $\alpha(x,t) \Leftarrow \frac{g}{2}|\psi(x,t)|^2$, where $\alpha(x,t)$ is a modified coefficient dependent on the density of the wavepackets. In real space, the state of one condensate can be described using a Guassian ansatz:

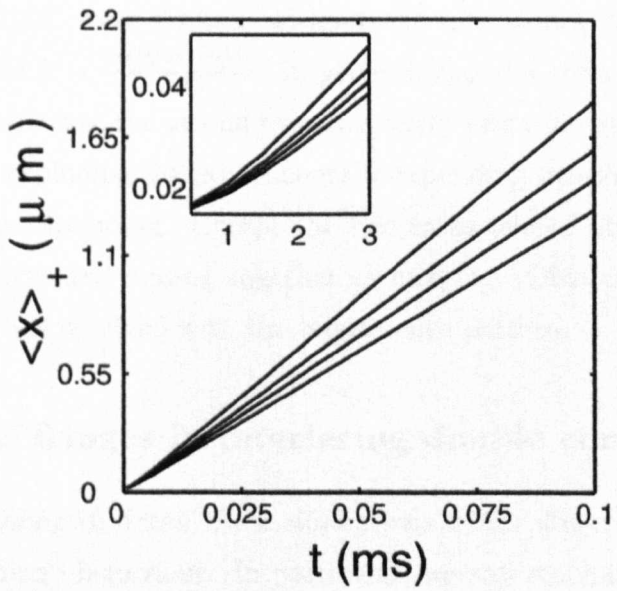

FIGURE 3.2: The c.m. trajectories of half condensate versus process time t from 1D simulation of freely expanding single condensate with parameters of $g = 2\hbar\omega_r a$ and total number of atoms N varied from 10 (bottom) to 1000 (top); Insert: short-time behavior of the trajectory.

$$\psi_0(x,t) = (2\pi l_0^2)^{-1/4} \frac{l_0}{\sigma(l)} e^{-\frac{x^2}{4\sigma^2(t)}} \tag{3.9}$$

where $\sigma(t) = \sqrt{l_0^2 + i(\frac{\hbar t}{2m} + \frac{\alpha t}{\hbar})}$. Now we consider a pair of wavepackets initially at positions $\pm L/2$, $\Psi(x,0) = \frac{1}{\sqrt{2}}(\psi_0(x - \frac{L}{2}, 0) + \psi_0(x + \frac{L}{2}, 0))$ so that, this pair of

wavepackets at later time t with the same speed $v = \hbar k'/m$ toward each other, $\Psi(x,t) = \frac{1}{\sqrt{2}}(\psi_0(x-\frac{L}{2},t)e^{-ik'x} + \psi_0(x+\frac{L}{2},t)e^{ik'x})$, where wavevector k' is modulated by the variation of trap potential. Thus, we can obtain the effective wavelength for the interference fringes through $|\Psi(x,t)|^2$,

$$\lambda = \frac{4\pi[l_0^4 + (\frac{\hbar t}{2m} + \frac{\alpha t}{\hbar})^2]}{I_{\prime}(\frac{\hbar t}{2m} + \frac{\alpha t}{\hbar}) + [l_0^4 + (\frac{\hbar t}{2m} + \frac{\alpha t}{\hbar})^2]4k'} \tag{3.10}$$

Under the condition that the nonlinear term is extremly small, there exists the highest-visibility interference fringe with $\lambda = \frac{\pi}{k'} = \frac{h}{mv}$ and the expansion of the atomic cloud is almost zero; that is analogous to classical interference. We define this process as colliding. In the other extreme condition, $k' \approx 0$ and $g|\psi|^2 \approx 0$, it describes free expansion of two BEC wave packets without the interatomic interaction and interference fringe period $\lambda = \frac{2\pi(4l_0^4 m + \frac{\hbar^2 t^2}{m})}{\hbar t L}$. In general, the first term in the bracket can be neglected with respect to the second term in a fairly long time so that the fringe spacing $\lambda = \frac{ht}{mL}$ used in explaning the experiments of expanding two condensates [35]. We refer this process as expanding. Except the two cases refered above, we define the process of two condensates coming together as merging. Obviously the role of interatomic interaction has involved with the interference pattern.

3.4 Distortion of fringes in interfering double condensates

We will begin by describing in detail three simulations which illustrate "collision", "merging" and "expanding" behaviour. In particular, we will emphasize the role of the repulsive interatomic interaction in the distortion of fringes in interfering double condensates and the resulting spontaneous vortex formation. Furthermore, we summarize the general relations between "collision", "merging" and "expanding" behaviour.

3.4.1 System I: Free Expansion of Well Separated Clouds

The initial state is chosen such that the peak density in each component is $n_0 = 6.9 \times 10^{19}\mathrm{m}^{-3}$, the trap frequencies are $\omega_{\parallel,0} = 2\pi \times 180\mathrm{Hz}$ and $\omega_{\perp,0} = 2\pi \times 120\mathrm{Hz}$,

the displacment from the centre of the trap is $\Delta = 4.8 l_{\|} = 9.5 \times 10^{-6}$m where

$$l_{\|} = \sqrt{\frac{\hbar}{m\omega_{\|}}} \tag{3.11}$$

is the oscillator length for the trap. The initial state corresponds to two well separated low density clouds: the Thomas-Fermi lengths being $R_{\|} = 3.5 l_{\|} = 5.5 \times 10^{-6}$m and $R_{\perp} = 8.2 \times 10^{-6}$m. The total number of atoms being $N \sim 8 \times 10^{4}$. Hence we have, initially, two well separated high density clouds. After preparation, the system is allowed to evolve freely, i.e. with the trap frequencies set to $\omega_{\|} = \omega_{\perp} = 0$. Such free expansions are well studied, in particular it is straightforward to show that, in the absence of interactions, the order parameter has the form $\phi_0(r, z-\Delta, t)+\phi_0(r, z+\Delta, t)$ where [4]

$$\begin{aligned} \phi_0(r,z,t) = \left(\frac{m\overline{\omega}}{\pi\hbar}\right)^{3/4} \frac{1}{1+i\omega_{\perp}t}\sqrt{\frac{1}{1+i\omega_{\|}t}} \\ \times e^{-\left(\alpha_{\|}(t)-i\beta_{\|}(t)\right)z^2/2l_{\|}^2} e^{-(\alpha_{\perp}-i\beta_{\perp})r^2/2l_{\perp}^2} \end{aligned} \tag{3.12}$$

and

$$\begin{aligned} \alpha_j &= \frac{1}{1+\omega_j^2 t^2} \\ \beta_j &= \frac{\omega_j t}{1+\omega_j^2 l^2} \end{aligned}$$

Hence at arbitrary time t we have

$$\phi(r,z,t) = A(t) e^{-2\alpha_{\perp}(t) r^2/l_{\perp}^2} e^{-2\alpha_{\|} z^2/l_{\perp}^2} \tag{3.13}$$

$$\times \left(\cosh\left(\frac{2\alpha_{\|}(t)\Delta z}{l_{\|}^2}\right) + \cos\left(\frac{2\beta_{\|}(t)\Delta z}{l_{\|}^2}\right)\right) \tag{3.14}$$

From this we deduce that the length scale characterizing the interference fringes is

$$\lambda(t) = \frac{l_{\|}^2}{2\Delta}\frac{1+\omega_{\|}^2 l^2}{\omega_{\|} t} \tag{3.15}$$

which, at times larger than $2\pi/\omega_{\|}$ behaves as $\lambda(t) \sim (l_{\|}^2/2\Delta)\omega_{\|} t$ as observed in our simulations (see Fig.3.5 Ia and Ib). From our simulations, with the more overlapping,

the more number of interference fringes appear and the period of fringes become larger. Meanwhile the peak density of the fringes also increases until the time of point in which two clouds expand fully, i.e., the peak density of fringes is comparable to the peak density in two clouds. After the time of point, the peak density of fringes will reduce but the width of fringes still increase.

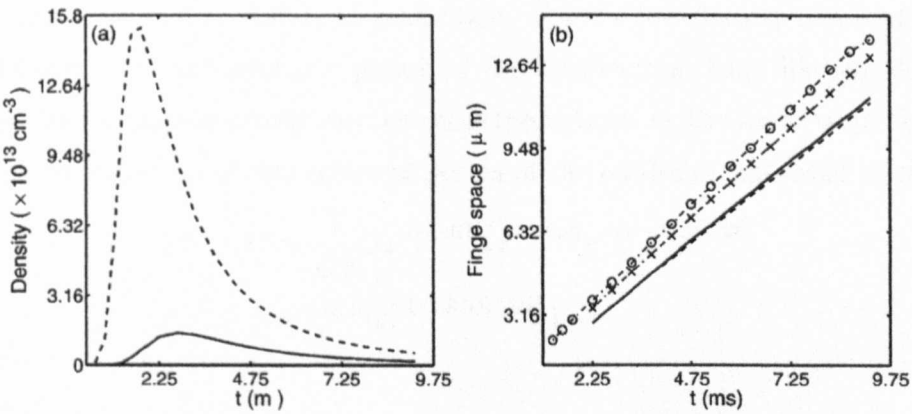

FIGURE 3.3: Left: The central density peak of interference versus time t in the process of expansion with $N = 3 \times 10^4$ (solid line) and 4×10^5 (dashed line). Right: The central fringe spacing versus time t in the process of expansion with $N = 3 \times 10^4$ (solid line) and 4×10^5 (circled line) and the first-order finge spacing for $N = 3 \times 10^4$ (dashed line) and 4×10^5 (crossed line).

In Fig.3.3, the linear fringe spacing versus time in the weakly interacting regime agrees qualitatively with the formula $\lambda = \frac{ht}{md}$, where d refers to the separation of two condensates and t process time [35]. However, beyond the weakly interacting regime, the central and first-order fringe spacings become different and the uniform pattern of interference in the weakly interacting regime is broken (see Fig.3.3 (b)) so that the distorted fringe pattern appears. Meanwhile the high-density clouds speed up the the expansion of clouds and produce larger fringe spacings than the low-density clouds (see Fig.3.3 (a)). Based on Eq.(3.10), the high-density central fringe has larger α than the first-order fringe so that the larger fringe spacing occurs on the central fringe. Thus, the role of interatomic interaction has been involved in the interference pattern so that this process becomes the process of merging. Suppose that there are external potential gradients along the direction of merging and the initial density of

the expanding clouds are sufficient high, the nonlinear excitations in Fig.3.5 can be produced.

3.4.2 System II: Collision of Well Separated Clouds

The clouds are prepared in the same manner as for system I. But by holding the traps, two clouds are allowed to collide to each other. For the low-density condensates, the system behaves, at least over one period of the longitudinal trap, like an ideal Bose gas. Since the preparation trap has the same frequencies as the main trap, the initial state is a superposition of two coherent states of the oscillator potential so that

$$\begin{aligned}\psi(r,z,t) = \frac{1}{\sqrt{2}} C e^{-r^2/2l_\perp^2} \Big(& e^{-iK(t)} e^{-(z-Z(t))^2/2l_\parallel^2} \\ & + e^{iK(t)} e^{-(z+Z(t))^2/2l_\parallel^2} \Big)\end{aligned} \tag{3.16}$$

where

$$\begin{aligned} Z(t) &= \Delta \cos\left(\omega_\parallel t\right) \\ K(t) &= \frac{\Delta}{l_\parallel^2} \sin\left(\omega_\parallel t\right) \end{aligned} \quad .$$

Hence when the clouds are maximally overlapped (at $\bar{t} = \pi/2\omega_\parallel$) the finge spacing is given by

$$\lambda = \frac{2\pi}{K\bar{t}} = \frac{2\pi l_\parallel^2}{\Delta}. \tag{3.17}$$

Fig.3.5 panel IIa shows the density distribution for the initial state, while Fig.3.5 panel IIb shows the fringes formed when the clouds are maximally overlapping. Subsequently the two clouds separate with their density peaks following classical trajectories. Each time the clouds overlap plane fringes form with the ideal spacing. The classical argument being that the velocity at $\bar{t}$ is given by

$$\frac{1}{2} m \bar{v}^2 = \frac{1}{2} m \omega_\parallel^2 \Delta^2 \tag{3.18}$$

which gives $v = \omega_\parallel \Delta$ and $\lambda = h/m\bar{v} = 2\pi l_\parallel^2/\Delta$. In this case the collision velocity is $\bar{v} = 6.08 l_\parallel \omega_\parallel = 1.07 \times 10^{-2}\mathrm{ms}^{-1}$ and $\lambda = 1.036 l_\parallel = 1.62 \times 10^{-6}\mathrm{m}$.

We increase the effect of the nonlinear term by increasing the number of atoms in the initial state. In Fig.3.4, for the initial peak density n_0 in the low density

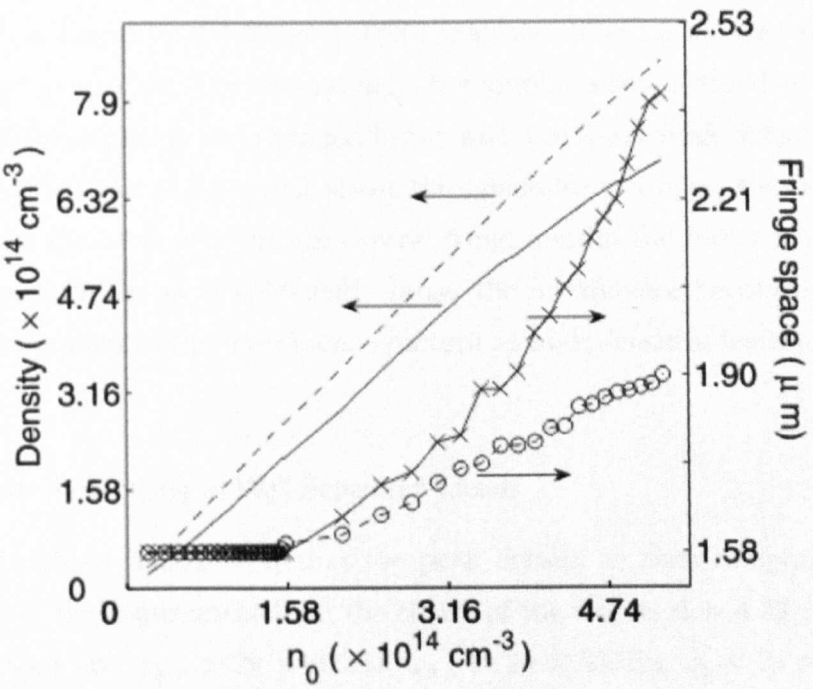

FIGURE 3.4: The central density peak (dash curve), the first-order density peak (solid curve) of interference, the central fringe spacing (crosses), and the first-order fringe spacing (circles) versus various initial peak density of condensates in the process of collision with fixed g .

regime, the amplification of the central and first-order peak of interference increases linearly, which is analogous to optical interference where the power spectrum of interference is raised linearly with the growth of optical resource power. In this regime, once the initial double trap frequencies and separation are fixed, the fringe spacings are *independent* on the density of initial condensates. However, when the nonlinear interaction is sufficiently strong, i.e. n_0 is larger than $1.58 \times 10^{14}\text{cm}^{-3}$, the central and the first-order fringe spacings become different and the uniform peak pattern is broken so that the distorted fringe pattern appears. The *higher* the peak density, the *larger* fringe spacing. Correspondingly, the amplification of the density peaks in the high density regime is not changed linear with the inital peak density. Also, our formula Eq.(3.10) can explain well about the nonuniform fringes; the larger α with respect to the higher density in the central fringe results the larger fringe spacing. Furthermore, once the n_0 is sufficiently large, the interference becomes unstable so that the deformation of the interference pattern at high densities leads to the vortex production.

3.4.3 System III: Merging of Well Separated Clouds

This initial state is chosen such that the peak density in each component is $n_0 = 4.6 \times 10^{21}\text{m}^{-3}$, the displacment from the centre of the trap is $\Delta = 4.33 \times 10^{-6}\text{m}$, the trap frequencies are: $\omega_{\parallel,0} > 2\pi \times 800\text{Hz}$, $\omega_{\perp,0} > 2\pi \times 533\text{Hz}$, $\omega_{\parallel} = 2\pi \times 180\text{Hz}$ and $\omega_{\perp} = 2\pi \times 120\text{Hz}$. Becuase the trap used for the simulation is much less confining than the trap used in preparing the clouds, each clouds expands due to internal pressure as well as undergoing bulk motion. Because the initial displacement from the centre of the trap is smaller than in system I the relative velocity of the two clouds when they overlap is much smaller, $\overline{v} = 2.8 l_{\parallel} \omega_{\parallel}$. Panels IIIa - IIIf of Fig.(3.5) show the time evolution of the density profile. As can be seen in panel IIIa, when the clouds are maximally overlapped a fringe pattern forms but it is distorted with "thicker" fringes in the centre of the cloud and a larger fringe spacing, towards the edge of the cloud the density is much lower so that interaction effects are negligible and the fringe spacing is closer to its non-interacting value.

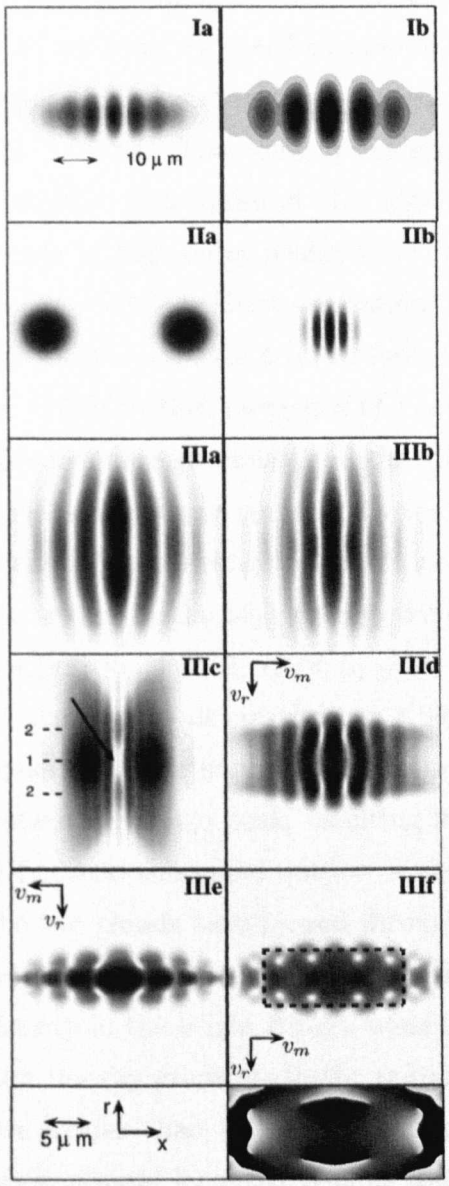

FIGURE 3.5: Gray-scale plots of atom density (black=high) in the x-r plane (axes inset) for double condensates, evolving with the process of expanding at t = 5.81ms(Ia), 10.21ms(Ib), colliding at t = 0ms(IIa), 2.01ms(IIb), and merging at t = 1.21ms(IIIa), 2.01ms(IIIb), 2.41ms(IIIc), 3.61ms(IIId), 4.11ms(IIIe), 4.41ms(IIIf); The phase of the BEC wave function within the dashed box in IIIf is shown in the gray-scale plot (black=2π, white=0) to the bottom of the density profile; arrowed v_m and v_r show the directions of motion in left-upper(bottom) part of clouds depended on the postion of speed coordinates.

From Eq.(3.10), in the process of merging, since the expanding speed of an atom cloud v_e is initially much larger than its speed of motion v_m, the pattern of interference fringes in the region of local strong interaction is dominated by the term $\alpha(x,t)t/\hbar$ in Eq.(3.10) at $t < 2.1$ms. Therefore, fringe spacings at the middle part of interference are larger slightly than those at the edge as well as the density of central peak larger than those of high-order peaks, which can explain the results of experiments in freely-expanding BECs in short separation, as shown in Fig.1 (left) in ref. [35] : condensates with short separation tend to form large variations of density in the region of mergence. With further mergence of two clouds in later time, the increasing k' and $\hbar t/2m$ predominate gradually and the differences of fringe spacing at the middle and edge have been reduced correpondly (seen IIIa-IIIb).

As can be seen in IIIb and IIIc the stronger interactions in the centre of the cloud lead to a net radial flow of atoms in the high density fringes. The speed for BECs to propagate radially from position 1 to 2, $v_r \approx L_{1,2}/t_{1,2} = 11.076\text{mms}^{-1}$, is more than twice as large as the center-of-mass speed $v_m \approx 4.8971\text{mms}^{-1}$. Thus the high transverse speed with respect to strong nonlinear interaction from merging two condensates tends to fragmentate the fringe peak, resulting in the formation of a dark soliton as seen in figure IIIc. Also this rapid outflow leads to complete depletion of the centre of trap after the two clouds have passed through one another. As can be seen in IIId when the two clouds recollide, at time $2\bar{t}$, both are recollapsing radially leading to an enhanced density in the bright fringes causing an even greater longitudinal expansion and greater density gradients in the radial direction. The curvature of the fringes is thus even greater than in the first collision, IIIe, and is sufficient to generate a net circulation around localized regions that are fully depleted: vortices are generated, as seen in IIIf. In general, due to strong interatomic interaction and the competition between v_m and v_r, additional degrees of freedom are generated, resulting that high-density areas from the second-time interference peaks reel around extremely low-density areas arising from the prior interference valleys (IIIe). The positions of four vortex rings correlate naturally with the previous positions of interference valleys. Actually, the formation of soliton and vortices from quantum reflection of high-density and low-velocity BEC is naturally analogous with our results;

the low velocity enables the interference between the incident and reflected parts of the condensate, which has been shown as fringe patterns in Fig.2(b) in [86], and the high density and trap potentials incite inner degree of freedom for high-density parts of the condensate. Through analysis of much simulation and known experiments, we argue that the role of interference of BECs is of critical importance for the spontaneous vortex formation: interference of atom clouds generates high-density peaks and extremely low-density valleys, and additional degrees of freedom possibly produced by thermal (quantum) fluctuations [25], dynamic instability [103], external potential or perturbation [36,92,94] might excitate high-density region from original peaks or condensate patches reeling around low-density region evolved from initial valleys, resulting in the formation of vortices.

3.5 General Features in the parameter space

Here, we identify approximately three processes through their interference characters. In the process of expansion, the interference fringes are time-dependent and uniform, and in colliding process are confirmed and uniform in the fully overlapping, and the interference pattern in expanding process are time-dependent and nonuniform. Based on simulations of a large range parameters, we describe heuristically the interference properties and the creation principles of nonlinear excitations shown in Fig.3.6. In merging and expanding process, the creation principles of soliton and vortex are naturally dependent on the competition between expanding (merging) speed and motion speed of condensates. The moving speed is too large (position **C** in solid line) and small (**A**), it is not easy to observe the excitations. Thus, we can explain the experiments in which more vortices in merging and interfereing region except the central vortex which is formed by phase mechanics, are formed provided that three components of clouds are merged more quickly. Due to high potential barrier, three parts of condensates expand rapidly and fast merging might avoid the loss of rapidly expanding condensates and form high-density condensates in merging region so that the strong nonlinear interaction can easily generate inner degrees of freedom. Meanwhile, the interference pattern is of critical importance in the formation of vortices.

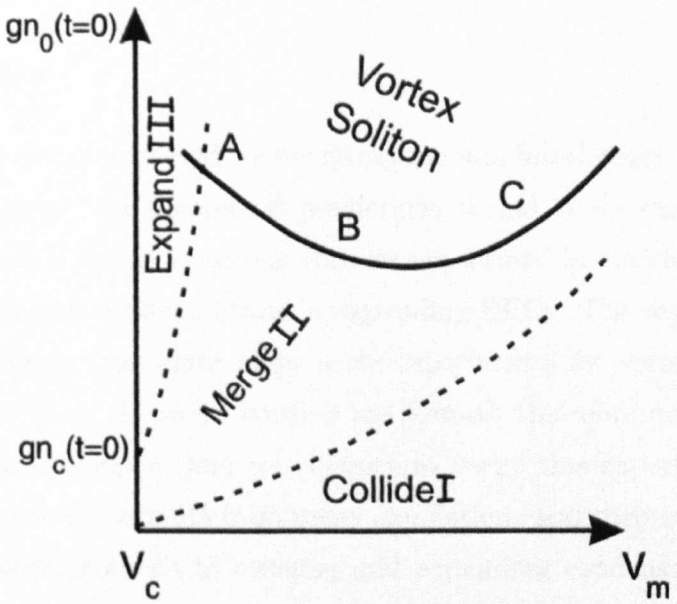

FIGURE 3.6: Heuristic description of the parameter space for v_m and $gn_0(t = 0)$. Dash lines are drawn through identifying different interference patterns: fringes vary approximately linearly with t for the case of expanding, are nonuniform and time-dependent for merging, and uniform and fixed highest-contrast period for colliding. Solid lines are drawn through identifying whether there exists nonlinear excitations. We must emphasis that $gn_c(t = 0)$ is determined by v_c and v_c is determined by size of condensate for which the dynamics and interference pattern corresponding to too small separation is naturally equivalent to merging case.

The faster merging produces more interference fringes so that there is the possibility for the formation of more vortices. In addition, for a qualitative depict of differences among colliding, merging and expanding processes in Fig.3.6, the dashed line can be altered by different parameters. In general, for the small nonlinear constant with the large atoms numbers, it is more easy to observe the crossover from colliding process to merging process.

3.6 Summary

In summary, we have investigated vortex formation and interference instability of two merging condensates. Our theoretical predictions should verify recent some experimental work in which the spontaneous vortices are formed in merging BECs and the nonuniform interference pattern forms in expanding BECs. The regularity of vortex formation and interference might allow some experiments for vortex creation. Our latest calculations show the more vortices are formed, the more interference fringes occur in the unstable region, and we propose to verify this experimentally. Additionally, the interference formula from many simulations and theoretical analysis can explain well some phenomena in merging and expanding condensates. However, a completely confirmed formula is needed from more rigorous theoretic deductions and experimental tests.

3.7 Vortex Decay and Dynamics in Merging BECs

3.7.1 Motivation and Findings

As seen in the above section, the dynamics and decay of the spontaneous vortices might be of importance for studies of quantum turbulence in the system of mixing superfluids or classical fluids. On the other hand, in the experiment [103], vortices are observed by probing for merging dynamics by releasing all traps and viewing the atom cloud using absorption imaging after a period of ballistic expansion. In general, the excitation energy of a vortex is macroscopically large and those off-center vortices in merging clouds might decay and vanish rapidly [4]. It is required to answer whether

this measure of time of flight can reflect the production of vortices in merging BECs.

In this work, we study the factors affecting the spontaneous formation of vortices when merging two atomic BECs. In the *non-uniform* condensates, two factors are of critical importance for the formation: interference and strong nonlinear interaction. The interference of condensates plays an important role in the formation of the vortex core. The strong nonlinear interaction triggers the interference peaks or condensate patches reeling around the vortex core. Through simulation and analysis, a feasible criteria for this formation has been shown. In addition, our simulations show that vortices decay from high-density regions into low-density regions, disappear ultimately on the edge of the condensate, with their cores becoming correspondingly larger. The fragmentation of atom clouds is caused by vortices with opposite rotation which are analogous to magnets. Finally, we demonstrate that the measure results for vortices through releasing all traps can reflect the dynamics of BECs with traps in real experiments when vortex decays can be neglected. The role of two other factors in the formation of this kind of vortices, i.e., relative phase of merging two clouds and quantum (thermal) fluctuations, has been discussed in the papers [39, 86].

3.7.2 Exemplar Model

In this work, the dilute double condensates are realized with total number 4×10^5 ^{23}Na atoms in the same traps used in the above part. The process I in this part is similar to the process of merging in the above part. Process II is modulated by the similar evolution to some experiments [103], where they removed all trapping potential after merging and viewed the atom cloud using absorption imaging. After the formation of vortices, all trapping potentials are removed and the atomic clouds are released completely from traps, expand freely. We record the dynamics of BECs in this process during a long time.

3.7.3 Results and discussion

We now explore the dynamics of vortices in two processes. As has been shown the above part, the interference of atom clouds generates high-density peaks and ex-

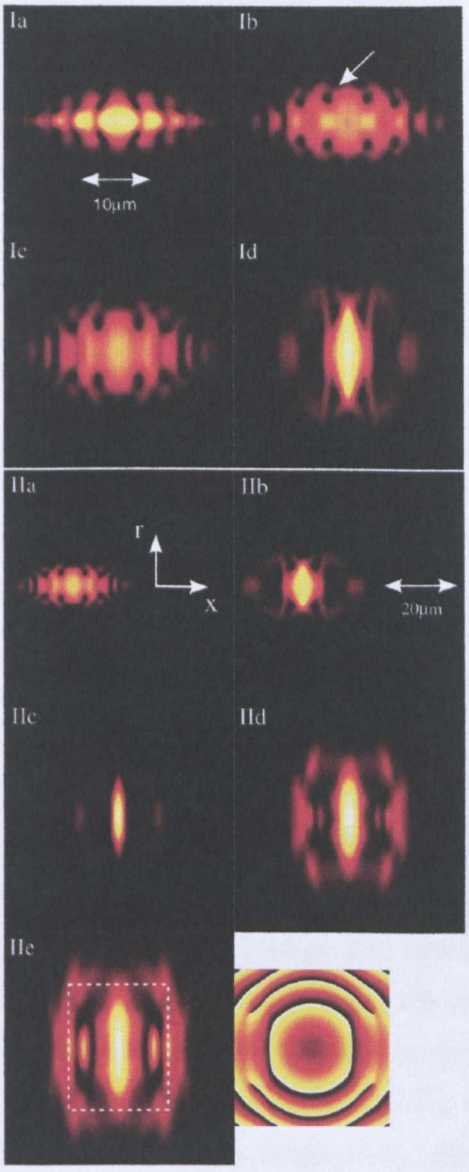

FIGURE 3.7: Hot-scale plots of atom density (white=high) in the x-r plane for double condensates, evolving with process I at t = 6.02ms(Ia), 6.46ms(Ib), 6.74ms(Ic), 7.46ms(Id), and process II at t = 6.74ms(IIa), 7.44ms(IIb), 8.34ms(IIc), 9.74ms(IId), 10.64ms(IIe); The phase of the BEC wave function within the dashed box in IIe is shown in the hot scale plot (white=2π, black=0) to the right of the density profile; Coordinate axes are inserted in IIa and length scales are labeled separately for both processes (see Ia and IIa).

tremely low-density valleys (Ia), and additional degrees of freedom produced by dynamical instabilities might excite high-density region from original peaks or condensate patches reeling around low density region evolved from initial valleys, resulting in the formation of vortices (Ib). Since four vortex rings are created at the ramp located between the high-density region (around $x = 0$ and $r = 0$) and low-density region (far from center of trap), they are highly unstable and thus tend to decay into more "stable" areas. As seen in Fig.(3.7) Ic and Id, the vortex rings propagate to the low-density region far from the center of trap although the trap potential in x-axis direction compresses them into the center, and later disappear at the edge of main clouds. The competition between the force of "dragging" the outer two vortices into high-density region from trap potential and expelling force originating from the variation of strongly interatomic interaction around them results in the clouds fragmenting into three parts from the region of vortex disappearance. In process II, the decay of vortices is similar to process I and the time of decay is a little shorter (IIa and IIb), since strong interaction can excitate faster dynamics in the absence of a trap potential. Thereafter, three parts of the clouds fragmented by the outer two vortex rings expand further as well as the compressed central part (IIc). After 1.4ms, the outer two parts interfere with the expanding center part and a vortex pattern is reformed in the freely expanding process. Contrasted with the rapid variation of the vortex pattern in the interval of 6.74ms to 7.44ms, the latter interference and vortices are more stable and last much a longer time. Indeed, the pattern of interference and vortex reformation will remain unchanged because the interaction energy of atom clouds is approximatly zero at $t > 10$ms. Although the method of creating these vortices has not been changed, the possibly results from releasing all traps might not show the nature of initial vortex formation in a long time, i.e. $t > 12ms$, because macroscopic nonlinear excitations might decay, merging, or disappear in this period. It indicates that there might exist some discrepancies between the dynamics of BECs with traps and the results from experimental observation at comparatively long times, in particular, in presence of nonlinear excitations [103], thermal fluctuation [25] and

dynamical instabilities [1].

We explore the dynamics of vortices by tracking one vortex (arrowed in Fig.(3.7)) in process I, based on two reasons: 1. due to the weak variation of the trap potential and strong excitation energy including kinetic energy and interaction of nonlinear excitation in the bottom of traps, the confining potential does not alter naturally the results of vortex decay and the dynamics of a vortex in confined potential; 2. four vortex rings decay entirely from high-density regions into low-density ones and disappear at the edge of main condensates. We characterize the size of the core by

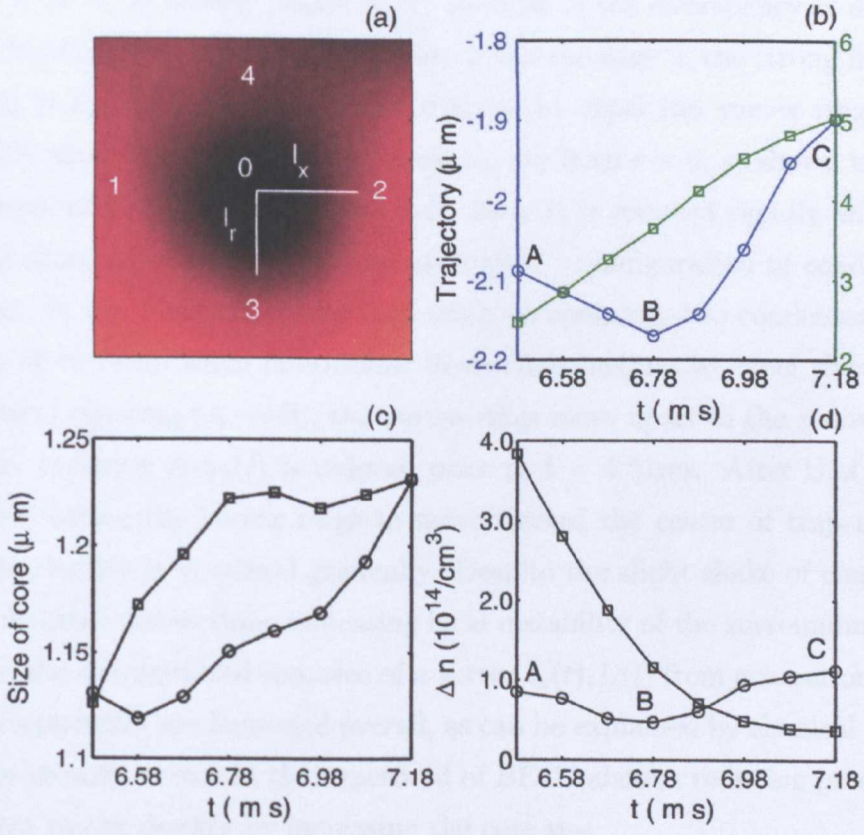

FIGURE 3.8: Vortex configuration arrowed in the Ib of Fig.(3.7) (a); Vortex core trajectory in x direction (circles) and r direction (squares) versus time (b); The size of core l_x (circles), l_r (squares) versus time (c); Density variation Δn_{12} (circles), Δn_{34} (squares) versus time (d).

[1]Our recent results demonstrate that thermal(quantum) fluctuations can alter strongly the dynamics of interference in a short time.

integrating the smooth part of distribution function from core center 0 to position 2, where the variation of density is very small, in Fig.(3.8) (a) along x direction with $l_x(t) = \int_{x_0}^{x_2}(x - x_0)|\psi(x,t)|^2dx / \int_{x_0}^{x_2}|\psi(x,t)|^2dx$ and $l_r(t)$ is defined similarly to $l_x(t)$. To figure out the relation between the trajectory of a vortex and its surroundings, we define the variation of density function in x and r directions by calculating $\Delta n_{12}(t) = \bar{n}_2(t) - \bar{n}_1(t)$ and $\Delta n_{34}(t) = \bar{n}_3(t) - \bar{n}_4(t)$ separately. Here $\bar{n}_{i(=1,2,3,4)}$ is the mean density around the high-density position i. For convenient contrast in the dynamics, we integrate $l_x(t)$ and $l_r(t)$ in a fixed interval of $x_2 - x_0(r_3 - r_0)$ and use the mean value of 30 density points as $\bar{n}_i$. Because of the discrepancy of density distribution between the center of condensates 3 and the edge 4, the strong interatomic interaction of condensates around $r = 0$ tends to expel the vortex ring from the high-density area into the low-density area, i.e. far from $r = 0$, as shown in Fig.(3.8) (b). Correspondingly the density variation $\Delta n_{34}(t)$ is reduced rapidly with respect to process time, reflecting the " Gaussian-shaped " configuration of condensates in r direction. In the x direction, the trap tends to compress two condensates toward the center of the trap while interatomic interaction inclines to expel them. During the domain of repelling (A$\longrightarrow$B), the vortex rings move apart in the x direction and the density variation $\Delta n_{12}(t)$ is reduced prior to $t = 4.51$ms. After that (B$\longrightarrow$C), compression causes the vortex rings to move toward the center of trap and consequently the density is increased gradually. Despite the slight shake of characteristic core size of vortex versus time, indicating local instability of the surroundings around the vortex, the characterized core size of a vortex $l_x(t), l_r(t)$ from generation of vortex rings to disappearing are increased overall, as can be explained by classical dynamics: fixed angle-velocity vortex in the superfluid of BEC balances reducing pressure force with respect to low density by increasing the core size.

We analyze the vortex dynamics through macroscopic vortex-vortex interaction, with analogy to spin-spin interaction. In Fig.(3.9), since vortex ring 1 (3) and 2 (4) have the same spin direction, and 2 and 3 have the different spin direction, vortex ring 1 (3) and 2 (4) expel each other while 2 and 3 attract one other. Consequently, vortex rings 2 and 3 move toward each other and the fragmentation of atom clouds is presented in the regions between vortex 1 (3) and 2 (4) as shown in Fig.(3.7) Id and

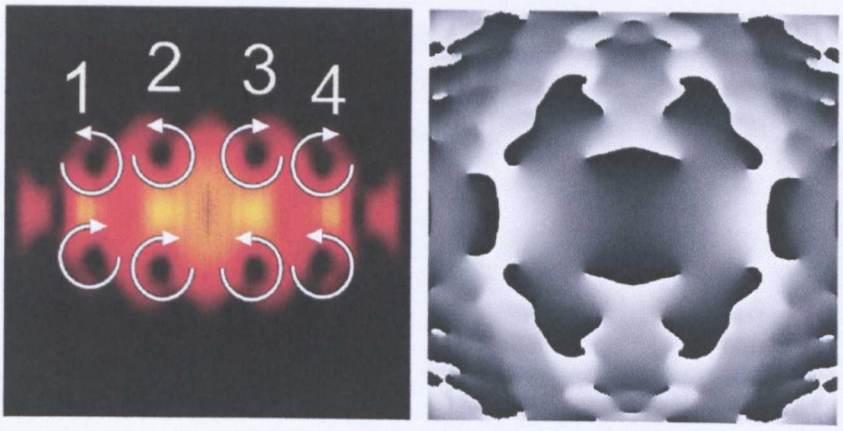

FIGURE 3.9: Vortex configuration of density at $t = 6.46$ms (left) and corresponding phase plot (white= 0, black= 2π)

IIc.

In condition of interference of merging two condensates, the possibility of forming vortices is determined by the velocity direction of superfluid. Oscillation, expansion and compression respond to case (a) and (b) in Fig.(3.10) and there is little possibility of forming a vortex. In case (c) and (d), there are enormously large possibility for the formation of vortex.

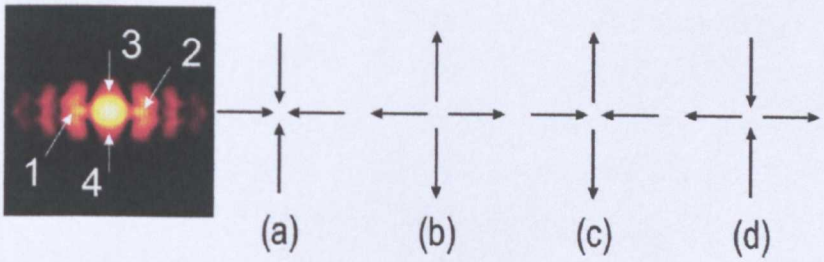

FIGURE 3.10: Four possibilities ((a), (b), (c), (d)) of velocity directions of two condensates during the process of mergence: left (right) arrow labels velocity direction arrowed separatively by 1 and 2 in the $r = 0$; up (down) arrow labels velocity directions in radial direction arrowed by 3 and 4.

3.7.4 Summary

In conclusion, we have investigated the spontaneous formation and dynamics of vortices in two merging BECs. Interference and strong nonlinear interaction play an

important role on the formation of vortices. Our results should guide experiments to produce spontaneous vortices. Meanwhile it should be taken as a model for studies of quantum turbulence and topological defect formation in mixing superfluids or classical fluids.

CHAPTER 4

Interference Properties of Colliding Bose-Einstein Condensates: from Mean Field Theory to Classical Field Theory

4.1 Introduction

Atom interferometer technology has been developed for various novel applications such as characterizing atomic and molecular properties [111], precision measurements in fundamental physics [112,113], and planetery gravity field mapping [114]. Research on matter wave interference in Bose-Einstein condensates(BECs) has significant effect on the optimization of atom interferometer techonology. Previous studies of interference phenomena in BEC were mainly based on freely expanding BECs. Experimentally, the techniques for division and manipulation of cold atom condensates have evolved from early experiments in which a magnetically trapped condensate is split with a blue-detuned laser beam [35], to later work in which a single laser beam is passed through an acousto-optic modulator [105] and most recently to an experiment in which a magnetically trapped condensate is split with an atom chip [94].

Recently, the evidence for quantum entanglement between matter waves generated by these techniques has demonstrated that the collisional four-wave mixing process is coherent. This coherent collision process indicates the applicability of quantum interference in colliding BECs [115], as has been verified in the recent experiment [103].

Thus this applicability stimulated huge interest in quantum interference and interference instability in colliding BECs. On the one hand, previous experiments and theories for the interference based on freely expanding BECs have shown some correlations between interference fringe spacing and initial separation [35], the relative phase between two separated condensates and the spatial phase of their interference [105], and uniform and nonuniform interference fringe spacing [116]. To explore properties of the interference in the colliding BECs, it might be valuable to understand previous theories based on the interference in freely expanding BECs. Also the research in the area of colliding BECs will extend further to understand the interference phenomena such as instability, coherence and decoherence, and quantum collision effect. On the other hand, some experiments in quantum interference in (quasi-)BECs have revealed that the true condensate cannot be described by a "pure" multimode coherent state [1] and it should also include the effect of quantum(or thermal) fluctuation [25, 117]. In general, the coherence of the condensate state can be suppressed during the collision process. Thus, the bare Gross-Pitaevskii equation (GPE) based on a pure coherent state can not explain completely all phenomenon that occured in experiments, in particular the case that the collision of many atoms is involved.

Indeed, a recent theoretical treatment in terms of a classical field with added quantum fluctuations (Truncated Wigner Approximation; TWA) beyond the bare

[1] If a condensate wave function is constructed by $\psi(x_1)$. Such a coherent state is the eigenstate of the annihilation operators $\hat{b}(x_1)$ at the location x_1, and can be expressed explicitly as

$$|\psi>= exp[\int dx_1 \psi(x_1)\hat{b}^\dagger(x_1)]|vac> \cdot A(\psi), \tag{4.1}$$

where the normalization factor is $A(\psi) = exp[-\frac{1}{2}\int dx|\psi(x)|^2]$. Moreover if a condensate wave function is constructed by different functional forms $\psi^{(k)}$, we can write the coherent state of condensate corresponding to the wave packet $\psi^{(k)}$ as

$$|\psi^{(k)}>= A_k e^{N^{(k)}(\hat{b}^{(k)})^\dagger}|vac>, \tag{4.2}$$

where $N^{(k)} = \int dx|\psi^{(k)}(x)|^2$ and $\hat{b}^{(k)} = \frac{1}{N^{(k)}}\int dx(\psi^{(k)})^*(x)\hat{b}(x)$. Thus the condensate state with respect to all wave packets can be described as the multiple coherent state [132]

$$|\psi>= \prod_k A_k e^{N^{(k)}(\hat{b}^{(k)})^\dagger}|vac> . \tag{4.3}$$

GPE has produced the scattering halo and predicted the unobserved phenomenon of quantum turbulence in the colliding BECs [52,118]. The method of TWA for a bosonic field originally devised for quantum optics and was first applied to BECs by Steel [53]. Later, this method was applied successfully in describing the damping of a collective excitation of a one-dimensional Bose gas [121] and disruption of reflection of three dimensional BECs [77]. Thus the introduction of quantum fluctuations to colliding BECs probes the robustness of interference, which has been exhibited previously in expanding BECs. The underlying correlations in colliding BECs, caused by quantum fluctuations, are valuable to understand experimental phenomena and the detection of coherence might have important implications for atom interferometers and quantum entanglement.

In this chapter, within the region of coherence, we show that once the initial confinement and geometry of double condensates are formed, the relative phase variation of condensates will not alter essentially the spatial fringe period, although the relative phase between the two separated condensates has a pronounced effect on the spatial phase of interference pattern. Our results demonstrate the hyperbolic relation between the absolute velocity of double condensates modulated by different trap separations, and the fringe period, which is expected for the behavior of single-particle waves. This fringe pattern is determined by the center of mass motion unaffected essentially by interactions up to the point where a nonuniform fringe pattern appears. Despite the reservation of hyperbolic fringe pattern versus displacement, due to interatomic interaction, the velocity of atom clouds is reduced a little so that the fringes are widened slightly. Moreover, we also discuss the effect of quantum noise on the low-density BECs interference in colliding condensates. The ratio of coherent atom number to incoherent atom number affects essentially the visibility and phase fluctuation of interference in the process of collision. The incoherent atom number is increased rapidly during the process of merger while it is increased much more slowly in the other process. The detailed analysis is shown through a correlation function.

4.2 Model and Numerical Methods

For the bare GPE calculation, we consider initially very dilute BECs of 4×10^5 ^{87}Rb atoms in two pancake-shaped traps with cylindrical symmetry and trap frequencies of $\omega_x = 2\pi \times 50$ rads s^{-1} (longitudinal) and $\omega_r = 2\pi \times 35$ rads s^{-1} (radial) in the x and r directions respectively, which produce two atom clouds of equilibrium peak density $n_0 = 2.7 \times 10^{11} cm^{-3}$. The two condensates are realized by the double harmonic traps in the x direction (Fig.1(a)):

$$V_d(x) = \frac{1}{2} m\omega_x^2 (x + \Delta x)^2 \qquad x < 0$$

and

$$V_d(x) = \frac{1}{2} m\omega_x^2 (x - \Delta x)^2 \qquad x \geq 0,$$

where Δx is the distance from symmetry point $x = 0$ to the center of each trap, i.e., half the BEC seperation, and in the r direction: $V(r) = \frac{1}{2} m\omega_r^2 r^2$, so that the total trap potential is $V(x, r) = V_d(x) + V(r)$. Although there are some discrepancies between our theoretical double traps and experimental traps, our double-well system can produce excellent insights for understanding substantially the process of interference of double condensates in the experiments where a single well is curved into a double well by a laser beam passing through an acousto-optic modulator (AOM) [105]. At time $t = 0$, we abruptly change the double trap into a single trap with the same frequency along the x direction (Fig.(4.1) (b)), $V_d(x, t = 0) = \frac{1}{2} m\omega_x^2 x^2$, and hence accelerate the two BECs toward one another. An interference pattern can be observed after the two condensates meet and overlap well. The amplitude and contrast of the interference pattern depends on the overlap between two condensates and our discussions in this work are based on the highest-contrast interference pattern.

Within mean-field theory, we determine the dynamics of the BEC in two dimensions by using the Crank-Nicolson method [78] to solve the time-dependent Gross-Pitaevskii equation

$$i\hbar \frac{\partial \Psi}{\partial t} = \left[-\frac{h^2}{2m} \nabla^2 + V(x, r) + \frac{4\pi a h^2}{m} |\Psi|^2 \right] \Psi, \tag{4.4}$$

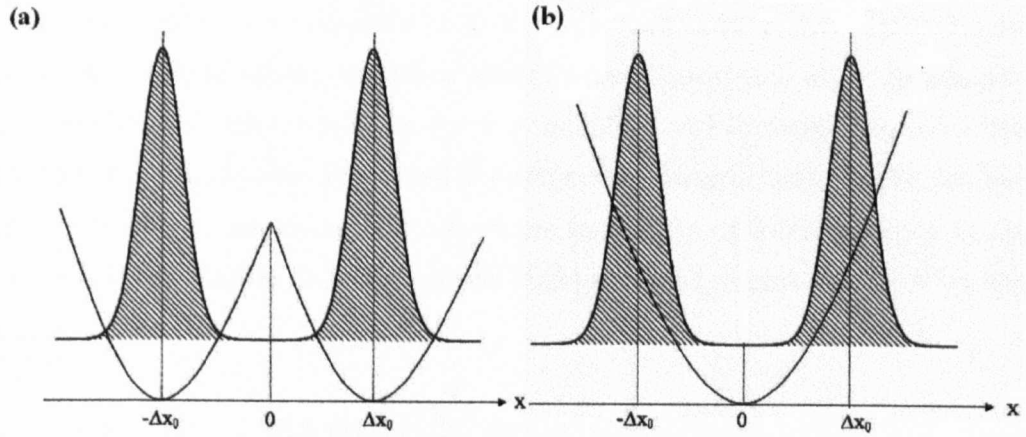

FIGURE 4.1: Solid curves show the effective potential and Shaded areas in the two pictures represent the initial atom density profile $|\Psi(x,0,0)|^2$.

where ∇^2 is the Laplacian in cylindrical coordinates, $a = 5.4$nm is the s-wave scattering length of ^{87}Rb, and $\Psi(x,r,t)$ is the axially symmetric condensate wave function at time t [2], normalized so that $|\Psi|^2$ is the number of atoms per unit volume.

In the calculation of TWA on bosonic field, our model system is a little different from the system of bare GPE calculation. Two quasi-condensates are formed by 4×10^4 ^{87}Rb atoms in a two dimensional system with trap frequencies of $\omega_x = 2\pi \times 50$rads s^{-1} and $\omega_y = 2\pi \times 35$rads s^{-1}. The separation of two quasi-condensates and the switch from initial double trap into single trap in the treatment of TWA are identical to mean field treatment. The critical difference is the coefficient of interatomic interaction $g = \frac{\hbar^2 a}{m}\sqrt{\frac{8\pi m\omega_z}{\hbar}}$ (See Appendix D) in the TWA rather than $g = \frac{4\pi a\hbar^2}{m}$ in the treatment of bare GPE. In order to avoid the effect of strong nonlinear interaction on the interference (has been discussed before) and focus on the role of quantum noise in the interference and colliding coherent atoms, we choose z-component trap frequency $\omega_z = 2\pi \times 35$rads s^{-1}.

As is well known, a uniform two-dimensional fluid cannot undergo BEC, in contrast to the three-dimensional case. However the two-dimensional system can form

[2] In the initial condition, the condensate wave function $\Psi(x,r,0)$ is symmetric about $x = 0$, i.e., $\Psi(-x,r,0) = \Psi(x,r,0)$. Due to the symmetry of $\Psi(x,r,0)$, Eq.(4.4) is symmetric about $x = 0$ at time $t = 0$. Since no external force alters the symmetry of $\Psi(x,r,t)$, the wave function $\Psi(x,r,t)$ is symmetric about $x = 0$ for all time t.

a 'quasi-condensate', i.e., condensed atoms with fluctuations [25]. We hope to understand the role of strong quantum noise in interfering two atom clouds so that two-dimensional system should be more reasonable. Additionally, we solve numerically the Eq.(4.4) by the Projected Fourth-order Runge-Kutta in the Interaction Picture (RK4IP-P) algorithm. Details of the numerical method are given in appendix C. In this calculation, we choose a two dimensional harmonic-oscillator basis using the mode expansion,

$$\Psi(x,y,t) = \sum_{n,n'=0}^{M} \alpha(n,n',t)\phi_n(x)\phi_{n'}(y), \tag{4.5}$$

where $\alpha(n,n',t)$ is the amplitude for the oscillator mode (n,n') and $\phi_n(x)$ is the nth single harmonic-oscillator wave function. The quantum fluctuations are introduced in the initial condition for $\Psi(x,y,t)$, which is given by the sum $\Psi(x,y,t=0) = \psi(x,y) + \chi(x,y)$, where $\psi(x,y)$ and $\chi(x,y)$ are, respectively, the real and virtual particle fields. We express the field of virtual particles using $\chi(x,y) = \sum_{n,n'=0}^{M} \chi(n,n')\phi_n(x)\phi_{n'}(y)$, where the amplitude in each mode is Gaussian with the properties $< \chi^*(n,n')\chi(m,m') >= \frac{1}{2}\delta_{n,m}\delta_{n',m'}$, $< \chi(n,n')\chi(m,m') >= 0$. The mean value of the total virtual population is thus $M/2$. To choose M, we confirm firstly the minimum value of mode n_1 above which the energy is larger than the chemical potential μ of groundstate. Due to the variation of traps, the potential energy is increased with $\frac{1}{2}m\omega_x^2(\Delta x)^2$ for each atom in the cloud so that the maximum value of n_{max} should satisfy $n_{max} > n_1 + \frac{m\omega_x(\Delta x)^2}{\hbar}$ where the effect of collision has been considered. Also n_{max} should be fulfilled in y direction. In order to satisfy the requirement, we choose $M \approx 11000$ in this work.

4.3 Results and discussion

4.3.1 Mean field theory for colliding BECs

The initial ground state of the atomic clouds in the double well potential is calculated numerically by an explicit imaginary time evolution [85]. For coupled condensates this method unambiguously yields the nondegenerate ground state. However, for well

separated condensates [94, 105], the ground state is virtually *degenerate* and can be written as a coherent superposition

$$\Psi(x,r) = \left(\Psi_1(x,r)e^{i\theta} + \Psi_2(x,r)\right) c \tag{4.6}$$

of the two independent condensate wave functions $\Psi_{1,2}(x,r)$ with an(a priori) arbitrary relative phase θ [4, 107, 108]. Here c is determined by the normalization condition, $\int\int |\Psi(x,r)|^2 2\pi r dx dr = N$. It is worth noticing that numerically $\theta = 0$ in the imaginary time evolution but we can choose the θ in the initial state, corresponding to the experiment where the phase in one condensate can be adjusted by applying ac Stark phase shifts [105]. This state does not correspond to definite numbers in each well. As is well known, even when the numbers in each well have definite values (Fock states), interference patterns are still observed in experiments. It is supposed that the imaging process used in the experiments, projects the state onto a coherent state with a randomly chosen phase [4, 107, 108].

To confirm the effect of an alteration of the initial condensate's phase on the matter wave interference pattern, we adjust the phase θ of the left condensate from 0 to 2π and switch rapidly the double trap into single trap at time $t = 0$ms. Thus, the potential energy of each BEC is increased by $\Delta V \approx \frac{1}{2}m\omega_x^2\Delta x^2$, causing the atoms of each condensate to move toward the areas of lower potential field with a maximum velocity of $v_x \approx \omega_x \Delta x = 2$ mms^{-1}. This evolution is equivalent to two isolated condensates with different phase moving together. As seen in the Fig.4.2, the relative phase of two condensates is changed, however the fringe period is not altered intrinsically and retains the same value of the fringe spacing, $\lambda_0 = 1.6\mu$m, indicating that the interference period is not dependent on the initial phase, as would occur in a noninteracting system. The interference plots reveal that the distance of two closest-neighbor valleys is quite similar and all equal to λ_0, which is consistent with the recent theoretical prediction that the fringes are uniform for large separations and weak interatomic interaction of the two BEC clouds [116]. Furthermore, contrasting the interference profiles from $\theta = 0$ to $\theta = 3/2\pi$, we can infer that when the initial phase θ of the left condensate is changed with a period of 2π, the atomic spatial distribution of the interference pattern is also moved forward to the positive x direction

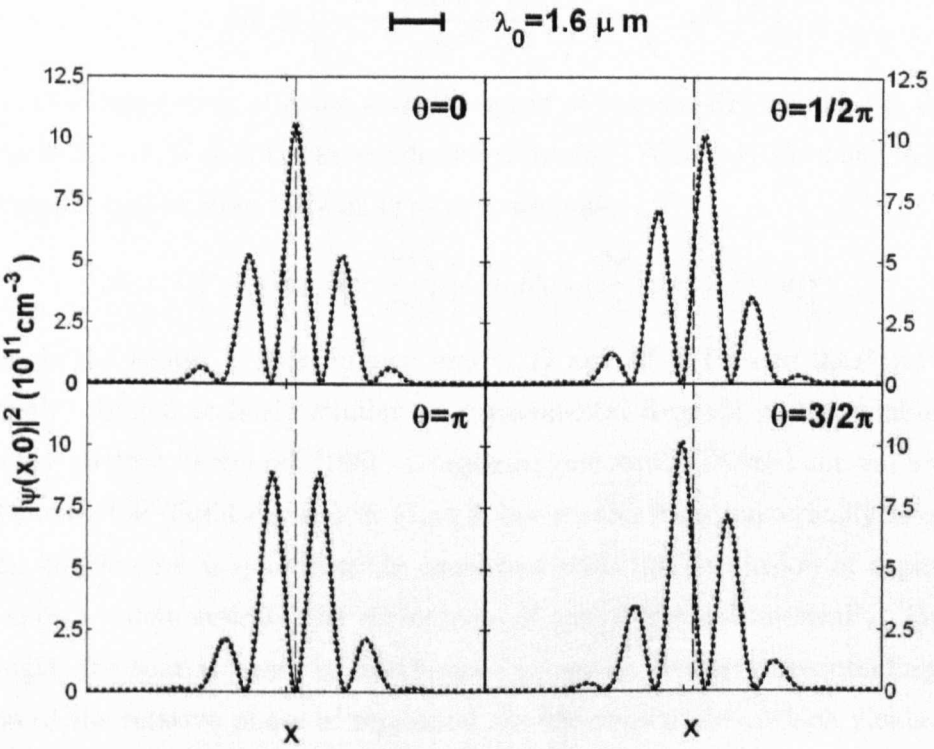

FIGURE 4.2: Dotted curves: atom density profiles of interference pattern at $t = 7.21$ms with different initial relative phase θ along $r = 0$. Solid curves: density profiles of fitting our data to experimental formula with $C = 5.625$, $D = 1$, $x_c = 0$, $\sigma^2 \approx 2/m\omega_x^2$, $\lambda = \lambda_0$, and $\theta = 0, \pi/2, \pi, 3\pi/2$ respectively.

with a length of fringe period λ_0; that is, the spatial phase of interference pattern varies with a period of 2π again as occurs in a non-interacting system. A possible theoretical interpretation in our system is that we initially show double condensates with Gaussian distribution in x direction as follows:

$$\begin{aligned}\Psi(x,t) = \Big[& A exp\left(-\frac{(x+d/2-vt)^2}{2\sigma^2}\right) exp\left(i\frac{2\pi vt}{\lambda} + i\theta\right) \\ & + B exp\left(-\frac{(x-d/2+vt)^2}{2\sigma^2}\right) exp\left(-i\frac{2\pi vt}{\lambda}\right)\Big],\end{aligned} \tag{4.7}$$

where d is the separation, v is the absolute speed of the two BECs, and λ is the wave length as well as A, B denote two condensates density. When the double condensates move together and overlap fully at $vt = d/2$, we have

$$|\Psi(x,t)|^2 = C exp\left(-\frac{x^2}{\sigma^2}\right)\left[1 + D cos(\frac{2\pi}{\lambda}(x - x_c) - \theta)\right], \tag{4.8}$$

where x_c is the center of interference and C, D are $A^2 + B^2$ and $2AB/(A^2 + B^2)$ respectively. Eq.4.8 is fairly similar to experimental formula about double BECs interference pattern in the ref. [105]. Comparing our result (Dotted curves) with theoretical prediction (Solid curves) in Fig.4.2, our results from numerically anomalous quantum interference is quantitativly consistent with the conclusion of experiments and thereby we demonstrate the correctness of this formula numerically. From another angle, the spatial phase of interference occurs to change corresponding to the variation of the relative phase of separated double condensates, which yields perfect agreement for the results of the experiment [105] where the phase sensitivity of the trapped-atom interferometer was demonstrated by applying ac Stark phase shifts to two separated condensates.

Previous experiments [35] have revealed the hyperbolic relation between interference fringe and expanding speed. In the ref. [35], the double condensate's relative speed v at any point in space is d/t, where d refers to the separation between two point-like condensates and t can be regarded as the time of atom cloud expansion. The fringe period is the de Broglie wavelength λ associated with the relative motion of atoms with mass m,

$$\lambda = \frac{h}{mv},$$

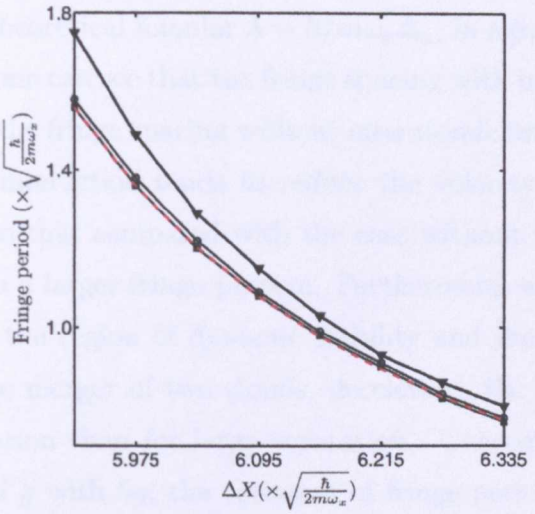

FIGURE 4.3: Fringe period versus trap displacement Δx: Dashed red curve from the results of theory formula, Open squared-lined curve without interatomic interaction, Open circle-lined curve with interatomic interaction g, and Solid triangle-lined curve for slightly larger interatomic interaction $5g$.

where h is Planck's constant. A similar conclusion has been presented in the classical interference for two colliding waves in which the interference fringe $\lambda = \frac{h}{mv}$ where v is the absolute speed for each wave. Thus this analogy should be replanted into two colliding non-interacting BECs. However, the situation might be a little complex for nonuniform interacting BECs. For the nonuniform spatial distribution of two clouds, maximum contrast of the interference occurs when clouds are fully overlapping. Distinguishing classical wave interference, the repulsive interatomic interaction will decelerate the center-of-mass motion during the overlapping of two clouds so that $v < \omega_x \Delta_x$ for $g \neq 0$.

To quantify how the absolute velocity of two BECs affects their interference fringe period, we produce a linearly increasing relative speed by regularly adjusting different Δx at the fixed frequencies [Fig.4.3]. Consequently, each condensate's velocity of propagation can be regarded approximately as $\omega_x \Delta x$. Fig.4.3 shows that increasing the separation of potential trap in the x direction tend to shorten the interference fringe spacing. It is worth putting forward that there exists an explicitly hyperbolic relation between the fringe period of the interference and Δx by contrasting the results

from simulation and theoretical formular $\lambda = h/m\omega_x\Delta_x$, in agreement with our initial prediction. However, one can see that the fringe spacing with interatomic interactions is slightly larger than the fringe spacing without interatomic interaction. This implies that the interatomic interaction tends to reduce the velocity of two clouds during the merging process so that compared with the case without interaction, the slower velocity contributes to a larger fringe pattern. Furthermore, we increase interatomic interaction a little in the region of dynamic stability and find that the interatomic interaction, during the merger of two clouds, decelerates the velocity of two clouds more for short separation than for large separation. Consequently, comparing the interference pattern of g with $5g$, the variation of fringe period is slightly larger for short separation than for large separation. Here, we perform our analysis by modeling the center-of-mass motion of one cloud as

$$\ddot{x} = -\omega_x^2 x - \eta(x)\dot{x}, \tag{4.9}$$

where

$$\eta(x) = \begin{cases} 2\gamma & |x| \leq \sigma \\ 0 & |x| > \sigma \end{cases}. \tag{4.10}$$

Here σ is the width of the cloud, and the damping γ is related to the interaction constant g and the spatial density distribution of two clouds during the mergence. Thus the stronger interatomic interaction corresponds to the stronger damping. If we suppose that at $t = 0$ we have $x(0) = \Delta > \sigma$ and $\dot{x}(0) = 0$, then the solution has the form

$$x(t) = \begin{cases} \Delta cos(\omega_x t) & 0 < t \leq t_0 \\ Ce^{-\gamma(t-t_0)}cos(\Omega(t-t_0)+\psi) & t_0 < t \end{cases} \tag{4.11}$$

where $\Omega = \sqrt{\omega_x^2 - \gamma^2}$, C and ψ are, as yet, undetermined constants and t_0 is the earliest time at which $x(t_0) = \sigma$. Calculating the velocity then gives

$$v(t) = \dot{x}(t) = \begin{cases} -\omega_x \Delta sin(\omega_x t) & 0 < t \leq t_0 \\ -\gamma x(t) - C\Omega e^{-\gamma(t-t_0)}sin(\Omega(t-t_0)+\psi) & t_0 < t \end{cases}. \tag{4.12}$$

Hence we have

$$\begin{aligned} x(t_0) = \sigma &= \Delta cos(\omega_x t_0) = C cos(\psi) \\ v(t_0) &= -\Delta\omega_x sin(\omega_x t_0) = \gamma\sigma - C\Omega sin\psi \end{aligned} \tag{4.13}$$

which can be solved to give

$$\begin{aligned} C cos\psi &= \sigma \\ C sin\psi &= \frac{1}{\Omega}\left(\omega_x\sqrt{\Delta^2-\sigma^2}+\gamma\sigma\right) \end{aligned} \tag{4.14}$$

or

$$\begin{aligned} C &= \sqrt{\sigma^2+\frac{1}{\Omega^2}\left(\omega_x\sqrt{\Delta^2-\sigma^2}+\gamma\sigma\right)^2} \\ \psi &= arctan\left(\frac{\omega_x\sqrt{\Delta^2-\sigma^2}+\gamma\sigma}{\Omega\sigma}\right). \end{aligned} \tag{4.15}$$

Now we define T to be the first time at which $x = 0$ so that

$$x(T) = 0 = Ce^{-\gamma(T-t_0)}cos(\Omega(T-t_0)+\psi) \tag{4.16}$$

so that

$$\Omega(T-t_0)+\psi = \frac{\pi}{2} \tag{4.17}$$

and

$$v(T) = -C\Omega e^{-\gamma(\frac{\pi}{2}-\psi)/\Omega} = -\Delta\omega_x f(\sigma/\Delta, \gamma/\omega_x) \tag{4.18}$$

where

$$\begin{aligned} f(\alpha,\beta) &= \sqrt{1-2\alpha\beta\sqrt{1-\alpha^2}} \\ &\times exp\left\{-\frac{\beta}{\sqrt{1-\beta^2}}\left[\frac{\pi}{2}-arctan\left(\frac{\sqrt{1-\alpha^2}+\alpha\beta}{\alpha\sqrt{1-\beta^2}}\right)\right]\right\} \end{aligned} \tag{4.19}$$

so that

$$\lambda = \frac{h}{mv(T)} = \frac{h}{m\omega_x\Delta}\frac{1}{f(\frac{\sigma}{\Delta},\frac{\gamma}{\omega_x})}. \tag{4.20}$$

From Fig.4.4, the interference pattern for $\gamma = 0$ (corresponding to $g = 0$) satisfies the hyperbolic relation. With increasing interatomic interaction (γ), fringe period is also growing for the different seperations. In addition, the variation of fringe period is larger for small separation than for large separation. These results from our analytic model are identical to our simulation, implying the applicability of this model for the colliding BECs.

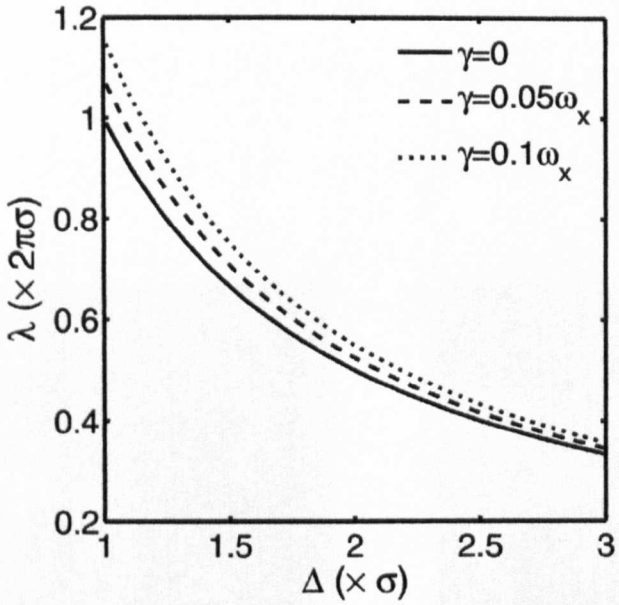

FIGURE 4.4: Fringe period versus trap displacement Δ from our analytic formula 4.20.

4.3.2 Classical field theory for colliding BECs

There is considerable interest in the way that quantum and thermal fluctuation will decrease the contrast of the interference patterns of two BECs and how the phase coherence is broken when the BECs experience impurity and dynamic instability. The following parts concentrate on the role of quantum noise in the interference pattern of low-density colliding atom clouds, using the Truncated Wigner method.

First, we show the spatial atomic density distribution from single realization in the calculation of TWA. In Fig.(4.5(a)), in presence of quantum noise, the smooth density distribution in the mean field theory is broken and there are some fragments of atom clouds in the outer region of the main clouds. As the two clouds move toward each other, the initial interference fringe is created by the overlapping wings of the two clouds (see Fig.(4.5(b))). One can see easily that the initial fringe is obviously distorted, but with more merger of the two clouds, the fringes are more stable and visible (see Fig.(4.5(c))). Since the wings of the atom clouds are composed of noncondensed atoms, the ratio of condensed atom number to noncondensed atom

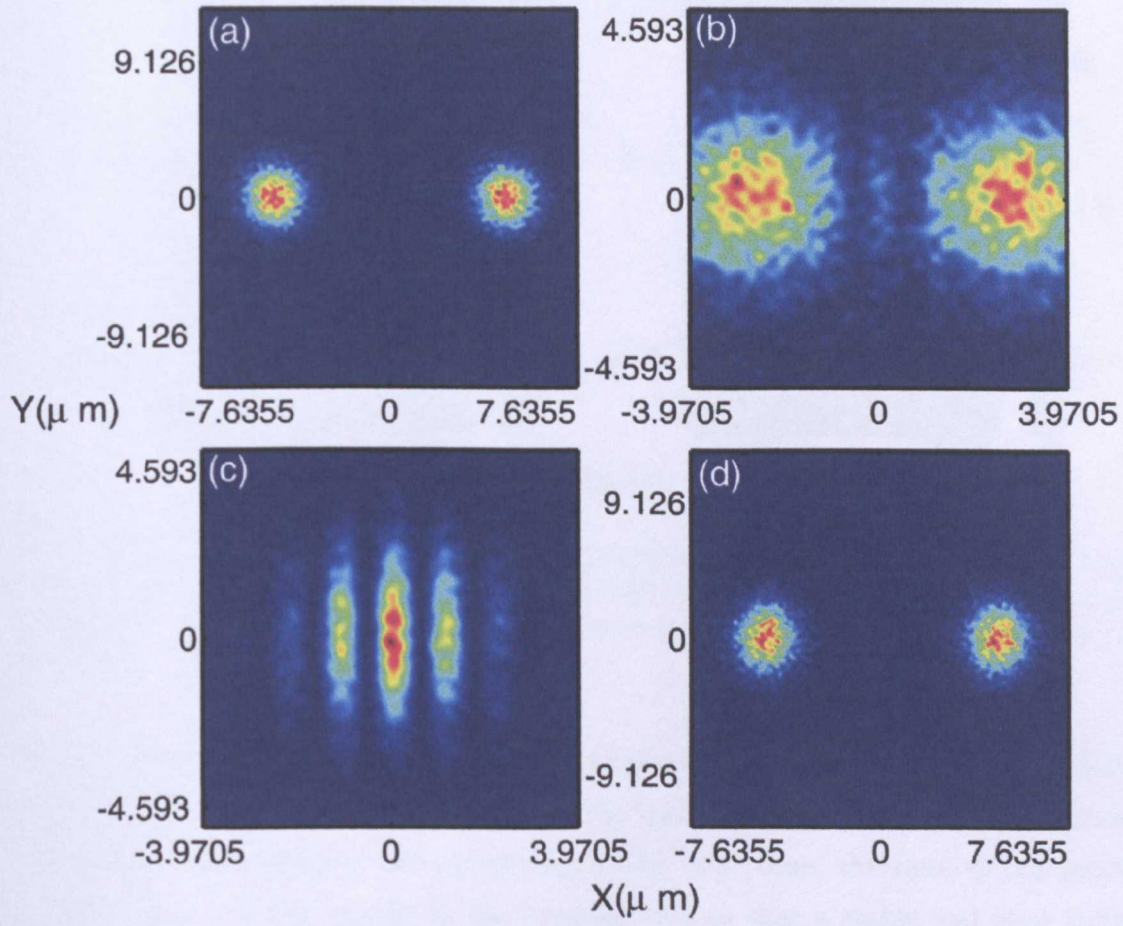

FIGURE 4.5: Jet-scale plots of atom density at times $t = 0$ (a), 3.61ms (b), 5.11ms (c), 7.81ms (d). Note the small population particles.

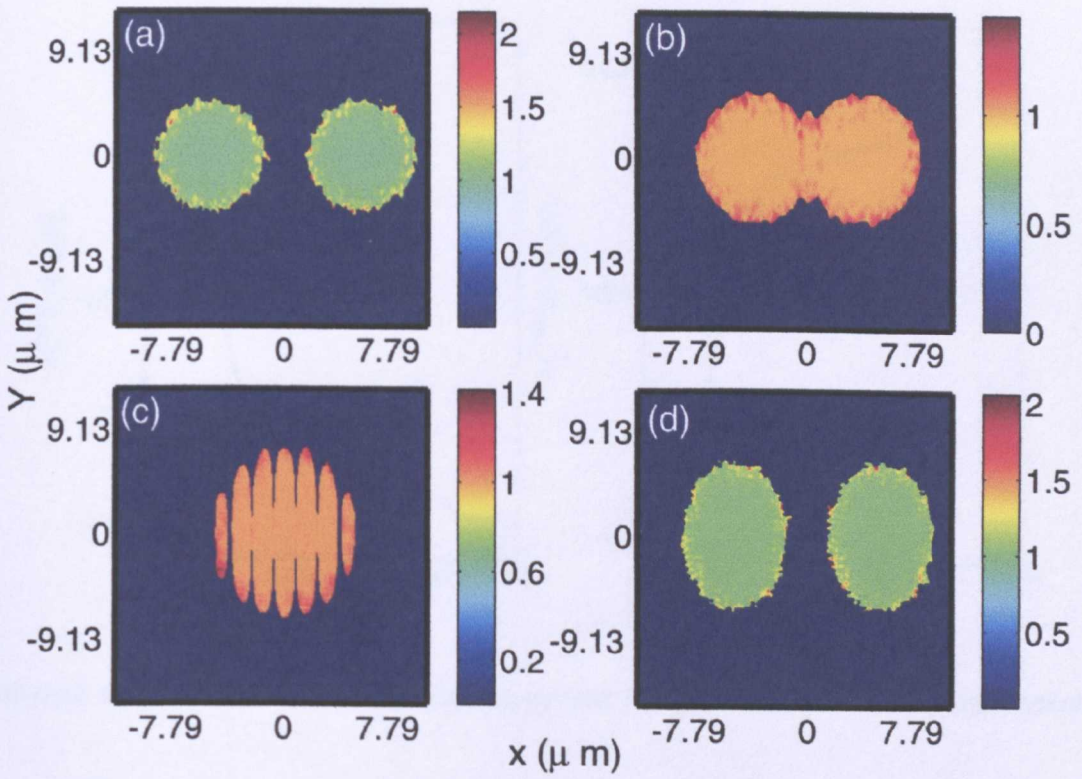

FIGURE 4.6: Normalized second-order equiposition coordinate-space correlation function $g^{(2)}(\mathbf{r}, t)$ at times 1.21ms (a), 2.11ms (b), 3.61ms (c), 5.71ms (d). Reults are shown only for those coordinate space points for which the real particle density exceeds 3.

number in the initial area of mergence is very low so that the strong phase fluctuations, derived from noncondensed atoms, distort the fringe pattern in the area. With more condensed atoms merging and interfering in the later time, the ratio of condensed atom number is rising rapidly in the merging area so that a stable and clear fringe pattern appears. Correspondingly phase fluctuations are much weaker than in the initial period of merger. Contrasting Fig.(4.5(a)) and (d), there is not much change in the shape of atom clouds. This implies that the collision and quantum noise cannot significantly alter the Bose gases in the current conditions and the interference is robust.

Furthermore, through many realizations in the calculation of TWA, the normalised second-order correlation function, coherent and incoherent atom number can be ob-

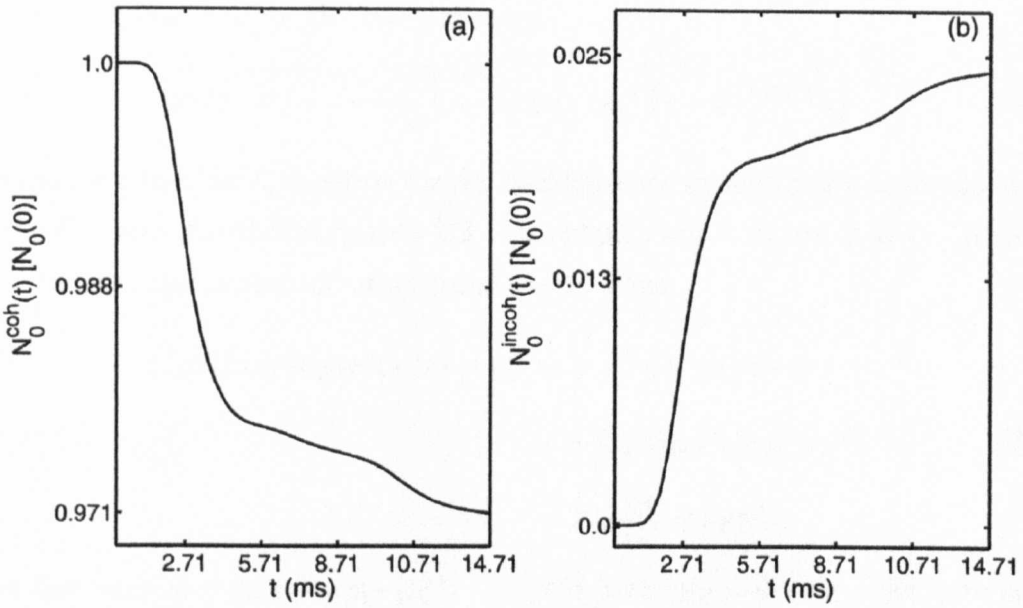

FIGURE 4.7: Total coherent (a) and incoherent (b) populations for colliding system

tained. These quantities are related directly to the measurement of experiments and thus some results might be contracted with experimental results. In particular, the second-order correlation function can be measured experimentally by detecting noise correlation [70, 71]. We evaluate these various quantum statistics of the colliding system by using an ensemble of 100 individual trajectories. Following [56], we define the normalised second-order correlation function in coordinate space

$$g^{(2)}(\mathbf{r}, l) = \frac{< \hat{\psi}_{\mathcal{P}}^{\dagger}(\mathbf{r})\hat{\psi}_{\mathcal{P}}^{\dagger}(\mathbf{r})\hat{\psi}_{\mathcal{P}}(\mathbf{r})\hat{\psi}_{\mathcal{P}}(\mathbf{r}) > (t)}{\left[< \hat{\psi}_{\mathcal{P}}^{\dagger}(\mathbf{r})\hat{\psi}_{\mathcal{P}}(\mathbf{r}) > (l)\right]^2}. \tag{4.21}$$

Now we show the underlying physical meaning of this correlation function. If the regions of coherently distributed density are concerned, we define a coherent state in coordinate space as $|\alpha(\mathbf{r}) >$ which has the form of $exp(-\int \alpha(\mathbf{r})\hat{\psi}^{\dagger}(\mathbf{r})dr)|vac >$ where α is complex function. Thus it is easily seen that $g^{(2)}(\mathbf{r}) = 1$. For a thermal state, one can define the Q-function corresponding to a density operator ρ [56]

$$Q(\alpha, \alpha^*) = \frac{1}{\pi} < \alpha|\rho|\alpha >, \tag{4.22}$$

so that the Q-function for the thermal state

$$Q_T(\alpha,\alpha^*) = \frac{1-e^{-\hbar\omega/KT}}{\pi} exp\left\{-|\alpha|^2\left(1-e^{-\hbar\omega/KT}\right)\right\}. \tag{4.23}$$

One can infer that the Q-function for the thermal state in coordinate space also satisfies the Gaussian distributed density [52]. For simplification, we use $Q_T(\alpha(x),\alpha^*(x)) \approx exp(-|\alpha(x)|^2)$ and neglect all other parameters. Thus

$$\begin{aligned} < \hat{\psi}^\dagger_{\mathcal{P}}(\mathbf{r})\hat{\psi}^\dagger_{\mathcal{P}}(\mathbf{r})\hat{\psi}_{\mathcal{P}}(\mathbf{r})\hat{\psi}_{\mathcal{P}}(\mathbf{r}) > (t) &= \int d^2\alpha(\alpha^*)^2(\alpha)^2 exp(-|\alpha|^2) \\ &= 2\int d^2\alpha|\alpha|^2 exp(-|\alpha|^2) \\ &= 2 < \hat{\psi}^\dagger_{\mathcal{P}}(\mathbf{r})\hat{\psi}_{\mathcal{P}}(\mathbf{r}) > . \end{aligned} \tag{4.24}$$

Since the integral $\int d\alpha|\alpha|^2 exp(-|\alpha|^2) = 1$, the normalised second-order correlation function in coordinate space $g^{(2)}(\mathbf{r},t) = 2$ for a thermal distributed density. If $g^{(2)}(\mathbf{r})$ is bracketed in the regime $(1,2)$, one can infer that one part of atoms at the position $\mathbf{r}$ are thermalized.

Expanding Eq.4.21 in terms of harmonic-oscillator modes and using the multimode correspondence between Wigner function averages and expectation values,

$$< \{a^r(a^\dagger)^s\}_{sym} >= \int d^2\alpha\alpha^r(\alpha^*)^s W(\alpha,\alpha^*),$$

we find that the second-order normalized correlation function in coordinate space can be expressed as

$$g^{(2)}(\mathbf{r},t) = \frac{< |\Psi(\mathbf{r},t)|^4 >_W - 2 < |\Psi(\mathbf{r},t)|^2 >_W \delta_{\mathcal{P}}(\mathbf{r},\mathbf{r}) + \frac{1}{2}\delta^2_{\mathcal{P}}(\mathbf{r},\mathbf{r})}{\left[< |\Psi(\mathbf{r},t)|^2 >_W - \frac{1}{2}\delta_{\mathcal{P}}(\mathbf{r},\mathbf{r})\right]^2}. \tag{4.25}$$

Here, the *restricted delta function* $\delta_{\mathcal{P}}(\mathbf{r},\mathbf{r}') = \sum_{j\in L}\phi^*_j(\mathbf{r}')\phi_j(\mathbf{r})$ where L means low-energy modes. The coherent and incoherent population in all modes are defined separately as

$$N_0^{coh}(t) \equiv \sum_{j\in L} | < \alpha_j(t) >_W |^2, \tag{4.26}$$

and

$$N_0^{incoh} \equiv \sum_{j\in L} < |\alpha_j(t)|^2 >_W - | < \alpha_j(t) >_W |^2 - \frac{1}{2}. \tag{4.27}$$

Some details of numerically solving the normalised second-order correlation function, coherent and incoherent atom number, are shown below. The coherent number in the numerical process is calculated as

$$N_0^{coh}(l) = \sum_{j \in L} \left| \frac{1}{N_{max}} \sum_{m=1}^{N_{max}} \alpha_j^{(m)}(l) \right|^2 \tag{4.28}$$

where N_{max} is the number of realizations (100 in our calcuations), (m) labels $m-lh$ realization, and $\alpha_j^{(m)}(t)$ means the amplitude of $j-th$ field mode at time t in $(m)-th$ realization. Also the incoherent number can be written as

$$N_0^{incoh} = \sum_{j \in L} \left(\frac{1}{N_{max}} \sum_{m=1}^{N_{max}} |\alpha_j^{(m)}(t)|^2 - \left| \frac{1}{N_{max}} \sum_{m=1}^{N_{max}} \alpha_j^{(m)}(t) \right|^2 - \frac{1}{2} \right). \tag{4.29}$$

In a similar way, one can deduce the numerical form of $g^{(2)}(\mathbf{r}, t)$.

From Fig.4.6 (a) and (d), we can see that the second-order correlation functions before and after interference are similar; that is to say, incoherent atoms occupy the edge of the cloud ($g^{(2)}(\mathbf{r}) > 1$) and coherent condensate atoms ($g^{(2)}(\mathbf{r}) = 1$) are located in the central areas of the cloud. Although the process of mergence and interference for two atom clouds is exceedingly stable, the incoherent atoms around interference valley (Fig.4.6 (b)) are expelled by condensed atoms to the edge of fringes during the process and correspondingly the visibility of the interference at the edge of condensates is much lower than in the central areas. Contrasting Fig.4.6 and Fig.4.5, it is seen that although the visibility and phase fluctuations are affected by the ratio of non-condensed atom number to condensed atom number, the detailed dynamics and correlations are very complex. The non-condensed atoms at the beginning of the merger and interference occupy the periphery of the cloud and interference valleys. Correspondingly, the visibility is very low where phase fluctuations are very strong. However, with more merger, the non-condensed atoms are expelled by the condensed atoms to the edge of the cloud so that the visibility becomes high and phase fluctuations become weak. Moreover, the effect of collision in the low-velocity and low-density condensates is shown in Fig.4.7. The fact that the number of incoherent atoms is increased significantly during the process of the collision implies

that, because in the process of collision the interaction between condensed atoms and virtual particles is much stronger than other processes, the quantum fluctuations excite more condensed atoms into non-condensed atoms in this process than other processes. Although the interference pattern is not broken by quantum fluctuations, indicating the robust character of this interference, the process of inner correlations and dynamics is very complex and can not be understood purely within mean-field theory.

4.4 Conclusion

In conclusion, in the mean-field approximation, the effect of variations of the relative phase & separation of two clouds and trap frequency on quantum interference of two BECs has been studied. Our results demonstrate the possibility of using a single-particle wave function to describe some phenomena of interference of two BECs in some experiments. Distinguishing classical wave interference, the fringe period of the colliding condensates is slightly smaller than the fringe formula from classical wave interference when the interatomic interaction becomes larger (still much smaller than the point at which instabilities occur) although the classical character of the matter wave fringe pattern is preserved. Furthermore, the Truncated Wigner method provides a description of the many-body state of two coherent BECs. The underlying dynamics of noncondensed atoms is of critical importance to understand the properties of the interference of colliding BECs.

CHAPTER 5

Quantum Transport of a 1D Degenerate Bose Gas in a Lattice: The Role of Different Quantum Fluctuations

5.1 Introduction

An optical lattice provides a versatile testbed for exploring the quantum transport of Bose-Einstein condensates (BECs) through the energy bands of a periodic quantum system. By accelerating condensed atoms through an optical lattice, experimentalists have investigated the quantum transport of BECs in periodic potentials, and successfully observed Bloch oscillations [58, 60, 61, 93]. These experiments stimulated considerable theoretical interest, which focused on damping mechanisms and the disruption of the Bloch oscillations. Much theoretical work has shown that the damping of Bloch motion is attributed to strong nonlinear interactions [62–67]. Recently, the strongly damped oscillation of a 1D Bose gas in a combined harmonic and optical lattice potential has been observed experimentally [17], under conditions for which undamped motion has been observed previously for 3D BECs [72]. Distinguishing some experiments on the damping of transport in OL [73–75], the inhibited transport of the degenerate 1D Bose gas is not due to Bloch oscillations, where transport is frustrated by Bragg reflection at the Brillouin zone boundary. Theoretical work has suggested that quantum fluctuations can strongly damp dipole oscillations of a 1D

atomic Bose gas, providing an accessible manner to explain these observations [76].

The truncated Wigner approximation (TWA) has been utilized extensively for the dynamics of BECs with quantum fluctuations. It provides a description of quantum field theory based on the Gross-Pitaevskii equation in which quantum-mechanical vacuum fluctuations are simulated by adding appropriate classical fluctuations in addition to the coherent field of the initial state of the BEC. These amount to half a quantum per degree of freedom, corresponding to the zero-point energy of the harmonic oscillator which represents each mode of the field [47]. Recently, the TWA has predicted quantum turbulence in the collisions of two condensates [47] and explained the disruption of reflecting BECs from Silicon surface [77]. In these theoretical works, zero-temperature quantum fluctuations, i.e. quantum noise, are modeled by adding, on average, half quantum into low-energy plane-wave (PW) modes, with a Gaussian distribution in amplitude. Therefore the average uniform quantum fluctuations in the coordinate space are added into the nonuniform condensates. It seems that the distribution of quantum fluctuations does not depend on the shape of atom clouds and interatomic interaction. Although the mean-field dynamics without quantum fluctuations does not depend on the choice of basis [79], initial wave functions are definitely different in the treatment of TWA when noise is added into distinct *limited* bases. These differences might cause some variation in local correlations and dynamic properties, in particular when quantum fluctuations dominate physical phenomenon. Moreover, the wave vector should not be a good quantum number for harmonically trapped condensates [80].

Although some work has been involved in the limitation of TWA [81] and the effect of cutoff [50], little work shows the discrepancies of quantum fluctuations in different forms, especially in local correlation functions and microscopic dynamics. Quantum fluctuations in correct form are of critical importance to explain some experimental phenomenon. Very recently, the distribution of quantum fluctuations of trapped atoms, determined from the Bogoliubov approximation, has shown reasonable results in the nonadiabatic dynamics and dissipative dynamics of quantum transport in optical lattices [55]. Consequently, under the ultracold condition, Bogoliubov theory might be an appropriate way to consider the effect of quantum fluctuations, which

depend on the shape of atom clouds and interatomic interaction.

Motivated by the effect of quantum fluctuation in distinct forms on the transport properties, in this chapter we demonstrate the discrepancies between the dynamics of a 1D degenerate Bose gas with respect to quantum fluctuations separately in PW and SHO modes. Despite slight difference in two trajectories of the center of mass (c.m.) motion, calculated respectively in PW and SHO modes, there exists some *intrinsic* differences which are characterized by phase coherence, number fluctuations and density distribution, especially in the short-time behavior. These discrepancies in short time indicate that local correlations depend definitely on the forms of initial quantum fluctuations. Quantum fluctuations from PW modes tends to kick some atoms out of the main part of atom cloud while quantum fluctuation from SHO modes break slightly the structure of the whole cloud. In addition, the results in PW modes do not agree completely with the observation in recent experiments [17] while the calculations respectively based on SHO and Bogoliubov modes show rational density function in agreement with experiments. Comparatively, in the same number of modes, Bogoliubov theory can offer stronger damping of c.m. trajectory than PW and SHO and thus the results from Bogoliubov theory is closer to the results of experiments [17]. This implies that quasiparticle excitation due to the strong confinement and optical lattice is critical factor in the strong damping of c.m. trajectory. Finally, to show robust proofs and a rigorous investigation of numerical methods, we contrast some results from mean-field approximate Gross-Pitaeviskii equation solved numerically by the Crank-Nicolson method [67,78,86] and TWA solved numerically by the Projected Fourth-order Runge-Kutta in the Interaction Picture (RK4IP-P) algorithm [47,84]. We also calculate statistical results using different number of realizations. Since results from 100 realizations are similar to ones from 200, we show results in this chapter with respect to 200 realizations.

5.2 Theoretical model and numerical methods

Our theoretical model is based on the experiment [17] where an array of independent 1D atom "tubes" were generated by applying a strong transverse 2D optical lattice

potential. Next, the tubes are corrugated by applying a very shallow 1D lattice along the axial direction. The dipole oscillations of atoms along the weak axial lattice were excited by suddently displacing the harmonic trap by means of applying a linear magnetic field gradient and the center-of-mass (c.m.) velocity was imaged. In the experimental condition, which the transverse 2D confining potential is much larger than the axial potential, and the chemical potential μ is smaller than the lowest energy $\hbar\omega_\perp$, contributed by 2D confining potential, the 3D dynamics of the bosonic atoms in each tube can be simplified into 1D dynamics.

We consider the potential energy profile of the 1D optical lattice is characterized by $V_{OL}(x,t) = V(t)sin^2(\pi x/d)$, where $d = 405$nm. The amplitude $V(t)$ is set to zero initially, ramped up to half photon recoil energy E_r in 2.653ms as $exp(kt) - 1$ where k is an constant determined from the ramping time, and after that remains unchanged. Consequently the total confining potential is $V(x,t) = V_{OL}(x,t) + \frac{1}{2}m\omega^2x^2$, where m is ^{87}Rb atom mass and $\omega = 2\pi \times 60$Hz is angular frequency of the harmonic trap, similar to experimental parameters [17]. At time $t = 2.653$ms, we abruptly displace the harmonic trap through a distance $\Delta x = 3\mu$m, and hence accelerate the BEC in the optical lattice.

To explore the effect of quantum fluctuation in different forms on the quantum transport of BECs, we consider four dissimilar dynamic cases. In case I, the atom condensates propagate in the optical lattice without any quantum fluctuation. Case II is allowed for the transport of condensates with 1/2 amplitude of virtual particle in every low-energy PW modes in the initial state [47, 77]. That is to say, the c-number field amplitude $\Psi(x,t)$ satisfies Gross-Pitaeviskii Equation (GPE) and in the initial condition, $\Psi(x, t = 0) = \psi(x) + \xi(x)$, where $\psi(x)$ and $\xi(x)$ are, respectively, the real and virtual particle fields. We express the field of virtual particles using $\xi(x) = \sum_{j=1}^{M} \xi_j exp(ik_jx)/\sqrt{L}$, where k_j is the wave vector in the j-th mode and the amplitude in each mode is a Gaussian random variable with the properties $< \xi_i^*\xi_j >= \frac{1}{2}\delta_{i,j}, < \xi_i\xi_j >= 0$. The mean value of the total virtual population is thus $M/2$. In case III, quantum noise is added into low-energy SHO modes. The field of virtual particles $\xi(x) = \sum_{n=0}^{M} \xi(n)\phi_n(x)$, where the amplitude in each mode is a Gaussian

random variable with the properties $< \xi^*(n)\xi(m) >= \frac{1}{2}\delta_{n,m}, < \xi(n)\xi(m) >= 0$. In case IV, we consider quantum fluctuation in the quasiparticle modes of SHO energy based on Bogoliubov theory. We approximate the field operator $\hat{\psi}(x, t = 0)$, within the Bogoliubov theory:

$$\hat{\psi}(x) = \psi_0(x)\hat{a}_0 + \sum_{j>0}[u_j(x)\hat{a}_j - v_j^*(x)\hat{a}_j^\dagger]. \tag{5.1}$$

Here ψ_0 is the ground state solution of the GPE and $< \hat{a}_0^\dagger\hat{a}_0 >= N_0$, the number of ground state atoms. we diagonalize the Bogoliubov equation,

$$\begin{aligned} \mathcal{L}u_j(x) - g_0N_0\psi_0^2(x)v_j(x) &= F_ju_j(x) \\ \mathcal{L}v_j(x) - g_0N_0\psi_0^{*2}(x)u_j(x) &= -E_jv_j(x), \end{aligned} \tag{5.2}$$

based on the SHO modes in the subspace orthogonal to $\psi_0(\xi)$ and get the quasiparticle amplitude $u_j(x)$, $v_j(x)$ and excitation spectrum E_j. The detailed analysis of the Bogliubov excitation spectra and mode functions is shown in next chapter. Here $\mathcal{L} = H_0 - \mu + 2g_0N_0|\psi_0(x)|^2$ and $H_0 = -\frac{\hbar^2}{2m}\frac{\partial^2}{\partial x^2} + V_{ext}$. Since TWA is valid providing the density of real particles is much larger than the density of virtual particles, we consider the total atom number $N = 1.0 \times 10^3$ and virtual particle number is less than 150 in all cases. Two groundstates with optical lattice amplitude $V(t) = 0$ and $E_r/2$ are calculated numerically by an explicit imaginary time propagation [85].

The dynamics of quantum transport of the atom cloud in the lattice is studied using the TWA method. The basic idea of the TWA is shown below. We expand the field operators $\hat{\Psi}(r), \hat{\Psi}^\dagger(r)$ in suitable basis, i.e., PW or SHO. In Wigner representation, some terms among Heisenberg equation of density operator $\hat{\rho}(t)$ might be truncated under certain conditions, resulting in deriving a generalized Fokker-Planck equation. The corresponding stochastic differential equation of Fokker-Planck equation is simplified into the Gross-Pitaevskii equation [55]

$$i\partial_t\Psi_W = H_0\Psi_W + g_0|\Psi_W|^2\Psi_W. \tag{5.3}$$

Here, $H_0 \equiv -\frac{\hbar^2}{2m}\frac{\partial^2}{\partial x} + V(x,t)$ and $g_0 = 2\hbar\omega_\perp a$ (see appendix D) where $\omega_\perp = 2\pi \times 38\text{kHz}$ is derived from theoretical analysis for 2D optical lattice used in the experiments

[17, 55] (see appendix E). Here $a = 5.4$nm is the s-wave scattering length of ^{87}Rb and Ψ_W is the 1D classical stochastic field. The thermal and quantum fluctuations are included in the initial state of Ψ_W in Eq.(5.3), which represents an ensemble of Wigner distributed wave functions [55]. The TWA and closely related approaches have previously been successful in describing atomic BECs [47, 53] and optical squeezing. In case IV, the initial state can be obtained through Eq.(5.1) and the excited state quantum operators $(\hat{a}_j, \hat{a}_j^\dagger)$ (for $j > 0$) are replaced by the random variables (α_j, α_j^*), obtained by sampling the corresponding Wigner distribution of the quasiparticles in a thermal bath,

$$W(\alpha_j, \alpha_j^*) = \frac{2}{\pi} tanh(\xi_j) exp[-2|\alpha_j|^2 tanh(\xi_j)], \tag{5.4}$$

where $\xi_j = E_j/2k_BT$. In this chapter, we concentrate on the case $T = 0$ where the Bogoliubov approximation can be justified.

To the precision and validity of results, different numerical methods are applied in our simulation. In case I, we obtain dynamic results by using the Crank-Nicolson method to integrate the time-dependent Gross-Pitaevskii equation. In case II, we apply a distinctive numerical method, RK4IP-P [47, 84]. In case III-IV, both methods are used in order to investigate their equivalence. For the solutions of c.m. trajectory, phase coherence and number fluctuation in truncated Wigner method, we have calculated them numerically using different numbers of realizations. We found that some results can be significantly different when the number of realizations is small, i.e. less than 50. However, all results have little difference when the number of realizations is more than 100. Here, we show all results in case II-IV based on 200 realizations. Although more realizations might increase the precision of results, it should not alter the nature of physics in our calculations.

5.3 Results and discussion

5.3.1 Analysis of groundstate

We now explore the properties of the groundstate of a quasi-1D Bose gas in a 1D elongated trap in the extreme situation where the properties of the ultracold Bose gas

are dominated by condensed atoms. This hypothesis is based on the fact that in TWA the introduction of quantum fluctuations in the equilibrium state are determined mainly by the groundstate of condensate wavefunction. Under the condition of atom number conservation, we set the nonlinear term g to the value of g_0 which is expected by experiments [17]. Some corresponding ground states versus various g are obtained through strict numerical calculations [1]. If the nonlinear term is strong and the trap

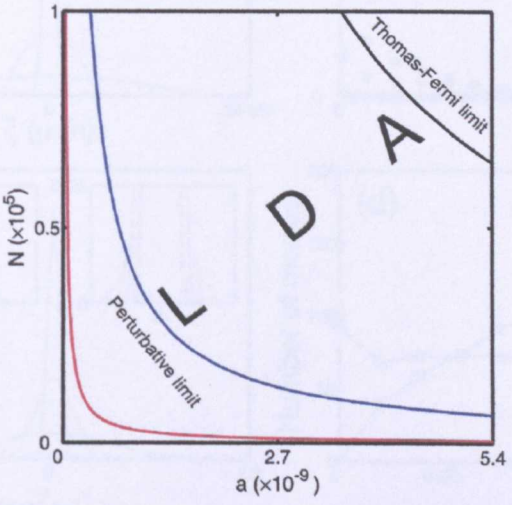

FIGURE 5.1: Parameter space for which LDA is applicable (above red line) and our method of calculations is applicable (below red line). In the regime of LDA, there are two solvable areas: perturbative limit (between red and blue line) and Thomas-Fermi limit (above black line).

potential in the axis direction is very weak, the local density approximation (LDA) should be applied to explain the properties of the groundstate. The conditions of applicability of the LDA is $(N\frac{aa_z}{a_\perp^2})^{1/3} >> 1$ where a is s-wave scattering length and a_z ($a_\perp$) is the longitude (vertical) characteristic length corresponding to the harmonic trap frequency ω_z ($\omega_\perp$) [4]. implying that the scattering length a should be large in a fixed total atom number of N. But it is not true in our case though we take the full value of g_0 and $(N\frac{aa_z}{a_\perp^2})^{1/3} \approx 13.5$. The regime of our calculations should be below the red line in Fig.5.1. With g increased from 0 to g_0, the interatomic interaction

[1] Unlike normal imaginary time method, we detect the variation of atomic number in every SHO mode rather than the variation of density until an extremely small difference at one time step among all SHO modes so that the stable groundstate is obtained.

tends to smooth the middle part of density distribution and expels the "Gaussian-shaped" part far from the center of trap (Fig.5.2(a)). Correspondingly the central

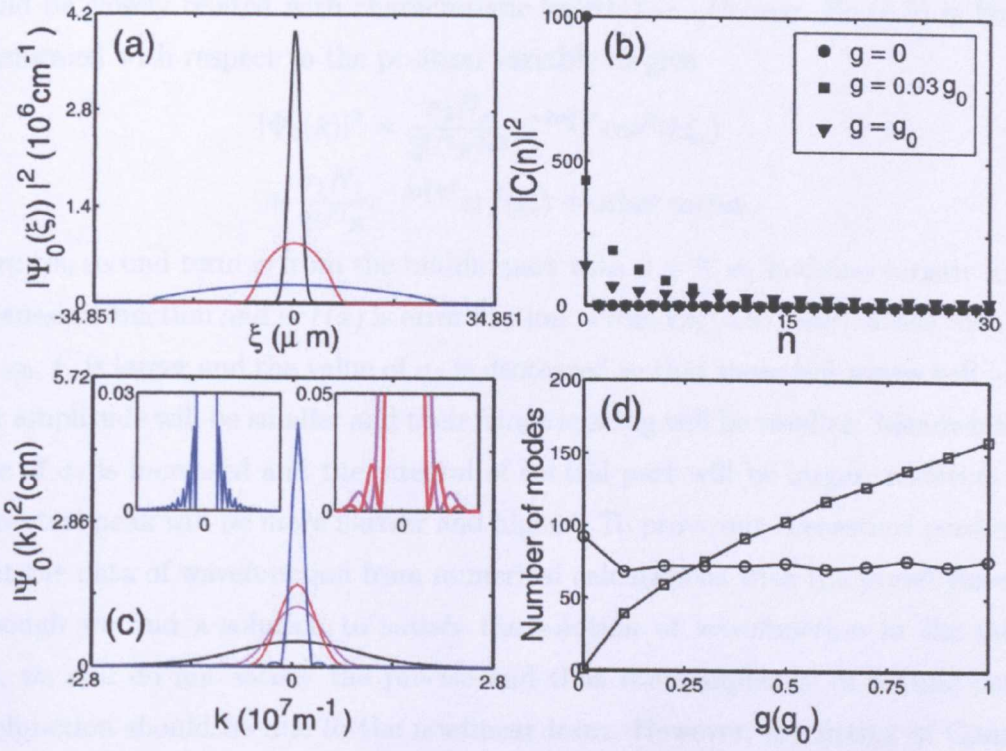

FIGURE 5.2: The configuration of groundstate density distribution (a), distribution function in SHO modes (b) and PW modes (c); (insert) momentum distribution function zoomed out. Different interaction coefficient g scaled by different color; $g = 0$(black), $0.01g_0$(magenta), $0.03g_0$(red), and g_0(blue). The number of the largest occupied modes in SHO presentation (Square) and PW presentation (Circle) versus interaction coefficient g (d).

part of momentum distribution becomes more narrow, and more importantly, there exist periodic tail waves of which the number becomes more, the amplitude becomes narrow, and the spacings become smaller (Fig.5.2(c)). To explain this phenomenon, we divide approximately the condensate into three parts:

$$\Psi_0(\xi) = \begin{cases} \frac{N_s^{1/2}}{(2\pi\sigma_2^2)^{1/4}} e^{-\frac{(\xi-\xi_c)^2}{4\sigma_2^2}} & \xi_c < \xi < \infty \\ \sum_n N_n e^{-\xi^2} H_n(\xi) & -\xi_c < \xi < \xi_c \\ \frac{N_s^{1/2}}{(2\pi\sigma_2^2)^{1/4}} e^{-\frac{(\xi+\xi_c)^2}{4\sigma_2^2}} & -\infty < \xi < -\xi_c \end{cases} \tag{5.5}$$

where N_n is determined by the atom number of the central part and character of the wave function and N_s depends only on the atom number of the side part. σ_2 should be closely related with characteristic length $l \backsim \sqrt{\hbar/m\omega}$. Eq.(5.5) is Fourier transformed with respect to the position variable to give

$$|\Psi_0(k)|^2 = \frac{\sigma_2 N_s}{2^{1/2}\pi^{3/2}} e^{-2\sigma_2^2 k^2} cos^2(k\xi_c) + \frac{\sigma_1 N_1}{2^{1/2}\pi} e^{-2\sigma_1^2 k^2} erf(\xi_c) + \text{other terms}, \tag{5.6}$$

where the second term is from the middle part with $n = 0$, σ_1 is characteristic length of Gaussian function and $erf(x)$ is error funtion. From Eq.(5.6), one can see that with $g \to g_0$, ξ_c is larger and the value of σ_2 is decreased so that more tail waves will occur, their amplitude will be smaller and their fringe spacing will be smaller. Meanwhile the value of σ_1 is increased and the integral of central part will be larger, resulting that the central peak will be more narrow and higher. To prove our theoretical prediction, we fit the data of wavefunction from numerical calculations with the preset function. Although we find a solution to satisfy the solution of wavefunction in the middle part, we still do not satisfy the precise and thus the complexity of middle part of wavefunction should be due to the nonlinear term. However, the fitting of Gaussian formula is found to yield quantitative agreement with the side part of wavefunction for varied g. In Fig.5.3, we show only the fitting results of $g = g_0$.

As is well known, there is no pure BEC state for a homogeneous one-dimensional system. Most of 1D degenerate Bose gas is treated approximately by using condensed atoms with strong fluctuations. It should be true that the properties of quantum fluctuations depend crucially on the form of interacting condensed atoms and perturbations of external potential. Due to strong confinement of optical lattice potential, the initial state should occupy more energy modes and the selection of suitable initial state is of vital importance in the dynamics of transport with respect to quantum fluctuation. We investigate the role of nonlinear terms on the wave function of ground-state and the maximum number of occupied mode respectively in the SHO and PW representation. In Fig.5.2(d), the largest occupied mode in the SHO representation increases as a power of g, while the maximum modes in the PW representation is reduced at small g and remains nearly constant at large g. It seems reasonable that

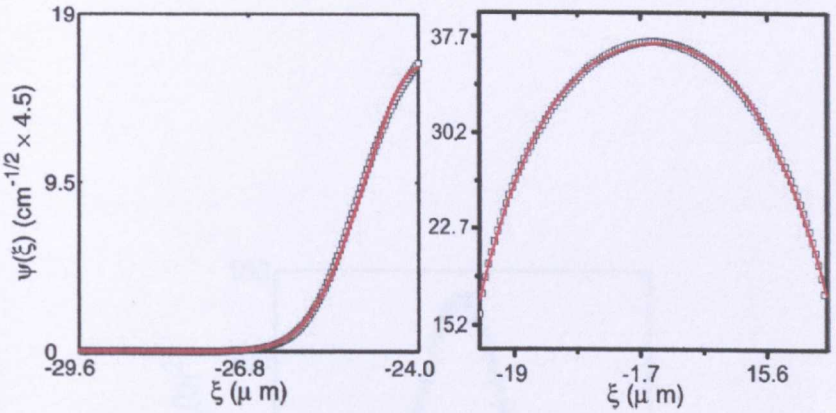

FIGURE 5.3: The configuration of groundstate wave function in $g = g_0$ (square). Data fittings from formulas: Guassian formula for side part with $N_s = 65$, $\sigma_2 = 0.63638\mu$m, $\xi_c = 24\mu$m; the formula $f(z) = y_0 + \frac{A}{w\sqrt{2\pi}} e^{-z^2/2} \left(1 + |\sum_{i=3}^{4} \frac{a_i}{i!} H_i(z)|\right)$, where $z = \frac{x-x_c}{w}$, $H_3 = z^3 - 3z$, $H_4 = z^4 - 6z^3 + 3$. The suitable parameters for middle part are $y_0 = -1.45 \times 10^5$, $x_c = 31.749\mu$m, $A = 7.7347 \times 10^8$. $w = 57\mu$m, $a3 = -1.98 \times 10^3$ and $a4 = -1.0 \times 10^4$.

the stronger interatomic interaction should excite more noise which are determined by more occupied modes in TWA. We argue that SHO representation in our system is more suitable to investigate quantum fluctuation than PW representation, especially for strong interactions. In order to include all information in low-energy modes and compare the role of the similar number of quantum noise in three different modes, we choose the number of low-energy modes as approximately 200.

5.3.2 Dynamics without fluctuation

Unlike previous work in which solitons and vortices cause the damping of the c.m. trajectory [67, 87, 88], the strong interaction here due to the lattice and the confinement does not trigger these excitations. In addition, in absence of quantum fluctuations, the extremely weak optical lattice in the axial direction can not damp the oscillation of 1D gas. Thus the dipole oscillation of the gas without fluctuation should keep the regularity that the matter wave oscillates in the space of energy modes [2]. In terms of

[2]In order to demonstrate this point of view, we define $\psi(x,t)$ as the wave function of the gas and thus $< x > (t) = \int_{-\infty}^{\infty} \psi^*(x,t) x \psi(x,t)$. In the treatment of semiclassical method, we support that the shape of wave function is not changed versus time exept its position so $< x > (t) =$

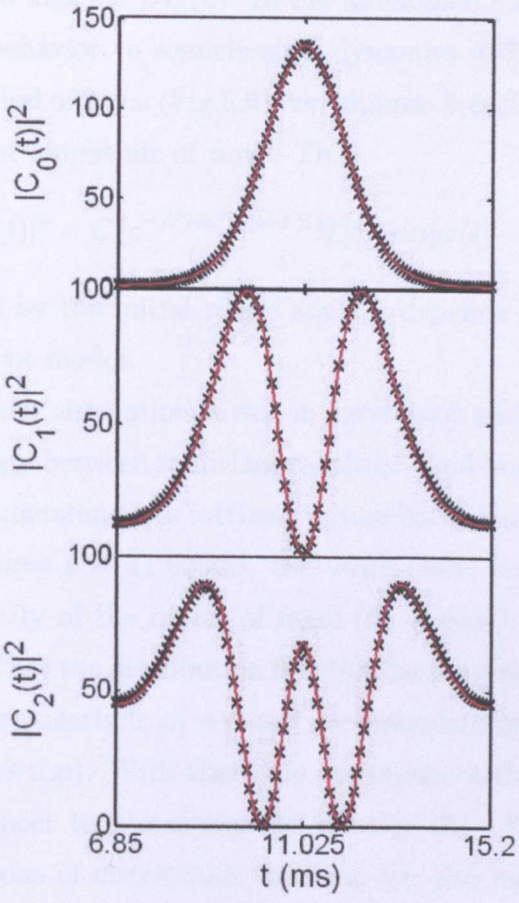

FIGURE 5.4: Plots of atom number $|C_n(t)|^2$ versus time t in one period in n-th SHO mode from simulation (Cross plots), and theoretical formula (Red line): $\omega = 2\pi \times 60$, $t' = 11.025$ms, $A = 2.1592$ for all modes and $B = 135.314078, 270.0407, 17.0516$ respectively for $n = 0, 1, 2$.

$\Psi_0(\xi) = \sum_n C_n e^{-\frac{\xi^2}{2}} H_n(\xi)$, we define

$$C_n(k) = \int_{-\infty}^{\infty} C_n e^{ik\xi} e^{-\frac{\xi^2}{2}} H_n(\xi) d\xi = (2\pi)^{1/2} C_n e^{-\frac{k^2}{2}} H_n(k) i^n, \tag{5.7}$$

we might infer that the distribution function $|C_n(k)|^2$ in SHO modes should have similar configuration to $exp(-k^2)H_n^2(k)$. In the undamped c.m. trajectory, the wave vector k has similar behavior to semiclassical dynamics [67]. Considering the cos-shaped $< x >$ with period of $2\pi/\omega$ (Fig.5.6), we suppose k with the shape of $Asin(\omega t)$, where A is the constant amplitude of wave. Thus,

$$|C_n(t)|^2 = C_n^2 e^{-\Lambda^2 sin^2|\omega(t-t')|} H_n^2(\Lambda sin[\omega(t-t')]). \tag{5.8}$$

where t' is determined by the initial phase and C_n depends critically on the initial atom number in different modes.

Fig.5.2 shows that our simulation is well in agreement with this prediction. More importantly, this analogy between semiclassical theory and quantum-mechanical simulation is *crucial* to understand the intrinsic dynamics of transport in the representation of energy. At time $t = 11.025$ms, the atom cloud moves up to the highest potential and the velocity of the center of mass (k) is nearly equal to zero. Consequently the properties that the distribution function have maximum value in $n \in even$ and minimum value, i.e., nearly 0, in $n \in odd$ are embodied by the period 2 of distribution function (Fig.5.3 top). With time, the variations of the distribution function are increased with respect to increasing the velocity (k). Even at the same time $t = 15.2$ms, the variations of distribution function are also increased versus larger n (Fig.5.3 inset). For simplification, the variations depended on k or t are named as *period*, and the variations depended on SHO mode n as *modulation period*. Also the variation of distribution function depends on the energy mode n; the larger modulation period, the larger SHO mode. It is worth *stressing* that one can identify the

$\int_{-\infty}^{\infty} \psi^*(x - Asin\omega t) x \psi(x - Asin\omega t) dx$ where we regard the variation of position of the wave function as $Acos\omega t$. It is easy to see that $< x > (t) =< x > (t = 0) - Asin\omega t$ is a periodic function. In a similar way, we define the variation of atom number in one mode n of SHO base as $< n > (t) = \int \phi_n^*(x)\psi^*(x,t)\phi_n(x)\psi(x,t)dx$ where $\phi_n(x)$ is the eigen function of single harmonic osillator in the energy level n and $\phi_n^*(x) = \phi_n(x)$. In the semiclassical method, $< n > (t) = \int \phi_n^2(x)\psi^*(x - Asin\omega t)\psi(x - Asin\omega t)dx$. Since $\phi_n(x)$ is a localized function in a limited region of space and $\psi(x - Asin\omega t)$ is a periodic function, $< n > (t)$ should be a periodic function versus time t.

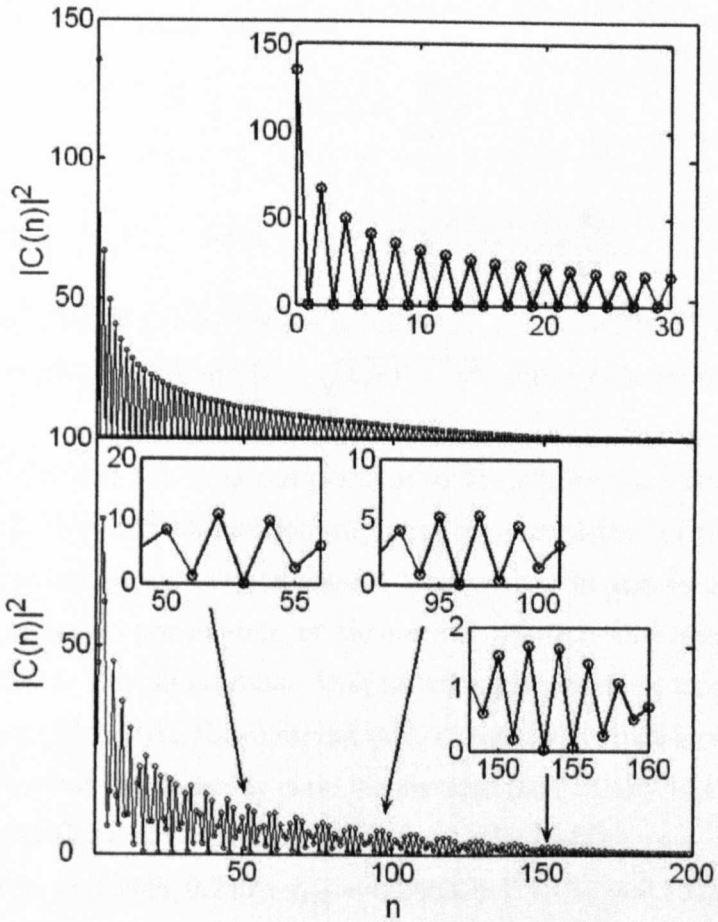

FIGURE 5.5: Plots of atom number $|C(n)|^2$ versus mode n in time $t = 11.025$ms (top) and 15.2ms (bottom); different scaled plots (Insert).

dissipative dynamics of condensates directly from distribution function in SHO modes rather than c.m. trajectory and phase coherence in the representation of coordinate or momentum.

5.3.3 Dynamics with different fluctuations

Since there is an analogy between the explanation of semiclassical dynamics and quantum mechanics on the transport of condensate without quantum fluctuation, we hope to implement further semiclassical dynamics of dissipation to explain the role of diverse quantum fluctuations on the c.m. motion. We attempt to model the c.m.

motion as a damped harmonic oscillator

$$\ddot{X}_{c.m.} + 2\gamma\dot{X}_{c.m.} + \frac{k}{m^*}X_{c.m.} = 0 \tag{5.9}$$

where

$$X_{c.m.} = < x > (t) = \frac{\int_{-\infty}^{\infty} x|\psi(x,t)|^2 dx}{\int_{-\infty}^{\infty} |\psi(x,t)|^2 dx}.$$

In underdamped case, Eq.(5.9) have a solution $X_{c.m.} = -e^{-\gamma(t-t_0)}(Acos\Omega(t-t_0) + Bsin\Omega(t-t_0))$, with $B = \frac{\gamma A}{\Omega}$ and $\Omega = \sqrt{k/m^* - \gamma^2}$, where t_0 is determined by initial phase.

From Fig.5.6(b) and (d), it is not possible to fit definite parameters through the solution of Eq.(5.9) to our simulation, implying the complexity of the role of different quantum fluctuation on the condensate transport. For convenient comparison, we show the applicable parameters of theoretical solution that satisfy the results of the first period in our simulation. Despite stronger damping amplitude prior to $t < 15.2$ms in cases II and III, the damping ratio in case IV is much larger than in cases II and III. To contrast the damping ratio versus time particularly in cases III and IV, we perform the similar definition from ref. [89], $\gamma_0 = \ln(D_0/D_1)$, $\gamma_{1/2} = \ln(D_{1/2}/D_{3/2})$. Our results give $\gamma_0 = 0.3049, 0.2309, \gamma_{1/2} = 0.2003, 0.2745, \gamma_1 = 0.1873, 0.2514$ respectively for cases III and IV. Although quantum fluctuations from the PW and the SHO modes cause stronger damping behavior in the initial movement of clouds ($\gamma_0 = 0.3049, 0.2309$), quantum fluctuations from the Bogoliubov theory trigger a stronger damping movement in a long later time ($\gamma_{1/2} = 0.2003, 0.2745, \gamma_1 = 0.1873, 0.2514$). It demonstrates directly that quantum fluctuations from Bogoliubov calculation dissipates the Bose gas more rapidly than the fluctuations from the low-energy PW and SHO modes.

Additionally, one can see in Fig.5.6(a) that there are slight differences of the trajectories of c.m. motion according to two forms of quantum noise. Does it indicates that there are completely identical dynamics in case II and III?

Since the trajectory of the c.m. motion does not reflect the local correlations and phase information of the condensate dynamics, we explore the properties of local phase coherence and number fluctuations. In order to avoid the complications arising

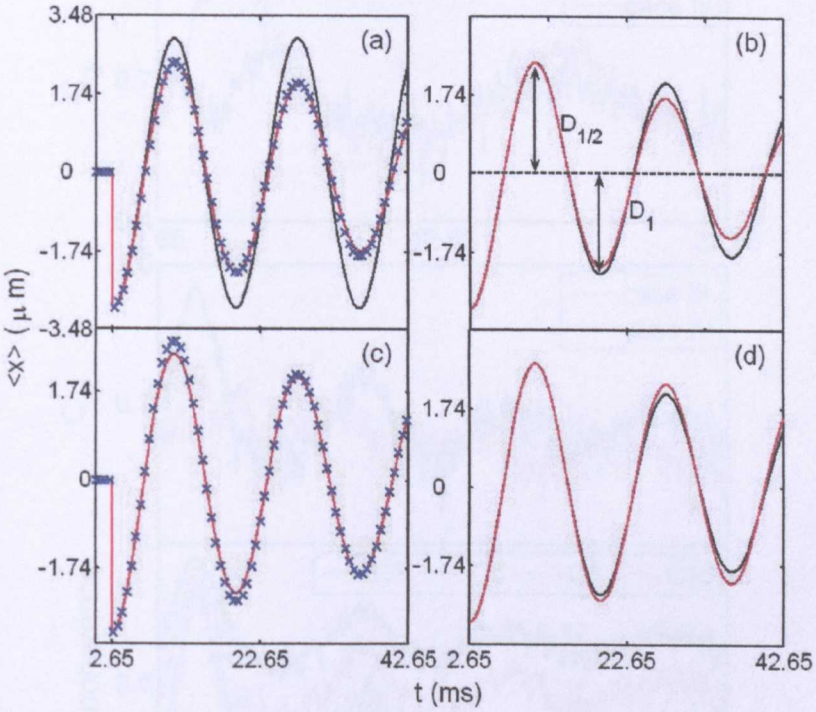

FIGURE 5.6: The plots of c.m. trajectory of BECs versus time with $\Delta x = 3\mu$m in case I (black in (a)); in case II (red in (a)); in case III (cross in (a), black in (b) and red in (c)); in case IV (cross in (c) and black in (d)). Theoretical formula: $B = 0.2218\mu$m, 0.1039μm and $\gamma = 22.88632492, 10.43904930$ separately for cases III (red in (b)) and IV (red in (d)); $\Omega = 2\pi \times 60$ and $A = 3.0\mu$m for both cases.

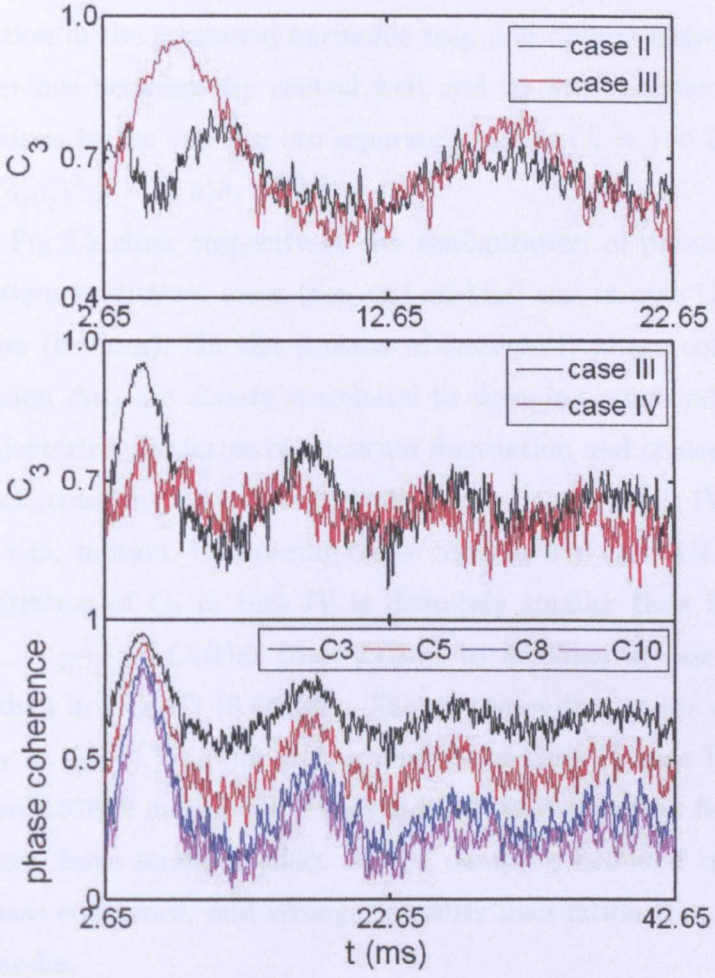

FIGURE 5.7: Plots of phase coherence in different cases with the same neighbor (top, middle) and in case III with different neighbors (bottom).

from the symmetrically ordered multimode field ψ_W [55], we define the ground state operators a_j for each individual lattice site j:

$$a_j(t) = \int_{j^{th}well} dx \psi_0^*(x)\psi_W(x,t), \tag{5.10}$$

where $\psi_W(x,t)$ is the stochastic field, determined by Eq.(5.3) and $\psi_0(x)$ is the ground-state wave function in the combined harmonic trap and optical lattice. The normalized phase coherence between the central well and its jth neighbor and the atom number fluctuations in the jth site are separately set as $C_j = | < \hat{a}_0^\dagger \hat{a}_j > |/\sqrt{n_0 n_j}$ and $\Delta n_j = [< (\hat{a}_j^\dagger \hat{a}_j)^2 > - < \hat{a}_j^\dagger \hat{a}_j >^2]^{1/2}$.

Fig.5.7 and Fig.5.8 show respectively the configuration of phase coherence and number fluctuations in distinct cases (top and middle) and in case III with different spatial neighbors (bottom). In the process of transport, phase coherence C_j and number fluctuation Δn_j are *closely* correlated to damping amplitude and damping rate of c.m. trajectories, the forms of quantum fluctuation and spatial length j. The variation of phase coherence is reduced identically in cases II, III, IV corresponding to the damping c.m. motion. Comparing phase coherence in cases III and IV (Fig.5.5 middle), the variation of C_3 in case IV is definitely smaller than in case III. The mean value $\bar{C}_3 = \frac{1}{t_2-t_1}\int_{t_1}^{t_2} C_3(t)dt$ from 2.65ms to 42.65ms in case IV is 0.62973, 5.21% smaller than in case III (0.66435). The corresponding mean value of number fluctuation $\bar{\Delta n}_3 = \frac{1}{t_2-t_1}\int_{t_1}^{t_2} n_3(t)dt$ in the interval of time in case IV is 3.94849, a little higher than 3.87862 in case III. These indicate that quantum fluctuations from Bogoliubov theory have stronger effect on the damping behavior of c.m. motion, more loss of phase coherence, and stronger number fluctuation than quantum noise in low-energy modes.

From Fig.5.7 bottom, we see that the larger the phase coherence and number fluctuation, the closer is the referred site of the condensate to the central well. However, from our full simulation, there is small difference of phase coherence from 10th neighbor to 60th neighbor while there exists an obvious difference in Δn_{20} and Δn_{50}. Since we consider only the correlation functions in left sites from central well, the number fluctuation in the site farther from the central well is affected more by low-density gas when the clouds move to right site, so that there exists large variation of fluctuations

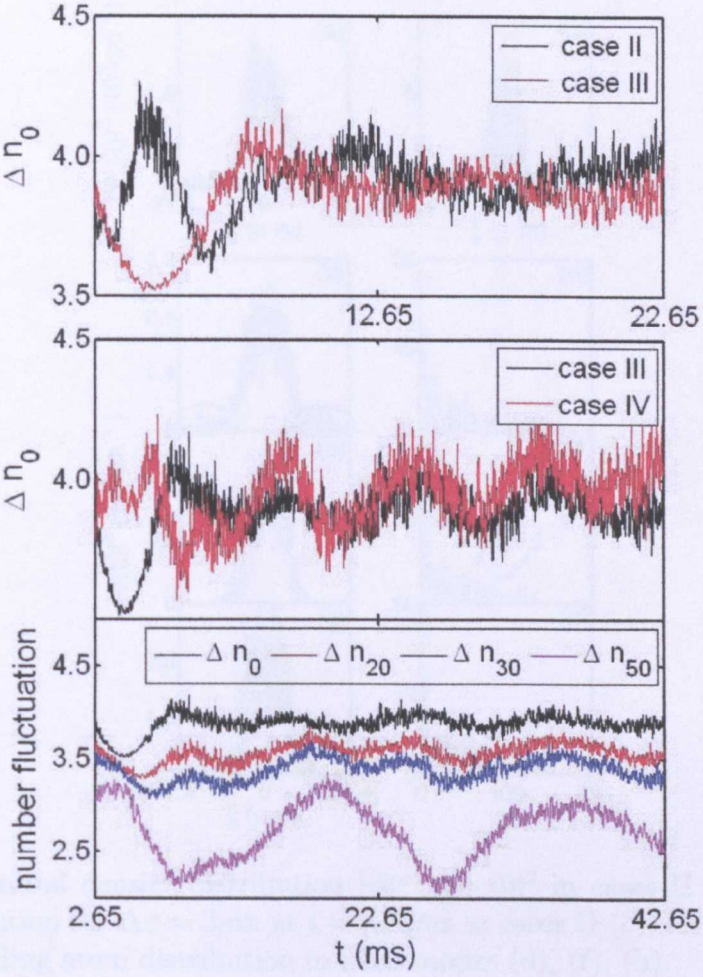
4.5
4.0
3.5
Δ n0
case II
case III
12.65
22.65
4.5
4.0
Δ n0
case III
case IV
number fluctuation
4.5
3.5
2.5
Δ n0
Δ n20
Δ n30
Δ n50
2.65
22.65
42.65
t (ms)

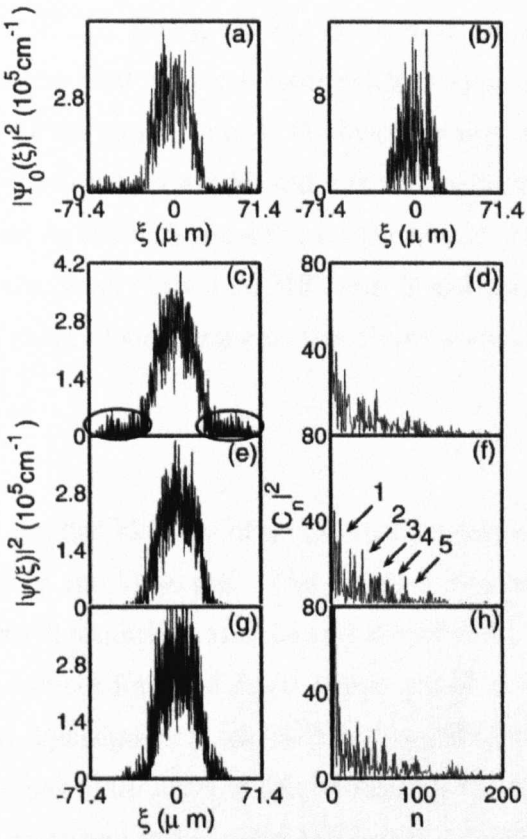

FIGURE 5.9: Initial density distribution $|\psi(\xi, t = 0)|^2$ in cases II (a) and III (b). Density distribution for $\Delta x = 3\mu$m at $t = 8.65$ms in cases II (c), III (e), IV (g), and their corresponding atom distribution in SHO modes (d), (f), (h).

over the whole real space (Fig.5.9(a)) while the space with the length, compared to the width of atom cloud, is occupied by noise from SHO modes (Fig.5.9(b)). During the transport process, one can see that some atoms, labeled by two ellipses (Fig.5.9(c)), are kicked out of main part of atom cloud in case II while it is not present in case III (Fig.5.9(d)). Correspondingly, there are a large number of atoms localized in some energy modes in case III (arrowed) while this does not occur apparently in case II (Fig.5.9(d)). Based on Fig.5.7, 5.8 and 5.9, we infer that the damping of c.m. trajectory in case II is attributed to PW-mode quantum fluctuations which tend to kick some atoms out of main region of atom cloud while SHO-mode quantum fluctuations are included to break slightly the inner configuration of condensates [3]. In addition,

[3]We also analyse dynamic distribution function from the mean of many trajectories and the

in the experiments [17], C. D. Fertig, et al. did not see a significant difference in TOF width between atoms that undergo damped harmonic motion and those that are unexcited but held for an equal time. It is obviously not true for the calculations in PW modes. Those atoms which are kicked out and occupy high-energy potential position can be observed in the experiments and the length of atom cloud should be extended. Conversely, the results based on SHO and Bogoliubov modes do not modify obviously the width of atom cloud, closer to the observation of the experiments.

5.4 Summary

In conclusion, we have studied the role of quantum fluctuations in different forms on the transport behavior of the Bose gas. The intrinsic discrepancy with respect to phase coherence, number fluctuation, and density distribution at short time behavior demonstrates that the correct forms of fluctuations are of critical importance in the dynamics of a Bose gas. Quasiparticle excitations from Bogliubov theory cause more loss of phase coherence and more number fluctuation on the damping dynamics than quantum noise from low-energy modes and condensate modes. Moreover, distribution function in SHO modes is an useful tool for identifying dissipative dynamics for trapped condensates, even in 2D and 3D system.

function shows also the results similar to Fig.5.9 but plots are more smooth

CHAPTER 6

Elementary excitations of a trapped Bose condensed gas: the role of interatomic interaction

6.1 Introduction

The term quasiparticle refers to a particle-like entity arising in a certain system of *interacting* particles. Since the quasiparticle is one of the known ways of simplifying the quantum mechanical many-body problem and is applicable to an extremely wide range of many-body systems, the quasiparticle concept is one of the most important in condensed matter physics. In the language of many-body quantum mechanics, a quasiparticle is a type of *low-lying excited* state of the system (a state possessing energy very close to the ground state energy) that is known as an elementary excitation. This means that most of the other low-lying excited states can be viewed as states in which multiple quasiparticles are present. It turns out that the interactions between quasiparticles become negligible at sufficiently low temperature, in which case we can obtain a great deal of information about the system as a whole including the flow properties and heat capacity by investigating the properties of individual quasiparticles.

The Bogoliubov approximation scheme leads naturally to a discussion of interacting bosons in terms of quasiparticles. As seen in chapter 2 the field operator for the

real bosons is expanded as

$$\widehat{\Psi}(\mathbf{r}) = N_0\widehat{a}_0 + \sum_{j>0}\left\{u_j(\mathbf{r})\widehat{a}_j^\dagger + v_j^*(\mathbf{r})\widehat{a}_j\right\}$$

where $\widehat{a}_0$ is an annihilation operator for the condensate and N_0 the number of bosons in the condensate. The mode functions u_j and v_j are chosen so that the $\widehat{a}_j$ and $\widehat{a}_j^\dagger$ operators satisfy bosonic commutation relations and such that the Hamiltonian can be written in the form

$$\widehat{H} = F_0 + \sum_{j>0} F_j\widehat{a}_j^\dagger\widehat{a}_j + \ldots$$

so that $\widehat{a}_j^\dagger$ and $\widehat{a}_j$ can naturally be interpreted as creation and annihilation operators for bosonic quasiparticles. The terms omitted in the Hamiltonian in the Bogoliubov approximation can then naturally be interpreted in terms of processes involving quasiparticle scattering.

In this chapter we study the influence of interatomic interactions on the Bogoliubov mode functions and excitation spectra of a quasi-1D bose system confined to a parabolic trap by numerically solving the Bogoliubov equation. We aim to understand the distribution of quasiparticles. The intensive analysis of excitation spectra and mode functions with respect to different nonlinear interactions are shown. Also the details of numerical calculations of the Bogoliubov spectrum in single-harmonic-oscillator basis are presented here.

6.2 Model and Numerical method

The Bogoliubov equations in real space were derived in chapter 2 and are reproduced below

$$\begin{pmatrix} \mathcal{L} - \mu + 2g|\psi_0(x)|^2 & -g(\psi_0(x))^2 \\ g(\psi_0^*(x))^2 & -(\mathcal{L} - \mu + 2g|\psi_0(x)|^2) \end{pmatrix} \begin{pmatrix} u(x) \\ v(x) \end{pmatrix} = E \begin{pmatrix} u(x) \\ v(x) \end{pmatrix} \quad (6.1)$$

where the one-body Hamiltonian is

$$\mathcal{L} = -\frac{\hbar^2}{2m}\frac{d^2}{dx^2} + \frac{1}{2}m\omega^2x^2 \quad . \quad (6.2)$$

If we work in terms of the dimensionless variables $\xi = x/x_0$, $\varepsilon = E/\hbar\omega$, $\lambda = \mu/\hbar\omega$, $\gamma = g/x_0 l\omega$, $\psi_0(\xi) = \sqrt{x_0}\psi_0(x)$ where $x_0 = \sqrt{l/m\omega}$ and $g = 2l\omega_\perp a_s$ is the effective 1d coupling constant ($\omega_\perp$ being the frequency of the transverse confining potential) then we have

$$\begin{pmatrix} -\frac{1}{2}\frac{d^2}{d\xi^2} + \frac{1}{2}\xi^2 - \lambda + 2\gamma\left|\psi_0(\xi)\right|^2 & -\gamma\left(\psi_0(\xi)\right)^2 \\ \gamma\left(\psi_0^*(\xi)\right)^2 & -\left(-\frac{1}{2}\frac{d^2}{d\xi^2} + \frac{1}{2}\xi^2 - \lambda + 2\gamma\left|\psi_0(\xi)\right|^2\right) \end{pmatrix} \begin{pmatrix} u(\xi) \\ v(\xi) \end{pmatrix} = \varepsilon \begin{pmatrix} u(\xi) \\ v(\xi) \end{pmatrix} \tag{6.3}$$

To solve Eq.(6.3), one general method is to expand the condensate wavefunction $\psi_0(\xi)$ and the amplitudes of quasiparticle $u(\xi)$ and $v(\xi)$ in a suitable basis which is related closely to the characters of these wave function. Thus we choose to use the Simple-Harmonic-Oscillator (SHO) basis $\phi_n(\xi)$ here. One might notice that it should be much easier numerically to use the plane-wave basis in our system. However, the momentum p (or wave vector k) is not good quantum number to describe the condensate confined in a harmonic trap, and fewer basis states should be neccessary in the SHO basis to give an accurate account of the Bogoliubov excitations. Now we set

$$u(\xi) = \sum_{n=0}^{\infty} a_n \phi_n(\xi) \tag{6.4}$$

$$v(\xi) = \sum_{n=0}^{\infty} b_n \phi_n(\xi) \tag{6.5}$$

so that

$$\sum_{n=0}^{\infty} a_n \left(-\frac{1}{2}\frac{d^2}{d\xi^2} + \frac{1}{2}\xi^2 - \lambda + 2\gamma\left|\psi_0(\xi)\right|^2\right)\phi_n(\xi) - \gamma\sum_{n=0}^{\infty} b_n\left(\psi_0(\xi)\right)^2\phi_n(\xi) = \varepsilon\sum_{n=0}^{\infty} a_n\phi_n(\xi) \tag{6.6}$$

$$-\gamma\sum_{n=0}^{\infty}a_n\left(\psi_0^*(\xi)\right)^2\phi_n(\xi)+\sum_{n=0}^{\infty}b_n\left(-\frac{1}{2}\frac{d^2}{d\xi^2}+\frac{1}{2}\xi^2-\lambda+2\gamma\left|\psi_0(\xi)\right|^2\right)\phi_n(\xi)$$
$$=-\varepsilon\sum_{n=0}^{\infty}b_n\phi_n(\xi) \tag{6.7}$$

which simplifies using

$$\left(-\frac{1}{2}\frac{d^2}{d\xi^2}+\frac{1}{2}\xi^2\right)\phi_n(\xi)=\left(n+\frac{1}{2}\right)\phi_n(\xi) \tag{6.8}$$

to

$$\sum_{n=0}^{\infty}a_n\left(n+\frac{1}{2}-\lambda\right)\phi_n(\xi)+2\gamma\sum_{n=0}^{\infty}a_n\left|\psi_0(\xi)\right|^2\phi_n(\xi)-\gamma\sum_{n=0}^{\infty}b_n\left(\psi_0(\xi)\right)^2\phi_n(\xi)$$
$$=\varepsilon\sum_{n=0}^{\infty}a_n\phi_n(\xi) \tag{6.9}$$

$$-\gamma\sum_{n=0}^{\infty}a_n\left(\psi_0^*(\xi)\right)^2\phi_n(\xi)+\sum_{n=0}^{\infty}b_n\left(n+\frac{1}{2}-\lambda\right)\phi_n(\xi)+2\gamma\sum_{n=0}^{\infty}b_n\left|\psi_0(\xi)\right|^2\phi_n(\xi)$$
$$=-\varepsilon\sum_{n\ 0}^{\infty}b_n\phi_n(\xi) \tag{6.10}$$

Now we premultiply each side of each equation by $\phi_j(\xi)$ and integrate over ξ to give, using the result

$$\int d\xi\phi_j(\xi)\,\phi_n(\xi)=\delta_{n,j}\qquad, \tag{6.11}$$

$$\sum_{n\ 0}^{\infty}\left(n+\frac{1}{2}-\lambda\right)a_n\delta_{n,j}+2\gamma\sum_{n\ 0}^{\infty}a_n\int d\xi\phi_j(\xi)\left|\psi_0(\xi)\right|^2\phi_n(\xi)$$
$$-\gamma\sum_{n\ 0}^{\infty}b_n\int d\xi\phi_j(\xi)\left(\psi_0(\xi)\right)^2\phi_n(\xi)=\varepsilon a_n\delta_{n,j} \tag{6.12}$$

$$
\begin{aligned}
&-\gamma\sum_{n=0}^{\infty}a_n\int d\xi\phi_j\left(\xi\right)\left(\psi_0^*\left(\xi\right)\right)^2\phi_n\left(\xi\right)+\sum_{n=0}^{\infty}\left(n+\frac{1}{2}-\lambda\right)b_n\delta_{n,j}\\
&+2\gamma\sum_{n=0}^{\infty}b_n\int d\xi\phi_j\left(\xi\right)\left|\psi_0\left(\xi\right)\right|^2\phi_n\left(\xi\right)=-\varepsilon b_n\delta_{n,j}
\end{aligned}
\tag{6.13}
$$

Now we write

$$
\psi_0\left(\xi\right)=\sum_{m=0}^{\infty}c_m\phi_m\left(\xi\right) \tag{6.14}
$$

so that

$$
\begin{aligned}
\gamma\int d\xi\phi_j\left(\xi\right)\left|\psi_0\left(\xi\right)\right|^2\phi_n\left(\xi\right)&=\gamma\int d\xi\phi_j\left(\xi\right)\left|\sum_{m=0}^{\infty}c_m\phi_m\left(\xi\right)\right|^2\phi_n\left(\xi\right)\\
&=\gamma\int d\xi\phi_j\left(\xi\right)\sum_{m=0}^{\infty}c_m\phi_m\left(\xi\right)\sum_{m'=0}^{\infty}c_{m'}^*\phi_m\left(\xi\right)\phi_n\left(\xi\right)\\
&=\sum_{m,m'=0}^{\infty}c_mc_{m'}^*\gamma\int d\xi\phi_j\left(\xi\right)\phi_m\left(\xi\right)\phi_{m'}\left(\xi\right)\phi_n\left(\xi\right)\\
&=\sum_{m,m'=0}^{\infty}c_mc_{m'}^*\Gamma_{j,m,m',n}
\end{aligned}
\tag{6.15}
$$

$$
\begin{aligned}
\gamma\int d\xi\phi_j\left(\xi\right)\left(\psi_0\left(\xi\right)\right)^2\phi_n\left(\xi\right)&=\gamma\int d\xi\phi_j\left(\xi\right)\left(\sum_{m=0}^{\infty}c_m\phi_m\left(\xi\right)\right)^2\phi_n\left(\xi\right)\\
&=\sum_{m,m'=0}^{\infty}c_mc_{m'}\gamma\int d\xi\phi_j\left(\xi\right)\phi_m\left(\xi\right)\phi_{m'}\left(\xi\right)\phi_n\left(\xi\right)\\
&=\sum_{m,m'=0}^{\infty}c_mc_{m'}\Gamma_{j,m,m',n}
\end{aligned}
\tag{6.16}
$$

$$
\begin{aligned}
\gamma\int d\xi\phi_j\left(\xi\right)\left(\psi_0^*\left(\xi\right)\right)^2\phi_n\left(\xi\right)&=\gamma\int d\xi\phi_j\left(\xi\right)\left(\sum_{m=0}^{\infty}c_m^*\phi_m\left(\xi\right)\right)^2\phi_n\left(\xi\right)\\
&=\sum_{m,m'=0}^{\infty}c_m^*c_{m'}^*\gamma\int d\xi\phi_j\left(\xi\right)\phi_m\left(\xi\right)\phi_{m'}\left(\xi\right)\phi_n\left(\xi\right)\\
&=\sum_{m,m'=0}^{\infty}c_m^*c_{m'}^*\Gamma_{j,m,m',n}
\end{aligned}
\tag{6.17}
$$

where

$$\Gamma_{i,j,m,n} = \gamma \int d\xi \phi_i(\xi)\, \phi_j(\xi)\, \phi_m(\xi)\, \phi_n(\xi) \tag{6.18}$$

Now we can use the standard form for the harmonic oscillator basis functions

$$\phi_n(\xi) = F_n \exp -\xi^2/2 H_n(\xi)$$

where $H_n(\xi)$ is the nth Hermite polynomial and

$$F_n = \frac{1}{\sqrt{2^n n! \sqrt{\pi}}}$$

is the appropriate dimensionless normalization constant. Hence we have

$$\begin{aligned} \Gamma_{i,j,m,n} &= F_i F_j F_n F_m \gamma & (6.19) \\ &\times \int d\xi e^{-2\xi^2} H_i(\xi) H_j(\xi) H_m(\xi) H_n(\xi) \quad . & (6.20) \end{aligned}$$

The Bogoliubov equations thus become

$$\sum_{n=0}^{\infty} X_{j,n} a_n - \sum_{n=0}^{\infty} Y_{j,n} b_n = \varepsilon a_n \delta_{j,n}$$

$$-\sum_{n=0}^{\infty} Y^*_{j,n} a_n + \sum_{n=0}^{\infty} X_{j,n} b_n = -\varepsilon b_n \delta_{j,n}$$

where

$$X_{j,n} = \left(n + \frac{1}{2} - \lambda\right) \delta_{j,n} + 2 \sum_{m,m'=0}^{\infty} c_m c^*_{m'} \Gamma_{j,m,m',n}$$

$$Y_{j,n} = \sum_{m,m'=0}^{\infty} c_m c_{m'} \Gamma_{j,m,m',n}$$

or, in matrix form,

$$\begin{pmatrix} X_{j,n} & -Y_{j,n} \\ Y^*_{j,n} & -X_{j,n} \end{pmatrix} \begin{pmatrix} \mathbf{a}_n \\ \mathbf{b}_n \end{pmatrix} = \varepsilon \delta_{j,n} \begin{pmatrix} \mathbf{a}_n \\ \mathbf{b}_n \end{pmatrix} \quad . \tag{6.21}$$

Normalization

As described in the last chapter, the "quasiparticle" creation and annihilation operators $\hat{a}_j$, $\hat{a}_j^\dagger$ obey boson commutation relations which lead to the constraints on $u_j(r)$ and $v_j(r)$

$$\sum_j [u_j(r)u_j^*(r') - v_j(r)v_j^*(r')] = \delta(r, r') \tag{6.22}$$

$$\sum_j [u_j(r)v_j^*(r') - v_j^*(r)u_j(r')] = 0 \tag{6.23}$$

$$\sum_j [u_j^*(r)v_j(r') - v_j(r)u_j^*(r')] = 0. \tag{6.24}$$

Here we will deduce the normalization condition for the mode functions in our numerical calculation through Eq.(6.22). By analogy with $\psi_0(x)$, we expand $u^{(j)}(r)$ amd $v^{(j)}(r)$ (notice that to demonstrate the application of the normalization condition in a numerical calculation clearly, we have changed the notation $u_j(r)$ and $v_j(r)$ into $u^{(j)}(r)$ and $v^{(j)}(r)$) in the SHO basis so that

$$\begin{aligned} u^{(j)}(r) &= \sum_i a_i^{(j)} \phi_i(r) \\ v^{(j)}(r) &= \sum_i b_i^{(j)} \phi_i(r) \end{aligned} \tag{6.25}$$

where $a_i^{(j)}$ is the $j-$th Bogoliubov mode amplitude coefficient of the SHO eigenstate $\phi_i(r)$; that is to say, every Bogoliubov mode is expanded in the SHO basis. Inserting Eq.(6.25) into Eq.(6.22), one can obtain

$$\sum_j \sum_i (|a_i^{(j)}|^2 - |b_i^{(j)}|^2) \phi_i^*(r)\phi_i(r') = \sum_i \phi_i^*(r)\phi_i(r'). \tag{6.26}$$

One can see easily that the condition Eq.(6.26) must be fulfilled as

$$\sum_j (|a_i^{(j)}|^2 - |b_i^{(j)}|^2) = 1 \tag{6.27}$$

for every SHO basis state. Compared with the matrix (6.21) for Bogoliubov equation, one can find that the normalization condition for the mode functions $a_n^{(i)}$, $b_n^{(i)}$ for every

energy level i must satisfy

$$\sum_n (|a_n^{(i)}|^2 - |b_n^{(i)}|^2) = 1. \tag{6.28}$$

The integrals c_m and Γ_{ijmn} which are needed for the matrix elements were calculated using the Gauss-Hermite quadrature method [130]. The matrix diagonalization was carried out using the standard EISPACK routines.

6.3 Results and Discussion

The standard structure of the matrix in Eq.(6.21), which is composed of four real symmetric tridiagonal matrices $X_{j,n}, -X_{j,n}, Y_{j,n}, -Y_{j,n}$ providing the phase of condensed atomic wave function is zero, determines essentially the Bogoliubov spectra and mode functions. In principle, the mean-field nonlinear terms $2\hbar\omega_\perp a|\psi(x)|^2$ influences the structure of matrices $X_{j,n}, Y_{j,n}$, which has internal relation with the Bogoliubov spectra and mode functions. Thus the role of the nonlinear term in the excitation spectra and mode functions becomes an immediate requirement of explaining some elementary excitation phenomena in cold atoms. To discuss conveniently

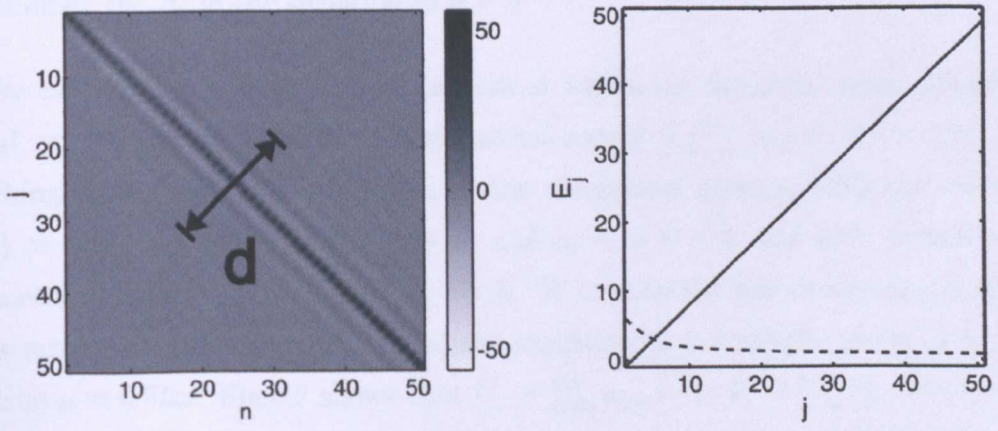

FIGURE 6.1: The plot of the characterized matrix $X_{j,n}$ (left) in the case of $g = 0.05g_0$; plots of two energy parts (right), $\left(n + \frac{1}{2} - \lambda\right)$ (solid line) and $\sum_{m,m'=0}^{\infty} c_m c_{m'} \Gamma_{j,m,m',j}$ (dash line).

our results, we define some quantities to characterize the matrix $X_{j,n}$ and mode functions. In Fig.6.1, we show the distribution of elements in the real matrix $X_{j,n}$ (Fig.6.1

Left) [1] and the distribution of two parts of its diagonal elements $\left(n+\frac{1}{2}-\lambda\right)\delta_{j,n}$ and $\sum_{m,m'\ 0}^{\infty} c_m c_{m'} \Gamma_{j,m,m',j}$ (Fig.6.1 Right). As will be seen in this part, the matrix $X_{j,n}$ and its diagonal elements play a crucial role in the excitation spectra and mode functions. In general, the width of nonzero elements in (sub)diagonal parts d (labeled in Fig.6.1 left) and the width of high-amplitude modes (labeled in Fig.6.5) grow with increasing interatomic interaction. Moreover, the competition between $\left(n+\frac{1}{2}-\lambda\right)$ and $\sum_{m,m'=0}^{\infty} c_m c_{m'} \Gamma_{j,m,m',j}$ leads to some odd excitation energy and mode functions.

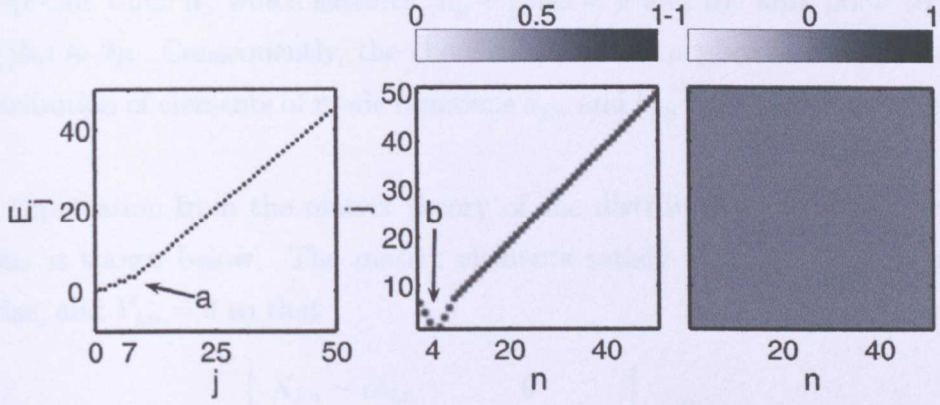

FIGURE 6.2: The plots of Bogoliubov excitation spectrum E_j (Left), mode functions a_n (middle) and b_n in the situation of $g = 0$

We explore firstly an extreme condition in which the nonlinear term $g|\psi_0(x)|^2$ is trivial, specifically the interatomic interaction energy $\frac{g}{2}\int_{-\infty}^{+\infty}|\psi_0(x)|^4 dx << \hbar\omega$. The matching groundstate wave function of the condensed atoms fulfills the criterion, $\psi_0(x) \approx c_0\phi_0(x) + c_2\phi_2(x) \ \ \forall\ c_0 >> c_2$ and $c_n = 0\ \forall\ n \in odd$ with regard to the symmetry of the wave function about $x = 0$. To explore the role of chemical potential in the eigenvalue and eigenstate, we adjust artificially $\mu = 4.9992\hbar\omega$ much larger than the true $\mu \approx 0.5\hbar\omega$. Fig.6.2 shows that $U_j = \sum_n a_{j,n} = 1$, $V_j = \sum_n b_{j,n} = 0$ for each excitation energy E_j so that the mode function $a_{j,n}$ for every j is identical with Kronecker delta function. Apparently $d' = 1$ for U_j in this case as well as $d = 1$. The fact that the amplitude of mode functions is identical for all modes implies

[1] Since the global phase θ in condensed wave function $\psi_0(\xi)$ cannot affect the elementary excitation spectra, for simplification, we choose $\theta = 0$. One notices that mode functions are Gauge invarient only for the number-conserving Bogoliubov equation [32] but it is not true for the normal Bogoliubov equation.

that quantum noises from TWA based on Bogoliubov modes do not depend on the mode functions, and is determined merely by the number of modes. This property coincides with the TWA used in ref. [47, 77]. In addition, the positions of the kink and V-junction, arrowed separately by a and b in Fig.6.2, demonstrate that the linear structure of the excitation spectra and the distribution of mode elements is broken with respect to the introduction of distinct chemical potential. Indeed, for some n of which $(n+\frac{1}{2})\hbar\omega < \mu$, the value of the abscissa in the position of V-junction refers to the specific value n_μ which satisfies $(n_\mu+\frac{1}{2})\hbar\omega \approx \mu$ and the kink point to n' with $(n'+\frac{1}{2})\hbar\omega \approx 2\mu$. Consequently, the chemical potential μ plays a role in displacing the distribution of elements of mode functions $a_{j,n}$ and $b_{j,n}$ in the direction of abscissa axis n.

An explanation from the matrix theory of the distribution of elements of mode functions is shown below. The matrix elements satisfy $X_{j,n} \neq 0 \ \forall \ j = n$ and 0 otherwise, and $Y_{j,n} = 0$ so that

$$\begin{vmatrix} X_{j,n} - \epsilon\delta_{j,n} & 0 \\ 0 & -X_{j,n} - \epsilon\delta_{j,n} \end{vmatrix} = 0. \tag{6.29}$$

Eq.(6.29) can be simplified as

$$(X_{1,1}-\epsilon)(X_{2,2}-\epsilon)\cdots(x_{n_{max},n_{max}}-\epsilon)(-x_{n_{max},n_{max}}-\epsilon)\cdots(-X_{1,1}-\epsilon)(-X_{2,2}-\epsilon) = 0, \tag{6.30}$$

and correspondingly the eigenvalue $\epsilon = \pm X_{n,n}$. According to the orthogonality and normalization of a_n and b_n, for a given value of n' $\epsilon = X_{n',n'}$, $a_n = 1 \ \forall \ n = n'$ and $a_n = 0$ otherwise while $b_n = 0$ for all values of n.

The next case, in which $g = 0.05g_0$ (a little stronger than the above case), is considered and the matching groundstate wave function $\psi_0(x) = \sum_n c_n\phi_n(x)$ where $c_0 \approx 2.04c_2$, $c_0 \approx 6c_4$, and $c_n \approx 0 \ \forall \ n \neq 0, 2, 4$. Our simulations show the width $d \approx 8$ for $X_{j,n}$. Since $|c_4|^2$ is much smaller than $|c_0|^2$, for brevity we ignore its contribution to $\Gamma_{j,n}$. Thus the analytic formula for diagonal elements and subdiagonal elements

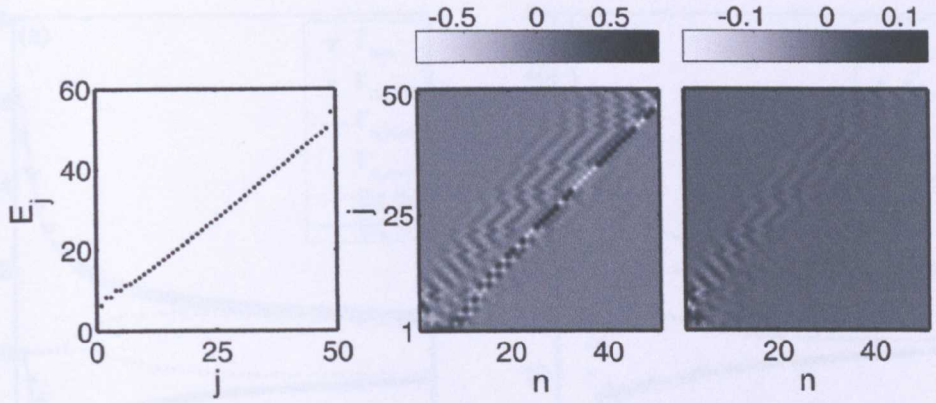

FIGURE 6.3: The plots of Bogoliubov excitation spectrum E_j (Left), mode functions a_n (middle) and b_n in the situation of $g = 0.05g_0$.

are respectively

$$\begin{aligned}\Gamma_{n,n} &= \sum_{i,j} c_i c_j \Gamma_{i,j,n,n} \\ &= \frac{\gamma\Gamma(n-\frac{3}{2})}{\Gamma(n+1)2^{3/2}\pi}\left[2(c_0^2+c_2^2)(n-\frac{1}{2})(n-\frac{3}{2})\right. \\ &\left.+(\frac{3}{4}c_2)^2+(c_2^2+\frac{c_0c_2}{\sqrt{2}})(n-\frac{3}{2})\right]\end{aligned} \tag{6.31}$$

$$\begin{aligned}\Gamma_{n,n+2} = \sum_{i,j} c_i c_j \Gamma_{i,j,n,n+2} &= \frac{\gamma\Gamma(n-\frac{1}{2})}{\Gamma(n+1)2^{3/2}\pi[(n+2)(n+1)]^{1/2}} \\ \times\left[2(c_0^2+c_2^2)(n^2-\frac{1}{4})+\frac{15}{16}c_2^2+3(c_2^2+\frac{c_0c_2}{\sqrt{2}})(n-\frac{1}{2})\right],&\end{aligned} \tag{6.32}$$

where $\Gamma(x)$ function satisfies the property $\Gamma(x+1) = x\Gamma(x)$.

Fig.6.3 (a) shows that $\Gamma_{n,n}$ and $\Gamma_{n,n+2}$ from our simulations are identical to the semianalytic formulas (6.31), (6.32). A slight difference for $\Gamma_{n,n+2}$ in the regime of small n can be found while there does not exist for $\Gamma_{n,n}$ in the whole regime. It is derived from the fact that, due to $|c_0|^2 >> |c_4|^2$, the contribution of c_4 to $\Gamma_{n,n}$ can be neglected safely but the terms including c_4 in $\Gamma_{n,n+2}$ might not be neglected in that c_2 is not much larger than c_4. However, the contribution of c_4 for $\Gamma_{n,n}$ and $\Gamma_{n,n+2}$ is reduced rapidly with increasing n and there is little difference between the fomulae (6.31), (6.32) and our simulations for large n. Although we can not give the confirmed value of d' for mode functions $a_{j,n}$, $b_{j,n}$ from Fig.6.3, it can be seen that d' grows with

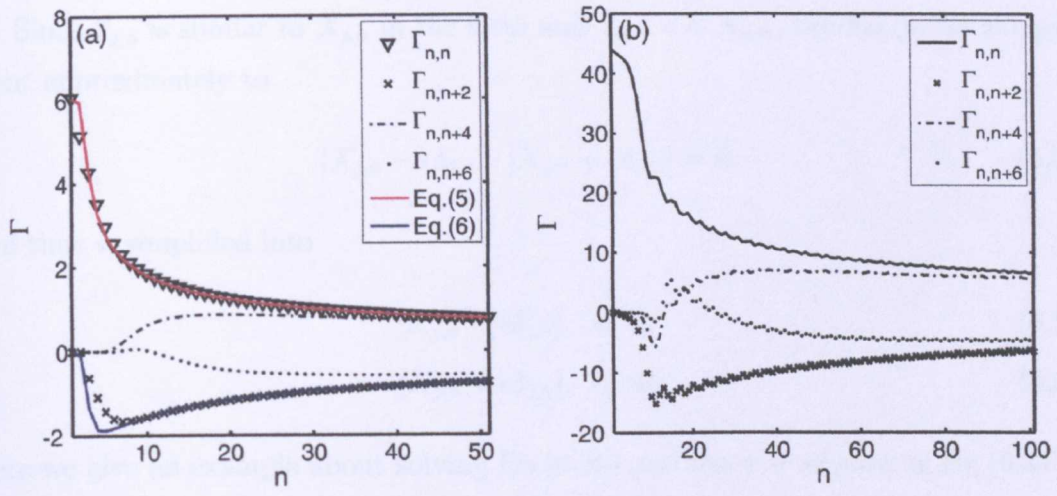

FIGURE 6.4: The plots of $\Gamma_{j,n}$ from our simulation and corresponding fittings from our fomulars for $\Gamma_{n,n}$ and $\Gamma_{n,n\pm 2}$ in the situation with $g = 0.05g_0$ (a); The plots of $\Gamma_{j,n}$ from our simulation in the situation with $g = g_0$ (b).

increasing d. This demonstrates that the stronger interatomic interaction in Bose gas tends to produce some excitations occupying more oscillator modes.

An explanation from matrix theory for $g = 0.05g_0$ is shown below. To simplify the complex Bogoliubov matrix and confirm the validity of conclusions, we suppose that the elements of Bogoliubov matrix $X_{n,n-2}, X_{n,n}, X_{n,n+2}$ $(Y_{n,n-2}, Y_{n,n}, Y_{n,n+2})$ are nonzero and otherwise $X_{j,n} = 0$ $(Y_{j,n} = 0)$. We also assume $X_{n,n-2} = X_{n-2,n} << X_{n,n}$ $(Y_{n,n-2} = Y_{n-2,n} << Y_{n,n})$ and $Y_{n,n} << X_{n,n}$. In general, the constraint conditions are valid for the case in which the condensate wave function occupies a limited number of harmonic modes. The Bogoliubov equation (6.21) is written into

$$\begin{vmatrix} X_{j,n} - \epsilon\delta_{j,n} & -Y_{j,n} \\ Y_{j,n} & -X_{j,n} - \epsilon\delta_{j,n} \end{vmatrix} = 0, \tag{6.33}$$

and also

$$|X_{j,n} - \epsilon\delta_{j,n}| \cdot |X_{j,n} + \epsilon\delta_{j,n}| - |Y_{j,n}|^2 = 0. \tag{6.34}$$

If we define ϵ' as the eigenvalue of $|X_{j,n} - \epsilon'\delta_{j,n}| \cdot |X_{j,n} + \epsilon'\delta_{j,n}| = 0$, $|Y_{j,n}|^2$ in the Eq.(6.34), contributed by the nonlinear interaction, plays a role in "displacing" the eigenvalue ϵ'.

Since $Y_{j,n}$ is similar to $X_{j,n}$ in the form and $Y_{n,n} << X_{n,n}$, the Eq.(6.34) is equivalent approximately to

$$|X_{j,n} - \epsilon\delta_{j,n}| \cdot |X_{j,n} + \epsilon\delta_{j,n}| = 0, \tag{6.35}$$

and thus is simplified into

$$|X_{j,n} - \epsilon\delta_{j,n}| = 0 \tag{6.36}$$

$$|X_{j,n} + \epsilon\delta_{j,n}| = 0. \tag{6.37}$$

Here we give an example about solving Eq.(6.36) and the way of solving Eq.(6.37) is similar. Use Laplace's formula to expand Eq.(6.36) so

$$(X_{1,1} - \epsilon)|M_{1,1}| + X_{1,3}|M_{1,3}| = 0, \tag{6.38}$$

where $M_{j,n}$ is the minor of matrix $X_{j,n}$. If we define ϵ'' as the eigenvalue of $(X_{1,1} - \epsilon'')|M_{1,1}| = 0$, the term of $X_{1,3}|M_{1,3}|$ in Eq.(6.38) plays the role in "displacing" the eigenvalue ϵ''. Since $X_{1,3} << X_{1,1}$ and $|M_{1,3}| << |M_{1,1}|$, Eq.(6.38) is changed into

$$(X_{1,1} - \epsilon)|M_{1,1}| \approx 0. \tag{6.39}$$

In a similar way, one can deduce

$$(X_{1,1} - \epsilon)(X_{2,2} - \epsilon) \cdots (X_{n_{max},n_{max}} - \epsilon) \approx 0. \tag{6.40}$$

Eq.(6.40) implies that when the excitation spectra with respect to weak nonlinear interaction are perturbed around the excitation spectra in absence of the nonlinear interaction. Furthermore, we give a deduction, which is not rigorous in mathematics, about the eigenvector equations. The eigenvector equations are written as

$$\begin{aligned} &X_{j,n}a_{n-2}\delta_{j,n-2} + (X_{j,n} - \epsilon)a_n\delta_{j,n} + X_{j,n}a_{n+2}\delta_{j,n+2} + \\ &Y_{j,n}b_{n-2}\delta_{j,n-2} + Y_{j,n}b_n\delta_{j,n} + Y_{j,n}b_{n+2}\delta_{j,n+2} = 0 \quad \forall j \in (1, n_{max}). \end{aligned} \tag{6.41}$$

If we ignore the contribution of $Y_{j,n}$, Eq.(6.41) becomes the standard triangular equations. Thus for a given eigenvalue $\epsilon_{j'}$ close to $X_{j',j'}$, a_j is nonzero for $j = j' - m, \cdots, j' - 2, j', j' + 2, \cdots, j' + m$ where m is positive integer and close to 2, and

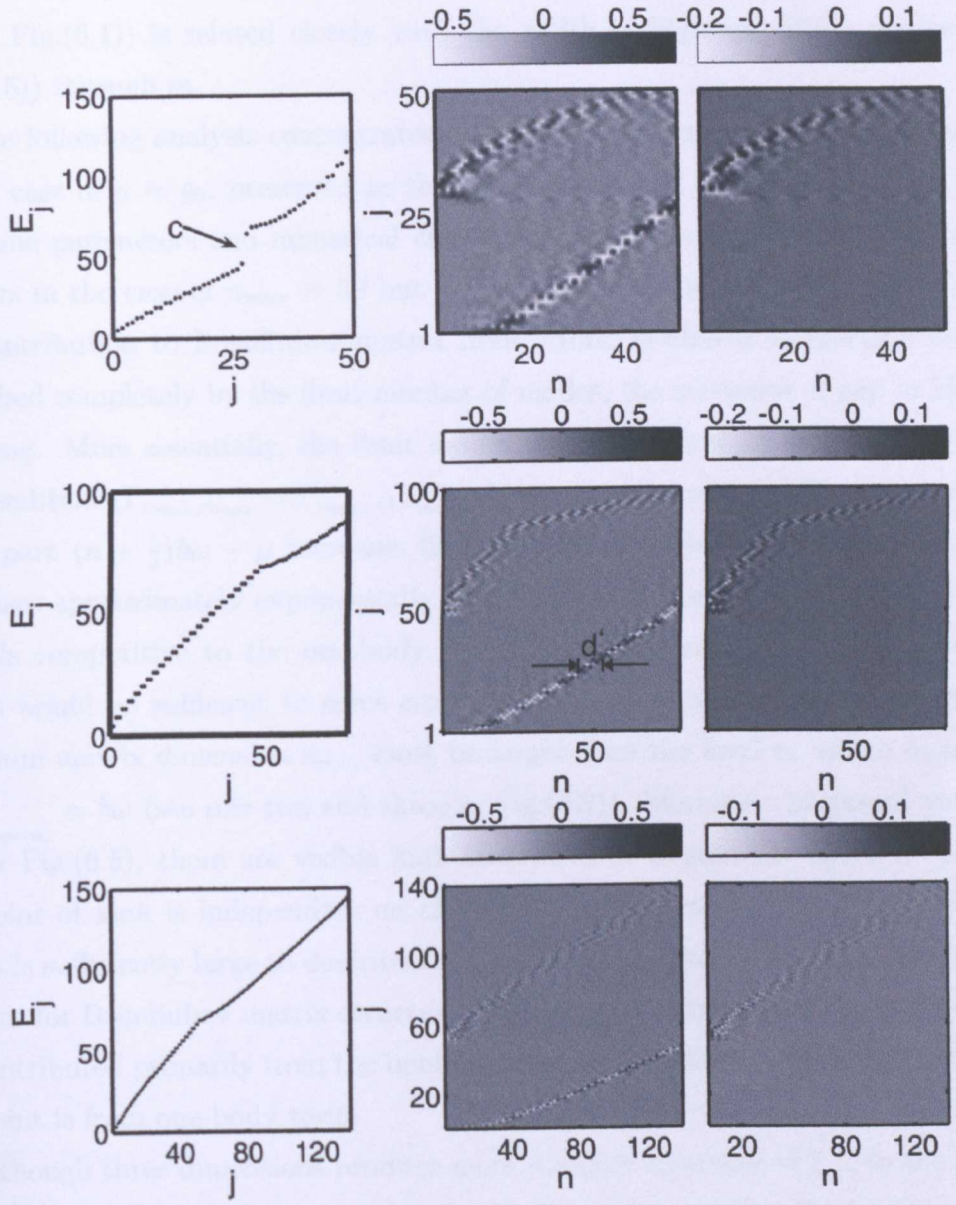

FIGURE 6.5: The plots of Bogoliubov excitation spectrum F_j (Left), mode functions a_n (middle) and b_n for all j; first, second and third row for the situation of $g = g_0$ but the results obtained by using seperately 50 (first row), 100 (second row) and 150 SHO modes (third row).

approximately zero otherwise. m should depend on the value of the non-diagonal elements. Consequently, we can infer that the width of elements in (sub)diagonal parts d (see Fig.(6.1)) is related closely with the width of high-amplitude modes d'(see Fig.(6.5)) through m.

The following analysis concentrates on the excitation spectra and mode function in the case of $g = g_0$, presented in the first, second and third row in Fig.6.5. For the same paremeters and numerical calculation, a visible gap of excitation spectra appears in the case of $n_{max} = 50$ but does not exist for $n_{max} = 100$. Indeed, since the contribution to Bogoliubov matrix from strong nonlinear interaction does not described completely by the limit number of modes, the existence of gap in Fig.(6.5) is wrong. More essentially, the limit modes (for example $n_{max} = 50$) do not fulfill the condition $(\Gamma_{n_{max},n_{max}} - \Gamma_{n_{max}-1,n_{max}-1}) << \hbar\omega$. As seen in Fig.(6.4), the one-body part $(n + \frac{1}{2})\hbar\omega - \mu$ increases linearly with n while the two-body part $\Gamma_{n,n}$ decreases approximately exponentially. This results in some special point m where $\Gamma_{m,m}$ is competitive to the one-body part. An important *criteria* for how many modes would be sufficient to solve correctly the Bogoliubov excitation, is that the minimum matrix dimension n_{min} must be larger than the level n_c where n_c satisfies $\frac{\Delta\Gamma_{n,n}}{\Delta n}\Big|_{n=n_c} \approx \hbar\omega$ (see row two and three in Fig.(6.5)). Moreover, in second and third row in Fig.(6.5), there are visible kink structures of Bogoliubov spectra, in which the point of kink is independent on the number of modes provided the number of modes is sufficiently large to describe the properties of system. Through the previous analysis for Bogoliubov matrix structure, the energy spectra below the point of kink are contributed primarily from the nonlinear term of Hamiltonian and the part above the point is from one-body term.

Although three dimensions produce more complex structure of $\Gamma_{j,n}$ in the Bogoliubov equation, there exist some analogies for $\Gamma_{j,n}$ between 3D and 1D in the case of extremely week interatomic interaction. These analogies imply that some conclusions drawn above for 1D situation might be also effective in 3D situation. If the occupied modes of the condensate wave function in 3D are only four and $n_{0,0,0}$ is much larger

than any one of $n_{2,0,0}$, $n_{0,2,0}$, and $n_{0,0,2}$[2], the form of quantum noise from the TWA in Bogoliubov modes should be independent on the mode and thus it is identical to TWA in PW mode.

In conclusion, we have investigated different forms of quantum fluctuation contributed by different interatomic interaction by solving numerically Bogoliubov equation. In the regime of extremely weak interaction, the contribution of quantum fluctuations from the TWA based on Bogoliubov modes and the TWA based on plan-wave modes are equivalent but they are definitely distinct in the regime of strong interaction, such as in the presentation of normal 1D Bose gas in experiments [17]. Our analysis of eigenvalue and eigenvector for distinct matrix structure might be practical for the Hamiltonian matrix in strongly correlated system such as spin-grid system and superconduction system.

6.4 More work on rigorous mathematics for future

Our simulations have revealed some regularities in the excitation spectrum E_j and mode functions a_n, b_n, derived from an underlying matrix configuration in the Bogoliubov equation. For simplification, one can consider only the case of nondegenerated energy. [3] In general, the equation has the form,

$$\begin{pmatrix} X_{j,n} & Y_{j,n} \\ -Y_{j,n} & -X_{j,n} \end{pmatrix} \begin{pmatrix} \mathbf{a}_n \\ \mathbf{b}_n \end{pmatrix} = \varepsilon \begin{pmatrix} \mathbf{a}_n \\ \mathbf{b}_n \end{pmatrix} \quad , \tag{6.42}$$

where $X_{j,n}$ and $Y_{j,n}$ are $N \times N$ real symmetric tridiagonal matrices. Here we define d is the width of band tridiagonal elements (see Fig.(6.1)); that is to say, $d = 1$ means there are nonzero elements only in the diagonal part. $d = 2$ means there are nonzero elements only in the diagonal and sub-diagonal parts. Meanwhile the matrix $X_{j,n}$ has the following characters,

$$|A_{j,j}| > |A_{j,j+1}| = |A_{j+1,j}| > |A_{j,j+2}| = |A_{j+2,j}| > \dots .$$

[2]Here, we consider the wave function describing Bose gas with center symmetry.

[3]In special case, i.e. attractive interatominc interaction and low dimension, there exist some complex excitations such as roton-like excitation.

Also $|A_{j,j+m}| > |A_{j,j+m'}|$ $\forall m < m'$ with m, m' are positive integer.

We use two matrices $M_{j,n}, N_{j,n}$ to save eigenstates a_n and b_n separately for all j-level energy under an ascending order; that is to say, the corresponding eigenstates a_n and b_n for E_1, defined the lowest excited energy, are deposited respectively into $M_{1,n}$ and $N_{1,n}$.

Here, we define d' as the width of continuous high-amplitude modes in the a_n or b_n. One needs to investigate the way in which with increasing d, d' increases correspondingly.

CHAPTER 7

Conclusion

7.1 Summary and overview

This thesis has explored the role of repulsive interatomic interaction in the spontaneous formation of vortices and interference pattern in merging BECs, the role of quantum fluctuation in colliding BECs and transport properties of 1D degenerate Bose gas.

In the mean-field approximation, the single particle wave, describing the BEC state, is affected strongly by interatomic interaction. The competition between the centre of mass speed due to an initial displacement and expansion speed due to interatomic interactions for merging BECs exhibits complex interference phenomenon such as non-uniform and distorted fringes. Meanwhile the essential relations between the spontaneous formation of vortices and interference have been shown clearly in Chapter 3. In many cases, these results should motivate some experiments on vortex creation.

Quantum fluctuations are always present in real systems. Beyond mean-field theory, the Truncated Wigner method described in Chapter 4, is one way of including some fluctuations, shows that they have a significant effect on interference visibility and internal correlations. In particular, the detailed dynamics of non-condensed atoms, and the interaction between non-condensed atoms and condensed atoms are of critical importance to understand the phenomenon of interference in quasi-condensates.

Finally, both mean-field method and the classical-field method with Bogoliubov theory are used to discuss the quantum transport of Bose gas in strongly confining potential. We have shown the internal relation between interatomic interaction and the form of excitations and have explored how the form of excitations influences the dynamics of the transport.

7.2 Suggestions for further study

In Chapter 4, we find that the fringe spacing in colliding BECs is sensitive for the repulsive short-range interatomic interaction. This stimulates us to explore the interference properties in merging BECs with different interaction. For example novel phenomena may occur in merging BECs when there are strong dipole-dipole interactions (DDI). As distinct from the repulsive interatomic interaction in Alkali metal atoms, the DDI is long-range and anisotropic (partially attractive) so that it leads to some new interference phenomena if two clouds merge in different directions or in different DDI.

Another promising research direction is to explore the properties of BECs, or Fermi gases when a disorder potential is present in these systems. It should be meaningful to study how and why the internal correlations are lost with the disorder potential and reformed without this potential. Obviously this work should be done beyond mean-field theory. More theoretical tools and mathematical methods should be required for this region. The Bogoliubov theory might be a possible way to begin to study this kind of problem.

APPENDIX A

Derivation of equations 2.2, 2.5, 2.52, 2.53, 2.54

A.1 Understanding Eq.2.2 and 2.5

The kinetic energy operator of Eq.2.2 is manipulated slightly with Green formula,

$$-\frac{\hbar^2}{2m}\int \hat{\psi}^\dagger(r)\nabla^2\hat{\psi}(r)dr = \frac{\hbar^2}{2m}\int \nabla\hat{\psi}^\dagger(r)\nabla\hat{\psi}(r)dr - \frac{\hbar^2}{2m}\int \nabla(\hat{\psi}^\dagger(r)\nabla\hat{\psi}(r))dr. \quad \text{(A.1)}$$

The second part of Eq.A.1 is changed by Gaussian formula into

$$-\frac{\hbar^2}{2m}\int \nabla(\hat{\psi}^\dagger(r)\nabla\hat{\psi}(r))dr = -\frac{\hbar^2}{2m}\int\int_s (\hat{\psi}^\dagger(r)\nabla\hat{\psi}(r))\cdot ds. \quad \text{(A.2)}$$

If the integral area s is sufficient large so that there is no "current" $(\hat{\psi}^\dagger(r)\nabla\hat{\psi}(r))$ passing through the surrounding area s, the final result of Eq.A.2 is zero and thus

$$-\frac{\hbar^2}{2m}\int \hat{\psi}^\dagger(r)\nabla^2\hat{\psi}(r)dr = \frac{\hbar^2}{2m}\int \nabla\hat{\psi}^\dagger(r)\nabla\hat{\psi}(r)dr. \quad \text{(A.3)}$$

As a two-body operator, $\hat{V}$ on a state $|\alpha_1...\alpha_n>$ of N particles is the sum of the action of V on all distinct pairs of particles:

$$\hat{V}|\alpha_1...\alpha_N> = \sum_{1\le i<j\le N}\hat{V}_{ij}|\alpha_1...\alpha_N> = \frac{1}{2}\sum_{1\le i\ne j\le N}\hat{V}_{ij}|\alpha_1...\alpha_N>. \quad \text{(A.4)}$$

So

$$<\alpha_1'...\alpha_N'|\hat{V}|\alpha_1...\alpha_N> = <\alpha_1'...\alpha_N'|\frac{1}{2}\sum_{\alpha\beta}V_{\alpha\beta}\hat{P}_{\alpha\beta}|\alpha_1...\alpha_N>, \quad \text{(A.5)}$$

where $\hat{P}_{\alpha\beta} = \hat{n}_\alpha \hat{n}_\beta - \delta_{\alpha\beta}\hat{n}_\alpha = \hat{a}^\dagger_\alpha \hat{a}^\dagger_\beta \hat{a}_\alpha \hat{a}_\beta$ is counting-operator for pairs of particles in the states $|\alpha>$ and $|\beta>$. So the second term of Eq.(2.2) is similar to two-body operator $\hat{V} = \frac{1}{2}\sum_{\alpha\beta} V_{\alpha\beta}\hat{P}_{\alpha\beta}$.

The deduction of Eq.(2.5) is shown below. Insert the Eq.(2.4) into Eq.(2.3),

$$\begin{aligned}\hat{II} &= \frac{1}{V}\sum_{p,p'}\frac{p\cdot p'}{2m}\hat{a}^\dagger_{p'}\hat{a}_p \int c^{i\frac{(p-p')}{\hbar}\cdot r}dr + \frac{g}{2V^2}\sum_{p'p''pp_0}\hat{a}^\dagger_{p'}\hat{a}^\dagger_{p''}\hat{a}_p\hat{a}_{p_0}\int c^{i\frac{(p\,|\,p_0-p'-p'')}{\hbar}\cdot r}dr \\ &= \sum_p \frac{p^2}{2m}\hat{a}^\dagger_p\hat{a}_p + \frac{g}{2V}\sum_{p,p_0,q}\hat{a}^\dagger_{p+q}\hat{a}^\dagger_{p_0-q}\hat{a}_p\hat{a}_{p_0}.\end{aligned} \tag{A.6}$$

A.2 Derivation of Eq.2.52, 2.53, and 2.54

Inserting Eq.(2.50) into Eq.(2.48), we can obtain the following parts

$$\begin{aligned}\text{Eq.2.48} = {} & \hat{\boldsymbol{\alpha}}^\dagger\mathbf{X}\boldsymbol{\epsilon}\mathbf{X}\hat{\boldsymbol{\alpha}} + \hat{\boldsymbol{\alpha}}^\dagger\mathbf{X}\boldsymbol{\epsilon}\mathbf{Y}\hat{\boldsymbol{\alpha}}^{\dagger T} + \hat{\boldsymbol{\alpha}}^\dagger\mathbf{X}\boldsymbol{\epsilon}\mathbf{z} \\ & + \hat{\boldsymbol{\alpha}}^T\mathbf{Y}\boldsymbol{\epsilon}\mathbf{X}\hat{\boldsymbol{\alpha}} + \hat{\boldsymbol{\alpha}}^T\mathbf{Y}\boldsymbol{\epsilon}\mathbf{Y}\hat{\boldsymbol{\alpha}}^{\dagger T} + \hat{\boldsymbol{\alpha}}^T\mathbf{Y}\boldsymbol{\epsilon}\mathbf{z} \\ & + \mathbf{z}^T\boldsymbol{\epsilon}\mathbf{X}\hat{\boldsymbol{\alpha}} + \mathbf{z}^T\boldsymbol{\epsilon}\mathbf{Y}\hat{\boldsymbol{\alpha}}^{\dagger T} + \mathbf{z}^T\boldsymbol{\epsilon}\mathbf{z} \\ & + 2\lambda\sqrt{N}\big(\hat{\boldsymbol{\alpha}}^\dagger\mathbf{X}\mathbf{A}_n + \hat{\boldsymbol{\alpha}}^T\mathbf{Y}\mathbf{A}_n + \mathbf{z}^T\mathbf{A}_n \\ & + \hat{\boldsymbol{\alpha}}^T\mathbf{X}^T\mathbf{A}_n + \hat{\boldsymbol{\alpha}}^\dagger\mathbf{Y}^T\mathbf{A}_n + \mathbf{z}^T\mathbf{A}_n\big) \\ & + \lambda\Big(4\hat{\boldsymbol{\alpha}}^\dagger\mathbf{X}\mathbf{A}_{m,n}\mathbf{X}\hat{\boldsymbol{\alpha}} + 4\hat{\boldsymbol{\alpha}}^\dagger\mathbf{X}\mathbf{A}_{m,n}\mathbf{Y}\hat{\boldsymbol{\alpha}}^{\dagger T} + 4\hat{\boldsymbol{\alpha}}^\dagger\mathbf{X}\mathbf{A}_{m,n}\mathbf{z} \\ & + 4\hat{\boldsymbol{\alpha}}^T\mathbf{Y}\mathbf{A}_{m,n}\mathbf{X}\hat{\boldsymbol{\alpha}} + 4\hat{\boldsymbol{\alpha}}^T\mathbf{Y}\mathbf{A}_{m,n}\mathbf{Y}\hat{\boldsymbol{\alpha}}^{\dagger T} + 4\hat{\boldsymbol{\alpha}}^T\mathbf{Y}\mathbf{A}_{m,n}\mathbf{z} \\ & + 4\mathbf{z}^T\mathbf{A}_{m,n}\mathbf{X}\hat{\boldsymbol{\alpha}} + 4\mathbf{z}^T\mathbf{A}_{m,n}\mathbf{Y}\hat{\boldsymbol{\alpha}}^{\dagger T} + 4\mathbf{z}^T\mathbf{A}_{m,n}\mathbf{z} \\ & + \hat{\boldsymbol{\alpha}}^\dagger\mathbf{X}\mathbf{A}_{m,n}\mathbf{X}^T\hat{\boldsymbol{\alpha}}^{\dagger T} + \hat{\boldsymbol{\alpha}}^\dagger\mathbf{X}\mathbf{A}_{m,n}\mathbf{Y}^T\hat{\boldsymbol{\alpha}} + \hat{\boldsymbol{\alpha}}^\dagger\mathbf{X}\mathbf{A}_{m,n}\mathbf{z} \\ & + \hat{\boldsymbol{\alpha}}^T\mathbf{Y}\mathbf{A}_{m,n}\mathbf{X}^T\hat{\boldsymbol{\alpha}}^{\dagger T} + \hat{\boldsymbol{\alpha}}^T\mathbf{Y}\mathbf{A}_{m,n}\mathbf{Y}^T\hat{\boldsymbol{\alpha}} + \hat{\boldsymbol{\alpha}}^T\mathbf{Y}\mathbf{A}_{m,n}\mathbf{z} \\ & + \mathbf{z}^T\mathbf{A}_{m,n}\mathbf{X}^T\hat{\boldsymbol{\alpha}}^{\dagger T} + \mathbf{z}^T\mathbf{A}_{m,n}\mathbf{Y}^T\hat{\boldsymbol{\alpha}} + \mathbf{z}^T\mathbf{A}_{m,n}\mathbf{z} \\ & + \hat{\boldsymbol{\alpha}}^T\mathbf{X}^T\mathbf{A}_{m,n}\mathbf{X}\hat{\boldsymbol{\alpha}} + \hat{\boldsymbol{\alpha}}^T\mathbf{X}^T\mathbf{A}_{m,n}\mathbf{Y}\hat{\boldsymbol{\alpha}}^{\dagger T} + \hat{\boldsymbol{\alpha}}^T\mathbf{X}^T\mathbf{A}_{m,n}\mathbf{z} \\ & + \hat{\boldsymbol{\alpha}}^\dagger\mathbf{Y}^T\mathbf{A}_{m,n}\mathbf{X}\hat{\boldsymbol{\alpha}} + \hat{\boldsymbol{\alpha}}^\dagger\mathbf{Y}^T\mathbf{A}_{m,n}\mathbf{Y}\hat{\boldsymbol{\alpha}}^{\dagger T} + \hat{\boldsymbol{\alpha}}^\dagger\mathbf{Y}^T\mathbf{A}_{m,n}\mathbf{z} \\ & + \mathbf{z}^T\mathbf{A}_{m,n}\mathbf{X}\hat{\boldsymbol{\alpha}} + \mathbf{z}^T\mathbf{A}_{m,n}\mathbf{Y}\hat{\boldsymbol{\alpha}}^{\dagger T} + \mathbf{z}^T\mathbf{A}_{m,n}\mathbf{z}\Big)\end{aligned} \tag{A.7}$$

Due to $X^T = X$ and $Y^T = Y$, we rearrange Eq.(A.7) in the order of $\hat{\boldsymbol{\alpha}}$ so

$$\begin{aligned}
\text{Eq.(2.51)} = {} & \mathbf{z}^T\big(\boldsymbol{\epsilon}\mathbf{z} + 4\lambda\sqrt{N}\mathbf{A}_n + 6\mathbf{A}_{m,n}\mathbf{z}\big) \\
& + \hat{\boldsymbol{\alpha}}^T\mathbf{Y}\big(\boldsymbol{\epsilon}\mathbf{z} + 2\lambda\sqrt{N}\mathbf{A}_n + 6\lambda\mathbf{A}_{m,n}\mathbf{z}\big) \\
& + \hat{\boldsymbol{\alpha}}^T\mathbf{X}\big(\boldsymbol{\epsilon}\mathbf{z} + 2\lambda\sqrt{N}\mathbf{A}_n + 6\lambda\mathbf{A}_{m,n}\mathbf{z}\big) \\
& + \hat{\boldsymbol{\alpha}}^\dagger\mathbf{X}\big(\boldsymbol{\epsilon}\mathbf{z} + 2\lambda\sqrt{N}\mathbf{A}_n + 6\lambda\mathbf{A}_{m,n}\mathbf{z}\big) \\
& + \hat{\boldsymbol{\alpha}}^\dagger\mathbf{Y}\big(\boldsymbol{\epsilon}\mathbf{z} + 2\lambda\sqrt{N}\mathbf{A}_n + 6\lambda\mathbf{A}_{m,n}\mathbf{z}\big) \\
& + \hat{\boldsymbol{\alpha}}^\dagger\big(\mathbf{X}\boldsymbol{\epsilon}\mathbf{X} + \mathbf{Y}\boldsymbol{\epsilon}\mathbf{Y} + 4\lambda\mathbf{X}\mathbf{A}_{m,n}\mathbf{X} \\
& + 4\lambda\mathbf{Y}\mathbf{A}_{m,n}\mathbf{Y} + 2\lambda\mathbf{X}\mathbf{A}_{m,n}\mathbf{Y} + 2\lambda\mathbf{Y}\mathbf{A}_{m,n}\mathbf{X}\big)\hat{\boldsymbol{\alpha}} \\
& + \hat{\boldsymbol{\alpha}}^\dagger\big(\mathbf{X}\boldsymbol{\epsilon}\mathbf{Y} + 4\lambda\mathbf{X}\mathbf{A}_{m,n}\mathbf{Y} + \lambda\mathbf{X}\mathbf{A}_{m,n}\mathbf{X} + \lambda\mathbf{Y}\mathbf{A}_{m,n}\mathbf{Y}\big)\hat{\boldsymbol{\alpha}}^{\dagger T} \\
& + \hat{\boldsymbol{\alpha}}^T\big(\mathbf{Y}\boldsymbol{\epsilon}\mathbf{X} + 4\lambda\mathbf{Y}\mathbf{A}_{m,n}\mathbf{X} + \lambda\mathbf{Y}\mathbf{A}_{m,n}\mathbf{Y} + \lambda\mathbf{X}\mathbf{A}_{m,n}\mathbf{X}\big)\hat{\boldsymbol{\alpha}}.
\end{aligned} \tag{A.8}$$

We use the property $\mathbf{A}^T\mathbf{B}\mathbf{C}\mathbf{D} = \mathbf{D}^T\mathbf{C}\mathbf{B}\mathbf{A}$ where $\mathbf{A}, \mathbf{D}$ are vectors and $\mathbf{B}, \mathbf{C}$ are Hermitian matrices. From Eq.(2.52), one can see that the linear terms in Eq.(2.48) produce only a shift of the energy levels but do not affect the distance between them. Moreover, to eliminate the linear in $\hat{\boldsymbol{\alpha}}$ terms from $\hat{H}$, the vector $\mathbf{z}$ must be

$$\mathbf{z} = -2\lambda\sqrt{N}(\boldsymbol{\epsilon} + 6\lambda\mathbf{A}_{m,n})^{-1}\mathbf{A}_n. \tag{A.9}$$

For the purpose of $\hat{\boldsymbol{\alpha}}^\dagger\hat{\boldsymbol{\alpha}}^{\dagger T}$ and $\hat{\boldsymbol{\alpha}}^T\hat{\boldsymbol{\alpha}}$ to vanish in the Hamiltonian, the following matrix equation should be fulfilled,

$$\mathbf{X}\boldsymbol{\epsilon}\mathbf{Y} + 4\lambda\mathbf{X}\mathbf{A}_{m,n}\mathbf{Y} + \lambda\mathbf{X}\mathbf{A}_{m,n}\mathbf{X} + \lambda\mathbf{Y}\mathbf{A}_{m,n}\mathbf{Y} = 0 \tag{A.10}$$

$$\mathbf{Y}\boldsymbol{\epsilon}\mathbf{X} + 4\lambda\mathbf{Y}\mathbf{A}_{m,n}\mathbf{X} + \lambda\mathbf{Y}\mathbf{A}_{m,n}\mathbf{Y} + \lambda\mathbf{X}\mathbf{A}_{m,n}\mathbf{X} = 0. \tag{A.11}$$

Finally the energy matrix $\boldsymbol{\mathcal{E}}$ is

$$\boldsymbol{\mathcal{E}} = \mathbf{X}\boldsymbol{\epsilon}\mathbf{X} + \mathbf{Y}\boldsymbol{\epsilon}\mathbf{Y} + 4\lambda\mathbf{X}\mathbf{A}_{m,n}\mathbf{X} + 4\lambda\mathbf{Y}\mathbf{A}_{m,n}\mathbf{Y} + 2\lambda\mathbf{X}\mathbf{A}_{m,n}\mathbf{Y} + 2\lambda\mathbf{Y}\mathbf{A}_{m,n}\mathbf{X} \tag{A.12}$$

and its eigenvalues define the energy spectrum.

APPENDIX B

The Crank-Nicolson method for solving numerically Gross-Pitaevskii equation

B.1 Three dimensition system

In general, the 3D time-independent Gross-Pitaevskii equation with harmonic traps can be written as

$$i\hbar\frac{\partial\psi}{\partial t} = -\frac{\hbar^2}{2m}\nabla^2 + (\frac{1}{2}m\omega_x^2x^2 + \frac{1}{2}m\omega_y^2y^2 + \frac{1}{2}m\omega_z^2z^2) + \frac{4\pi\hbar^2a}{m}|\psi|^2\psi, \tag{B.1}$$

where ω_x, ω_y, ω_z are trap frequencies separately in x, y and z direction, and a is the s-wave scattering length of Alkali atom with mass m. $\psi(x, y, z, t)$ is normalized so that $|\psi(x, y, z, t)|^2$ is the number of atoms per unit volume.

In order to ensure maximum numerical accuracy and to identify the irreducible minimum of independent system parameters, it is customary in computational treatments of physical systems to express the relevant equations in dimensionless computational units. Here, we select natural units of length, time and energy to be

$$\begin{aligned} x_0 &= \sqrt{\frac{\hbar}{2m\omega_x}} \\ t_0 &= \frac{1}{\omega_x} \\ \epsilon_0 &= \hbar\omega_x, \end{aligned} \tag{B.2}$$

so that the original equation can be changed into

$$i\frac{\partial\tilde{\psi}}{\partial\tilde{t}} = [-\tilde{\nabla}^2 + \frac{1}{4}[\tilde{x}^2 + (\lambda_y\tilde{y})^2 + (\lambda_z\tilde{z})^2] + \tilde{U}_0|\tilde{\psi}(\tilde{r}, \tilde{t})|^2]\tilde{\psi}. \tag{B.3}$$

Here,

$$\begin{aligned}
\lambda_y &= \frac{\omega_y}{\omega_x}; \\
\lambda_z &= \frac{\omega_z}{\omega_x}; \\
\tilde{U}_0 &= 8\pi a\sqrt{\frac{2m\omega_x}{\hbar}}, \\
\tilde{\psi}(\tilde{r},\tilde{t}) &= \psi(r,t)x_0^{3/2}
\end{aligned} \tag{B.4}$$

In order to maintain a simple relationship between the wavefunction at time step n and the wavefunction at time step $n+1$, the first order temporal derivative in Eq.(B.3) is approximated by

$$\frac{\partial\psi_{j,l,k}}{\partial t} \approx \frac{\psi_{j,l,k}^{n+1} - \psi_{j,l,k}^{n}}{\Delta_t}, \tag{B.5}$$

where Δ_t is the size of each time step, and the integers j, l and k are the coordinates of a particular point on the cubic wavefunction gride in the x, y and z direction. The spatial derivatives with respect to x are approximated by taking the Taylor expansions

$$\psi_{j+1,l,k} \approx \psi_{j,l,k} + \Delta_x\frac{\partial\psi}{\partial x}|_{j,l,k} + \frac{\Delta_x^2}{2}\frac{\partial^2\psi}{\partial x^2}|_{j,l,k}, \tag{B.6}$$

and

$$\psi_{j-1,l,k} \approx \psi_{j,l,k} - \Delta_x\frac{\partial\psi}{\partial x}|_{j,l,k} + \frac{\Delta_x^2}{2}\frac{\partial^2\psi}{\partial x^2}|_{j,l,k}, \tag{B.7}$$

where Δ_x is the grid spacing in the x-direction. Adding Eq.(B.6) and Eq.(B.7) yields

$$\frac{\partial^2\psi}{\partial x^2}|_{j,l,k} \approx \frac{\psi_{j+1,l,k} - 2\psi_{j,l,k} + \psi_{j-1,l,k}}{\Delta_x^2}. \tag{B.8}$$

Subtracting Eq.(B.7) from Eq.(B.6) yields

$$\frac{\partial\psi}{\partial x}|_{j,l,k} \approx \frac{\psi_{j+1,l,k} - \psi_{j-1,l,k}}{2\Delta_x} \tag{B.9}$$

Using approximations Eq.(B.5), (B.8) and (B.9), together with equivalent expressions for derivatives with respect to y and z, the Eq.(B.3) can be rewrited as

$$\begin{aligned}
i\frac{\psi_{j,l,k}^{n+1} - \psi_{j,l,k}^{n}}{\Delta_t} = -(&\frac{\psi_{j+1,l,k}^{n} - 2\psi_{j,l,k}^{n} + \psi_{j-1,l,k}^{n}}{\Delta_x^2} + \frac{\psi_{j,l+1,k}^{n} - 2\psi_{j,l,k}^{n} + \psi_{j,l-1,k}^{n}}{\Delta_y^2} \\
&+ \frac{\psi_{j,l,k+1}^{n} - 2\psi_{j,l,k}^{n} + \psi_{j,l,k-1}^{n}}{\Delta_z^2}) + V_{j,l,k}^{n}\psi_{j,l,k}^{n},
\end{aligned} \tag{B.10}$$

and

$$i\frac{\psi_{j,l,k}^{n+1}-\psi_{j,l,k}^{n}}{\Delta_t}=-(\frac{\psi_{j+1,l,k}^{n+1}-2\psi_{j,l,k}^{n+1}+\psi_{j-1,l,k}^{n+1}}{\Delta_x^2}+\frac{\psi_{j,l+1,k}^{n+1}-2\psi_{j,l,k}^{n+1}+\psi_{j,l-1,k}^{n+1}}{\Delta_y^2}$$
$$+\frac{\psi_{j,l,k+1}^{n+1}-2\psi_{j,l,k}^{n+1}+\psi_{j,l,k-1}^{n+1}}{\Delta_z^2})+V_{j,l,k}^{n+1}\psi_{j,l,k}^{n+1}. \tag{B.11}$$

Adding Eq.(B.10) and Eq.(B.11) and simplifying it to

$$\psi_{j,l,k}^{n+1}=\psi_{j,l,k}^{n}+\frac{i\Delta_t}{2}(\frac{\psi_{j+1,l,k}^{n}-2\psi_{j,l,k}^{n}+\psi_{j-1,l,k}^{n}}{\Delta_x^2}+\frac{\psi_{j+1,l,k}^{n+1}-2\psi_{j,l,k}^{n+1}+\psi_{j-1,l,k}^{n+1}}{\Delta_x^2}$$
$$+\frac{\psi_{j,l+1,k}^{n}-2\psi_{j,l,k}^{n}+\psi_{j,l-1,k}^{n}}{\Delta_y^2}+\frac{\psi_{j,l+1,k}^{n+1}-2\psi_{j,l,k}^{n+1}+\psi_{j,l-1,k}^{n+1}}{\Delta_y^2}$$
$$+\frac{\psi_{j,l,k+1}^{n}-2\psi_{j,l,k}^{n}+\psi_{j,l,k-1}^{n}}{\Delta_z^2}+\frac{\psi_{j,l,k+1}^{n+1}-2\psi_{j,l,k}^{n+1}+\psi_{j,l,k-1}^{n+1}}{\Delta_z^2}) \tag{B.12}$$
$$-\frac{i\Delta_t}{2}(V_{j,l,k}^{n}\psi_{j,l,k}^{n}+V_{j,l,k}^{n+1}\psi_{j,l,k}^{n+1}).$$

By using *three times time-operator and spatial operator splitting*, the Eq.(B.12) can be splitted into three small equations:

$$\psi_{j,l,k}^{n+1/3}=\psi_{j,l,k}^{n}+\frac{i\Delta_t}{2}(\frac{\psi_{j+1,l,k}^{n+1/3}-2\psi_{j,l,k}^{n+1/3}+\psi_{j-1,l,k}^{n+1/3}}{\Delta_x^2}$$
$$+\frac{\psi_{j,l+1,k}^{n}-2\psi_{j,l,k}^{n}+\psi_{j,l-1,k}^{n}}{\Delta_y^2})-\frac{i\Delta_t}{6}(V_{j,l,k}^{n}\psi_{j,l,k}^{n}+V_{j,l,k}^{n+1/3}\psi_{j,l,k}^{n+1/3}), \tag{B.13}$$

$$\psi_{j,l,k}^{n+2/3}=\psi_{j,l,k}^{n+1/3}+\frac{i\Delta_t}{2}(\frac{\psi_{1,l+l,k}^{n+2/3}-2\psi_{j,l,k}^{n+2/3}+\psi_{j,l-1,k}^{n+2/3}}{\Delta_y^2}$$
$$+\frac{\psi_{j,l,k+1}^{n+1/3}-2\psi_{j,l,k}^{n+1/3}+\psi_{j,l,k-1}^{n+1/3}}{\Delta_z^2})-\frac{i\Delta_t}{6}(V_{j,l,k}^{n+1/3}\psi_{j,l,k}^{n+1/3}+V_{j,l,k}^{n+2/3}\psi_{j,l,k}^{n+2/3}), \tag{B.14}$$

$$\psi_{j,l,k}^{n+1}=\psi_{j,l,k}^{n+2/3}+\frac{i\Delta_t}{2}(\frac{\psi_{j,l,k+1}^{n+1}-2\psi_{j,l,k}^{n+1}+\psi_{j,l,k-1}^{n+1}}{\Delta_z^2}$$
$$+\frac{\psi_{j+1,l,k}^{n+2/3}-2\psi_{j,l,k}^{n+2/3}+\psi_{j-1,l,k}^{n+2/3}}{\Delta_x^2})-\frac{i\Delta_t}{6}(V_{j,l,k}^{n+1}\psi_{j,l,k}^{n+1}+V_{j,l,k}^{n+2/3}\psi_{j,l,k}^{n+2/3}), \tag{B.15}$$

Rearranging Eq.(B.13), (B.14) and (B.15) yields

$$-\frac{i\Delta_t}{2\Delta_x^2}\psi_{j+1,l,k}^{n+1/3}+(1+\frac{i\Delta_t}{\Delta_x^2}+\frac{i\Delta_t}{6}V_{j,l,k}^{n+1/3})\psi_{j,l,k}^{n+1/3}-\frac{i\Delta_t}{2\Delta_x^2}\psi_{j-1,l,k}^{n+1/3}=$$
$$\frac{i\Delta_t}{2\Delta_y^2}\psi_{j,l+1,k}^{n}+(1-\frac{i\Delta_t}{\Delta_y^2}-\frac{i\Delta_t}{6}V_{j,l,k}^{n})\psi_{j,l,k}^{n}+\frac{i\Delta_t}{2\Delta_y^2}\psi_{j,l-1,k}^{n}, \tag{B.16}$$

$$-\frac{i\Delta_t}{2\Delta_y^2}\psi_{j,l+1,k}^{n+2/3}+(1+\frac{i\Delta_t}{\Delta_y^2}+\frac{i\Delta_t}{6}V_{j,l,k}^{n+2/3})\psi_{j,l,k}^{n+2/3}-\frac{i\Delta_t}{2\Delta_y^2}\psi_{j,l-1,k}^{n+2/3}=$$
$$\frac{i\Delta_t}{2\Delta_z^2}\psi_{j,l,k+1}^{n+1/3}+(1-\frac{i\Delta_t}{\Delta_z^2}-\frac{i\Delta_t}{6}V_{j,l,k}^{n+1/3})\psi_{j,l,k}^{n+1/3}+\frac{i\Delta_t}{2\Delta_z^2}\psi_{j,l,k-1}^{n+1/3}, \tag{B.17}$$

$$-\frac{i\Delta_t}{2\Delta_z^2}\psi_{j,l,k+1}^{n+1}+(1+\frac{i\Delta_t}{\Delta_z^2}+\frac{i\Delta_t}{6}V_{j,l,k}^{n+1})\psi_{j,l,k}^{n+1}-\frac{i\Delta_t}{2\Delta_z^2}\psi_{j,l,k-1}^{n+1}=$$
$$\frac{i\Delta_t}{2\Delta_x^2}\psi_{j+1,l,k}^{n+2/3}+(1-\frac{i\Delta_t}{\Delta_x^2}-\frac{i\Delta_t}{6}V_{j,l,k}^{n+2/3})\psi_{j,l,k}^{n+2/3}+\frac{i\Delta_t}{2\Delta_x^2}\psi_{j-1,l,k}^{n+2/3}. \tag{B.18}$$

The exact process of Crank-Nicolson method for numerically solving 3D Gross-Pitaevskii equation has been show above. The following thing is involved in the general realization of codes. To solve Eq.B.16, B.17, and B.18 numerically, one can use the technique of *LU decomposition followed by forward and backward substitution* [130] to solve these equations. The detailed process has been shown in the thesis [131]. Also, one can utilize more simple technique, *Tridiagonal Systems of Equations* to solve them [130]. Normally, the first method is more stable than the second one but the later is more efficient than the former. Since the elements on the diagonal plus and minus one column are normally nonzero and a series of regular values, the second method should be sufficient and stable to solve these equations.

Moreover, there are two methods inplemented to realize the code. The first method is involved in using some natural units of length, time and energy to reduce constants as far as possible. The above process of Crank-Nicolson method is attibuted to this method. The second method is to realize the code directly from the original equation and some constants such as $\hbar, m, a$ can be adjusted in a rational range so that these constants behave as some variables. According to two methods, they have different advantages separately in real applications. If one hopes to contrast numerical results with analytic results or to explore some physical properties which are correlated closely with known parameters, such as characteristic length of single harmonic oscillator, we suggest to realize the code in the first method. If one hopes that their simulation results satisfy well the results of experiments, the second method should be better in that real experiments are generally not more "perfect" than theoritic prediction and altering properly the values of those constants might cause more ideal results.

B.2 The 3D system with cylindrical symmetry

We consider the 3D time-independent Gross-Pitaevskii equation in the harmonic traps with cylindrical symmetry as

$$i\hbar\frac{\partial\psi}{\partial t} = -\frac{\hbar^2}{2m}\nabla^2 + (\frac{1}{2}m\omega_r^2 r^2 + \frac{1}{2}m\omega_z^2 z^2) + \frac{4\pi\hbar^2 a}{m}|\psi|^2\psi, \tag{B.19}$$

where ω_r, ω_z are trap frequencies respectively in the radial and longitudinal directions, and a is the s-wave scattering length of Alkali atom with mass m. $\psi(r,z,t)$ is normalized so that $|\psi(r,z,t)|^2$ is the number of atoms per unit volume.

We select the units of length, time and energy and evolve the process in analogy to three dimensional Crank-Nicolson method. Thus the orignal equation is split into

$$\begin{aligned} i\frac{\psi_{j,l}^{n+1}-\psi_{j,l}^{n}}{\Delta_t} = -(&\frac{\psi_{j+1,l}^{n}-2\psi_{j,l}^{n}+\psi_{j-1,l}^{n}}{\Delta_z^2} + \frac{\psi_{j,l+1}^{n}-2\psi_{j,l}^{n}+\psi_{j,l-1}^{n}}{\Delta_r^2} \\ &+ \frac{\psi_{j,l+1}^{n}-\psi_{j,l-1}^{n}}{2r\Delta_r}) + V_{j,l}^{n}\psi_{j,l}^{n}, \end{aligned} \tag{B.20}$$

and

$$\begin{aligned} i\frac{\psi_{j,l}^{n+1}-\psi_{j,l}^{n}}{\Delta_t} = -(&\frac{\psi_{j+1,l}^{n+1}-2\psi_{j,l}^{n+1}+\psi_{j-1,l}^{n+1}}{\Delta_z^2} + \frac{\psi_{j,l+1}^{n+1}-2\psi_{j,l}^{n+1}+\psi_{j,l-1}^{n+1}}{\Delta_r^2} \\ &+ \frac{\psi_{j,l+1}^{n+1}-\psi_{j,l-1}^{n+1}}{2r\Delta_r}) + V_{j,l}^{n+1}\psi_{j,l}^{n+1}. \end{aligned} \tag{B.21}$$

Adding Eq.(B.20) and Eq.(B.21) and simplifying it to

$$\begin{aligned} \psi_{j,l}^{n+1} = \psi_{j,l}^{n} + \frac{i\Delta_t}{2}(&\frac{\psi_{j+1,l}^{n}-2\psi_{j,l}^{n}+\psi_{j-1,l}^{n}}{\Delta_z^2} + \frac{\psi_{j+1,l}^{n+1}-2\psi_{j,l}^{n+1}+\psi_{j-1,l}^{n+1}}{\Delta_z^2} \\ &+ \frac{\psi_{j,l+1}^{n}-2\psi_{j,l}^{n}+\psi_{j,l-1}^{n}}{\Delta_r^2} + \frac{\psi_{j,l+1}^{n+1}-2\psi_{j,l}^{n+1}+\psi_{j,l-1}^{n+1}}{\Delta_r^2} \\ &+ \frac{\psi_{j,l+1}^{n}-\psi_{j,l-1}^{n}}{2r\Delta_r} + \frac{\psi_{j,l+1}^{n+1}-\psi_{j,l-1}^{n+1}}{2r\Delta_r}) - \frac{i\Delta_t}{2}(V_{j,l}^{n}\psi_{j,l}^{n} + V_{j,l}^{n+1}\psi_{j,l}^{n+1}). \end{aligned} \tag{B.22}$$

By using two times time-operator and spatial operator splitting, the Eq.(B.22) can be splitted into two small equations:

$$\begin{aligned} \psi_{j,l}^{n+1/2} = \psi_{j,l}^{n} + \frac{i\Delta_t}{2}(&\frac{\psi_{j+1,l}^{n+1/2}-2\psi_{j,l}^{n+1/2}+\psi_{j-1,l}^{n+1/2}}{\Delta_z^2} + \frac{\psi_{j,l+1}^{n}-2\psi_{j,l}^{n}+\psi_{j,l-1}^{n}}{\Delta_r^2} \\ &+ \frac{\psi_{j,l+1}^{n}-\psi_{j,l-1}^{n}}{2r\Delta_r}) - \frac{i\Delta_t}{4}(V_{j,l}^{n+1/2}\psi_{j,l}^{n+1/2} + V_{j,l}^{n}\psi_{j,l}^{n}), \end{aligned} \tag{B.23}$$

and

$$\psi_{j,l}^{n+1} = \psi_{j,l}^{n+1/2} + \frac{i\Delta_t}{2}\left(\frac{\psi_{j+1,l}^{n+1/2} - 2\psi_{j,l}^{n+1/2} + \psi_{j-1,l}^{n+1/2}}{\Delta_z^2} + \frac{\psi_{j,l+1}^{n+1} - 2\psi_{j,l}^{n+1} + \psi_{j,l-1}^{n+1}}{\Delta_r^2}\right.$$
$$\left. + \frac{\psi_{j,l+1}^{n+1} - \psi_{j,l-1}^{n+1}}{2r\Delta_r}\right) - \frac{i\Delta_t}{4}(V_{j,l}^{n+1/2}\psi_{j,l}^{n+1/2} + V_{j,l}^{n+1}\psi_{j,l}^{n+1}). \tag{B.24}$$

Rearranging Eq.(B.23) and Eq.(B.24) yields

$$-\frac{i\Delta_t}{2\Delta_z^2}\psi_{j+1,l}^{n+1/2} + (1 + \frac{i\Delta_t}{\Delta_z^2} + \frac{i\Delta_t}{4}V_{j,l}^{n+1/2})\psi_{j,l}^{n+1/2} - \frac{i\Delta_t}{2\Delta_z^2}\psi_{j-1,l}^{n+1/2} =$$
$$(\frac{i\Delta_t}{2\Delta_r^2} + \frac{i\Delta_t}{4r\Delta_r})\psi_{j,l+1}^{n} + (1 - \frac{i\Delta_t}{\Delta_r^2} - \frac{i\Delta_t}{4}V_{j,l}^{n})\psi_{j,l}^{n} + (\frac{i\Delta_t}{2\Delta_r^2} - \frac{i\Delta_t}{4r\Delta_r})\psi_{j,l-1}^{n}, \tag{B.25}$$

and

$$(-\frac{i\Delta_t}{2\Delta_r^2} - \frac{i\Delta_t}{4r\Delta_r})\psi_{j,l+1}^{n+1} + (1 + \frac{i\Delta_t}{\Delta_r^2} + \frac{i\Delta_t}{4}V_{j,l}^{n+1})\psi_{j,l}^{n+1} + (-\frac{i\Delta_t}{2\Delta_r^2} + \frac{i\Delta_t}{4r\Delta_r})\psi_{j,l-1}^{n+1}$$
$$= \frac{i\Delta_t}{2\Delta_z^2}\psi_{j+1,l}^{n+1/2} + (1 - \frac{i\Delta_t}{\Delta_z^2} - \frac{i\Delta_t}{4}V_{j,l}^{n+1/2})\psi_{j,l}^{n+1/2} + \frac{i\Delta_t}{2\Delta_z^2}\psi_{j-1,l}^{n+1/2} \tag{B.26}$$

The realization of codes is basically similar to 3D case except that the normalization of condensate wave function is a little different.

Appendix C

RK4IP-P algorithm for solving numerically Gross-Pitaevskii equation

C.1 Gross-Pitaevskii equation in the mode space and interaction picture representation

A generalized Gross-Pitaevskii equation has the form as

$$i\hbar\frac{\partial\Psi(\mathbf{r},t)}{\partial t}=\left[-\frac{\hbar^2}{2m}\nabla^2+U_{ext}(\mathbf{r},t)+\delta U_{ext}(\mathbf{r},t)+U_0|\Psi(\mathbf{r},t)|^2\right]\Psi(\mathbf{r},t). \tag{C.1}$$

Normally, we choose special basis $\phi_j(\mathbf{r})$ which are closest to the character of condense wave function to expand $\Psi(\mathbf{r},t)$ in low-energy mode space [1] , i.e.,

$$\Psi_P(\mathbf{r},t)=\sum_{j\in L}\phi_j(\mathbf{r})\alpha_j(t). \tag{C.2}$$

Here, $\phi_j(\mathbf{r})$ satisfies the eigenvalue equation,

$$-\frac{\hbar^2}{2m}\nabla^2\phi_j(\mathbf{r})+U_{ext}(\mathbf{r},t)\phi_j(\mathbf{r})=\hbar\omega_j\phi_j(\mathbf{r}). \tag{C.3}$$

Thus Eq.(C.1) is rewriten as

$$\frac{d\alpha_j(t)}{dt}=-i\left\{\omega_j\alpha_j+\int d\mathbf{r}\phi_j^*\left[\delta U_{ext}(\mathbf{r},t)+U_0|\Psi_P(\mathbf{r},t)|^2\right]\Psi_P(\mathbf{r},t)\right\}. \tag{C.4}$$

[1] The reason of choosing only low-energy mode space for Bose field is based on three factors. Firstly, condensed atoms occupy the lowest energy modes. Secondly, the interatomic interaction between low-energy modes and high-energy modes are extremely weak. Thirdly, it might be difficult for experiments to probe for the behavior of atoms in the high-energy modes. One can infer that this method might be improper used in strongly correlated system.

The Eq.(C.4) in the Schrödinger picture representation can be simplified more in the interaction picture representation. Defining

$$\alpha_j(t) = e^{-i\omega_j(t-t_{ref})}\bar{\alpha}_j(t), \tag{C.5}$$

where the equivalence time between the pictures t_{ref} is choosn shortly, the Eq.(C.4) is changed into

$$\frac{d\bar{\alpha}_j(t)}{dt} = -ie^{i\omega_j(t-t_{ref})}\int d\mathbf{r}\phi_j^*(\mathbf{r})\left[\delta U_{ext}(\mathbf{r},t) + U_0|\Psi_P(\mathbf{r},t)|^2\right]\Psi_P(\mathbf{r},t) \quad (j \in L), \tag{C.6}$$

where the coordinate space field is now calculated using

$$\Psi_P(\mathbf{r},t) = \sum_{j\in L}\phi_j(\mathbf{r})e^{-i\omega_j(t-t_{ref})}\bar{\alpha}_j(t). \tag{C.7}$$

C.2 RK4IP-P algorithm for Eq.(C.6)

The stardard fourth-order Runge-Kutta (RK4) method can be used to deal with differential equation with the general form,

$$\frac{d\mathbf{f}(t)}{dt} = \mathbf{g}[\mathbf{f}(t), t], \tag{C.8}$$

where $\mathbf{f}(t)$ is the vector-valued function. Then, we advance the vector $\mathbf{f}(t)$ between discrete time steps, such that

$$t_{i+1} = t_i + \Delta t,$$

where Δt is the time increment between numerically integrated solutions. Thus in the RK4, the vector at the discrete time is written

$$\mathbf{f}(t_{i+1}) = \mathbf{f}(t_i) + \frac{1}{6}\left[\mathbf{h}_1 + 2(\mathbf{h}_2 + \mathbf{h}_3) + \mathbf{h}_4\right] + O(\Delta t^5), \tag{C.9}$$

where the individual Runge-Kutta terms are calculated as

$$\begin{aligned}
\mathbf{h_1} &= \mathbf{g}\left[\mathbf{f}(t_i), t_i\right]\Delta t \\
\mathbf{h_2} &= \mathbf{g}\left[\mathbf{f}(t_i) + \frac{\mathbf{h}_1}{2}, t_i + \frac{\Delta t}{2}\right]\Delta t \\
\mathbf{h_3} &= \mathbf{g}\left[\mathbf{f}(t_i) + \frac{\mathbf{h}_2}{2}, t_i + \frac{\Delta t}{2}\right]\Delta t \\
\mathbf{h_4} &= \mathbf{g}\left[\mathbf{f}(t_i) + \mathbf{h}_3, t_i + \Delta t\right]\Delta t.
\end{aligned} \tag{C.10}$$

Contrasting Eq.(C.6) and (C.7) with Eq.(C.10), one can see easily that when choosing $t_{ref} = t_i + \Delta t/2$, we can remove a large number of the exponential multiplications. Thus the final process of the projected fourth-order Runge-Kutta algorithm in the interaction picture algorithm (RK4IP-P) for numerically sovling Gross-Pitaevskii equation is shown completely below. The evolution of $\bar{\alpha}_j(t)$ in RK4 algorithm is

$$\bar{\alpha}_j(t_{i+1}) = \bar{\alpha}_j(t_i) + \frac{1}{6}\left[\bar{\alpha}_j^{h_1} + 2(\bar{\alpha}_j^{h_2} + \bar{\alpha}_j^{h_3}) + \bar{\alpha}_j^{h_4}\right], \tag{C.11}$$

where the Runge-Kutta increments to

$$\begin{aligned}
\bar{\alpha}_j^{h_1} &= -i\Delta t e^{-i\omega_j \frac{\Delta t}{2}} \int d\mathbf{r}\phi_j^* \left[\delta U_{ext}(t_i) + U_0|\Psi_P^{h_1}|^2\right] \Psi_P^{h_1} \\
\bar{\alpha}_j^{h_2} &= -i\Delta t \int d\mathbf{r}\phi_j^* \left[\delta U_{ext}\left(t_i + \frac{\Delta t}{2}\right) + U_0|\Psi_P^{h_2}|^2\right] \Psi_P^{h_2} \\
\bar{\alpha}_j^{h_3} &= -i\Delta t \int d\mathbf{r}\phi_j^* \left[\delta U_{ext}\left(t_i + \frac{\Delta t}{2}\right) + U_0|\Psi_P^{h_3}|^2\right] \Psi_P^{h_3} \\
\bar{\alpha}_j^{h_4} &= -i\Delta t e^{i\omega_j \frac{\Delta t}{2}} \int d\mathbf{r}\phi_j^* \left[\delta U_{ext}(t_i + \Delta t) + U_0|\Psi_P^{h_4}|^2\right] \Psi_P^{h_4}.
\end{aligned} \tag{C.12}$$

The corresponding coordinate fields are now

$$\begin{aligned}
\Psi_P^{h_1}(\mathbf{r}) &= \sum_{j\in L} \phi_j(\mathbf{r}) c^{i\omega_j \frac{\Delta t}{2}} \bar{\alpha}_j(t_i) \\
\Psi_P^{h_2}(\mathbf{r}) &= \sum_{j\in L} \phi_j(\mathbf{r}) \left[\bar{\alpha}_j(t_i) + \frac{1}{2}\bar{\alpha}_j^{h_1}\right] \\
\Psi_P^{h_3}(\mathbf{r}) &= \sum_{j\in L} \phi_j(\mathbf{r}) \left[\bar{\alpha}_j(t_i) + \frac{1}{2}\bar{\alpha}_j^{h_2}\right] \\
\Psi_P^{h_4}(\mathbf{r}) &= \sum_{j\in L} \phi_j(\mathbf{r}) c^{-i\omega_j \frac{\Delta t}{2}} \left[\bar{\alpha}_j(t_i) + \frac{1}{2}\bar{\alpha}_j^{h_3}\right].
\end{aligned} \tag{C.13}$$

Appendix D

Interatomic interaction in low dimensional system within mean-field theory

The interaction energy in the mean-field approximation for Bose-Einstein condensate in full space is writen as

$$E_{int} = g_{3D} \int\int\int |\Psi_0(x,y,z,t)|^4 dxdydz. \tag{D.1}$$

If we consider a quasi-2D system and z-component is independent on time, the wavefunction of condensate can be read as $\Psi_0(x,y,z,t) = \Psi_0(x,y,t)\Psi_0(z)$. With ansaz of $|\Psi_0(z)|^2 = \frac{1}{\sqrt{\pi\sigma_z^2}} e^{-z^2/(\sigma_z^2)}$, the above equation can be writen into

$$\begin{aligned} E_{int} &= \frac{g_{3D}}{\pi\sigma_z^2} \int_{-\infty}^{\infty} e^{-\frac{2z^2}{\sigma_z^2}} dz \int\int |\Psi_0(x,y,t)|^4 dxdy \\ &= \frac{g_{3D}}{\sqrt{2\pi}\sigma_z} \int\int |\Psi_0(x,y,t)|^4 dxdy. \end{aligned} \tag{D.2}$$

Here, the characteristic quantum-mechanical length scale for the harmonic oscillator in z-component $\sigma_z = \sqrt{\hbar/(m\omega_z)}$ so one can define new interatomic interaction coefficient in the quasi-2D system

$$g_{2D} = \frac{g_{3D}}{\sqrt{2\pi}\sigma_z} = \frac{\hbar^2 a}{m}\sqrt{\frac{8\pi m\omega_z}{\hbar}}. \tag{D.3}$$

Similarly, one can deduce the interatomic interaction coefficient in 1D system

$$g_{1D} = \frac{g_{2D}}{\sqrt{2\pi}\sigma_y} = 2\hbar a\sqrt{\omega_z\omega_y}. \tag{D.4}$$

Appendix E

Thomas-Fermi density envelope in a strong 2D optical lattice and harmonic potential

If the density of atomic gas changes slowly in space, the kinetic energy term in Gross-Pitaevskii equation (or the quantum pressure term in the corresponding hydrodynamic equations) can be neglected and the GPE can be simplified into

$$[V(r) + U_0|\psi(r)|^2]\psi(r) = \mu\psi(r), \tag{E.1}$$

where μ is the chemical potential. Eq.(E.1) has the solution

$$n(r) = |\psi(r)|^2 = [\mu - V(r)]/U_0 \tag{E.2}$$

in the region where the right hand side is positive, while $n(r) = 0$ outside this region. The boundary of the cloud is therefor given by

$$V(r_{boud}) = \mu. \tag{E.3}$$

We shall determine the ground-state energy for a gas trapped in an anisotropic three-dimensional harmonic-oscillator potential V given by

$$V(x, y, z) = \frac{1}{2}m(\omega_1^2 x^2 + \omega_2^2 y^2 + \omega_3^2 z^2) \tag{E.4}$$

where the three oscillator frequencies $\omega_i (i = 1, 2, 3)$ may differ from each other. In the TFA the extension of the cloud in the three directions is given by the three semi-axes

R_i obtained by inserting Eq.(E.4)into Eq.(E.3),

$$R_i^2 = \frac{2\mu}{m\omega_i^2}, i = 1, 2, 3. \tag{E.5}$$

The normalization condition for $n(r)$ in Eq.(E.2), yields a relation between the chemical potential μ and the total number of particles N. For a harmonic trap with a potential given by Eq.(E.4), one finds

$$N = \frac{8\pi}{15}(\frac{2\mu}{m\bar{\omega}^2})^{3/2}\frac{\mu}{U_0} \tag{E.6}$$

where $\bar{\omega}^3 = \omega_x\omega_y\omega_z$.

The deduce of Eq.(E.6) is shown below. First, we set $u = \omega_x x$, $v = \omega_y y$, $w = \omega_z z$ to give

$$N = \frac{1}{U_0\bar{\omega}^3}\int\int\int dudvdw(\mu - \frac{1}{2}m(u^2 + v^2 + w^2)), \tag{E.7}$$

where $\bar{\omega}^3 = \omega_x\omega_y\omega_z$. Exchange the integral in the Cartesian coordinates into the spherical polar coordinates and give

$$\begin{aligned} N &= \frac{4\pi}{U_0\bar{\omega}^3}\int_0^{\sqrt{2\mu/m}} r^2(\mu - \frac{1}{2}mr^2)dr \\ &= \frac{8\pi}{15}(\frac{2\mu}{m\bar{\omega}^2})^{3/2}\frac{\mu}{U_0}. \end{aligned} \tag{E.8}$$

Through Eq.(E.6) and $U_0 = \frac{4\pi\hbar^2 a}{m}$, one obtain the following relation between μ and N:

$$N = \frac{4\sqrt{2}}{15}\frac{l}{a}(\frac{\mu}{\hbar\bar{\omega}})^{5/2} \tag{E.9}$$

$$\mu = \frac{\hbar\bar{\omega}}{2}(\frac{15aN}{l})^{2/5}, \tag{E.10}$$

where $l = \sqrt{\frac{\hbar}{m\bar{\omega}}}$.

Insert Eq.(E.10) into Eq.(E.5), three semi-axes

$$R_i = l_i\frac{\bar{\omega}}{\omega_i}(\frac{15aN}{l})^{1/5}, \tag{E.11}$$

where

$$l_i = \sqrt{\frac{\hbar}{m\omega_i}}.$$

The quantity $\bar{R} = (R_1 R_2 R_3)^{\frac{1}{3}}$ is a convenient measure of the spatial extent of the cloud and through Eq.(E.2), $\bar{R} = (15l^4 aN)^{1/5}$. Thus

$$|\psi(\mathbf{r})| = \begin{cases} \frac{15N}{8\pi R^3}(1 - (\frac{x^2}{R_x^2} + \frac{y^2}{R_y^2} + \frac{z^2}{R_z^2})) & (\frac{x^2}{R_x^2} + \frac{y^2}{R_y^2} + \frac{z^2}{R_z^2}) < 1 \\ 0 & (\frac{x^2}{R_x^2} + \frac{y^2}{R_y^2} + \frac{z^2}{R_z^2}) > 1 \end{cases}$$

We now turn on a deep 2d optical lattice potential of strength v of the form

$$v(x, y) = v(2 + cos(kx) + cos(ky)) \tag{E.12}$$

where $k = 2\pi/d$ which generates an array of tubular minima at $x_l = (2l + 1)\pi/k = (2l + 1)d/2, y_n = (2n + 1)\pi/k = (2n + 1)d/2$. We suppose that this redistributes the density so that the wavefunction becomes

$$\psi(x, y, z) = \sum_{l,n} \psi_t(x_l, y_n, z)\phi(x - x_l, y - y_n) \tag{E.13}$$

where $\phi(x - x_l, y - y_n)$ is the ground state wavefunction of the potential within a single unit cell. If the potential is deep we can approximate

$$\begin{aligned} V(x_l + \xi, y_n + \theta) &= v(2 + cos(k((2l + 1)d/2 + \xi)) \\ &\quad + cos(k((2n + 1)d/2 + \theta))) \\ &\approx (2 - 1 + \frac{1}{2}k^2\xi^2 - 1 + \frac{1}{2}k^2\theta^2) \\ &= \frac{1}{2}m\Omega^2(\xi^2 + \theta^2) \end{aligned} \tag{E.14}$$

where

$$\Omega = \sqrt{\frac{vk^2}{m}}$$

so that the tube potential is harmonic with natural frequency Ω and zero point amplitude $\lambda = \sqrt{\hbar/m\Omega}$. Hence the ground state wave function is

$$\phi(\xi, \theta) = ce^{-(\xi^2+\theta^2)/2\lambda^2} \tag{E.15}$$

The constant C must be chosen so that the presence of the lattice does not change the total number of atoms in a given unit cell. Hence we must have

$$\int_{-d/2}^{d/2} d\xi \int_{-d/2}^{d/2} d\theta |\phi|^2 = d^2 \tag{E.16}$$

which gives (assuming that $\lambda << d$ so that the limits of the integration can be extended to $\pm\infty$ which leads to an error of order e^{-d^2/λ^2})

$$\begin{aligned} C^2\pi\lambda^2 &= d^2 \\ C &= \frac{d}{\lambda\sqrt{\pi}} \end{aligned} \tag{E.17}$$

and, close to the l, n tube we have

$$\begin{aligned} \rho(x_l+\xi, y_n+\theta, z) &= \frac{15N}{8\pi R^3}\Big(1-\big(\frac{x_l^2}{R_x^2}+\frac{y_n^2}{R_y^2}+\frac{Z^2}{R_z^2}\big)\Big)\frac{d^2}{\lambda^2\pi}e^{-(\xi^2+\theta^2)/\lambda^2} \\ &= \frac{15Nd^2}{8\pi^2R^3\lambda^2}\Big(1-\big(\frac{x_l^2}{R_x^2}+\frac{y_n^2}{R_y^2}+\frac{Z^2}{R_z^2}\big)\Big)e^{-(\xi^2+\theta^2)/\lambda^2}. \end{aligned} \tag{E.18}$$

Appendix F

Numerically solving time-dependent Bogoliubov-deGenne equation for Bose gas in a harmonic trap

The first order in Bose field operator $\hat{\Psi}$ through number-conserving Bogobiubov theory (see chapter 2) provides the equation of motion for quasiparticle wavefunction,

$$i\hbar\partial_t \begin{pmatrix} |u_j(t)> \\ |v_j(t)> \end{pmatrix} = \mathcal{L}(t) \begin{pmatrix} |u_j(t)> \\ |v_j(t)> \end{pmatrix}, \tag{F.1}$$

where the Bogoliubov operator

$$\mathcal{L} = \begin{pmatrix} \hat{H}(t) + g\hat{Q}(t)|\psi(\hat{x},t)|^2\hat{Q}(t) & g\hat{Q}(t)\psi(\hat{x},t)^2\hat{Q}^*(t) \\ -g\hat{Q}^*(t)\psi(\hat{x},t)^{*2}\hat{Q}(t) & -\hat{H} - g\hat{Q}^*(t)|\psi(\hat{x},t)|^2\hat{Q}^*(t) \end{pmatrix}. \tag{F.2}$$

Here the Hamiltonian is given by

$$\hat{H}(t) = \frac{\hat{p}^2}{2m} + \frac{1}{2}m\omega\hat{x}^2 + g|\psi(\hat{x},t)|^2 - \mu(t), \tag{F.3}$$

where the phase factor $\mu(t)$ is equal to the ground state chemical potential μ when $\psi(x,t)$ is the ground state of Gross-Pitaevskii equation. Since the space of quasiparticle is orthogonal to the space of condensates, $\hat{Q}$ projects orthogonally to $\psi(x,t)$:

$$\hat{Q} = 1 - |\psi><\psi|. \tag{F.4}$$

Eq.(F.2) corresponds to the time evolution operator

$$\mathcal{L}(t) = \begin{pmatrix} \hat{Q}(t) & 0 \\ 0 & \hat{Q}^*(t) \end{pmatrix} \mathcal{L}_{all}(t) \begin{pmatrix} \hat{Q}(t) & 0 \\ 0 & \hat{Q}^*(t) \end{pmatrix}, \tag{F.5}$$

where $\mathcal{L}_{all}(t)$ is the full-space evolution operator. Now we explore the numerical skills for Eq.(F.1). we can do the integration of the Bogoliubov equation without the state projection $\hat{Q}$,

$$i\hbar\partial_t \begin{pmatrix} |U_j(t)> \\ |V_j(t)> \end{pmatrix} = \mathcal{L}_{all}(t) \begin{pmatrix} |U_j(t)> \\ |V_j(t)> \end{pmatrix}. \tag{F.6}$$

where apply the projection $\begin{pmatrix} |u_j(t)> \\ |v_j(t)> \end{pmatrix} = \begin{pmatrix} \hat{Q}(t)|U_j(t)> \\ \hat{Q}^*(t)|V_j(t)> \end{pmatrix}$ whenever we need to export the states. Notice that $\mathcal{L}_{all}(t)$ is in principle time dependent through $\psi(\hat{x}, t)$. In a small time step Δt, the evolution may be adiabatical, given approximately by

$$\begin{pmatrix} |U_j(t+\Delta t)> \\ |V_j(t+\Delta t)> \end{pmatrix} \approx e^{-i\mathcal{L}_{all}(t)\Delta t/\hbar} \begin{pmatrix} |U_j(t)> \\ |V_j(t)> \end{pmatrix}. \tag{F.7}$$

The time evolution operator $e^{-i\mathcal{L}_{all}(t)\Delta t/\hbar}$ can be split into position- and energy-dependent parts, that is, $e^{-i\mathcal{L}_{all}(t)\Delta t/\hbar} = e^{-iF\Delta t/2\hbar} e^{-iG\Delta t/\hbar} e^{-iF\Delta t/2\hbar}$, where the energy-dependent part $M = \begin{pmatrix} (n+1)\hbar\omega/2 & 0 \\ 0 & -(n+1)\hbar\omega/2 \end{pmatrix}$ and position dependent part $G = \begin{pmatrix} 2g|\psi(\hat{x},t)|^2 & g\psi(\hat{x},t)^2 \\ -g\psi^*(\hat{x},t)^2 & -2g|\psi(\hat{x},t)|^2 \end{pmatrix}$. The energy part is

$$\begin{pmatrix} |U_{j,n}(t)> \\ V_{j,n}(t)> \end{pmatrix} = \begin{pmatrix} e^{-i(n+1/2)\omega\Delta t/2}|U_{j,n}(t)> \\ e^{i(n+1/2)\omega\Delta t/2}|V_{j,n}(t)> \end{pmatrix} \tag{F.8}$$

Using Spectral method, we can transfer the state back to real space. The position-dependent part is

$$\begin{pmatrix} |U_j(t+\Delta t)> \\ |V_j(t+\Delta t)> \end{pmatrix} = e^{-iG\Delta t/\hbar} \begin{pmatrix} |U_j(t)> \\ |V_j(t)> \end{pmatrix}. \tag{F.9}$$

The eigenvalue of G are

$$\lambda = \pm\sqrt{3}g|\psi|^2 \tag{F.10}$$

and the corresponding eigenvectors are

$$\begin{pmatrix} e^{2i\theta} \\ -(\sqrt{3}+2) \end{pmatrix}$$

for $\lambda = \sqrt{3}g|\psi|^2$ and

$$\begin{pmatrix} e^{2i\theta} \\ (\sqrt{3}-2) \end{pmatrix}$$

for $\lambda = -\sqrt{3}g|\psi|^2$, where θ is the phase of the ground state wavefunction ψ. Therefore the solution can be written as

$$\begin{pmatrix} |U_j(t+\Delta t)> \\ |V_j(t+\Delta t)> \end{pmatrix} = A \begin{pmatrix} e^{2i\theta} \\ -(\sqrt{3}+2) \end{pmatrix} e^{i\sqrt{3}g|\psi|^2\Delta t} + B \begin{pmatrix} e^{2i\theta} \\ (\sqrt{3}-2) \end{pmatrix} e^{-i\sqrt{3}g|\psi|^2\Delta t}. \tag{F.11}$$

From the initial conditions

$$\begin{pmatrix} e^{2i\theta} & e^{2i\theta} \\ -(\sqrt{3}+2) & (\sqrt{3}-2) \end{pmatrix} \begin{pmatrix} A \\ B \end{pmatrix} = \begin{pmatrix} U_j(l) \\ V_j(t) \end{pmatrix}. \tag{F.12}$$

determine the coefficients

$$\begin{pmatrix} A \\ B \end{pmatrix} = \frac{1}{2\sqrt{3}} \begin{pmatrix} (\sqrt{3}-2)e^{-2i\theta}U_j(t) - V_j(t) \\ (\sqrt{3}+2)e^{-2i\theta}U_j(t) + V_j(t) \end{pmatrix}. \tag{F.13}$$

Finally, we have

$$\begin{aligned} U_j(t+\Delta t) &= \frac{1}{2\sqrt{3}} \begin{pmatrix} (2\sqrt{3}cos(\lambda\Delta t) - 4isin(\lambda\Delta t))U_j(t) \\ +(-2isin(\lambda\Delta t)cos(2\theta) + 2sin(\lambda\Delta t)sin(2\theta))V_j(t) \end{pmatrix} \\ V_j(t+\Delta t) &= \frac{1}{2\sqrt{3}} \begin{pmatrix} (2\sqrt{3}cos(\lambda\Delta t) + 4isin(\lambda\Delta t))V_j(t) \\ +(2isin(\lambda\Delta l)cos(2\theta) + 2sin(\lambda\Delta l)sin(2\theta))U_j(l) \end{pmatrix}. \end{aligned} \tag{F.14}$$

Although the central idea of solving numerically Bogoliubov-deGenne equation have been shown, the stability of this method is still of problem. We will not exhibit the results of dynamics about Bogoliubov-deGenne equation here until we find an elegent way to solve the problem of the stability.

References

[1] M. H. Anderson, J. R. Ensher, M. R. Matthews, C. E. Wieman and E. A. Cornell, Science, **269**, 198(1995).

[2] K. B. Davis, M. -O. Mewes, M. R. Andrews, N. J. van Druten, D. S. Durfee, D. M. Kurn and W. Keterle, Phys. Rev. Lett. **75**, 3969(1995).

[3] Naomi S. Ginsberg, Sean R. Garner and Lene Vestergaard Hau, Nature, **445**, 623(2007).

[4] L. Pitaevskii and S. Stringari, *Bose-Einstein Condensation* (Clarendon press, Oxford, England, 2003).

[5] Markus Greiner, Olaf Mandel, Tilman Esslinger, Theodor W. Hänsch and Immanuel Bloch, Nature, **415**, 39(2002).

[6] T. W. Hansch and A. L. Schawlow, Opt. Commun. **13**, 68(1975).

[7] W. Ketterle, D. S. Durfee, and D. M. Stamper-Kurn, cond-mat/9904034.

[8] M. H. Anderson, J. R. Ensher, M. R. Matthews, C. E. Wieman, E. A. Comell, Science, **269**, 198(1995).

[9] M. R. Andrews, M. -O. Mewes, N. J. van Druten, D. S. Durfee, D. M. Kurn, and W. Ketterle, Science, **273**, 84(1996).

[10] J. Stenger, S. Inouye, A. P. Chikkatur, D. M. Stamper-Kurn, D. E. Pritchard, and W. Ketterle, Phys. Rev. Lett. **82**, 4569(1999).

[11] P. R. Berman and B. Bian, Phys. Rev. A, **55**, 4382(1997).

[12] Kapitza, P. L., Nature, **141**, 913(1938).

[13] Allen, J. F. and Misener, A. D., Nature, **141**, 75(1938).

[14] A. J. Leggett, Rev. Mod. Phys., **71**, 5318(1999).

[15] E. M. Lifshitz and L. P. Pitaevskii *Statistical Physics, part2* (Butterworth-Heinemann, Oxford, England, 1980).

[16] S. Inouye, M. R. Andrews, J. Stenger, H. -J. Miesner, D. M. Stamper-Kurn, and W. Ketterle, Nature, **392**, 151(1998).

[17] C. D. Fertig, K. M. O'Hara, J. H. Huckans, S. L. Rolston, W. D. Phillips, and J. V. Porto, Phys. Rev. Lett. **94**, 120403(2005).

[18] D. A. W. Hutchinson, E. Zaremba, and A. Griffin, Phys. Rev. Lett. **78**, 1842(1997).

[19] V. V. Kocharovsky, Vl. V. Kocharovsky, and M. O. Scully, Phys. Rev. Lett. **84**, 2306(2000), and references therein.

[20] D. S. Jin, M. R. Matthews, J. R. Ensher, C. E. Wieman, and E. Cornell, Phys. Rev. Lett. **78**, 764(1997).

[21] D. N. Stamper-Kurn and H. -J. Miesner, S. Inouye, M. R. Andrews, and W. Ketterle, Phys. Rev. Lett. **81**, 500(1998).

[22] M. R. Matthews, B. P. Anderson, P. C. Haljan, D. S. Hall, C. E. Wieman, and E. A. Cornell, Phys. Rev. Lett. **83**, 2498(1999).

[23] K. W. Madison, F. Chevy, W. Wohlleben, and J. Dalibard, Phys. Rev. Lett. **84**, 806(2000).

[24] J. R. Abo-Shaeer, C. Raman, J. M. Vogels, and W. Ketterle, Science, **292**, 476(2001).

[25] Z. Hadzibabic et. al., Nature **441**, 1118(2006); S. Stock et. al., Phys. Rev. Lett. **95**, 190403(2005).

[26] Oliver Penrose and Lars Onsager, Phys. Rev. **104**, 576(1956).

[27] E. P. Gross, Phys. Rev. **106**, 61(1957).

[28] V. L. Ginzburg and L. P. Pitaevskii, *Sov. Phys. JETP* **7**, *858(1958)*.

[29] László Erdös, Benjamin Schlein, and Horng-Tzer Yau, Phys. Rev. Lett. **98**, 040404(2007).

[30] Alexander L. Fetter, Annals of Physics **70**, 67(1972).

[31] Andrij Rovenchak, J. Low Temp. Phys. **148**, 411(2007).

[32] Y. Castin and R. Dum, Phys. Rev. A **57**, 3008(1998).

[33] M. R. Andrews, D. M. Kurn, H. -J. Miesner, D. S. Durfee, C. G. Townsend, S. Inouye, and W. Ketterle, Phys. Rev. Lett. **79**, 553(1997).

[34] E. Zaremba, Phys. Rev. A **57**, 518(1998).

[35] M. R. Andrews, C. G. Townsend, H. -J. Miesner, D. S. Durfa, D. M. Kurn, and W. Ketterle, Science, **275**, 637(1997).

[36] T. F. Scott, R. J. Ballagh, and K. Burnett, J. Phys. B **31**, L329(1998).

[37] R. J. Ballagh, K. Burnett, and T. F. Scott, Phys. Rev. Lett. **78**, 1607(1997).

[38] D. R. Scherer, C. N. Weiler, T. W. Neely, and B. P. Anderson, Phys. Rev. Lett. **98**, 110402 (2007).

[39] R. Carretero-González et al., Phys. Rev. A, **77**, 033625(2008).

[40] R. Carretero-Gonz'alez, N. Whitaker, P. G. Kevrekidis and D. J. Frantzeskakis, Phys. Rev. A, **77**, 023605 (2008).

[41] M. S. Chapman, et al., Phys. Rev. Lett. **75**, 3783(1995).

[42] M. -O. Mewes, M. R. Andrews, D. M. Kurn, D. S. Durfee, C. G. Townsend, and W. Ketterle, Phys. Rev. Lett. **78**, 582(1997).

[43] C. Raman, J. R. Abo-Shaeer, J. M. Vogels, K. Xu, and W. Ketterle, Phys. Rev. Lett. **87**, 210402(2001).

[44] Subhasis Sinha and Yvan Castin, Phys. Rev. Lett. **87**, 190402(2001).

[45] E. A. Burt, R. W. Ghrist, C. J. Myatt, M. J. Holland, E. A. Cornell, and C. E. Wieman, Phys. Rev. Lett. **79**, 337(1997).

[46] D. S. Hall, M. R. Matthews, C. E. Wieman, and E. A. Cornell, Phys. Rev. Lett. **81**, 1543(1998).

[47] A. A. Norrie, R. J. Ballagh, and C. W. Gardiner, Phys. Rev. Lett. **94**, 040401(2005); Phys. Rev. A **73**, 043617(2006).

[48] A. J. Leggett, Rev. Mod. Phys., **73**, 307(2001).

[49] B. Xiong, S. Chen, T. Yang and Keith Benedict, *Quantum Transport of 1D Degenerate Bose Gas in the Lattice: The Role of Different Quantum Fluctuations.*

[50] A. S. Bradley, P. B. Blakie and C. W. Gardiner, J. Phys. B **38**, 4259(2005).

[51] S. A. Morgan, J. Phys. B, **33**, 3847(2002).

[52] A. A. Norrie, R. J. Ballagh, and C. W. Gardiner, Phys. Rev. A, **73**, 043617(2006).

[53] M. J. Steel, M. K. Olsen, L. I. Plimak, P. D. Drummond, S. M. Tan, M. J. Collett, D. F. Walls and R. Graham, Phys. Rev. A **58**, 4824(1998).

[54] P. Deuar and P. D. Drummond, Phys. Rev. Lett. **98**, 120402(2007).

[55] J. Ruostekoski and L. Isella, Phys. Rev. Lett. **95**, 110403(2005); Lorenzo Isella and Janne Ruostekoski, Phys. Rev. A **72**, 011601(2005); L. Isella and J. Ruostekoski, Phys. Rev. A **74**, 063625(2006).

[56] C. W. Gardiner and P. Zoller, *Quantum Noise* (Springer, Berlin, 1999).

[57] C. W. Gardiner, *Handbook of Stochastic Methods*, 3rd edition (Springer-Verlag, 2004).

[58] O. Morsch, J. H. Müller, M. Cristiani, D. Ciampini, and E. Arimondo, Phys. Rev. Lett. **87**, 140402(2001).

[59] B. P. Anderson and M. A. Kasevich, Science **282**, 1686(1998).

[60] B. Wu and Q. Niu, Phys. Rev. A **64**, 061603(2001).

[61] M. Holthaus, J. Opt. B: Quantum Semiclassical Opt. **2**, 589(2000).

[62] A. Trombettoni and A. Smerzi, Phys. Rev. Lett. **86**, 2353(2001).

[63] D. -I. Choi and Q. Niu, Phys. Rev. Lett. **82**, 2022(1999).

[64] K. Berg-Sørensen and K. Mølmer, Phys. Rev. A **58**, 1480(1998).

[65] M. Cerimele, M. Chiofalo, F. Pistella, S. Succi, and M. Tosi, Phys. Rev. E **62**, 1382(2000).

[66] D. -I. Choi and Q. Niu, Phys. Lett. A **318**, 558(2003).

[67] R. G. Scott et al., Phys. Rev. Lett. **90**, 110404(2003).

[68] S. Stock et. al., Phys. Rev. Lett. **95**, 190403 (2005).

[69] W.F. Vinen, J. Low. Temp. Phys., **145**, 7 (2006)

[70] Ehud Altman, Eugene Demler, and Mikhail D. Lukin, Phys. Rev. A **70**, 013603(2004).

[71] Simon Fölling, Fabrice Gerbier, Artur Widera, Olaf Mandel, Tatjana Gericke and Immanuel Bloch, Nature, **434**, 481(2005).

[72] F. S. Cataliotti et al., Science **293**, 843(2001).

[73] F. Ferlaino et al., Phys. Rev. A **66**, 011604(**R**) (2002).

[74] G. Modugno et al., Phys. Rev. A **68**, 011601(**R**) (2003).

[75] L. Pezzè et al., Phys. Rev. Lett. **93**, 120401(2004).

[76] T. Stöferle et al., Phys. Rev. Lett. **92**, 130403(2004).

[77] R. G. Scott, D. A. W. Hutchinson, and C. W. Gardiner, Phys. Rev. A **74**, 053605(2006); Laser Physics **17**, 527(2007).

[78] D. I. Choi and Q. Niu, Phys. Rev. Lett. **82**, 2022(1999).

[79] Sebastian Wüster, et al., Phys. Rev. A, **75**, 043611(2007).

[80] R. Ozeri, N. Katz, J. Steinhauer, and N. Davidson, Rev. Mod. Phys. **77**, 187(2005).

[81] Alice Sinatra, Carlos Lobo and Yvan Castin, J. Phys. B **35**, 3599(2002).

[82] M. L. Chiofalo, S. Succi, and M. P. Tosi, Phys. Rev. E **62**, 7438(2000).

[83] M. Lewenstein and L. You, Phys. Rev. Lett. **77**, 3489(1996).

[84] *A Classical Field Treatment of Colliding Bose-Einstein Condensates*, Adam Anson Norrie, A thesis submitted for the degree of Doctor of Philosophy at the University of Otago, Dunedin, New Zealand, June 2005.

[85] M. L. Chiofalo, S. Succi, and M. D. Tosi, Phys. Rev. A **62**, 7438(2000).

[86] R. G. Scott et al., Phys. Rev. Lett. **95**, 073201(2005).

[87] Z. Dutton et al., Science **293**, 663(2001).

[88] S. Burger et al., Phys. Rev. Lett. **86**, 4447(2001).

[89] Anatoli Polkovnikov and Daw-Wei Wang, Phys. Rev. Lett. **93**, 070401(2004).

[90] E. Hodby et al., Phys. Rev. Lett. **88**, 010405(2001).

[91] P. C. Haljan et al., Phys. Rev. Lett. **87**, 210403(2001).

[92] S. Inouye et. al., Phys. Rev. Lett. **87**, 080402(2001).

[93] B. P. Andrews et al., Phys. Rev. Lett. **86**, 2926(2001).

[94] Y. Shin et. al., Phys. Rev. A, **72**, 021604(2005).

[95] J. Javanainen and Sun Mi Yoo, Phys. Rev. Lett. **76**, 161(1996).

[96] T. Wong, M. J. Collett, and D. F. Walls, Phys. Rev. A **54**, 3718(1996).

[97] J. I. Cirac, C. W. Gardiner, M. Naraschewski, and P. Zoller, Phys. Rev. A **54**, 3714(1996).

[98] Y. Castin and J. Dalibard, Phys. Rev. A **55**, 4330(1997).

[99] P. Horak and S. M. Barnett, J. Phys. B **32**, 3421(1999).

[100] K. Mølmer, Phys. Rev. A **65**,021067(2003).

[101] F. Laloë, European Physics Journal D **33**, 87(2005).

[102] G. -B. Jo, J. -H. Choi, C. A. Christensen, Y. -R. Lee, T. A. Pasquini, W. Ketterle, and D. E. Pritchard, Phys. Rev. Lett. **99**, 240406(2007).

[103] David R. Scherer, Chad N. Weiler, Tyler W. Neely, and Brian P. Anderson, Phys. Rev. Lett. **98**, 110402(2007).

[104] C. Pethick and H. Smith, *Bose-Einstein Condensation in Dilute Gases* (Cambridge University Press, Cambridge, England, 2002).

[105] Y. Shin, M. Saba, T. A. Pasquini, W. Ketterle, D. E. Pritchard, and A. E. Leanhardt, Phys. Rev. Lett. **92**, 050405(2004).

[106] G.-B. Jo et al., Phys. Rev. Lett. **98**, 030407(2007).

[107] A. Röhrl, M. Naraschewski, A. Schenzle, and H. Wallis, Phys. Rev. Lett. **78**, 4143(1997).

[108] William Hostom and L. You, Phys. Rev. A, **53**, 4254 (1996).

[109] H. Wallis, A. Röhrl, M. Naraschewski, and A. Schenzle, Phys. Rev. A, **55**, 2109(1997).

[110] Y. Castin and R. Dum, phys. Rev. Lett. **77**, 5315(1996).

[111] C. R. Ekstrom, J. Schmiedmayer, M. S. Chapman, T. D. Hammond, and D. E. Pritchard, Phys. Rev. A, **51**, 3883(1995).

[112] A. Peters, K. Y. Chung, B. Young, J. Hensley, and S. Chu, *Philos. Trans. R. Soc, London, Ser.* A**355**, 2223(1997).

[113] S. Gupta, K. Dieckmann, Z. Hadzibabic, and D. E. Pritchard, Phys. Rev. Lett. **89**, 140401(2002).

[114] N. Yu, J. M. Kohel, J. Ramez-serrano, J. R. Kellogg, L. Lim, and L. Maleki, Earth Science Technology conference (2004).

[115] J. M. Vogels, J. K. Chin, and W. Ketterle, Phys. Rev. Lett. **90**, 030403(2003).

[116] Wu-Ming Liu, Biao Wu, and Qian Niu, Phys. Rev. Lett. **84**, 2294(2000).

[117] C. Orzel, A. K. Tuchman, M. L. Fenselau, M. Yasuda, M. A. Kasevich, Science, **291**, 2386(2001).

[118] A. A. Norrie, R. J. Ballagh, and C. W. Gardiner, Phys. Rev. Lett., **94**, 040401(2005).

[119] P. O. Fedichev and G. V. Shlyapnikov, Phys. Rev. A **60**, R1779(1999).

[120] Stephan Ritter, Anton Öttl, Tobias Donner, Thomas Bourdel, Michael Köhl, and Tilman Esslinger, Phys. Rev. Lett. **98**, 090402(2007).

[121] A. Sinatra, C. Lobo, and Y. Castin, Phys. Rev. Lett., **87**, 210404(2001).

[122] V. V. Konotop and M. Salerno, Phys. Rev. A **65**, 021602(R)(2002).

[123] B. B. Baizakov.et al., J. Phys. B **35**, 5105(2002).

[124] M. Abramowitz and I. Stegun, *Handbook of mathematical functions* (Dover books, 1965).

[125] K. Xu, Y. Liu, D. E. Miller, J. K. Chin, W. Setiawan, and W. Ketterle, Phys. Rev. Lett. **96**, 180405(2006).

[126] B. Wu, Q. Niu, cond-mat/0306411 (2003).

[127] V. I. Yukalov et al., Phys. Rev. A **66**, 043602(2002).

[128] J. C. Bronski et al., Phys. Rev. Lett. **86**, 1402(2001).

[129] B. Wu et al., Phys. Rev. A **65**, 025601(2002).

[130] W. H. Press, S. A. Teukolsky, W. T. Vetterling, and B. P. Flannery, *Numerical Recipes, the art of scientific computing* (Cambridge University Press, 1994).

[131] *Cold Atoms in Optical Lattices*, Robin George Scott, Thesis submitted to the University of Nottingham for the degree of Doctor of Philosophy March 2003.

[132] Huang Hu, Li Shi-qun, Chin. Phys. Lett. **16**, 9(1999).